ANALYTICAL LATERAL LOAD RESPONSE OF UNBONDED POST-TENSIONED CAST-IN-PLACE CONCRETE SPECIAL STRUCTURAL WALLS WITH BONDED OR DEBONDED LONGITUDINAL MILD STEEL REINFORCEMENT

Report to
Charles Pankow Foundation
RGA#3-10

by

Sonam Srivastava

Stephen Pessiki

Richard Sause

ATLSS Report No. 13-02

April 2013

ATLSS is a National Center for Engineering Research on Advanced Technology for Large Structural Systems

117 ATLSS Drive
Bethlehem, PA 18015-4729

Phone: (610)758-3525
Fax: (610)758-5902

www.atlss.lehigh.edu
Email:inatl@lehigh.edu

ANALYTICAL LATERAL LOAD RESPONSE OF UNBONDED POST-TENSIONED CAST-IN-PLACE CONCRETE SPECIAL STRUCTURAL WALLS WITH BONDED OR DEBONDED LONGITUDINAL MILD STEEL REINFORCEMENT

Report to
Charles Pankow Foundation
RGA#3-10

by

Sonam Srivastava
Graduate Research Assistant

Stephen Pessiki
Professor of Structural Engineering
pessiki@lehigh.edu

Richard Sause
Professor of Structural Engineering
rs0c@lehigh.edu

ATLSS Report No. 13-02

April 2013

ATLSS is a National Center for Engineering Research on Advanced Technology for Large Structural Systems

117 ATLSS Drive
Bethlehem, PA 18015-4729

Phone: (610)758-3525
Fax: (610)758-5902

www.atlss.lehigh.edu
Email:inatl@lehigh.edu

ACKNOWLEDGMENTS

The work presented in this report was supported by the Charles Pankow Foundation and conducted at the Department of Civil and Environmental Engineering, Lehigh University, Bethlehem, Pennsylvania. The support of the Charles Pankow Foundation in facilitating this project is gratefully acknowledged.

The opinions, findings, and conclusions expressed in this report are those of the author's and do not necessarily reflect the views of the individuals acknowledged above.

TABLE OF CONTENTS

LIST OF TABLES

LIST OF FIGURES

ABSTRACT

This research investigates the analytical lateral load responses of unbonded post-tensioned cast-in-place concrete special structural walls with bonded or debonded longitudinal mild steel reinforcement under the action of monotonic lateral load. Two sets of generalized closed-form expressions are derived for estimating the lateral load responses, base moment and lateral drift, of the walls for critical limit states. First set of equations is for cast-in-place special structural walls with bonded longitudinal reinforcement and the second for cast-in-place special structural walls with predetermined length of debonded longitudinal reinforcement at the base of the wall.

Analytical models for walls, with the two configurations of longitudinal reinforcement, using fiber elements are also presented for nonlinear analysis of walls under monotonic lateral load. In general, results of the closed-form expressions are in good agreement with the results of analytical models.

The analytical models and the closed-form expressions are also used for investigating effects of six design parameters in the lateral load response of the walls. The parameters considered are area of post-tensioning steel with constant initial prestress; initial prestress in post-tensioning steel with constant area of post-tensioning steel; constant initial prestress force with varying area and initial prestress; area of boundary longitudinal reinforcement; area of web longitudinal reinforcement; and spacing of web longitudinal reinforcement.

Debonding the longitudinal reinforcement over a predetermined height at the base of the wall significantly increased the lateral drift value with minimal effect on base moment. This additional deformation capacity of the walls was achieved by delaying the yielding of longitudinal reinforcement without any change in the restoring action of unbonded post-tensioning steel. With increase in the area or initial prestress of post-tensioning steel base moment value increases and drift value decreases for all the limit states. Increasing the area of boundary or web longitudinal reinforcement also increases the lateral load response values of the walls, whereas, spacing of web longitudinal reinforcement with constant longitudinal reinforcement area does not have any significant effect.

This research was sponsored by the Charles Pankow Foundation.

CHAPTER 1

INTRODUCTION

The structural damages observed in past earthquakes have demonstrated that structures with structural walls performed better than those without any walls. Two inherent limitations found in commonly used structural walls are: (1) the required nonlinearity or softening of the wall is caused by damage (i.e., yielding of reinforcing steel and softening of concrete in compression); and (2) residual lateral drift after a major seismic event. Both these limitations can be addressed through the use of post-tensioning. The post-earthquake residual lateral deformation of a structural can be controlled by use of post-tensioning which provides a restoring force against the lateral load which enables the wall to rock back to its original upright position. Using precast concrete panels accelerates the construction process as they can be fabricated in workshops and easily erected on-site. Therefore, several analytical and experimental studies have been conducted in last decade or two to combine the two components of precast construction and post-tensioning to improve lateral load behavior of structural walls.

Figure 1.1 shows a schematic of a traditional cast-in-place wall (ACI 318 compliant), an unbonded post-tensioned precast concrete wall, and an unbonded post-tensioned hybrid precast concrete wall. Also shown in this figure is the expected base moment-lateral drift of each wall. The structural wall (Figure 1.1(a)) is a cast-in-place concrete wall, without post-tensioning, with detailing according to ACI 318-11. Under the action of lateral load, the wall softens due to yielding of steel reinforcement and nonlinear stress-strain response of concrete. Upon reversal of lateral load F, the wall will not necessarily return to zero drift position. The unbonded post-tensioned precast concrete walls are the precast walls with post-tensioning for self-centering (Kurama et al. (1996), Kurama (1997), Perez (2004), Perez et al. (2007)). These walls have higher self-centering capacity but they do not have any mild steel reinforcement crossing the horizontal joint between vertically stacked panels or the panel at the base of the wall and the foundation. Therefore, these walls undergo large drift without dissipating any excitation energy as illustrated in Figure 1.1(b). The unbonded post-tensioned hybrid precast concrete walls include bonded longitudinal web reinforcement for energy dissipation. As shown in Figure 1.1, lateral load-deflection curve of the unbonded post-tensioned hybrid precast concrete walls is a combination of the energy dissipation as in structural walls and self-centering as in unbonded post-tensioned precast concrete walls. In an event of seismic excitation, use of unbonded post-tensioning provides the wall with self-centering capacity and the mild steel reinforcement is designed to dissipate energy.

Table 1.1 presents a summary of the various types of walls reviewed and studied in this report along with the structural elements included. For example, the structural wall consists of cast-in-place walls with bonded web and boundary longitudinal reinforcement. In an unbonded post-tensioned precast concrete wall, the post-tensioning steel is placed in ducts and stays ungrouted after prestressing. This eliminates strain compatibility between the post-tensioning steel and the surrounding concrete, unlike the bonded post-tensioned case. Since the post-tensioning steel is unbonded, it is assumed that the deformation in post-tensioning steel is distributed uniformly over the entire unbonded length. Therefore, the unbonded post-tensioned precast concrete wall can

achieve larger overall deformation before the post-tensioning steel reaches its yield strain (Kurama 1997).

Holden et al (2003) and Restrepo and Rahman (2007) showed that hybrid unbonded precast concrete walls with bonded mild steel extending from the bottom of the wall into the foundation provide the supplemental energy dissipation as in a cast-in-place concrete wall, but with less structural damage and less residual displacement, without compromising the self-centering capacity of the walls.

The current research is designed to study the lateral load behavior of a cast-in-place wall which incorporates the self-centering ability by using unbonded post-tensioning and energy dissipation capability by using longitudinal mild steel reinforcement.

1.1 OBJECTIVES

The primary objective of this study is to derive closed-form expressions to describe monotonic lateral load behavior of an unbonded post-tensioned cast-in-place special structural wall with bonded or debonded longitudinal mild steel reinforcement, as shown in Figure 1.2. Together the two types of reinforcement, post-tensioning steel for self-centering and mild steel reinforcement for energy dissipation, incorporate the features of both cast-in-place walls with energy dissipation and unbonded post-tensioned precast with higher lateral displacement and self-centering capacity. This study also investigates effects of different design parameters on the moment at the base of the wall and lateral drift response of these walls.

1.2 RESEARCH APPROACH

In order to achieve the objectives presented in Section 1.1, following approach is taken:

1. Perform a literature review of previous research related to lateral load response of unbonded post-tensioned precast walls with and without mild steel reinforcement.
2. Derive closed-form expressions for estimating lateral load responses, moment at the base and drift at the roof level, of two cases of unbonded post-tensioning cast-in-place special structural walls with longitudinal reinforcement: (a) the longitudinal mild steel reinforcement is bonded with the surrounding concrete and (b) the longitudinal reinforcement in debonded over a predetermined height at the base of the wall.
3. Design cast-in-place parametric walls with unbonded post-tensioning and longitudinal mild steel reinforcement.
4. Develop an analytical model for determining expected lateral load response of the parametric walls.
5. Establish accuracy of the closed-form expressions in estimating lateral load responses of the parametric walls using the results obtained from the analytical models under monotonic lateral load.
6. Conduct a parametric study by systematically varying design parameters and observing the expected lateral load response of the walls.

1.3 REPORT ORGANIZATION

The report is organized into six chapters (Chapters 2-7) in accordance with the research approach summarized in Section 1.2. Chapter 2 presents the literature review of walls with post-tensioning for self-centering and longitudinal mild steel for energy dissipation.

Chapter 3 derives two sets of closed-form expressions for unbonded post-tensioned special structural walls with longitudinal mild steel reinforcement, one set of closed-form expressions each for bonded longitudinal reinforcement and for debonded longitudinal reinforcement. Chapter 4 describes the design and detailing of the parametric walls used in the current research. Chapter 5 discusses the development of analytical models for the parametric walls under monotonic lateral load. Chapter 6 presents results of a parametric study conducted on the lateral load response of unbonded post-tensioned cast-in-place concrete special structural walls with longitudinal mild steel reinforcement by systematically varying design parameters of the parametric walls of Chapter 4. Lastly, Chapter 7 presents a summary and conclusions of the research, and identifies future research needs.

1.4 NOTATIONS

The following notations are used in this research report:

$A_{b,l}$ = Area of longitudinal mild steel reinforcement in boundary region

$A_{b,t}$ = Area of transverse mild steel reinforcement in boundary region

$A_{p,1}$ = Cross-sectional area of first post-tensioning steel group from right end of the wall

$A_{p,2}$ = Cross-sectional area of second post-tensioning steel group from right end of the wall

$A_{p,i}$ = Cross-sectional area of i^{th} group of post-tensioning steel from right end of the wall

A_{pt} = Total post-tensioning steel area in the wall cross-section

$A_{s,i}$ = Cross-sectional area of i^{th} reinforcement bar(s) from right end of the wall

$A_{w,l}$ = Area of longitudinal mild steel reinforcement in web region

$A_{w,t}$ = Area of transverse mild steel reinforcement in web region

A'_w = Gross cross-sectional area of the wall

a = Depth of equivalent rectangular compression stress block

a_{ccc} = Depth of equivalent rectangular compression stress block at the limit state of crushing of confined concrete

a_{ell-2} = Depth of equivalent rectangular compression stress block at the limit state of effective linear limit with non-linear behavior of unconfined concrete

a_{fms} = Depth of equivalent rectangular compression stress block when farthest longitudinal mild steel reinforcement bar(s) reaches its ultimate strength

a_{llp} = Depth of equivalent rectangular compression stress block when farthest post-tensioning steel begins to yield in tension

a_{yms} = Depth of equivalent compression stress block when farthest longitudinal mild steel reinforcement bar(s) begin to yield in tension (for debonded reinforcement)

C = Resultant of compressive force at the base of the wall

C_c = Resultant of compressive force in concrete

C_{ccc} = Resultant upward force at the base of the wall at the crushing of confined concrete

C_{dec} = Resultant upward force at the base of the wall at the limit state of decompression

C_{ell} = Resultant upward force at the base of the wall at the limit state of effective linear limit

C_{fms} = Resultant upward force at the base of the wall when farthest longitudinal mild steel reinforcement bar(s) reaches its ultimate strength

C_{llp} = Resultant upward force at the base of the wall when farthest post-tensioning steel begins to yield in tension

$C_{s,i}$ = Resultant compressive force in i^{th}longitudinal mild steel reinforcement bar(s)

C_{yms} = Resultant compressive force at the base of the wall when farthest longitudinal mild steel reinforcement bar(s) begin to yield in tension (for debonded reinforcement)

c_{ccc} = Neutral axis depth at crushing of confined concrete

c_{ell-2} = Neutral axis depth at effective linear limit with non-linear behavior of unconfined concrete

c_{ell-4} = Neutral axis depth at effective linear limit of yielding of bonded mild steel reinforcement

c_{fms} = Neutral axis depth when farthest longitudinal mild steel reinforcement bar(s) reaches its ultimate strength

c_{llp} = Neutral axis depth when farthest post-tensioning steel begins to yield in tension

c_{yms} = Neutral axis depth when farthest longitudinal mild steel reinforcement bar(s) starts yielding in tension

E_c = Young's modulus for concrete

E_p = Young's modulus for post-tensioning steel

E_s = Young's modulus for longitudinal mild steel reinforcement

e_p = Eccentricity of post-tensioning steel about the centerline of wall section

F = Lateral force acting on the wall

$f_{c,dec}$ = Maximum compressive stress in concrete at the limit state of decompression

$f_{csc,i}$ = Compressive stress in concrete at i^{th} longitudinal mild steel reinforcement bar(s) from right end of the wall

$f_{c,ell-1}$ = Maximum compressive stress in concrete at effective linear limit when neutral axis depth is 25% of l_w

$f_{c,ell-4}$ = Maximum compressive stress in concrete at effective linear limit when bonded longitudinal mild steel reinforcement bar(s) start yielding

$f_{p,i}$ = Initial prestress in the i^{th}post-tensioninag steel

$f_{p,2}$ = Stress in the second post-tensioning steel

f_{pu} = Ultimate strength of the post-tensioning steel

f_{py} = Yield strength of the post-tensioning steel

$f_{s,j}$ = Tensile stress in j^{th} longitudinal mild steel reinforcement bar(s)

f_{su} = Ultimate strength of longitudinal mild steel reinforcement

f_{sy} = Yield strength of longitudinal mild steel reinforcement

$f_c^{'}$ = Compressive strength of unconfined concrete

$f_{cc}^{'}$ = Compressive strength of confined concrete

$f_{s,i}^{'}$ = Compressive stress in i^{th} longitudinal mild steel reinforcement bar(s)

G_c = Shear modulus of concrete

H_{cr} = Critical confined concrete crushing height

H_F = Height of the applied equivalent later force from the base of the wall

$H_{ms,unb}$ = Debonded height of longitudinal mild steel reinforcement

H_{ph} = Plastic hinge length

$H_{pt,unb}$ = Unbonded height of post-tensioning steel

H_w = Total height of wall

I_w = Moment of inertia of the gross cross-section of the wall

$l_{p,1}$ = Distance of first post-tensioning steel group from right end of the wall

$l_{p,2}$ = Distance of second post-tensioning steel group from right end of the wall

$l_{s,i}$ = Distance of i^{th} longitudinal mild steel reinforcement bar(s) from right end of the wall

l_w = Length of the wall cross-section

$l_{p,1}^{\prime}$ = Effective distance of first post-tensioning steel group from right end of the wall (after spalling)

$l'_{p,2}$ = Effective distance of second post-tensioning steel group from right end of the wall (after spalling)

$l'_{P,i}$ = Effective distance of i^{th} post-tensioning steel group from right end of the wall (after spalling)

$l'_{s,i}$ = Effective distance of i^{th} longitudinal mild steel reinforcement bar(s) from right end of the wall (after spalling)

M_{ccc} = Base moment at the crushing of confined concrete

M_{dec} = Base moment at the limit state of decompression

M_{ell} = Base moment at the limit state of effective linear limit

M_{ell-1} = Base moment at effective linear limit when neutral axis depth is 25% of l_w

M_{ell-2} = Base moment at effective linear limit with non-linear behavior of unconfined concrete

M_{ell-3} = Base moment at effective linear limit when the moment at the base of the wall is $2.5M_{dec}$

M_{ell-4} = Base moment at effective linear limit when farthest bonded longitudinal reinforcement bar(s) begin to yield in tension

M_{fms} = Base moment when farthest longitudinal mild steel reinforcement bar(s) reaches its ultimate strength

M_{llp} = Base moment when farthest post-tensioning steel begins to yield in tension

M_{yms} = Base moment when farthest debonded longitudinal mild steel reinforcement bar(s) begin to yield in tension

N = Gravity load acting on the wall

n = Modular ratio for reinforcing steel and concrete

T_{ccc} = Resultant downward force at the base of the wall at the crushing of confined concrete

T_{dec} = Resultant downward force at the base of the wall at the limit state of decompression

T_{ell} = Resultant downward force at the base of the wall at the limit state of effective linear limit

T_{fms} = Resultant downward force at the base of the wall when farthest longitudinal mild steel reinforcement bar(s) reaches its ultimate strength

T_{llp} = Resultant downward force at the base of the wall when farthest post-tensioning steel begins to yield in tension

T_{pt} = Resultant initial post-tensioning force

$T_{p,1}$ = Resultant force in the first post-tensioning steel group (other than initial prestress force)

$T_{p,2}$ = Resultant force in the second post-tensioning steel group (other than initial prestress force)

$T_{p1,i}$ = Total initial prestress force in the first post-tensioning steel group after elastic shortening due to post-tensioning

$T_{p2,i}$ = Total initial prestress force in the second post-tensioning steel group after elastic shortening due to post-tensioning

$T_{s,j}$ = Tension force in j^{th} longitudinal mild steel reinforcement bar(s)

T_{yms} = Resultant tensile force at the base of the wall when farthest debonded longitudinal mild steel reinforcement bar(s) begin to yield in tension

t_w = Thickness of wall cross-section

t_w'' = Effective thickness of wall

V_{ccc} = Base shear at the crushing of confined concrete

V_{dec} = Base shear at the limit state of decompression

V_{ell} = Base shear at the limit state of effective linear limit

V_{fms} = Base shear when farthest longitudinal mild steel reinforcement bar(s) reaches its ultimate strength

V_{llp} = Base shear when farthest post-tensioning steel begins to yield in tension

V_{yms} = Base shear when farthest debonded longitudinal mild steel reinforcement bar(s) begin to yield in tension

$\Delta_{conc,ccc}$ = Compressive deformation of concrete at the crushing of confined concrete

Δ_{ccc} = Resultant lateral displacement of the wall at the crushing of confined concrete

$\Delta_{conc,fms}$ = Compressive deformation of concrete when farthest longitudinal mild steel reinforcement bar(s) reaches its ultimate strength

$\Delta_{conc,ell-1}$ = Compressive deformation of concrete at the limit state of effective linear limit when neutral axis depth is 25% of l_w

$\Delta_{conc,ell-2}$ = Compressive deformation of concrete at the limit state of effective linear limit with non-linear behavior of unconfined concrete

$\Delta_{conc,ell-4}$ = Compressive deformation of concrete at when farthest bonded longitudinal reinforcement bar(s) begin to yield in tension 4

Δ_{dec} = Resultant lateral displacement of the wall at the limit state of decompression

Δ_{ell} = Resultant lateral displacement of the wall at the limit state of effective linear limit

$\Delta_{F,ccc}$ = Elastic flexural displacement of the wall at the crushing of confined concrete

$\Delta_{F,dec}$ = Elastic flexural displacement of the wall at the limit state of decompression

$\Delta_{F,ell}$ = Elastic flexural displacement of the wall at the limit state of effective linear limit

$\Delta_{F,fms}$ = Elastic flexural displacement of the wall when farthest longitudinal mild steel reinforcement bar(s) reaches its ultimate strength

$\Delta_{F,llp}$ = Elastic flexural displacement of the wall when farthest post-tensioning steel begins to yield in tension

$\Delta_{F,yms}$ = Elastic flexural displacement of the wall when farthest debonded longitudinal mild steel reinforcement bar(s) begin to yield in tension

Δ_{fms} = Resultant lateral displacement of the wall when farthest longitudinal mild steel reinforcement bar(s) reaches its ultimate strength

$\Delta_{go,ccc}$ = Lateral displacement of the wall due to gap opening at the crushing of confined concrete

$\Delta_{go,ell}$ = Lateral displacement of the wall due to gap opening at the limit state of effective linear limit

$\Delta_{go,fms}$ = Lateral displacement of the wall due to gap opening when farthest longitudinal mild steel reinforcement bar(s) reaches its ultimate strength

$\Delta_{go,llp}$ = Lateral displacement of the wall due to gap opening when farthest post-tensioning steel begins to yield in tension

$\Delta_{go,yms}$ = Lateral displacement of the wall due to gap opening when farthest debonded longitudinal mild steel reinforcement bar(s) begin to yield in tension

Δ_{llp} = Resultant lateral displacement of the wall when farthest post-tensioning steel begins to yield in tension

$\Delta_{ms,fms}$ = Elongation of farthest longitudinal mild steel reinforcement bar(s) when farthest longitudinal mild steel reinforcement bar(s) reaches its ultimate strength

$\Delta_{ms,yms}$ = Elongation of farthest longitudinal mild steel reinforcement bar(s) when farthest debonded longitudinal mild steel reinforcement bar(s) begin to yield in tension

$\Delta_{p,2}$ = Elongation of second post-tensioning steel group due to lateral force

$\Delta_{P,i}$ = Elongation of i^{th} post-tensioning steel group due to lateral force

$\Delta_{S,ccc}$ = Elastic shear displacement at the crushing of confined concrete

$\Delta_{S,dec}$ = Elastic shear displacement at the limit state of decompression

$\Delta_{S,ell}$ = Elastic shear displacement at the limit state of effective linear limit

$\Delta_{S,fms}$ = Elastic shear displacement when farthest longitudinal mild steel reinforcement bar(s) reaches its ultimate strength

$\Delta_{S,llp}$ = Elastic shear displacement when farthest post-tensioning steel begins to yield in tension

$\Delta_{S,yms}$ = Elastic shear displacement when farthest debonded longitudinal mild steel reinforcement bar(s) begin to yield in tension

$\Delta_{s,j}$ = Deformation of j^{th} longitudinal mild steel reinforcement bar(s) in tension

Δ_{yms} = Resultant lateral displacement when farthest debonded longitudinal mild steel reinforcement bar(s) begin to yield in tension

$\Delta'_{s,i}$ = Deformation of i^{th} longitudinal mild steel reinforcement bar(s) in compression

Θ_{ccc} = Drift of the wall at the crushing of confined concrete

Θ_{dec} = Drift of the wall at the limit state of decompression

Θ_{ell} = Drift of the wall at the limit state of effective linear limit

Θ_{fms} = Drift of the wall when farthest longitudinal mild steel reinforcement bar(s) reaches its ultimate strength

Θ_{yms} = Drift of the wall farthest longitudinal mild steel reinforcement bar(s) begin to yield in tension (for debonded reinforcement)

Θ_{llp} = Drift of the wall when farthest post-tensioning steel begins to yield in tension

α = Strength reduction factor for confined concrete

β = Length reduction factor for confined concrete

β_1 = Length reduction factor for unconfined concrete

$\varepsilon_{c,ell-1}$ = Maximum compressive strain in concrete at effective linear limit when neutral axis depth is 25% of l_w

$\varepsilon_{c,ell-2}$ = Maximum compressive strain in concrete at effective linear limit with non-linear behavior of unconfined concrete

$\varepsilon_{c,ell-4}$ = Maximum compressive strain in concrete at effective linear limit when bonded longitudinal mild steel reinforcement bar(s) start yielding

$\varepsilon_{c,fms}$ = Compressive strain in extreme concrete fiber when farthest longitudinal mild steel reinforcement bar(s) reaches its ultimate strength

$\varepsilon_{c,llp}$ = Compressive strain in extreme concrete fiber when farthest post-tensioning steel begins to yield in tension

$\varepsilon_{csc,i}$ = Concrete strain at i^{th}reinforcement bar(s) location

ε_{cc} = Expected strain in concrete at f'_{cc}

ε_{co} = Expected strain in concrete at f'_{c}

ε_{cu} = Ultimate compressive strain of confined concrete

$\varepsilon_{p,i}$ = Initial strain in i^{th} post-tensioning steel group

ε_{pu} = Ultimate strain of the post-tensioning steel

ε_{py} = Yield strain of the post-tensioning steel

$\varepsilon_{s,j}$ = Tensile strain in j^{th} longitudinal mild steel reinforcement bar(s)

ε_{su} = Ultimate strain of longitudinal mild steel reinforcement

ε_{sy} = Yield strain of longitudinal mild steel reinforcement

$\varepsilon'_{s,i}$ = Compressive strain in i^{th} longitudinal mild steel reinforcement bar(s)

θ_{ccc} = Rigid body rotation due to gap opening at the crushing of confined concrete

θ_{ell} = Rigid body rotation due to gap opening at the limit state of effective linear limit

θ_{ell-1} = Rigid body rotation due to gap opening at effective linear limit when neutral axis depth is 25% of l_w

θ_{ell-2} = Rigid body rotation due to gap opening at effective linear limit with non-linear behavior of unconfined concrete

θ_{ell-4} = Rigid body rotation due to gap opening at effective linear limit when farthest bonded longitudinal reinforcement bar(s) begin to yield in tension

θ_{fms} = Rigid body rotation due to gap opening when farthest longitudinal mild steel reinforcement bar(s) reaches its ultimate strength

θ_{llp} = Rigid body rotation due to gap opening when farthest post-tensioning steel begins to yield in tension

θ_{yms} = Rigid body rotation due to gap opening when farthest debonded longitudinal mild steel reinforcement bar(s) begin to yield in tension

Table 1.1: Properties of various types of walls

Reference	Reference	Concrete		Post-tensioning steel	Longitudinal web reinforcement		Longitudinal boundary reinforcement	
		Cast-in-place	Precast	Unbonded	Bonded	Debonded	Bonded	Debonded
Structural wall	ACI 318-11	√			√		√	
Unbonded post-tensioned precast concrete wall	Kurama et al. (1996), Kurama (1997), Perez (2004), Perez et al. (2007)		√	√				
Unbonded post-tensioned hybrid precast concrete wall	Holden et al. (2003), Restrepo and Rahman (2007), Smith and Kurama (2009), Smith et al. (2011)		√	√	√			
Unbonded post-tensioned cast-in-place concrete special structural wall	This report, Lehigh University (in progress)	√		√	√		√	
Unbonded post-tensioned cast-in-place concrete special structural wall	This report	√		√		√		√

12

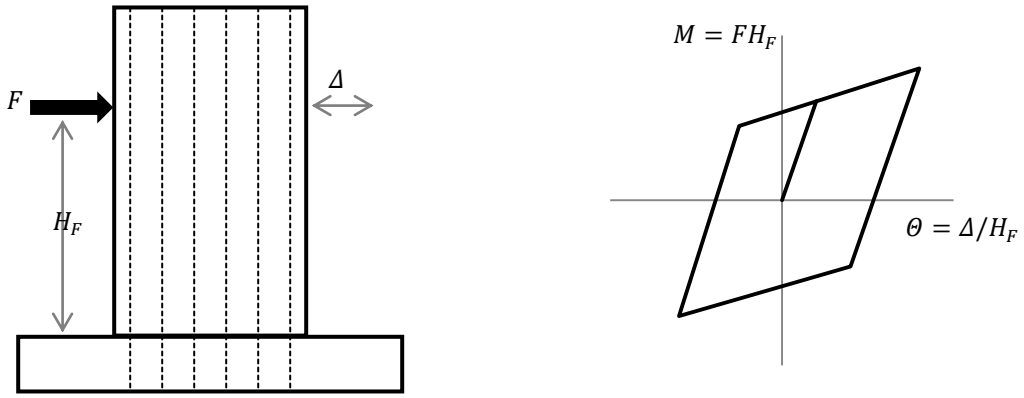

(a) ACI compliant cast-in-place wall and base moment-lateral drift curve

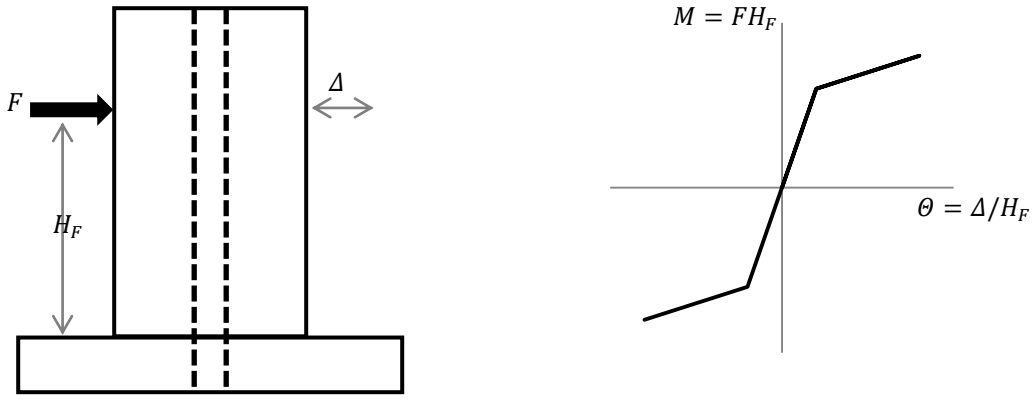

(b) Unbonded post-tensioned precast concrete wall and base moment-lateral drift curve

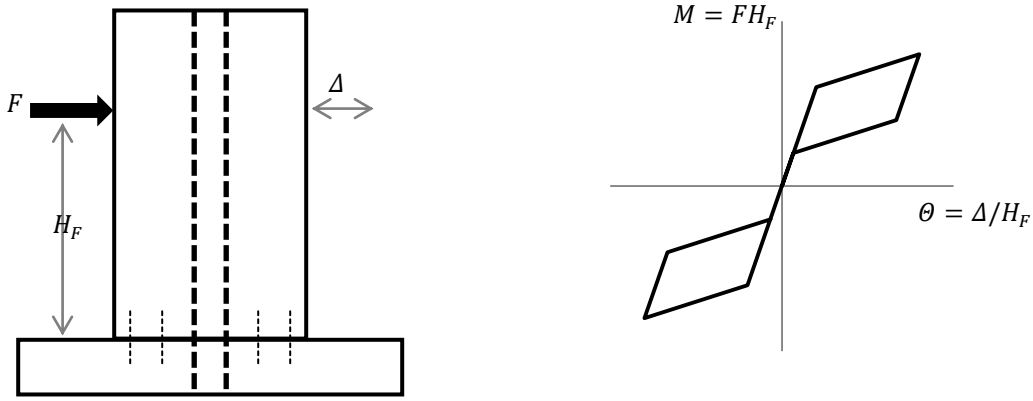

(c) Unbonded post-tensioned hybrid precast concrete wall and base moment-lateral drift curve

Figure 1.1: Base moment-lateral drift behavior of cast-in-place wall, unbonded post-tensioned precast wall and unbonded post-tensioned hybrid precast wall

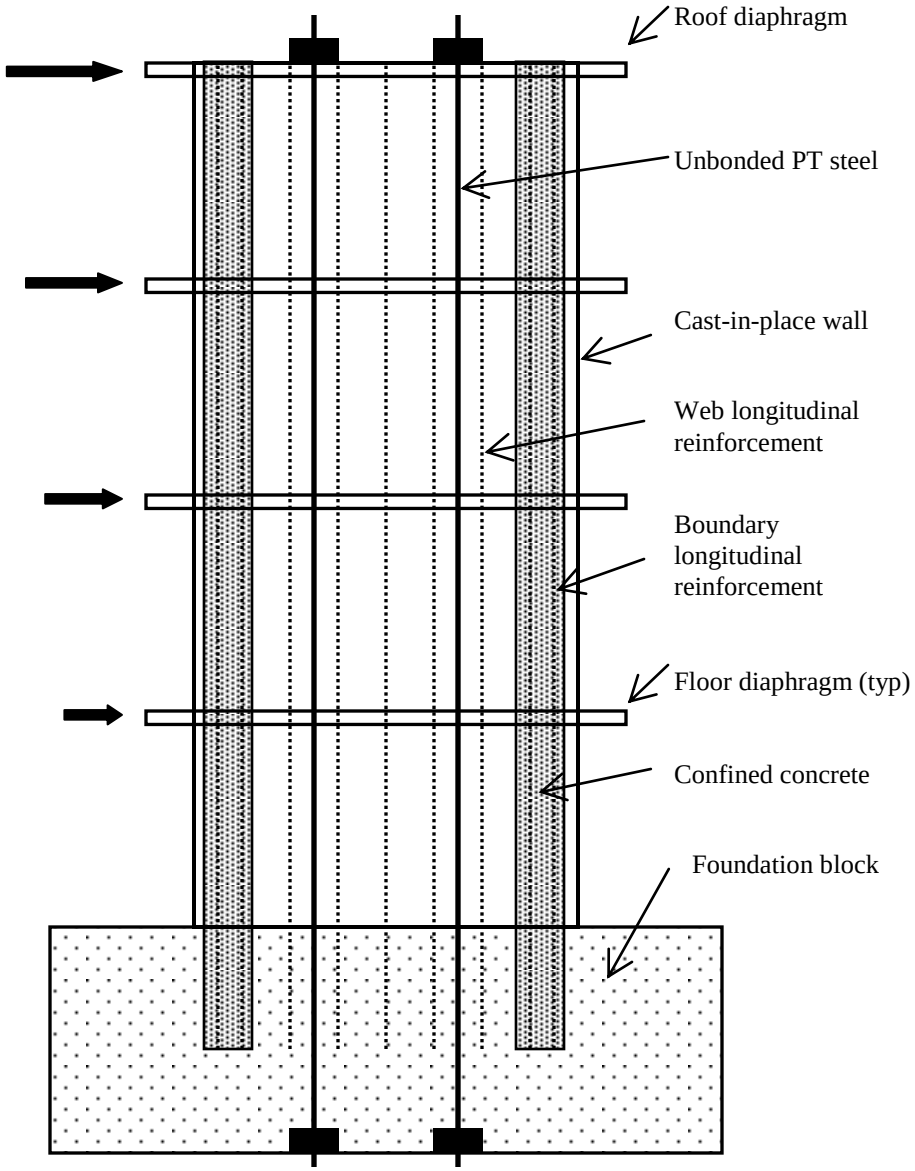

Figure 1.2: Elevation of an unbonded post-tensioned cast-in-place special structural wall with longitudinal mild steel reinforcement subjected to lateral load

CHAPTER 2

BACKGROUND

This chapter discusses background information which is relevant to the current study. Section 2.1 describes unbonded post-tensioned precast concrete walls. Section 2.2 reviews previous research on unbonded post-tensioned precast concrete walls without and with energy dissipating longitudinal mild steel reinforcement. Section 2.3 describes unbonded post-tensioned cast-in-place special structural walls with longitudinal mild steel reinforcement. Section 2.4 discusses wall parameters and forces considered in the derivation of closed-form expressions in Chapter 3.

2.1 UNBONDED POST-TENSIONED PRECAST CONCRETE WALLS

In an unbonded post-tensioned precast concrete wall, the post-tensioning steel is placed in ducts and stays ungrouted after prestressing. This eliminates strain compatibility between the post-tensioning steel and the surrounding concrete, unlike the bonded post-tensioned case. Since the post-tensioning steel is unbonded, it is assumed that the deformation in the post-tensioning steel is distributed uniformly over the entire unbonded length. Therefore, the unbonded post-tensioned precast concrete wall can achieve larger overall deformation before the post-tensioning steel reaches its yield strain (Kurama 1997).

2.2 PREVIOUS RESEARCH ON UNBONDED POST-TENSIONED PRECAST CONCRETE WALLS

Several analytical and experimental studies have been conducted on unbonded post-tensioned precast concrete walls with: (i) two or more panels stacked vertically and connected horizontally in the same plane, (ii) two or more panels connected by vertical joint connecters or coupling beams in the same plane, or (iii) two or more panels connected by vertical joint connecters or coupling beams in perpendicular planes.

The analytical and experimental investigation of the flexural behavior of unbonded post-tensioned precast concrete walls with horizontal joints under lateral loading was conducted at Lehigh University as presented in Kurama et al. (1996, 1997) and Perez (2004, 2007). These studies used the fiber beam column elements and truss bar elements of the DRAIN-2DX program (Prakash and Powell 1993) to model gap opening behavior of the walls. The analytical parametric study performed by Kurama et al. (1996) indicates that the base shear and roof drift depends on design and detailing parameters such as total post-tensioning force, unbonded length of the post-tensioning steel, eccentricity of the post-tensioning steel, initial stress in the prestress, amount of confinement reinforcement, axial force due to gravity, wall length, and wall thickness. The advantage of these walls over monolithic cast-in-place walls is the self-centering behavior with little damage at the toe of the wall and the only disadvantage is the small energy dissipation.

In order to increase the energy dissipation of unbonded post-tensioned walls, hybrid post-tensioned precast concrete walls that include energy dissipating longitudinal mild steel reinforcement but retain the self-centering behavior of the walls were studied by Restrepo and Rahman (2007), Smith and Kurama (2009) and Smith et al. (2011). The bonded mild steel, crossing the horizontal joint between the wall and the foundation, is designed to yield in tension and compression to provide energy dissipation. Smith et al. (2011)

studied the experimental lateral response of a 0.4-scale hybrid wall and an emulative precast concrete wall. The study concluded that the hybrid wall provided large energy dissipation and self-centering behavior compared to the emulative wall. Also, the hybrid wall had a smaller residual gap at the base, smaller horizontal slip, smaller strength and stiffness degradation compared to the emulative wall.

2.3 UNBONDED POST-TENSIONED CAST-IN-PLACE SPECIAL STRUCTURAL WALLS WITH LONGITUDINAL MILD STEEL REINFORCEMENT

Figure 2.1 shows an unbonded post-tensioned cast-in-place special structural wall with longitudinal mild steel reinforcement. Figure 2.2 is an example of detailing of the wall with distributed longitudinal mild steel reinforcement and PT steel configuration. The wall is cast-in-place monolithically with the foundation block. The post-tensioning (PT) steel is placed in a duct and unbonded over the whole length of the PT steel to improve lateral load response of the PT steel as discussed earlier. Figure 2.1 and 2.2 show two groups of PT steel groups. For the purposes of the current study, a PT steel group is defined as one or more PT bars, tendons or strands. The longitudinal mild steel reinforcement is extended far enough into the foundation block to develop yield strength of the reinforcement. The mild steel reinforcement can be bonded to the surrounding concrete or debonded over a certain height at the base of the wall. At the boundaries of the wall heavy transverse reinforcement is provided to confine the concrete.

2.4 WALL PARAMETERS

Figure 2.3 shows the vertical forces acting on a wall. As shown in Figure 2.1 length of the wall along the base is denoted as l_w, the vertical elevation is denoted as H_w, and the thickness is denoted as t_w. Lateral forces are assumed to act at the floor and roof diaphragm levels.

The gravity force, N, acting on the wall consists of gravity forces acting on the wall at all diaphragm levels and self-weight of the wall. The resultant post-tensioning forces from the PT steel groups are $T_{p1,i}$ and $T_{p2,i}$, after elastic shortening of the wall due to prestressing. The resultant post-tensioning forces act at an eccentricity, e_p, on either side of the wall centerline. $T_{s,i}$ is the tensile force acting on the i^{th}mild steel reinforcement bar in tension and $C_{s,j}$ is the compressive force acting on the j^{th} mild steel reinforcement bar in compression. The resultant compression force from the compression in the concrete, acting at the toe of the wall, is C_c. The total downward force on the wall, T, is sum of the gravity load, resultant post-tensioning forces, tensile forces in the distributed reinforcement bars. The total upward force, C, on the wall is sum of the resultant compressive force in concrete and compressive forces in the distributed reinforcement bars.

Experimental stress-strain data for mild steel reinforcement bars and PT steel indicate that when steel is strained beyond the yield strain, an increase in stress is required beyond the yielding point stress to produce plastic deformation. This increase in stress with strain beyond yield stress is termed strain-hardening. These strain hardening effects are also considered in the present research while determining forces in the longitudinal mild steel reinforcement and PT steel.

The base moment, M, is defined as the moment acting at the base of the wall due to lateral loads acting on the wall. These lateral loads also cause the wall to displace in the plane of the wall with maximum displacement at the roof diaphragm level which is denoted as the roof displacement. Roof displacement as a percentage of the wall height is called roof drift. The above parameters are used in Chapter 3 to present a derivation of closed-form expressions for calculating moment at the base and drift for a wall with single equivalent lateral force acting towards the right, i.e., the wall is displaced to the right. The closed-form expressions derived in Chapter 3 are applied to the walls discussed in Chapter 4 and the results are compared with the results obtained from DRAIN-2DX analytical models in Chapter 5. In Chapter 6, a comparative analysis of the effects of different parameters on the base moment and roof drift is conducted. Chapter 7 summarizes the results and findings of the present study.

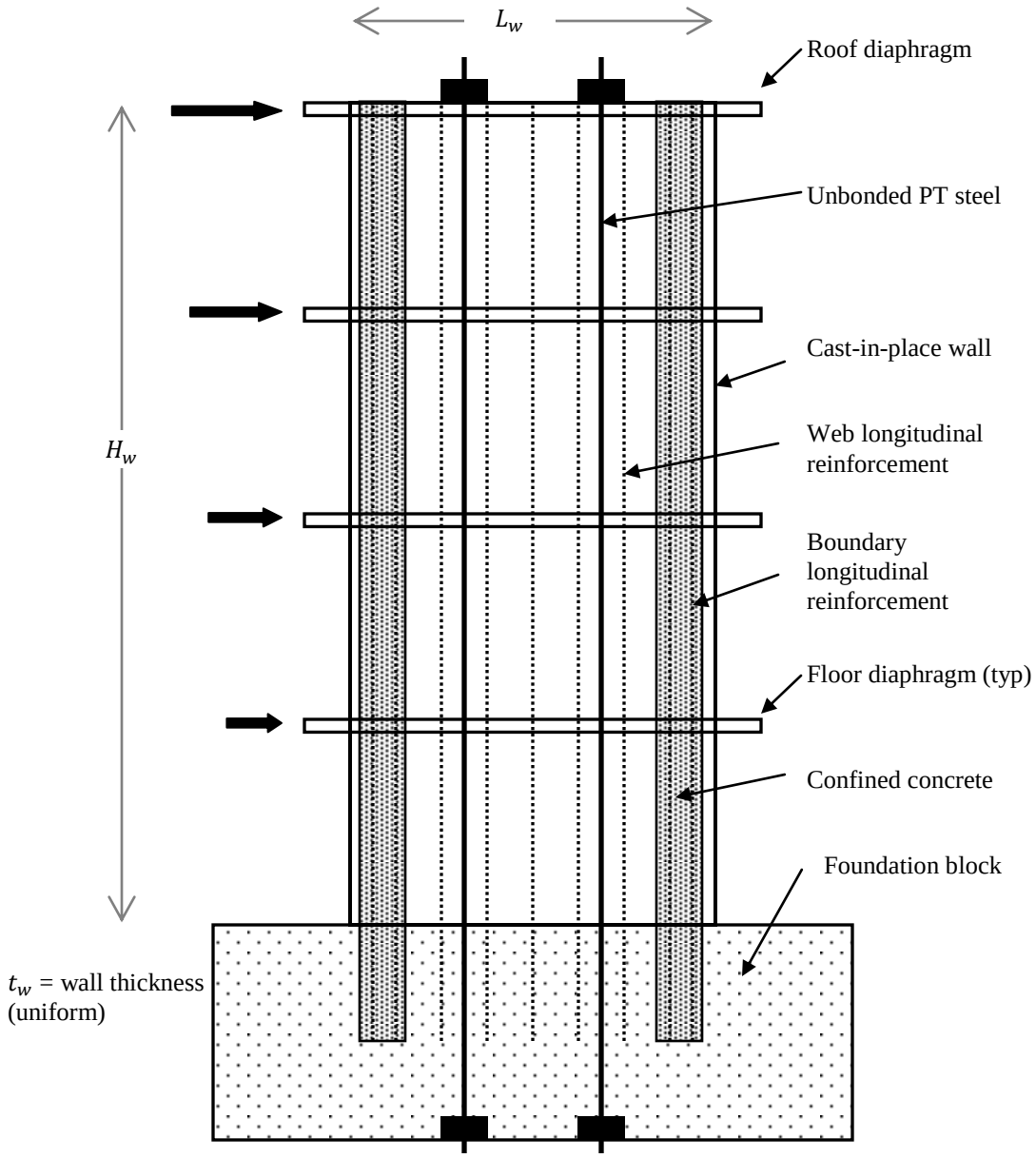

Figure 2.1: Elevation of an unbonded post-tensioned cast-in-place wall with longitudinal reinforcement and applied lateral load

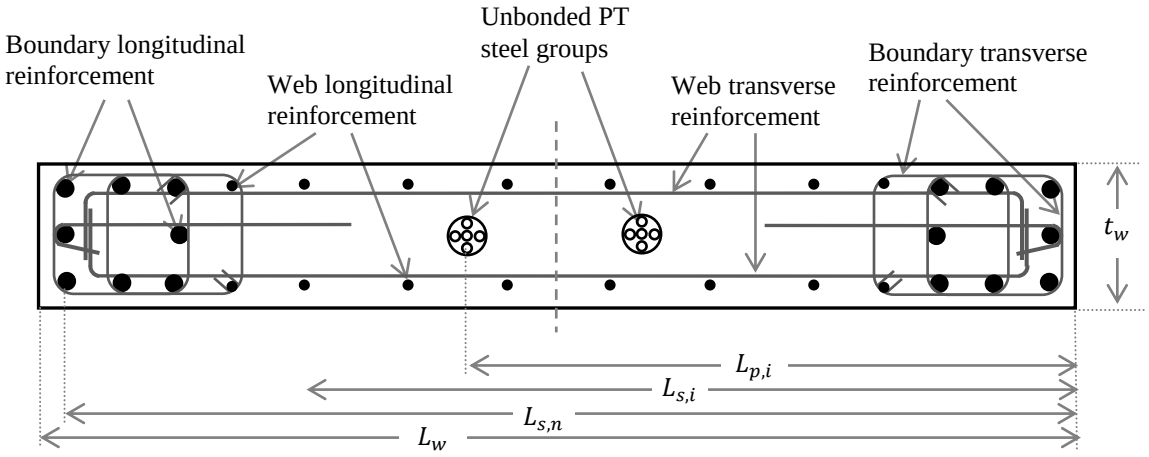

Figure 2.2: Section detailing of unbonded post-tensioned cast-in-place wall with longitudinal mild steel reinforcement and PT steel

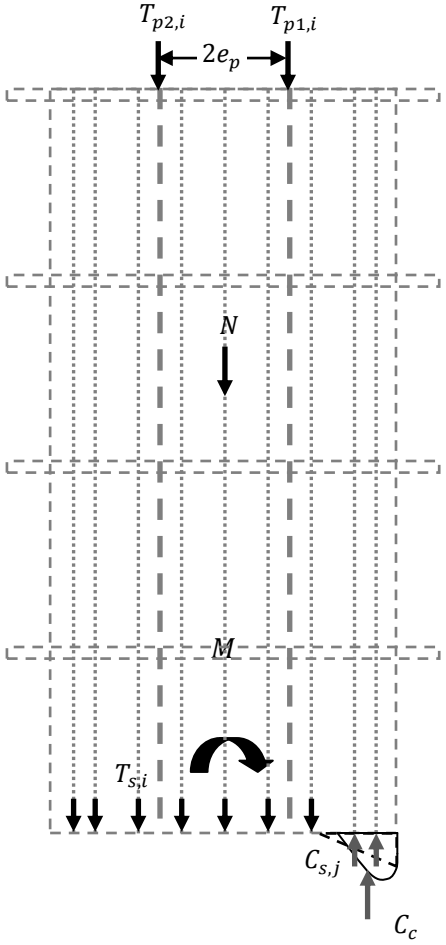

Figure 2.3: Forces acting on the wall

CHAPTER 3

DERIVATION OF CLOSED FORM EXPRESSIONS FOR STRUCTURAL LIMIT STATES OF UNBONDED POST-TENSIONED CAST-IN-PLACE SPECIAL STRUCTURAL WALLS WITH LONGITUDINAL MILD STEEL REINFORCEMENT

This chapter discusses the derivation of a set of closed-form expressions for structural limit states of an unbonded post-tensioned cast-in-place concrete wall with energy dissipating longitudinal mild steel reinforcement. Section 3.1 provides an overview of the key structural limit states used to describe the expected response of the wall subject lateral load. Section 3.2 discusses the basis for deriving the closed-form expressions for base moment and roof drift associated with each of the structural limit states described in Section 3.1 for a wall with unbonded PT steel and bonded longitudinal mild steel reinforcement. Section 3.3 discusses the basis for deriving the closed-form expressions for base moment and roof drift associated with each of the structural limit states described in Section 3.1 for a wall with unbonded PT steel and debonded longitudinal mild steel reinforcement.

3.1 KEY STRUCTURAL LIMIT STATES ASSOCIATED WITH IDEALIZED RESPONSE OF THE WALL SUBJECT TO LATERAL LOAD

Figure 3.1a is a schematic of the equivalent lateral loads acting at floor and roof diaphragm levels of a cast-in-place wall with debonded PT steel and longitudinal reinforcement. Figure 3.1b shows an example of detailing of the wall with distributed reinforcement and PT steel configuration. This section describes the idealized structural limit states considered in the current study, described in terms of the base moment and roof drift response of an unbonded post-tensioned cast-in-place concrete wall with longitudinal reinforcement for energy dissipation. It is assumed that the wall undergoes in-plane deformation only.

3.1.1 Wall Structural Limit States

A wall structural limit state is defined as the state of the wall beyond which the wall does not fulfill all the relevant criteria and assumptions associated with that state of the wall. These wall structural limit states may be based on strains, deformations, stresses, forces, or extent of damage to the wall.

Figure 3.2 shows the base moment-roof drift relationship with idealized structural limit states (based on Kurama (1997) and Perez (2004)) for a hybrid wall with longitudinal reinforcement under monotonic lateral load.

3.1.1.1 <u>Decompression (DEC)</u>

Decompression, denoted as DEC henceforth, is the limit state at which overturning moment at the base of the wall due to lateral load leads to zero strain at one edge of the wall. The base moment, roof displacement and roof drift associated with DEC are represented as M_{dec}, Δ_{dec} and θ_{dec}, respectively. DEC is followed by cracking and gap opening initiation at the base of the wall.

3.1.1.2 Effective linear limit (ELL)

Effective linear limit, represented as ELL, is the limit state up till which the base moment and roof drift response of the wall remains essentially linear elastic. After this limit state, significant reduction in stiffness of the wall, or softening, occurs due to increasing gap opening at the base of the wall. The base moment, roof displacement and roof drift corresponding to ELL are denoted as M_{ell}, Δ_{ell} and Θ_{ell}, respectively.

3.1.1.3 Yielding of longitudinal mild steel reinforcement (YMS)

Yielding of longitudinal mild steel reinforcement, YMS, is the limit state at which the strain in the farthest longitudinal reinforcement bar(s) on the tension side reaches the yield strain. The base moment, roof displacement and roof drift associated with yielding of this longitudinal reinforcement are denoted as M_{yms}, Δ_{yms} and Θ_{yms}, respectively. Depending upon the distribution and strength of PT steel and longitudinal reinforcement, and initial prestress in the PT steel, this limit state may be followed by fracture of longitudinal reinforcement or the linear limit (yielding) of the post-tensioning steel.

3.1.1.4 Fracture of longitudinal mild steel reinforcement (FMS)

Fracture of longitudinal mild steel reinforcement, FMS, is the limit state at which the farthest longitudinal reinforcement on tension side reaches the strain at its ultimate strength. According to the experimental stress-strain relationship of mild steel, strain-hardening, an increase in stress, is observed for strain beyond yield strain. The strain-hardening effects of mild steel are also considered in this limit state. The base moment, roof displacement and roof drift associated with fracture of longitudinal reinforcement are denoted as M_{fms}, Δ_{fms} and Θ_{fms}, respectively. Depending upon the distribution and strength of PT steel and longitudinal reinforcement, and initial prestress in PT steel, this limit state may be followed by the linear limit of the post-tensioning steel or crushing of the confined concrete.

3.1.1.5 Linear limit of post-tensioning steel (LLP)

Linear limit of post-tensioning steel, denoted as LLP, occurs when strain in the farthest group of PT bars, tendons or strands, henceforth referred to as a PT group, on the tension side reaches the yield strain. The base moment, roof displacement and roof drift associated with LLP are denoted as M_{llp}, Δ_{llp} and Θ_{llp}, respectively.

3.1.1.6 Crushing of confined concrete (CCC)

Crushing of confined concrete or CCC is the limit state at which the confined concrete at the toe of the wall fails in compression. In this study, this limit state is reached when strain in extreme concrete fiber reaches ε_{cu} which is the ultimate concrete compressive strain obtained from the Mander model for confined concrete (Mander et al. 1988a, 1988b). The base moment, roof displacement and roof drift associated with crushing of the confined concrete are denoted as M_{ccc}, Δ_{ccc} and Θ_{ccc} respectively. In an under-reinforced concrete wall, failure of the wall occurs when confined concrete at the base of the wall fails in compression after significant yielding of longitudinal reinforcement in tension.

In the current study, two sets of closed-form expressions are derived for unbonded post-tensioned cast-in-place concrete wall with longitudinal reinforcement. In the first case,

closed-form expressions for estimating the base moment and roof drift values for cast-in-place concrete walls with bonded longitudinal reinforcement are derived and in the second case, closed-form expressions for estimating the base moment and roof drift values for cast-in-place concrete wall with debonded longitudinal reinforcement are derived. The post-tensioning steel is unbonded in both cases.

3.2 CLOSED-FORM EXPRESSIONS FOR ESTIMATING BASE MOMENT AND ROOF DRIFT VALUES OF WALL WITH BONDED LONGITUDINAL REINFORCEMENT

This section derives the closed-form expressions to estimate the base moment and roof drift values corresponding to the limit states described in Section 3.1 for a wall with bonded longitudinal reinforcement. These expressions are derived for a cast-in-place concrete wall with a symmetric arrangement of two groups of debonded PT steel which may have different initial prestressing force, a symmetric arrangement of n groups of distributed bonded longitudinal reinforcement, a concentric gravity (axial) load and a single concentrated lateral load at the roof level as shown in Figure 3.3. These expressions can be extended to a wall with lateral load acting at more than one point, eccentric or varying gravity load, more or less than two groups of PT steel with different eccentricities and initial prestressing force, and unsymmetrical distribution of bonded longitudinal reinforcement. Any contribution of concrete in tension is neglected for calculating moment at the base.

3.2.1 Decompression (DEC)

Figure 3.4 shows the strains, stresses, resultant forces and moment acting at the base of the wall at the decompression limit state. The moment at the base of the wall at this limit state is M_{dec}, the base moment at decompression. At M_{dec}, it is assumed that the elongation of PT steel = due to the applied lateral load is small with respect to the unbonded height and can be neglected; therefore, the forces in the PT steel groups are the initial prestressing forces $T_{p1,i}$ and $T_{p2,i}$ (after losses). As the longitudinal reinforcement is completely bonded, it is assumed that strain compatibility between concrete and longitudinal reinforcement is maintained. It is also assumed that the stresses developed in the concrete are small so the concrete remains linear elastic. Hence net uncracked elastic section properties can be used.

The estimated base moment obtained by summing moment about the right edge is:

$$M_{dec} = N\frac{l_w}{2} + T_{p1,i}l_{p,1} + T_{p2,i}l_{p,2} - \frac{1}{2}f_{c,dec}l_w t_w \frac{l_w}{3} - \sum_i (n-1)f_{csc,i}A_{s,i}l_{s,i} \quad (3.1)$$

The compressive stress in the mild steel reinforcement can be calculated in terms of the compressive stress in concrete ($f_{c,dec}$), modular ratio (n) for mild steel reinforcement bar(s) and concrete, area of the reinforcement bars ($A_{s,i}$) and location of the reinforcement bars ($l_{s,i}$). Concrete compression stresses at longitudinal reinforcement locations, $f_{csc,i}$, and force, C_c, are:

$$f_{csc,i} = \frac{l_w - l_{s,i}}{l_w} f_{c,dec} \quad (3.2)$$

$$C_c = \frac{1}{2}f_{c,dec}l_w t_w - \sum_i f_{csc,i}A_{s,i} \quad (3.3)$$

Longitudinal reinforcement compression stresses, $f'_{s,i}$, and forces, $C_{s,i}$, are:

$$f'_{s,i} = nf_{csc,i} \tag{3.4}$$

$$C_{s,i} = f'_{s,i}A_{s,i} \tag{3.5}$$

Resultant upward force, C_{dec}, is:

$$C_{dec} = \frac{1}{2}f_{c,dec}l_w t_w + \sum_i (n-1)f_{csc,i}A_{s,i} \tag{3.6}$$

Resultant downward force, T_{dec}, is:

$$T_{dec} = T_{p1,i} + T_{p2,i} + N \tag{3.7}$$

The compressive stress in concrete, $f_{c,dec}$, is calculated by equating the upward and downward forces. This in turn can be used to determine forces in the reinforcement bars and the moment at the base of the wall.

Resultant shear force at the base, V_{dec}, is:

$$V_{dec} = \frac{M_{dec}}{H_w} \tag{3.8}$$

The roof drift at decompression is estimated by elastic analysis of the wall as cantilever beam subject to a point lateral load acting at the roof level, treating the base as fixed and using net section properties, Young's modulus (E_c) of concrete, shear modulus of concrete (G_c), moment of inertia (I_w) of gross-cross-section area the wall and area of gross-cross-section area (A'_w) of the wall. This gives rise to two deflection components; roof deflection in flexure due to the applied lateral load and roof deflection due to elastic shear deformation.

Elastic flexural deflection, $\Delta_{F,dec}$, is:

$$\Delta_{F,dec} = \frac{1}{2E_c I_w} V_{dec} \frac{2H_w^3}{3} \tag{3.9}$$

Elastic shear deflection, $\Delta_{S,dec}$, is:

$$\Delta_{S,dec} = \frac{1}{G_c A'_w} V_{dec} H_w \tag{3.10}$$

Total roof deflection, Δ_{dec}, is:

$$\Delta_{dec} = \Delta_{F,dec} + \Delta_{S,dec} \tag{3.11}$$

The roof drift at the decompression, Θ_{dec}, is calculated as:

$$\Theta_{dec} = \frac{\Delta_{dec}}{H_w} \tag{3.12}$$

3.2.2 Effective Linear Limit (ELL)

In a wall with bonded longitudinal reinforcement, a significant reduction in the lateral stiffness of the wall may occur due to one of the three possible events: (i) significant gap opening at the base of the wall, (ii) initiation of nonlinear behavior of unconfined

concrete, or (iii) initiation of yielding in longitudinal mild steel reinforcement. Figures 3.5, 3.6 and 3.7 show the strains, stresses, resultant forces and moment acting at the base of the wall due to gap opening, nonlinear behavior of unconfined concrete, and yielding of longitudinal mild steel reinforcement, respectively. As noted by Perez (2004)the base moment at the effective linear limit due to significant gap opening can be taken as equal to 2.5 times the base moment at DEC (as shown by El-Sheikh et al. (1997) and Kurama et al. (1997)). This is treated as a fourth possible value of effective linear limit and denoted as ELL-3 in the current study. The moment, M_{ell}, at the base of the wall at effective linear limit is defined as the minimum of the four values: M_{ell-1} at significant gap opening at the base of the wall, M_{ell-2} at initiation of nonlinear behavior of unconfined concrete, M_{ell-3} equal to 2.5 times of base moment at DEC, and M_{ell-4} at initiation of yielding of farthest longitudinal reinforcement on tension side.

The first alternative value of ELL corresponds to significant gap opening at the horizontal joint at the base of the wall Kurama et al. (1996) found that the reduction in lateral stiffness of the wall due to gap opening becomes apparent when about 25% of the cross-section is under compression. The strain distribution, stress distribution and resultant forces in concrete, PT steel and bonded longitudinal reinforcement at this limit state are as shown in Figure 3.5. In order to determine M_{ell-1}(moment at the base of the wall at significant gap opening) it is assumed that the elongation of PT steel due to the applied lateral load is small with respect to the debonded height of the PT steel and can be neglected; therefore, the forces in the PT steel groups remain at the initial values. As the longitudinal reinforcement is completely bonded, strain compatibility between concrete and longitudinal reinforcement is assumed. It is also assumed that the stresses developed in concrete are small and hence net section properties can be used. Further, it is assumed that plane sections remain plane for concrete and reinforcing steel.

The base moment is obtained by summing moment about the right edge :

$$M_{ell-1} = N\frac{l_w}{2} + T_{p1,i}l_{p,1} + T_{p2,i}l_{p,2} + \sum_j f_{s,j}A_{s,j}l_{s,j} - \frac{1}{2}f_{c,ell-1}\frac{l_w}{4}t_w\frac{l_w}{12} - \sum_i (n-1)f_{csc,i}A_{s,i}l_{s,i} \quad (3.13)$$

If $f_{c,ell-1}$ is the compressive stress in concrete at ELL-1, concrete compression stresses at longitudinal reinforcement locations, $f_{csc,i}$, and compressive force in concrete, C_c, are:

$$f_{csc,i} = \frac{\frac{l_w}{4} - l_{s,i}}{\frac{l_w}{4}} f_{c,ell-1} \quad (3.14)$$

$$C_c = \frac{1}{2}f_{c,ell-1}\frac{l_w}{4}t_w - \sum_i f_{csc,i}A_{s,i} \quad (3.15)$$

The longitudinal reinforcement compression stresses, $f'_{s,i}$, and forces, $C_{s,i}$, can be obtained in terms of the compressive stress in concrete ($f_{c,ell-1}$), modular ratio (n) for mild steel and concrete, area of the reinforcement bars ($A_{s,i}$) and location of the reinforcement bars ($l_{s,i}$):

$$f'_{s,i} = nf_{csc,i} \quad (3.16)$$

$$C_{s,i} = f'_{s,i}A_{s,i} \quad (3.17)$$

Resultant upward force C_{ell-1} is:

$$C_{ell-1} = \frac{1}{2} f_{c,ell-1} \frac{l_w}{4} t_w + \sum_i (n-1) f_{csc,i} A_{s,i} \quad (3.18)$$

Similar to the longitudinal mild steel in compression, tensile stresses, $f_{s,j}$, and forces, $T_{s,j}$, in longitudinal reinforcement are:

$$f_{s,j} = n \frac{l_{s,j} - \frac{l_w}{4}}{\frac{l_w}{4}} f_{c,ell-1} \quad (3.19)$$

$$T_{s,j} = f_{s,j} A_{s,j} \quad (3.20)$$

Resultant downward force, T_{ell-1} is:

$$T_{ell-1} = T_{p1,i} + T_{p2,i} + N + \sum_j T_{s,j} \quad (3.21)$$

The compressive stress in concrete, $f_{c,ell-1}$, at significant gap opening is calculated by equating the resultant upward and downward forces which is then used to calculate forces in the longitudinal mild steel reinforcement and moment at the base of the wall.

The second alternative value of ELL corresponds to initiation of nonlinear behavior of concrete in compression. Perez (2004) treated the concrete at the base of the wall as unconfined to account for the nonlinear behavior of concrete, and the same approach is used in the current work. The stress distribution and resultant forces in concrete, PT steel and bonded longitudinal reinforcement at this limit state are as shown in Figure 3.6. To calculate M_{ell-2} (i.e. the moment at the base of the wall at initiation of nonlinear behavior of unconfined concrete) elongation of PT steel due to the applied lateral load is assumed to be small and is neglected; therefore, the forces in the PT steel groups remain at the initial values. Strain in longitudinal reinforcement is calculated using strain compatibility with respect to the neutral axis depth and ultimate strain, ε_u, of unconfined concrete at the farthest concrete fiber in compression. It is assumed that no spalling takes place and hence net section properties can be used. It is also assumed that the plane sections remain plane for concrete and reinforcing steel. Also, impact of transverse reinforcement in the confinement region on concrete properties is ignored.

The estimated base moment obtained by summing moment about the right edge is:

$$M_{ell-2} = N \frac{l_w}{2} + T_{p1,i} l_{p,1} + T_{p2,i} l_{p,2} + \sum_j f_{s,j} A_{s,j} l_{s,j} - C_c \frac{a_{ell-2}}{2} - \sum_i C_{s,i} l_{s,i} \quad (3.22)$$

The length of equivalent compression stress block, a_{ell-2}, and compression force, C_c, is:

$$a_{ell-2} = \beta_1 c_{ell-2} \quad (3.23)$$

$$C_c = 0.85 a_{ell-2} t_w f_c' \quad (3.24)$$

where, β_1 is the length reduction factor, and 0.85 is the strength reduction factor for unconfined concrete (ACI 318-11).

Longitudinal reinforcement compression strains, $\varepsilon_{s,i}'$, and forces, $C_{s,i}$, with respect to expected strain at f_c' are:

$$\varepsilon_{s,i}' = \frac{c_{ell-2} - l_{s,i}}{c_{ell-2}} \varepsilon_{co} \quad (3.25)$$

$$C_{s,i} = f'_{s,i} A_{s,i} \quad (3.26)$$

where, $f'_{s,i}$ = stress in longitudinal reinforcement corresponding to $\varepsilon'_{s,i}$ strain

Resultant upward force, C_{ell-2}, is:

$$C_{ell-2} = C_c + \sum_i C_{s,i} \quad (3.27)$$

Longitudinal reinforcement tensile strains, $\varepsilon_{s,j}$, and forces, $T_{s,j}$, are:

$$\varepsilon_{s,j} = \frac{l_{s,j} - c_{ell-2}}{c_{ell-2}} \varepsilon_{co} E_s \quad (3.28)$$

$$T_{s,j} = f_{s,j} A_{s,j} \quad (3.29)$$

where, $f_{s,j}$ = stress in longitudinal reinforcement corresponding to $\varepsilon_{s,j}$ strain

Resultant downward force, T_{ell-2}, is:

$$T_{ell-2} = T_{p1,i} + T_{p2,i} + N + \sum_j T_{s,j} \quad (3.30)$$

The neutral axis depth, c_{ell-2} , is calculated by iteratively equating the upward and downward forces. Forces in longitudinal reinforcement can be calculated using equations 3.26 and 3.29, and the moment at the base can be estimated from equation 3.22.

The third alternative value of base momentELL-3, corresponding to decompression base moment, can be calculated as:

$$M_{ell-3} = 2.5 M_{dec} \quad (3.31)$$

The fourth alternative value of ELL corresponds to the initiation of yielding of farthest longitudinal reinforcement on tension side. The strain distribution, stress distribution and resultant forces in concrete, PT steel and bonded longitudinal reinforcement at this limit state are as shown in Figure 3.7. In order to determine M_{ell-4}, moment at the base of the wall due to initiation if yielding of longitudinal reinforcement, elongation of PT steel groups due to the applied lateral load is assumed to be small and is neglected; therefore, the forces in the PT steel groups remain at the initial values. As the longitudinal reinforcement is completely bonded, therefore, strain compatibility between concrete and longitudinal reinforcement is assumed. It is assumed that the stresses developed in concrete are small and hence uncracked net section properties can be used. It is also assumed that the plane sections remain plane for concrete and reinforcing steel. Also, impact of transverse reinforcement in the confinement region on concrete properties is ignored.

The estimated base moment obtained by summing moment about the right edge is:

$$M_{ell-4} = N \frac{l_w}{2} + T_1 l_{p,1} + T_2 l_{p,2} + \sum_j f_{s,j} A_{s,j} l_{s,j} - \frac{1}{2} f_{c,ell-4} c_{ell-4} t_w \frac{c_{ell-4}}{3} - \sum_i (n-1) f_{csc,i} A_{s,i} l_{s,i} \quad (3.32)$$

Yielding strain, ε_{sy}, of longitudinal reinforcement and the distance of farthest longitudinal reinforcement, $l_{s,m}$, are used to determine c_{ell-4}, neutral axis depth by iteratively equating the resultant upward and downward forces as given below.

Concrete compression stress, $f_{c,ell-4}$, stress at mild steel reinforcement locations in compression, $f_{csc,i}$, and compressive force in concrete, C_c, are:

$$f_{c,ell-4} = \frac{c_{ell-4}}{l_{s,m}} \varepsilon_{sy} E_c \tag{3.33}$$

$$f_{csc,i} = \frac{c_{ell-4} - l_{s,i}}{c_{ell-4}} f_{c,ell-4} \tag{3.34}$$

$$C_c = \frac{1}{2} f_{c,ell-4} c_{ell-4} t_w - \sum_i f_{csc,i} A_{s,i} \tag{3.35}$$

Longitudinal reinforcement compression stresses, $f'_{s,i}$, and forces, $C_{s,i}$, are:

$$f'_{s,i} = \frac{c_{ell-4} - l_{s,i}}{l_{s,n} - c_{ell-4}} f_{sy} \tag{3.36}$$

$$C_{s,i} = f'_{s,i} A_{s,i} \tag{3.37}$$

Resultant upward force, C_{ell-4}, is:

$$C_{ell-4} = C_c + \sum_i C_{s,i} \tag{3.38}$$

Longitudinal reinforcement tensile stresses, $f_{s,j}$, and forces, $T_{s,j}$, are:

$$f_{s,j} = \frac{l_{s,j} - c_{ell-4}}{l_{s,m} - c_{ell-4}} f_{sy} \tag{3.39}$$

$$T_{s,j} = f_{s,j} A_{s,j} \tag{3.40}$$

Resultant downward force, T_{ell-4}, is:

$$T_{ell-4} = T_{p1,i} + T_{p2,i} + N + \sum_j T_{s,j} \tag{3.41}$$

Minimum of the four alternative base moment values at the limit state of ELL is selected as the base moment at ELL. Therefore, Moment, M_{ell}, and base shear, V_{ell}, at the limit state of effective linear limit are:

$$M_{ell} = \min\{M_{ell-1}, M_{ell-2}, M_{ell-3}, M_{ell-4}\} \tag{3.42}$$

$$V_{ell} = \frac{M_{ell}}{H_w} \tag{3.43}$$

The roof drift at effective linear limit is estimated using a combination of elastic deflection and rigid body rotation at the base of the wall. To determine the elastic deflection, an elastic analysis of the wall as cantilever beam subject to a point lateral load acting at the roof level is used. The base is treated as fixed and net section properties are used. Therefore, the roof deflection at the effective linear limit is sum of roof deflection in flexure and roof deflection due to elastic shear deformation.

Elastic flexural deflection, $\Delta_{F,ell}$, is:

$$\Delta_{F,ell} = \frac{1}{2E_c I_w} V_{ell} \frac{2H_w^3}{3} \tag{3.44}$$

Elastic shear deflection, $\Delta_{S,ell}$, is:

$$\Delta_{S,ell} = \frac{1}{G_c A'_w} V_{ell} H_w \tag{3.45}$$

The added rigid body rotation, θ_{ell}, caused by deformation in concrete is calculated with respect to the plastic hinge length, H_{ph}, for the wall for the governing case of ELL. Plastic hinge length is defined as the minimum of twice of the neutral axis depth and twice of the wall thickness.

For ELL-1 with 25% of the cross-section in compression:

$$\Delta_{conc,ell-1} = \varepsilon_{c,ell-1} H_{ph} \tag{3.46}$$

$$H_{ph} = \min\{{}^{l_w}/_{2}, 2t_w\} \tag{3.47}$$

$$\theta_{ell-1} = \frac{\Delta_{conc,ell-1}}{{}^{l_w}/_{4}} \tag{3.48}$$

For ELL-2 with non-linear behavior of concrete in compression:

$$\Delta_{conc,ell-2} = \varepsilon_{co} H_{ph} \tag{3.49}$$

$$H_{ph} = \min\{2c_{ell-2}, 2t_w\} \tag{3.50}$$

$$\theta_{ell-2} = \frac{\Delta_{conc,ell-2}}{c_{ell-2}} \tag{3.51}$$

For ELL-4 with yielding of mild steel in tension:

$$\Delta_{conc,ell-4} = \varepsilon_{c,ell-4} H_{ph} \tag{3.52}$$

$$H_{ph} = \min\{2c_{ell-4}, 2t_w\} \tag{3.53}$$

$$\theta_{ell-4} = \frac{\Delta_{conc,ell-4}}{c_{ell-4}} \tag{3.54}$$

θ_{ell} = rigid body rotation corresponding to the governing ELL from eq. 3.42

The deflection at the roof due to rigid body rotation, $\Delta_{go,ell}$, is:

$$\Delta_{go,ell} = \theta_{ell} H_w \tag{3.55}$$

Total roof deflection, Δ_{ell}, is:

$$\Delta_{ell} = \Delta_{F,ell} + \Delta_{S,ell} + \Delta_{go,ell} \tag{3.56}$$

The roof drift at the limit state of effective linear limit is:

$$\Theta_{ell} = \frac{\Delta_{ell}}{H_w} \tag{3.57}$$

3.2.3 Fracture of Longitudinal Mild Steel Reinforcement (FMS)

Figure 3.8 shows the stresses, resultant forces and moment acting at the base of the wall at the limit state of fracture of longitudinal reinforcement, taken as when the farthest longitudinal reinforcement reaches its ultimate strain capacity ε_{su}. The moment at the base of the wall at this limit state is M_{fms}, the base moment at fracture of farthest longitudinal reinforcement in tension. As the longitudinal reinforcement is assumed to be perfectly bonded, strain compatibility between concrete and longitudinal reinforcement is assumed. The strains and stresses in remaining longitudinal reinforcement are determined with respect to the ultimate strain in the farthest longitudinal reinforcement including

effects of strain-hardening. Elongation of the PT steel is calculated using compatibility with the deformation of the concrete with a height of the wall denoted as the plastic hinge height (H_{ph}). Other assumptions for this limit state include plane sections remain plane in concrete and bonded longitudinal reinforcement, concrete cover is spalled and confined concrete properties with equivalent compression stress block are used. The equivalent stress block parameters a, strength reduction factor, and β, length reduction factor, are estimated for confined concrete using results in Park and Paulay (1975).

The estimated base moment obtained by summing moment about the right edge is:

$$M_{fms} = N\frac{l'_w}{2} + T_{p,1}l'_{p,1} + T_{p,2}l'_{p,2} + \sum_j T_{s,j}l'_{s,j} - \alpha a_{fms}t''_w f'_{cc}\frac{a_{fms}}{2} - \sum_i C_{s,i}l'_{s,i} \quad (3.58)$$

The length of the equivalent concrete stress block, a_{fms}, compressive strain, $\varepsilon_{c,fms}$, deformation $\Delta_{c,fms}$, and compression force C_c are:

$$a_{fms} = \beta c_{fms} \quad (3.59)$$

$$\varepsilon_{c,fms} = \frac{c_{fms}}{l'_{s,n} - c_{fms}}\varepsilon_{su} \quad (3.60)$$

$$\Delta_{conc,fms} = \varepsilon_{c,fms}H_{ph} \quad (3.61)$$

$$H_{ph} = \min\{2c_{fms}, 2t''_w\} \quad (3.62)$$

$$C_c = \alpha f'_{cc}a_{fms}t''_w \quad (3.63)$$

Longitudinal reinforcement compression strains, $\varepsilon_{csc,i}$, stresses, $f'_{s,i}$, and forces $C_{s,i}$, are calculated using strain compatibility with respect to the ultimate strain in the farthest longitudinal reinforcement:

$$\varepsilon_{csc,i} = \frac{c_{fms} - l'_{si}}{c_{fms}}\varepsilon_{su} \quad (3.64)$$

$$C_{s,i} = f'_{s,i}A_{s,i} \quad (3.65)$$

where, $f'_{s,i}$ = stress in longitudinal reinforcement corresponding to $\varepsilon_{csc,i}$ strain

Resultant upward force, C_{fms}, is:

$$C_{fms} = C_c + \sum_i C_{s,i} \quad (3.66)$$

Longitudinal reinforcement tensile strains $\varepsilon_{s,j}$, stresses, $f_{s,j}$, and forces, $T_{s,j}$, are calculated using strain compatibility with respect to the ultimate strain in the farthest longitudinal reinforcement:

$$\varepsilon_{s,j} = \frac{l'_{s,j} - c_{fms}}{l'_{s,n} - c_{fms}}\varepsilon_{su} \quad (3.67)$$

$$T_{s,j} = f_{s,j}A_{s,j} \quad (3.68)$$

where, $f_{s,j}$ = stress in longitudinal reinforcement corresponding to $\varepsilon_{s,j}$ strain

PT steel group elongation, $\Delta_{p,i}$, strain, $\varepsilon_{p,i}$, stress, $f_{p,i}$, and force, $T_{p,i}$, are:

$$\Delta_{p,i} = \frac{l'_{p,i} - c_{fms}}{l'_{s,n} - c_{fms}}\Delta_{conc,fms} \quad (3.69)$$

$$\varepsilon_{p,i} = \frac{\Delta_{p,i}}{H_{pt,unb}} \tag{3.70}$$

$$T_{p,i} = f_{p,i} A_{p,i} \tag{3.71}$$

where, $f_{p,i}$ = stress PT stress corresponding to $\left(\varepsilon_{p,i} + \frac{f_{pi}}{E_p}\right)$ strain

Resultant downward force, T_{fms}, is:

$$T_{fms} = T_{p,1} + T_{p,2} + N + \sum_j T_{s,j} \tag{3.72}$$

The neutral axis depth at FMS, c_{fms}, is calculated by iteratively using force equilibrium for the resultant downward and upward forces. The neutral axis depth is then be used to determine forces in concrete, PT steel and longitudinal reinforcement, and moment at the base of the wall.

Resultant shear force, V_{fms}, at the base is:

$$V_{fms} = \frac{M_{fms}}{H_w} \tag{3.73}$$

The roof drift at the fracture of longitudinal reinforcement is determined by adding roof deflection from the rigid body rotation due to gap opening at the base of the wall and the roof deflection from the elastic deflection of the wall.

Elastic flexural deflection, $\Delta_{F,fms}$, is:

$$\Delta_{F,fms} = \frac{1}{2E_c I_w} V_{fms} \frac{2H_w^3}{3} \tag{3.74}$$

Elastic shear deflection, $\Delta_{S,fms}$, is:

$$\Delta_{S,fms} = \frac{1}{G_c A'_w} V_{fms} H_w \tag{3.75}$$

Rigid body rotation, θ_{fms}, and deflection due to gap opening, $\Delta_{go,fms}$, is:

$$\Delta_{p,2} = \frac{(f_{P,2} - f_{Pi}) H_{pt,unb}}{E_P} \tag{3.76}$$

$$\theta_{fms} = \frac{\Delta_{p,2}}{l'_{p,2} - c_{fms}} \tag{3.77}$$

$$\Delta_{go,fms} = \theta_{fms} H_w \tag{3.78}$$

Total roof deflection, Δ_{fms}, is:

$$\Delta_{fms} = \Delta_{F,fms} + \Delta_{S,fms} + \Delta_{go,fms} \tag{3.79}$$

The roof drift, Θ_{fms}, at the fracture of longitudinal reinforcement is calculated as:

$$\Theta_{fms} = \frac{\Delta_{fms}}{H_w} \tag{3.80}$$

Depending on the distribution and relative strengths of longitudinal reinforcement and PT steel, and initial prestressing of the PT steel; the fracture of longitudinal reinforcement limit state may occur after the linear limit of post-tensioning limit state has occurred.

3.2.4 Linear Limit of Post-Tensioning Steel (LLP)

Figure 3.9 shows the stresses, resultant forces and moment acting at the base of the wall at the limit state of linear limit of post-tensioning steel. The moment at the base of the wall at this limit state is M_{llp}, the base moment at initiation of yielding of farthest PT steel group. Strains, stresses, and forces in the remaining PT groups are obtained using strain and deformation compatibility with respect to the yielded PT group. Deformation compatibility with respect to plastic hinge height (H_{ph}) of concrete in compression and yielded PT steel group is used to determine strain in concrete which in turn is used to obtain strains and stresses in the bonded longitudinal reinforcement. Other assumptions for this limit state include plane sections remain plane for concrete and bonded longitudinal reinforcement, concrete cover is spalled and equivalent stress block for confined concrete with strength reduction factor a and length reduction factor β, are used.

The estimated base moment obtained by summing moment about the right edge is:

$$M_{llp} = N\frac{l'_w}{2} + T_{p,1}l'_{p,1} + T_{p,y}l'_{p,2} + \sum_j T_{s,j}l'_{s,j} - \alpha a_{llp}t''_w f'_{cc}\frac{a_{llp}}{2} - \sum_i C_{s,i}l'_{s,i} \quad (3.81)$$

PT groups elongation, $\Delta_{p,i}$, strain $\varepsilon_{p,i}$, stress, $f_{p,i}$, and force, $T_{p,i}$ is calculated in terms of the yield strain, ε_{py}, and unbonded length, $H_{pt,unb}$, of PT steel:

$$\Delta_{p,i} = \left(\varepsilon_{py} - \frac{f_{p,i}}{E_p}\right) H_{pt,unb}\frac{l'_{p,i} - c_{llp}}{l'_{p,2} - c_{llp}} \quad (3.82)$$

$$T_{p,i} = f_{p,i}A_{p,i} \quad (3.83)$$

where, $f_{p,i}$ = PT stress corresponding to $\left(\varepsilon_{p,i} + \frac{f_{pi}}{E_p}\right)$ strain

Concrete length of equivalent stress block length,a_{llp}, compressive strain, $\varepsilon_{c,llp}$, and compression force, C_c, are:

$$a_{llp} = \beta c_{llp} \quad (3.84)$$

$$\varepsilon_{c,llp} = \left(\frac{c_{llp}}{l'_{p,2} - c_{llp}}\right)\left(\frac{\Delta_{p,2}}{H_{ph}}\right) \quad (3.85)$$

$$H_{ph} = \min\{2c_{llp}, 2t''_w\} \quad (3.86)$$

$$C_c = \alpha f'_{cc} a_{fms} t''_w \quad (3.87)$$

Longitudinal reinforcement compression strains, $\varepsilon_{csc,i}$, stresses, $f'_{s,i}$, and forces, $C_{s,i}$, are calculated using $\varepsilon_{c,llp}$, the strain in concrete:

$$\varepsilon_{csc,i} = \frac{c_{llp} - l_{si}}{c_{llp}}\varepsilon_{c,llp} \quad (3.88)$$

$$C_{s,i} = f'_{s,i}A_{s,i} \quad (3.89)$$

where, $f'_{s,i}$ = stress in longitudinal reinforcement corresponding to $\varepsilon_{csc,i}$ strain

Resultant upward force, C_{llp}, is:

$$C_{llp} = C_c + \sum_i C_{s,i} \tag{3.90}$$

Similarly, longitudinal reinforcement tensile strains, $\varepsilon_{s,j}$, stresses, $f_{s,j}$, and forces, $T_{s,j}$, are:

$$\varepsilon_{s,j} = \frac{l_{s,j} - c_{llp}}{c_{llp}} \varepsilon_{c,llp} \tag{3.91}$$

$$T_{s,j} = f_{s,j} A_{s,j} \tag{3.92}$$

where, $f_{s,j}$ = stress in longitudinal reinforcement corresponding to $\varepsilon_{s,j}$ strain

Resultant downward force, T_{llp}, is:

$$T_{llp} = T_{p,1} + T_{p,2} + N + \sum_j T_{s,j} \tag{3.93}$$

Using the vertical force equilibrium, neutral axis depth (c_{llp}) and strain in concrete can be calculated. As forces in the linear elastic PT steel group and the longitudinal mild steel reinforcement are dependent on the neutral axis depth, an iterative approach is required to solve for c_{llp}. The neutral axis depth is then used to calculate forces in the PT steel and mild steel, and base moment.

Resultant shear force, V_{llp}, at the base is:

$$V_{llp} = \frac{M_{llp}}{H_w} \tag{3.94}$$

As in Perez (2004), the roof drift at the linear limit of post-tensioning steel is determined by adding elastic flexural and shear deflection of the wall, and roof deflection from rigid body rotation due to gap opening at the base of the wall.

Elastic flexural deformation, $\Delta_{F,llp}$, is:

$$\Delta_{F,llp} = \frac{1}{2E_c I_w} V_{llp} \frac{2H_w^3}{3} \tag{3.95}$$

Elastic shear deformation, $\Delta_{S,llp}$, is:

$$\Delta_{S,llp} = \frac{1}{G_c A'_w} V_{llp} H_w \tag{3.96}$$

Rigid body rotation, θ_{llp}, deformation, $\Delta_{go,llp}$, due to gap opening can be calculated in terms of the elongation of the PT steel and its distance from the neutral axis:

$$\theta_{llp} = \frac{\Delta_{p2,llp}}{l'_{p2} - c_{llp}} \tag{3.97}$$

$$\Delta_{go,llp} = \theta_{llp} H_w \tag{3.98}$$

Total roof deflection, Δ_{llp}, is:

$$\Delta_{llp} = \Delta_{F,llp} + \Delta_{S,llp} + \Delta_{go,llp} \tag{3.99}$$

The roof drift, Θ_{llp}, at the linear limit of post-tensioning is calculated as:

$$\Theta_{llp} = \frac{\Delta_{llp}}{H_w} \tag{3.100}$$

3.2.5 Crushing of Confined Concrete (CCC)

Figure 3.10 shows the stresses, resultant forces and moment acting at the base of the wall at the limit state of crushing of confined concrete. The moment at the base of the wall at this limit state is M_{ccc}, the base moment at crushing of confined concrete. It is assumed that the concrete cover is spalled and cracked section properties are used for all calculations. It is also assumed that the extreme confined concrete fiber in compression is at its ultimate strain capacity ε_{cu}. Therefore, equivalent stress block parameters for confined concrete, α and β, as earlier in case of LLP, are used. Also, strain compatibility between concrete and bonded longitudinal reinforcement is used to obtain forces in the longitudinal reinforcement. Similarly, deformation compatibility with respect to critical confined concrete crushing height (H_{cr}) is used to determine elongation, strain and stress in the PT groups. It is also assumed that at this limit state plane sections remain plane for concrete and bonded longitudinal reinforcement.

The estimated base moment obtained by summing moment about the right edge is:

$$M_{ccc} = N\frac{l'_w}{2} + T_{p,1}l'_{p,1} + T_{p,2}l'_{p,2} + \sum_j T_{s,j}l'_{s,j} - \alpha a_{ccc}t''_w f'_{cc}\frac{a_{ccc}}{2} - \sum_i C_{s,i}l'_{s,i} \quad (3.101)$$

Concrete length of equivalent stress block, a_{ccc}, deformation $\Delta_{conc,ccc}$ corresponding to ultimate strain ε_{cu}, and compressive force, C_c, are calculated with respect to H_{cr}:

$$a_{ccc} = \beta c_{ccc} \quad (3.102)$$

$$\Delta_{conc,ccc} = \varepsilon_{cu}H_{cr} \quad (3.103)$$

$$H_{cr} = \min\{2t''_w, 2a_{ccc}\} \quad (3.104)$$

$$C_c = \alpha a_{ccc}t''_w f'_{cc} \quad (3.105)$$

Longitudinal reinforcement compression strains, $\varepsilon_{csc,i}$, stresses, $f'_{s,i}$, and forces, $C_{s,i}$, are:

$$\varepsilon_{csc,i} = \frac{c_{ccc} - l_{si}}{c_{ccc}}\varepsilon_{cu} \quad (3.106)$$

$$C_{s,i} = f'_{s,i}A_{s,i} \quad (3.107)$$

where, $f'_{s,i}$ = stress in reinforcement corresponding to $\varepsilon_{csc,i}$ strain

Resultant upward force, C_{ccc}, is:

$$C_{ccc} = C_c + \sum_i C_{s,i} \quad (3.108)$$

PT Groups elongation $\Delta_{p,i}$, strains $\varepsilon_{p,i}$, stresses $f_{p,i}$, and forces , $T_{p,i}$, in PT groups, obtained from the deformation in concrete, are:

$$\Delta_{p,i} = \frac{l'_{p,i} - c_{ccc}}{l'_{s,n} - c_{ccc}}\Delta_{conc,ccc} \quad (3.109)$$

$$\varepsilon_{p,i} = \frac{\Delta_{p,i}}{H_{pt,unb}} + \frac{f_{p,i}}{E_p} \quad (3.110)$$

$$T_{p,i} = f_{p,i}A_{p,i} \quad (3.111)$$

where, $f_{p,i}$ = PT stress corresponding to $\varepsilon_{p,i}$ strain

Longitudinal reinforcement tensile strains, $\varepsilon_{s,j}$, stresses, $f_{s,j}$, and forces, $T_{s,j}$, are:

$$\varepsilon_{s,j} = \frac{l_{s,j} - c_{ccc}}{c_{ccc}} \varepsilon_{cu} \quad (3.112)$$

$$T_{s,j} = f_{s,j} A_{s,j} \quad (3.113)$$

where, $f_{s,j}$ = stress in longitudinal reinforcement corresponding to $\varepsilon_{s,j}$ strain

Resultant downward force, T_{ccc}, is:

$$T_{ccc} = T_{p,1} + T_{p,2} + N + \sum_j f_{s,j} A_{s,j} \quad (3.114)$$

The unknown neutral axis depth, c_{ccc} , is calculated iteratively by equating the downward and upward forces(T_{ccc} and C_{ccc}).

Resultant shear force, V_{ccc}, at the base is:

$$V_{ccc} = \frac{M_{ccc}}{H_w} \quad (3.115)$$

Similar to LLP, roof drift at the crushing of confined concrete is also a sum of elastic flexural and shear deflection of the wall, and roof deflection from rigid body rotation due to gap opening at the base of the wall.

Elastic flexural deflection, $\Delta_{F,ccc}$, is:

$$\Delta_{F,ccc} = \frac{1}{2E_c I_w} V_{ccc} \frac{2H_w^3}{3} \quad (3.116)$$

Elastic shear deflection, $\Delta_{S,ccc}$, is:

$$\Delta_{S,ccc} = \frac{1}{G_c A'_w} V_{ccc} H_w \quad (3.117)$$

Rigid body rotation, θ_{ccc}, and deflection, $\Delta_{go,ccc}$, due to gap opening are calculated in terms of elongation op the farthest PT steel group:

$$\Delta_{p2} = \frac{(f_{P,2} - f_{Pi}) H_{pt,unb}}{E_P} \quad (3.118)$$

$$\theta_{ccc} = \frac{\Delta_{p,2}}{l'_{p2} - c'} \quad (3.119)$$

$$\Delta_{go,ccc} = \theta_{ccc} H_w \quad (3.120)$$

Total roof deflection, Δ_{ccc}, is:

$$\Delta_{ccc} = \Delta_{F,ccc} + \Delta_{S,ccc} + \Delta_{go,ccc} \quad (3.121)$$

The roof drift, Θ_{ccc}, at the linear limit of post-tensioning is calculated as:

$$\Theta_{ccc} = \frac{\Delta_{ccc}}{H_w} \quad (3.122)$$

3.3 CLOSED-FORM EXPRESSIONS FOR ESTIMATING BASE MOMENT AND ROOF DRIFT VALUES FOR WALL WITH DEBONDED LONGITUDINAL MILD STEEL REINFORCEMENT

This section derives the closed-form expressions to estimate base moment and roof drift values corresponding to the limit states described in Section 3.1 for a wall with debonded longitudinal reinforcement. The expressions derived below are for a post-tensioned cast-

in-place concrete wall with a symmetric arrangement of two groups of PT steel which may have different initial prestressing force, a symmetric arrangement of n groups of distributed longitudinal mild steel reinforcement debonded over a predetermined height at the base of the wall, a concentric gravity (axial) load and a single concentrated lateral load at the roof level as shown in Figure 3.11. These closed-form expressions can be extended to a general case wall with more than one story, eccentric or varying gravity load, more or less than two groups of PT steel with variable eccentricity and initial prestress, and unsymmetrical distribution of longitudinal reinforcement. For the closed-form expressions derived in this section, $H_{ms,unb}$, denotes the debonded height of the longitudinal mild steel reinforcement. It is assumed that all the longitudinal reinforcement bar(s) in a given wall have the same debonded height.

3.3.1 Decompression (DEC)

As for the bonded longitudinal reinforcement case, Figure 3.4 shows the strains, stresses, resultant forces and moment acting at the base of the wall at the decompression limit state for debonded longitudinal reinforcement. It is assumed that the debonded height is large compared to shortening in length at the limit state of decompression. Hence, longitudinal reinforcement is treated as bonded reinforcement for this limit state. Therefore, the same closed-form expressions of bonded reinforcement are applicable for the debonded reinforcement case as well.

The estimated base moment obtained by summing moment about the right edge is:

$$M_{dec} = N\frac{l_w}{2} + T_{p1,i}l_{p,1} + T_{p2,i}l_{p,2} - \frac{1}{2}f_{c,dec}l_w t_w \frac{l_w}{3} - \sum_i (n-1)f_{csc,i}A_{s,i}l_{s,i} \quad (3.123)$$

Concrete compression stresses, $f_{csc,i}$, and forces, C_c, are:

$$f_{csc,i} = \frac{l_w - l_{s,i}}{l_w} f_{c,dec} \quad (3.124)$$

$$C_c = \frac{1}{2}f_{c,dec}l_w t_w - \sum_i f_{csc,i}A_{s,i} \quad (3.125)$$

Longitudinal reinforcement compression stresses, $f'_{s,i}$, and forces, $C_{s,i}$, are:

$$f'_{s,i} = nf_{csc,i} \quad (3.126)$$

$$C_{s,i} = f'_{s,i}A_{s,i} \quad (3.127)$$

Resultant upward force, C_{dec}, is:

$$C_{dec} = \frac{1}{2}f_{c,dec}l_w t_w + \sum_i (n-1)f_{csc,i}A_{s,i} \quad (3.128)$$

Resultant downward force, T_{dec}, is:

$$T_{dec} = T_{p1,i} + T_{p2,i} + N \quad (3.129)$$

The compressive stress in concrete, $f_{c,dec}$, is calculated by equating the upward and downward forces. This in turn can be used to determine forces in the reinforcement bars and the moment at the base of the wall.

Resultant shear force, V_{dec}, at the base is:

$$V_{dec} = \frac{M_{dec}}{H_w} \quad (3.130)$$

The roof drift at decompression is estimated by elastic analysis of the wall as cantilever beam subject to a point lateral load acting at the roof level, same as for the bonded longitudinal reinforcement.

Elastic flexural deflection, $\Delta_{F,dec}$, is:

$$\Delta_{F,dec} = \frac{1}{2E_c I_w} V_{dec} \frac{2H_w^3}{3} \tag{3.131}$$

Elastic shear deflection, $\Delta_{S,dec}$, is:

$$\Delta_{S,dec} = \frac{1}{G_c A'_w} V_{dec} H_w \tag{3.132}$$

Total roof deflection, Δ_{dec}, is:

$$\Delta_{dec} = \Delta_{F,dec} + \Delta_{S,dec} \tag{3.133}$$

The roof drift, Θ_{dec}, at the decompression state is calculated as:

$$\Theta_{dec} = \frac{\Delta_{dec}}{H_w} \tag{3.134}$$

3.3.2 Effective Linear Limit (ELL)

As in the previous case, a significant reduction in the lateral stiffness of the wall with debonded longitudinal reinforcement may occur due to significant gap opening at the base of the wall (ELL-1) or initiation of nonlinear behavior of concrete (ELL-2). Figures 3.5 and 3.6 show the strains, stresses, resultant forces and moment acting at the bases of the wall due to gap opening and nonlinear behavior of concrete. As in the bonded longitudinal mild steel reinforcement case, a third possible value of effective linear limit and denoted as ELL-3 when moment at the base of the wall is 2.5 times the base moment at DEC (El-Sheikh et al. 1997, Kurama et al. 1997 and Perez 2004) is also included. The moment at the base of the wall, M_{ell}, at effective linear limit is defined as the minimum of the three values: M_{ell-1} at significant gap opening at the base of the wall, M_{ell-2} at initiation of nonlinear behavior of concrete, and M_{ell-3} equal to 2.5 times of base moment at DEC.

Estimation of value of M_{ell-1} corresponding to significant gap opening at the base of the wall with 25% of the cross-section under compression is based on the following assumptions: plane sections remain plane for both concrete and longitudinal reinforcement, elongation of PT at this limit state is assumed to be small and therefore the forces in the PT steel groups remain at the initial values , contribution of concrete in tension is neglected, contribution of confinement reinforcement on the compression side is neglected, all material remains linear elastic; therefore uncracked elastic section properties are used, and elongation of debonded longitudinal reinforcement is obtained by assuming deformation compatibility of longitudinal reinforcement with respect to plastic hinge height (H_{ph}) of concrete in compression. Figure 3.5 shows the strains, stresses and resultant forces in concrete, debonded longitudinal reinforcement and unbonded post-tensioning steel at the base of the wall.

The estimated base moment obtained by summing moment about the right edge is:

$$M_{ell-1} = N\frac{l_w}{2} + T_{p1i}l_{p,1} + T_{p2i}l_{p,2} + \sum_j f_{s,j}A_{s,j}l_{s,j} - \frac{1}{2}f_{c,ell-1}\frac{l_w}{4}t_w\frac{l_w}{12} - \sum_i f'_{s,i}A_{s,i}l_{s,i}$$

(3.135)

Concrete deformation, $\Delta_{conc,ell-1}$, and force, C_c, in terms of strain in concrete $\varepsilon_{c,ell-1}$ are:

$$\Delta_{conc,ell-1} = \varepsilon_{c,ell-1} H_{ph} \tag{3.136}$$

$$H_{ph} = \min\{{}^{l_w}/_{2}, 2t_w\} \tag{3.137}$$

$$C_c = \frac{1}{2} f_{c,ell-1} \frac{l_w}{4} t_w \tag{3.138}$$

Longitudinal reinforcement compressive deformation, $\Delta'_{si,ell-1}$, strain, , $\varepsilon'_{si,ell-1}$, stress, $f'_{s,i}$, and forces, $C_{s,i}$, are:

$$\Delta'_{si,ell-1} = \frac{\frac{l_w}{4} - l_{s,i}}{\frac{l_w}{4}} \Delta_{conc,ell-1} \tag{3.139}$$

$$\varepsilon'_{si,ell-1} = \frac{\Delta'_{si,ell-1}}{H_{ms,unb}} \tag{3.140}$$

$$C_{s,i} = f'_{s,i} A_{s,i} \tag{3.141}$$

where, $f'_{s,i}$ = stress in reinforcement corresponding to $\varepsilon'_{si,ell-1}$ strain

Resultant upward force, C_{ell-1}, is:

$$C_{ell-1} = C_c + \sum_i C_{s,i} \tag{3.142}$$

Longitudinal reinforcement tensile deformation, $\Delta_{si,ell-1}$, strain, $\varepsilon_{si,ell-1}$, stresses, $f_{s,j}$, and forces, $T_{s,j}$, are:

$$\Delta_{sj,ell-1} = \frac{l_{sj} - \frac{l_w}{4}}{\frac{l_w}{4}} \Delta_{conc,ell-1} \tag{3.143}$$

$$\varepsilon_{sj,ell-1} = \frac{\Delta_{sj,ell-1}}{H_{ms,unb}} \tag{3.144}$$

$$T_{s,j} = f_{s,j} A_{s,j} \tag{3.145}$$

where, $f_{s,j}$ = stress in reinforcement corresponding to $\varepsilon_{sj,ell-1}$ strain

Resultant downward force, T_{ell-1}, is:

$$T_{ell-1} = T_{p1,i} + T_{p2,i} + N + \sum_j T_{s,j} \tag{3.146}$$

The compressive stress in concrete, $f_{c,ell-1}$, at significant gap opening is calculated by equating the resultant upward and downward forces and used to moment at the base of the wall.

The second alternative value of ELL corresponds to initiation of nonlinear behavior of unconfined concrete in compression. The primary assumption for estimation of M_{ell-2}, moment at the base of the wall due to initiation of nonlinear behavior of concrete, is that the concrete at the base of the wall is unconfined and the compressive strain is ε_{cu}. Figure 3.6 shows the forces acting at the base of the wall under nonlinear behavior of concrete.

Also, it is assumed that elongation of PT at this limit state is very small and is neglected; therefore, the forces in the PT steel groups remain at the initial values. Other assumptions for deriving the closed form expressions for this limit state are: plane sections remain plane for concrete and longitudinal reinforcement, contribution of concrete in tension is neglected, all material remain linear elastic; therefore uncracked elastic section properties are used, elongation of debonded longitudinal reinforcement is obtained by assuming deformation compatibility of longitudinal reinforcement on tension side with respect to plastic hinge height (H_{ph}) of concrete in compression, and strains in the longitudinal reinforcement on the compression side is obtained using strain compatibility between the longitudinal reinforcements.

The estimated base moment obtained by summing moment about the right edge is:

$$M_{ell-2} = N\frac{l_w}{2} + T_{p1,i}l_{p,1} + T_{p2,i}l_{p,2} + \sum_j f_{s,j}A_{s,j}l_{s,j} - 0.85a_{ell-2}t_w f_c' \frac{a_{ell-2}}{2} - \sum_i f_{s,i}' A_{s,i} l_{s,i} \quad (3.147)$$

The length of equivalent compression stress block, a_{ell-2}, compressive strain, $\varepsilon_{c,ell-2}$, deformation , $\Delta_{c,ell-2}$,and compressive force, C_c, are:

$$a_{ell-2} = \beta_1 c_{ell-2} \quad (3.148)$$

where, $\beta_1 =$ is the length reduction factor for unconfined concrete (ACI 318-11)

$$\varepsilon_{conc,ell-2} = \varepsilon_{cu} \quad (3.149)$$

$$\Delta_{c,ell-2} = \varepsilon_{conc,ell-2} H_{ph} \quad (3.150)$$

$$C_c = 0.85 a_{ell-2} t_w f_c' \quad (3.151)$$

Longitudinal reinforcement compressive deformation, $\Delta_{si,ell-2}'$, strain, $\varepsilon_{si,ell-2}'$, stresses, $f_{s,i}'$, and forces, $C_{s,i}$, are:

$$\Delta_{si,ell-2}' = \frac{c_{ell-2} - l_{si}}{c_{ell-2}} \Delta_{conc,ell-2} \quad (3.152)$$

$$\varepsilon_{si,ell-2}' = \frac{\Delta_{si,ell-2}'}{H_{ms,unb}} \quad (3.153)$$

$$C_{s,i} = f_{s,i}' A_{s,i} \quad (3.154)$$

where, $f_{s,i}' =$ stress in longitudinal reinforcement corresponding to $\varepsilon_{si,ell-2}'$ strain

Resultant upward force, C_{ell-2}, is:

$$C_{ell-2} = C_c + \sum_i C_{s,i} \quad (3.155)$$

Longitudinal reinforcement tensile deformation, $\Delta_{si,ell-2}$, strain, $\varepsilon_{si,ell-2}$, stress, $f_{s,j}$, and force, $T_{s,j}$, are:

$$\Delta_{sj,ell-2} = \frac{l_{s,j} - c_{ell-2}}{c_{ell-2}} \Delta_{conc,ell-2} \quad (3.156)$$

$$\varepsilon_{sj,ell-2} = \frac{\Delta_{sj,ell-2}}{H_{ms,unb}} \quad (3.157)$$

$$T_{s,j} = f_{s,j} A_{s,j} \quad (3.158)$$

where, $f_{s,j}$ = stress in longitudinal reinforcement corresponding to $\varepsilon_{sj,ell-2}$ strain

Resultant downward force, T_{ell-2}, is:

$$T_{ell-2} = T_{p1,i} + T_{p2,i} + N + \sum_j T_{s,j} \quad (3.159)$$

The neutral axis depth, c_{ell-2} , is calculated by applying equilibrium on the vertical forces which is then used to determine moment at the base of the wall.

The third alternative value of base momentELL-4 is equal to 2.5 times decompression base moment:

$$M_{ell-3} = 2.5M_{dec} \quad (3.160)$$

Minimum of the three alternative base moment values at the limit state of ELL is selected as the base moment at ELL. Therefore, Moment, M_{ell}, and base shear, V_{ell}, at the limit state of effective linear limit are:

$$M_{ell} = \min\{M_{ell-1}, M_{ell-2}, M_{ell-3}\} \quad (3.161)$$

$$V_{ell} = \frac{M_{ell}}{H_w} \quad (3.162)$$

The roof drift at effective linear limit for a wall with debonded longitudinal reinforcement is a combination of elastic deflection and rigid body rotation at the base of the wall as in the bonded reinforcement case.

Elastic flexural deflection, $\Delta_{F,ell}$, is:

$$\Delta_{F,ell} = \frac{1}{2E_c I_w} V_{ell} \frac{2H_w^3}{3} \quad (3.163)$$

Elastic shear deflection, $\Delta_{S,ell}$, is:

$$\Delta_{S,ell} = \frac{1}{G_c A'_w} V_{ell} H_w \quad (3.164)$$

The added rigid body rotation, θ_{ell}, caused by deformation in concrete is calculated with respect to the plastic hinge length, H_{ph}, for the wall for the governing case of ELL. Rigid body rotation, θ_{ell}, and deflection due to gap opening, $\Delta_{go,ell}$, is:

For ELL-1 with 25% of the cross-section in compression:

$$\theta_{ell-1} = \frac{\Delta_{conc,ell-1}}{l_w/_4} \quad (3.165)$$

For ELL-2 with non-linear behavior of concrete in compression:

$$\theta_{ell-2} = \frac{\Delta_{conc,ell-2}}{c_{ell-2}} \quad (3.166)$$

θ_{ell} = rigid body rotation corresponding to the governing ELL from eq. 3.160

$$\Delta_{go,ell} = \theta_{ell} H_w \quad (3.167)$$

Total roof deflection, Δ_{ell}, is:

$$\Delta_{ell} = \Delta_{F,ell} + \Delta_{S,ell} + \Delta_{go,ell} \quad (3.168)$$

The roof drift, Θ_{ell}, at the limit state of effective linear limit is:

$$\Theta_{ell} = \frac{\Delta_{ell}}{H_w} \tag{3.169}$$

3.3.3 Yielding of Longitudinal Mild Steel Reinforcement (YMS)

Depending upon the distribution of longitudinal reinforcement, distribution of PT steel, relative strengths of longitudinal reinforcement and PT steel, initial prestress in the PT steel, debonded length of longitudinal reinforcement and unbonded length of PT steel, the limit state following effective linear limit may be initiation of yielding in farthest longitudinal reinforcement or linear limit (yielding) of post-tensioning steel. Assuming initiation of yielding in longitudinal reinforcement precedes linear limit of post-tensioning steel, Figure 3.7 shows the strain distribution, stress distribution and resultant forces in concrete, PT steel and debonded longitudinal reinforcement at this limit state. It is assumed that the concrete in compression shown nonlinear unconfined concrete behavior at initiation of yielding in longitudinal mild steel reinforcement. In order to determine M_{yms}, moment at the base of the wall due to initiation of yielding in longitudinal reinforcement, deformation compatibility with respect to the yielded mild steel bar(s) is used to determine elongation of PT steel groups and deformation in the extreme concrete fiber in compression. Also, strain compatibility amongst the longitudinal reinforcement is used to calculate strains, stresses and forces in the remaining longitudinal reinforcements.

The estimated base moment obtained by summing moment about the right edge is:

$$M_{yms} = N\frac{l_w}{2} + T_{p,1}l_{p,1} + T_{p,2}l_{p,2} + \sum_j f_{s,j}A_{s,j}l_{s,j} - 0.85a_{yms}t_w f_c'\frac{a_{yms}}{2} - \sum_i \sum_i f_{s,i}'A_{s,i}l_{s,i} \tag{3.170}$$

The length of equivalent compression stress block, a_{yms}, and compression force, C_c, are:

$$a_{yms} = \beta_1 c_{yms} \tag{3.171}$$

$$C_c = 0.85a_{yms}t_w f_c' \tag{3.172}$$

The elongation, $\Delta_{ms,yms}$, and stress (f_{sy}) of yielded longitudinal reinforcement is used to determine stresses, $f_{s,i}'$, and forces, $C_{s,i}$, in longitudinal reinforcement under compression:

$$\Delta_{ms,yms} = \varepsilon_{sy}H_{ms,unb} \tag{3.173}$$

$$f_{s,i}' = \frac{c_{yms} - l_{s,i}'}{l_{s,m}' - c_{yms}} f_{sy} \tag{3.174}$$

$$C_{s,i} = f_{s,i}'A_{s,i} \tag{3.175}$$

Resultant upward force, C_{yms}, is:

$$C_{yms} = C_c + \sum_i C_{s,i} \tag{3.176}$$

Similar to reinforcement in compression, longitudinal reinforcement tensile stresses, $f_{s,j}$, and forces, $T_{s,j}$, are:

$$f_{s,j} = \frac{l'_{s,i} - c_{yms}}{l'_{s,m} - c_{yms}} f_{sy} \quad (3.177)$$

$$T_{sj} = f_{sj} A_{sj} \quad (3.178)$$

PT groups elongation, $\Delta_{p,i}$, strain, $\varepsilon_{p,i}$, stresses, $f_{p,i}$, and forces, $T_{p,i}$, are obtained from deformation compatibility between longitudinal reinforcement and PT steel:

$$\Delta_{p,i} = \frac{l'_{p,i} - c_{fms}}{l'_{s,n} - c_{fms}} \Delta_{ms,yms} \quad (3.179)$$

$$\varepsilon_{p,i} = \frac{\Delta_{p,i}}{H_{pt,unb}} + \frac{f_{p,i}}{E_p} \quad (3.180)$$

$$T_{p,i} = f_{p,i} A_{p,i} \quad (3.181)$$

where, $f_{p,i}$ = stress PT stress corresponding to $\varepsilon_{p,i}$ strain

Resultant downward force, T_{yms}, is:

$$T_{yms} = T_{p,1} + T_{p,2} + N + \sum_j T_{s,j} \quad (3.182)$$

Equating the downward and upward forces gives an estimate of the neutral axis depth for subsequent calculations.

Resultant shear force, V_{yms}, at the base is:

$$V_{yms} = \frac{M_{yms}}{H_w} \quad (3.183)$$

Roof drift at the yielding of longitudinal reinforcement is contributed by elastic flexural and shear deflection and rigid body rotation due to gap opening at the base of the wall.

Elastic flexural deformation, $\Delta_{F,yms}$, is:

$$\Delta_{F,yms} = \frac{1}{2E_c I_w} V_{yms} \frac{2H_w^3}{3} \quad (3.184)$$

Elastic shear deformation, $\Delta_{S,yms}$, is:

$$\Delta_{S,yms} = \frac{1}{G_c A'_w} V_{yms} H_w \quad (3.185)$$

Rigid body rotation due to gap opening, θ_{yms}, and roof deflection due to gap opening, $\Delta_{go,yms}$, is:

$$\theta_{yms} = \frac{\Delta_{ms,yms}}{l_{s,n} - c_{yms}} \quad (3.186)$$

$$\Delta_{go,yms} = \theta_{yms} H_w \quad (3.187)$$

Total roof deflection, Δ_{yms}, is:

$$\Delta_{yms} = \Delta_{F,yms} + \Delta_{S,yms} + \Delta_{go,yms} \quad (3.188)$$

The roof deflection at the limit state of yielding of longitudinal reinforcement, Θ_{yms}, is:

$$\Theta_{yms} = \frac{\Delta_{yms}}{H_w} \quad (3.189)$$

3.3.4 Fracture of Longitudinal Reinforcement (FMS)

For derivation of closed-form expressions for the limit state of fracture of longitudinal reinforcement it is assumed that yielding of longitudinal reinforcement is followed by fracture of longitudinal reinforcement. Figure 3.8 shows the strain distribution, stress distribution and resultant forces in concrete, PT steel and debonded longitudinal reinforcement at this limit state. M_{fms}, is the base moment when the farthest longitudinal reinforcement reaches its ultimate strain capacity, ε_{su}, in tension. Deformation compatibility with respect to the longitudinal reinforcement bar(s), that reached its ultimate strain capacity, is used to determine elongation of PT steel groups, and deformation in the extreme concrete fiber in compression As in the case of yielding of longitudinal reinforcement, strain compatibility between longitudinal reinforcement bars is used to determine stresses and forces in the remaining longitudinal reinforcement bars, including strain-hardening effects. It is also assumed that plane sections remain plane in concrete and bonded longitudinal reinforcement, concrete cover is spalled and cracked section properties are used with equivalent compression block parameters (α and β) for confined concrete corresponding to the ultimate strain capacity. Iteratively using force equilibrium for vertical forces, location of neutral axis depth and resultant forces can be obtained.

The estimated base moment obtained by summing moment about the right edge is:

$$M_{fms} = N\frac{l'_w}{2} + T_{p,1}l'_{p,1} + T_{p,2}l'_{p,2} + \sum_j T_{s,j}l'_{s,j} - \alpha a_{fms}t''_w f'_{cc}\frac{a_{fms}}{2} - \sum_i C_{s,i}l'_{s,i} \quad (3.190)$$

Longitudinal reinforcement tensile deformation, $\Delta_{ms,fms}$, strain, $\varepsilon_{s,j}$, stress, $f_{s,j}$, and force, $T_{s,j}$, are:

$$\Delta_{ms,fms} = \varepsilon_{su}H_{ms,unb} \quad (3.191)$$

$$\varepsilon_{s,j} = \frac{l'_{s,j}-c_{fms}}{l'_{s,n}-c_{fms}}\varepsilon_{su} \quad (3.192)$$

$$T_{s,j} = f_{s,j}A_{s,j} \quad (3.193)$$

where, $f_{s,j}$ = stress in longitudinal reinforcement corresponding to $\varepsilon_{s,j}$ strain

PT group elongation, $\Delta_{p,i}$, strain, $\varepsilon_{p,i}$, stress, $f_{p,i}$, and force, $T_{p,i}$, are:

$$\Delta_{p,i} = \frac{l'_{p,i}-c_{fms}}{l'_{s,n}-c_{fms}}\Delta_{ms,fms} \quad (3.194)$$

$$\varepsilon_{p,i} = \frac{\Delta_{p,i}}{H_{pt,unb}} + \frac{f_{p,i}}{E_p} \quad (3.195)$$

$$T_{p,i} = f_{p,i}A_{p,i} \quad (3.196)$$

where, $f_{p,i}$ = stress PT corresponding to $\varepsilon_{p,i}$ strain

Resultant downward force, T_{fms}, is:

$$T_{fms} = T_{p,1} + T_{p,2} + N + \sum_j T_{s,j} \quad (3.197)$$

Concrete equivalent compression stress block length, a_{fms}, compressive deformation, $\Delta_{c,fms}$, compressive strain, $\varepsilon_{c,fms}$, and compressive force, C_c, are:

$$a_{fms} = \beta c_{fms} \tag{3.198}$$

$$\Delta_{conc,fms} = \frac{c_{fms}}{l'_{s,n} - c_{fms}} \Delta_{ms,fms} \tag{3.199}$$

$$\varepsilon_{c,fms} = \frac{\Delta_{c,fms}}{H_{ph}} \tag{3.200}$$

$$C_c = \alpha a_{fms} t''_w f'_{cc} \tag{3.201}$$

Longitudinal reinforcement compression strain, $\varepsilon'_{s,i}$, stress, $f'_{s,i}$, and force, $C_{s,i}$, are:

$$\varepsilon'_{s,i} = \frac{c_{fms} - l'_{s,i}}{l'_{s,n} - c_{fms}} \varepsilon_{su} \tag{3.202}$$

$$C_{s,i} = f'_{s,i} A_{s,i} \tag{3.203}$$

where, $f'_{s,i}$ = stress in longitudinal reinforcement corresponding to $\varepsilon'_{s,i}$ strain

Resultant upward force, C_{fms}, is:

$$C_{fms} = C_c + \sum_i C_{s,i} \tag{3.204}$$

The neutral axis depth (c_{fms}) is calculated by an iterative procedure of vertical force equilibrium. This is then used for calculating member deformations and forces.

Resultant shear force at the base, V_{fms}, is:

$$V_{fms} = \frac{M_{fms}}{H_w} \tag{3.205}$$

The roof drift at the fracture of longitudinal reinforcement is determined by adding roof deflection from the rigid body rotation due to gap opening at the base of the wall and the roof deflection from the elastic deflection of the wall.

As earlier, the roof drift at the fracture of longitudinal reinforcement is a sum of elastic flexural and shear deflection of the wall, and roof deflection from rigid body rotation due to gap opening at the base of the wall.

Elastic flexural deflection, $\Delta_{F,fms}$, is:

$$\Delta_{F,fms} = \frac{1}{2E_c I_w} V_{fms} \frac{2H_w^3}{3} \tag{3.206}$$

Elastic shear deflection, $\Delta_{S,fms}$, is:

$$\Delta_{S,fms} = \frac{1}{G_c A'_w} V_{fms} H_w \tag{3.207}$$

Rigid body rotation due to gap opening, θ_{fms}, and roof deflection due to gap opening, $\Delta_{go,fms}$, are:

$$\theta_{fms} = \frac{\Delta_{ms,fms}}{l'_{s,n} - c_{fms}} \tag{3.208}$$

$$\Delta_{go,fms} = \theta_{fms} H_w \tag{3.209}$$

Total roof deflection, Δ_{fms}, is:

$$\Delta_{fms} = \Delta_{F,fms} + \Delta_{S,fms} + \Delta_{go,fms} \quad (3.210)$$

The roof drift at the fracture of longitudinal reinforcement, Θ_{fms}, is calculated as:

$$\Theta_{fms} = \frac{\Delta_{fms}}{H_w} \quad (3.211)$$

3.3.5 Linear Limit of Post-Tensioning Steel (LLP)

Figure 3.9 shows the strains, stresses, resultant forces and moment acting at the base of the wall at the limit state of linear limit of post-tensioning steel. The moment at the base of the wall at this limit state is M_{llp}, the moment at initiation of yielding of farthest PT steel group. Strains, stresses, and forces in the remaining PT steel groups are obtained using deformation compatibility with respect to the yielded PT group. Deformation compatibility with respect to plastic hinge height (H_{ph}) for concrete in compression and yielded PT steel group is used to determine strain in concrete which in turn is used to calculate strains and stresses in the debonded longitudinal reinforcement using deformation compatibility. Other assumptions for this limit state include concrete cover is spalled and confined section properties are used with equivalent compression block parameters α and β.

The estimated base moment obtained by summing moment about the right edge is:

$$M_{llp} = N\frac{l'_w}{2} + T_{p,1}l'_{p,1} + T_{p,2}l'_{p,2} + \sum_j T_{s,j}l'_{s,j} - \alpha a_{llp}t''_w f'_{cc}\frac{a_{llp}}{2} - \sum_i C_{s,i}l'_{s,i} \quad (3.212)$$

PT group deformation, $\Delta_{p,i}$, stress, $f_{p,i}$, and force, $T_{p,i}$, are:

$$\Delta_{p,i} = \left(\varepsilon_{py} - \frac{f_{pi}}{E_p}\right) H_{pt,unb}\frac{l'_{p,i} - c_{llp}}{l'_{p,2} - c_{llp}} \quad (3.213)$$

$$T_{p,i} = f_{p,i}A_{p,i} \quad (3.214)$$

where, $f_{p,i}$ = PT stress corresponding to $\left(\frac{\Delta_{p,i}}{H_{pt,unb}} + \frac{f_{p,i}}{E_p}\right)$ strain

Longitudinal reinforcement tensile deformation, $\Delta_{s,j}$, strain, $\varepsilon_{s,j}$, stress, $f_{s,j}$, and force, $T_{s,j}$, are calculated using elongation of the yielded PT steel group:

$$\Delta_{s,j} = \frac{l'_{s,j} - c_{llp}}{l'_{p,2} - c_{llp}}\Delta_{p2,llp} \quad (3.215)$$

$$\varepsilon_{s,j} = \frac{\Delta_{s,j}}{H_{ms,unb}} \quad (3.216)$$

$$T_{s,j} = f_{s,j}A_{s,j} \quad (3.217)$$

where, $f_{s,j}$ = stress in longitudinal reinforcement corresponding to $\varepsilon_{s,j}$ strain

Resultant downward force, T_{llp}, is:

$$T_{llp} = T_{p,1} + T_{p,2} + N + \sum_j T_{s,j} \quad (3.218)$$

Concrete equivalent compression stress block length, a_{llp}, and compression force, C_c, are:

$$a_{llp} = \beta c_{llp} \tag{3.219}$$

$$C_c = \alpha a_{llp} t''_w f'_{cc} \tag{3.220}$$

Longitudinal reinforcement compression deformation, $\Delta'_{s,i}$, strain, $\varepsilon'_{s,i}$, stress, $f'_{s,i}$, and force, $C_{s,i}$, are:

$$\Delta'_{s,i} = \frac{c_{llp} - l'_{s,i}}{l'_{p,2} - c_{llp}} \Delta_{p2,llp} \tag{3.221}$$

$$\varepsilon'_{s,i} = \frac{\Delta'_{s,i}}{H_{ms,unb}} \tag{3.222}$$

$$C_{s,i} = f'_{s,i} A_{s,i} \tag{3.223}$$

where, $f'_{s,i}$ = stress in longitudinal reinforcement corresponding to $\varepsilon'_{s,i}$ strain

Resultant upward force, C_{llp}, is:

$$C_{llp} = C_c + \sum_i C_{s,i} \tag{3.224}$$

Strains, stresses and forces in longitudinal reinforcement, PT steel groups and concrete are calculated by using vertical force equilibrium

Resultant shear force at the base, V_{llp}, is:

$$V_{llp} = \frac{M_{llp}}{H_w} \tag{3.225}$$

Roof drift at the linear limit of post-tensioning steel is contributed by elastic flexural deflection and elastic shear deflection due to applied lateral load, and roof deflection from rigid body rotation due to gap opening.

Elastic flexural deflection, $\Delta_{F,llp}$, is:

$$\Delta_{F,llp} = \frac{1}{2E_c I_w} V_{llp} \frac{2H_w^3}{3} \tag{3.226}$$

Elastic shear deflection, $\Delta_{S,llp}$, is:

$$\Delta_{S,llp} = \frac{1}{G_c A'_w} V_{llp} H_w \tag{3.227}$$

Rigid body rotation due to gap opening, θ_{llp}, and roof deflection due to gap opening, $\Delta_{go,llp}$, are calculated with respect to the elongation of yielded PT steel group:

$$\theta_{llp} = \frac{\Delta_{p,2}}{l'_{p2} - c_{llp}} \tag{3.228}$$

$$\Delta_{go,llp} = \theta_{llp} H_w \tag{3.229}$$

Total roof deflection, Δ_{llp}, are:

$$\Delta_{llp} = \Delta_{F,llp} + \Delta_{S,llp} + \Delta_{go,llp} \tag{3.230}$$

The roof drift at the linear limit of post-tensioning, Θ_{llp}, is calculated as:

$$\Theta_{llp} = \frac{\Delta_{llp}}{H_w} \tag{3.231}$$

3.3.6 Crushing of Confined Concrete (CCC)

Figure 3.10 shows the stresses and resultant forces acting at the base of the wall at the limit state of crushing of confined concrete and the moment at the base of the wall M_{ccc}. It is assumed that the concrete cover is spalled and cracked section properties are used for all calculations. All expressions for this limit state are based on the assumption that the extreme confined concrete fiber in compression has reached it ultimate strain capacity ε_{cu}. Therefore, equivalent stress block parameters, α and β, for confined concrete are used. Also, deformation compatibility with respect to critical confined concrete crushing height (H_{cr}) of concrete in compression with debonded longitudinal reinforcement and PT steel is used to obtain forces in the longitudinal reinforcement and PT steel, respectively.

The estimated base moment obtained by summing moment about the right edge is:

$$M_{ccc} = N\frac{l'_w}{2} + T_{p,1}l'_{p,1} + T_{p,2}l'_{p,2} + \sum_j T_{s,j}l'_{s,j} - \alpha a_{ccc}t''_w f'_{cc}\frac{a_{ccc}}{2} - \sum_i C_{s,i}l'_{s,i} \quad (3.232)$$

The equivalent concrete compression stress block length, a_{ccc}, deformation, $\Delta_{conc,ccc}$, and compression force, C_c, are:

$$a_{ccc} = \beta c_{ccc} \quad (3.233)$$

$$H_{cr} = \min\{2t''_w, 2a_{ccc}\} \quad (3.234)$$

$$\Delta_{conc,ccc} = \varepsilon_{cu}H_{cr} \quad (3.235)$$

$$C_c = \alpha a_{ccc}t''_w f'_{cc} \quad (3.236)$$

Longitudinal reinforcement compression deformation, $\Delta'_{s,i}$, strain, $\varepsilon'_{s,i}$, stress, $f'_{s,i}$, and force, $C_{s,i}$, are obtained from the deformation in concrete $\Delta_{conc,ccc}$:

$$\Delta'_{s,i} = \frac{c_{ccc} - l'_{s,i}}{c_{ccc}}\Delta_{conc,ccc} \quad (3.237)$$

$$\varepsilon'_{s,i} = \frac{\Delta'_{s,i}}{H_{ms,unb}} \quad (3.238)$$

$$C_{s,i} = f'_{s,i}A_{s,i} \quad (3.239)$$

where, $f'_{s,i}$ = stress in longitudinal reinforcement corresponding to $\varepsilon'_{s,i}$ strain

Resultant upward force, C_{ccc}, is:

$$C_{ccc} = C_c + \sum_i C_{s,i} \quad (3.240)$$

Longitudinal reinforcement tensile deformation, $\Delta_{s,j}$, strain, $\varepsilon_{s,j}$, stress, $f_{s,j}$, and force, $T_{s,j}$, are also calculated in terms of $\Delta_{conc,ccc}$:

$$\Delta_{s,j} = \frac{l'_{s,j} - c_{ccc}}{c_{ccc}}\Delta_{conc,ccc} \quad (3.241)$$

$$\varepsilon_{s,j} = \frac{\Delta_{s,j}}{H_{ms,unb}} \quad (3.242)$$

$$T_{s,j} = f_{s,j}A_{s,j} \quad (3.243)$$

where, $f_{s,j}$ = stress in longitudinal reinforcement corresponding to $\varepsilon_{s,j}$ strain

Post-tensioning steel elongation, $\Delta_{p,i}$, strain, $\varepsilon_{p,i}$, stress, $f_{p,i}$, and force, $T_{p,i}$, are obtained from deformation compatibility between PT steel and concrete:

$$\Delta_{p,i} = \frac{l'_{p,i} - c_{ccc}}{c_{ccc}} \Delta_{conc,ccc} \tag{3.244}$$

$$\varepsilon_{p,i} = \frac{\Delta_{p,i}}{H_{pt,unb}} \tag{3.245}$$

$$T_{p,i} = f_{p,i} A_{pi} \tag{3.246}$$

where, $f_{p,i}$ = PT stress corresponding to $\left(\varepsilon_{p,i} + \frac{f_{pi}}{E_p}\right)$ strain

Resultant downward force, T_{ccc}, is:

$$T_{ccc} = T_{p,1} + T_{p,2} + N + \sum_j T_{s,j} \tag{3.247}$$

Iterative procedure is required to determine neutral axis depth, c_{ccc}, for this limit state. Deformations, strains, stresses and forces in PT steel groups and longitudinal reinforcement are estimated using c_{ccc}. The force values are then used in calculating M_{ccc}.

Resultant shear force at the base, V_{ccc}, is:

$$V_{ccc} = \frac{M_{ccc}}{H_w} \tag{3.248}$$

As in the previous case, roof drift at the crushing of confined concrete is also a sum of elastic flexural and shear deflection, and roof deflection from rigid body rotation due to gap opening at the base of the wall.

Elastic flexural deformation, $\Delta_{F,ccc}$, is:

$$\Delta_{F,ccc} = \frac{1}{2E_c I_w} V_{ccc} \frac{2H_w^3}{3} \tag{3.249}$$

Elastic shear deformation, $\Delta_{S,ccc}$, is:

$$\Delta_{S,ccc} = \frac{1}{G_c A'_w} V_{ccc} H_w \tag{3.250}$$

Rigid body rotation due to gap opening, θ_{ccc}, and roof deflection due to gap opening at the base, $\Delta_{go,ccc}$, are calculated with respect to the elongation of PT steel groups:

$$\theta_{ccc} = \frac{\Delta_{p,2}}{l'_{p,2} - c_{ccc}} \tag{3.251}$$

$$\Delta_{go,ccc} = \theta_{ccc} H_w \tag{3.252}$$

Total roof deflection, Δ_{ccc}, is:

$$\Delta_{ccc} = \Delta_{F,ccc} + \Delta_{S,ccc} + \Delta_{go,ccc} \tag{3.253}$$

The roof deflection at the linear limit of post-tensioning, Θ_{ccc}, is calculated as:

$$\Theta_{ccc} = \frac{\Delta_{ccc}}{H_w} \tag{3.254}$$

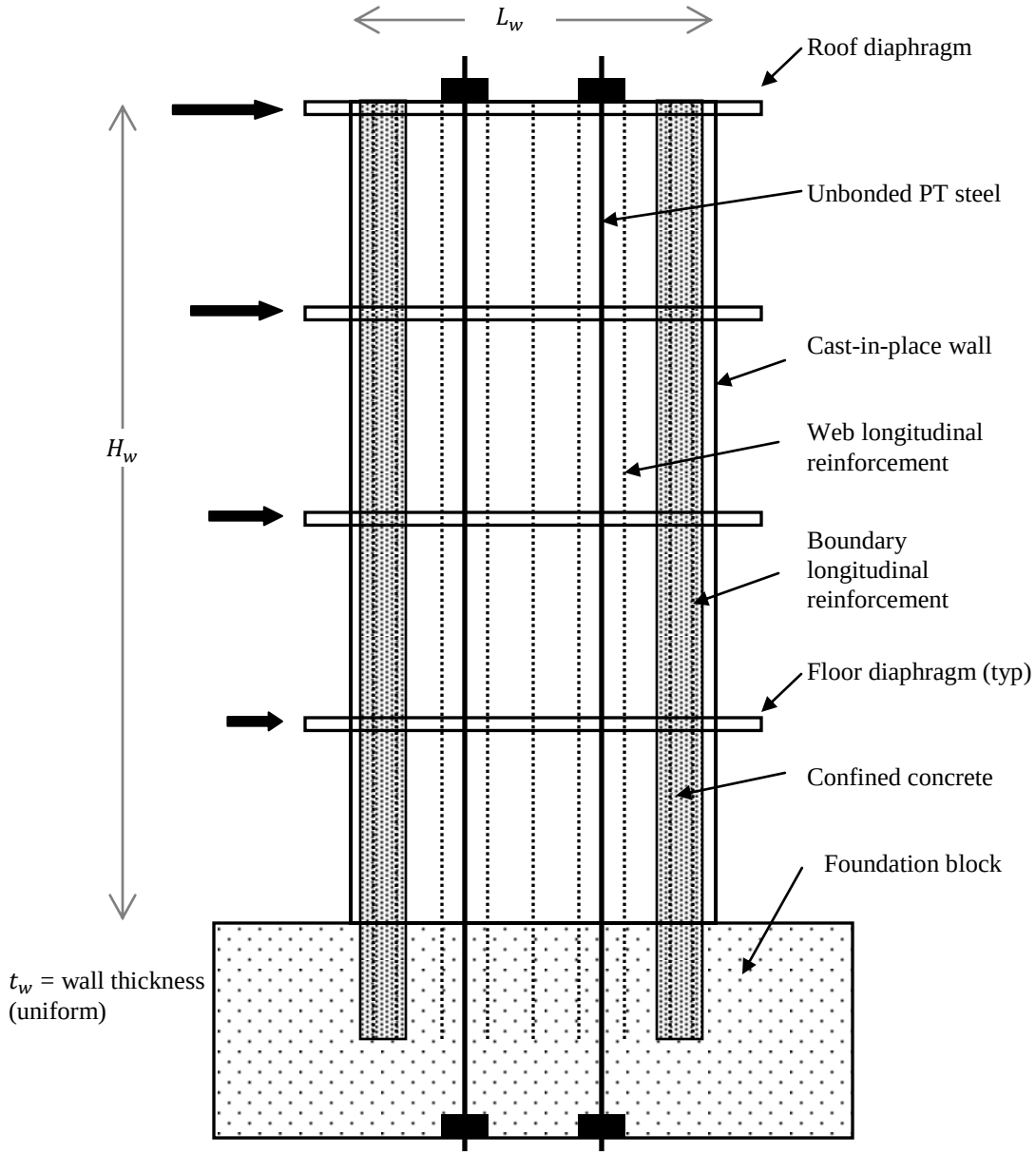

Figure 3.1(a): Elevation of cast-in-place wall with unbonded PT steel and longitudinal reinforcement and applied lateral force

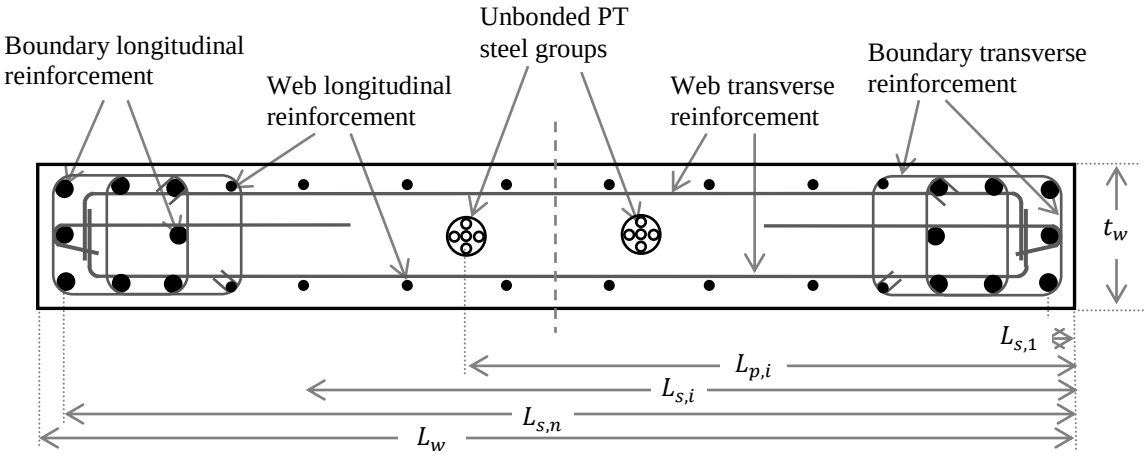

Figure 3.1(b): Section of Cast-in-place wall with unbonded PT steel and longitudinal reinforcement and applied lateral load

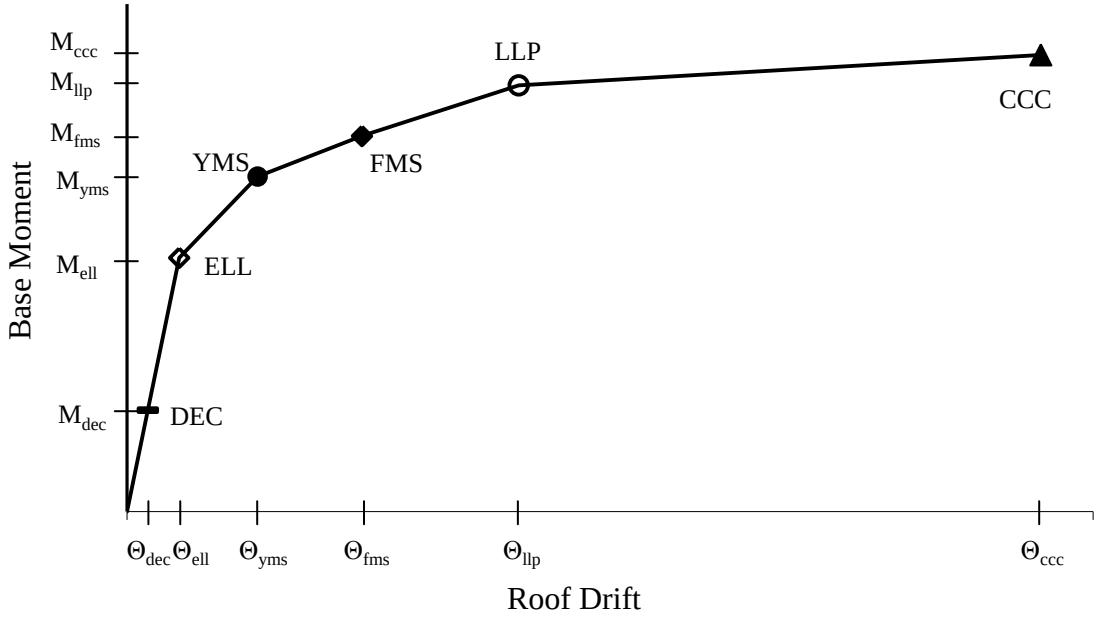

Figure 3.2: Structural limit states for a wall with unbonded PT steel and longitudinal reinforcement

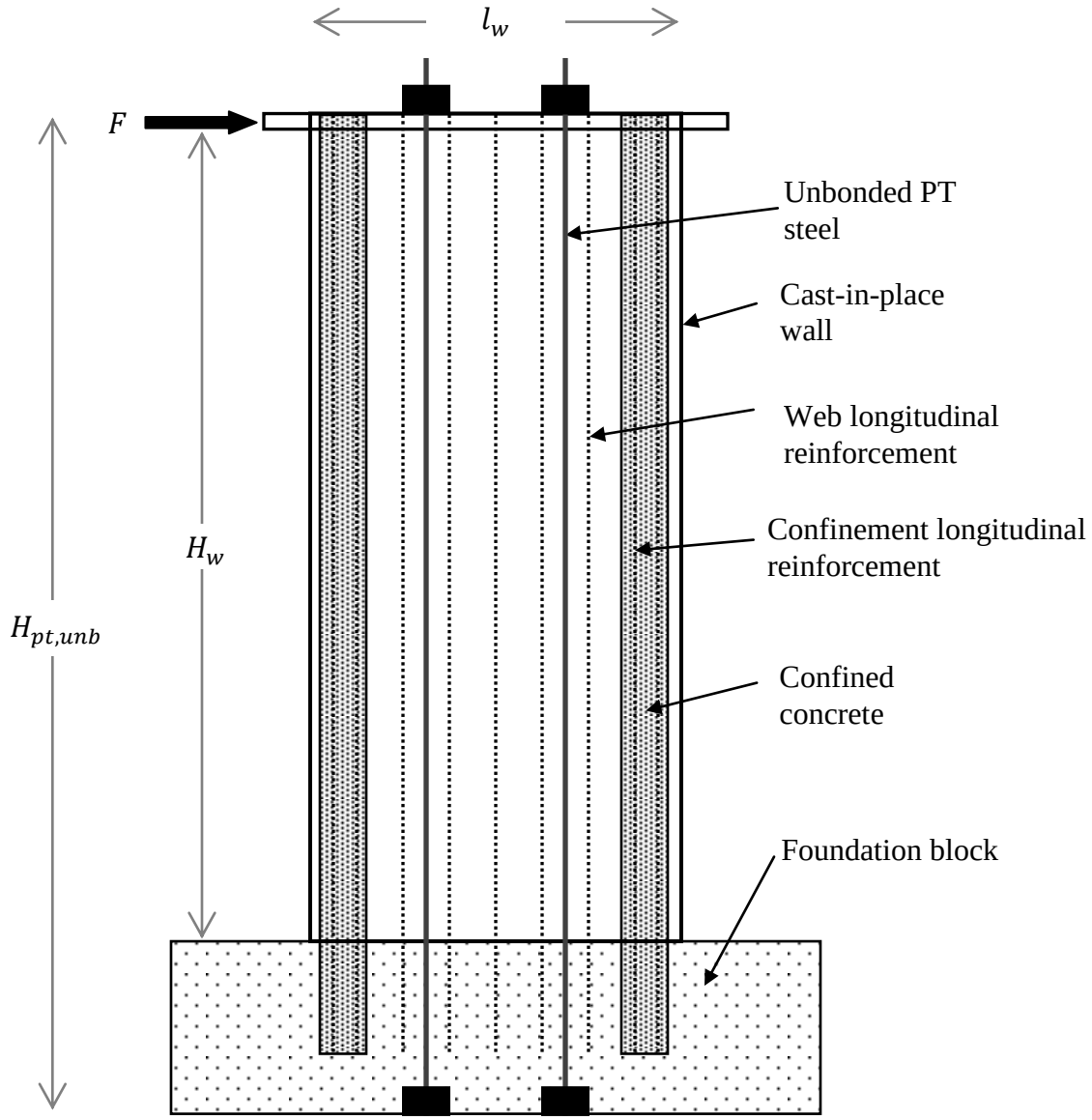

Figure 3.3: Schematic of a cast-in-place wall with unbonded PT steel and longitudinal mild steel reinforcement used for deriving the closed-form expressions

(a) Strain distribution in concrete at the base of the wall

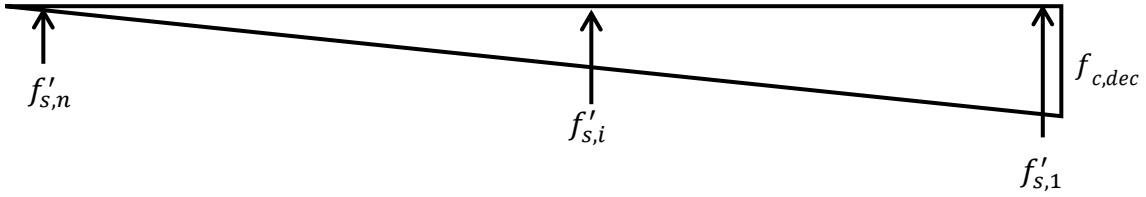

(b) Stress distribution in concrete and longitudinal reinforcement at the base of the wall

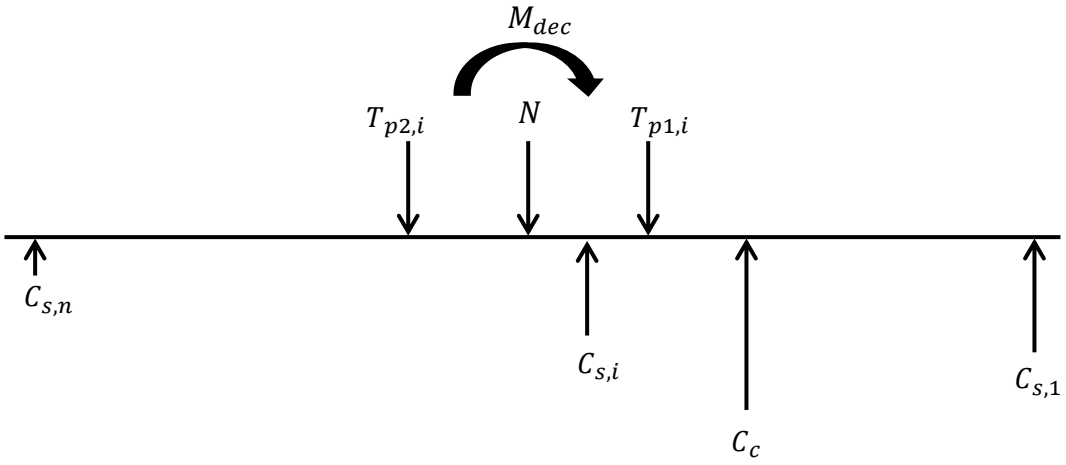

(c) Resultant forces acting at the base of the wall

Figure 3.4: Forces acting at the base of a wall at DEC

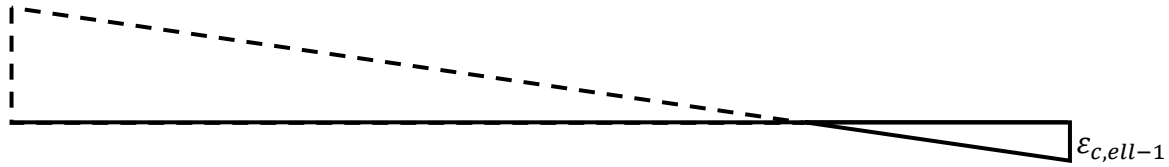

(a) Strain distribution in concrete

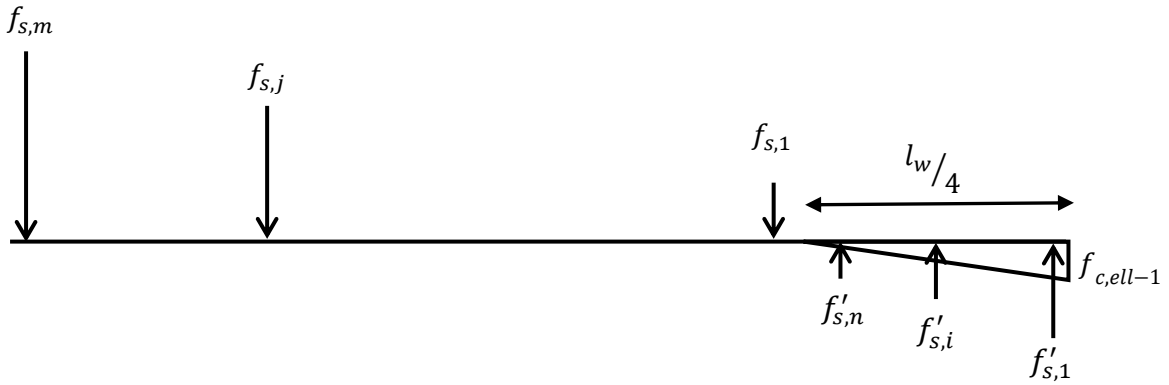

(b) Stress distribution in concrete and reinforcing steel

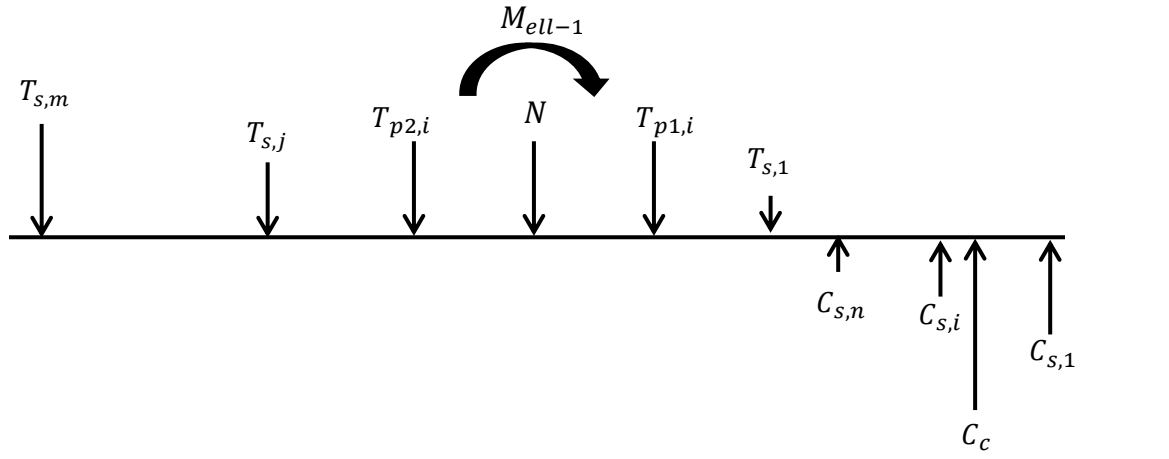

(c) Resultant forces acting at the base of the wall

Figure 3.5: Forces acting at the base of a wall at ELL-1 with 25% neutral axis depth

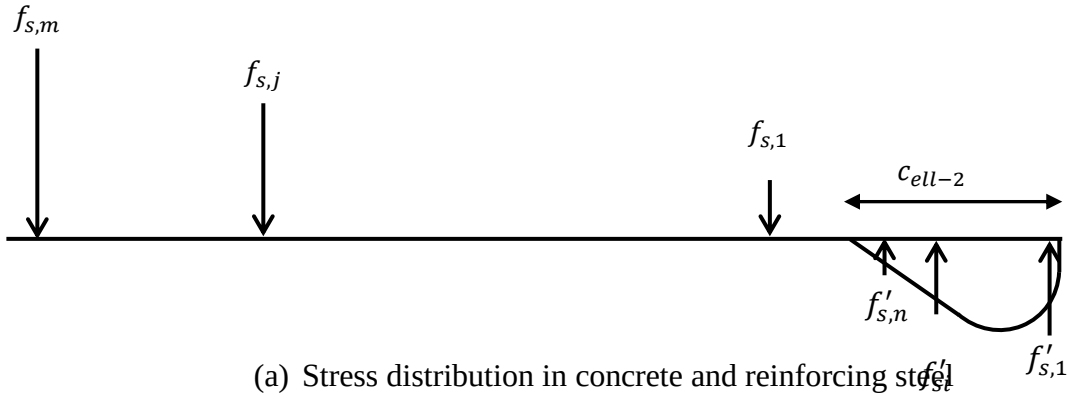

(a) Stress distribution in concrete and reinforcing steel

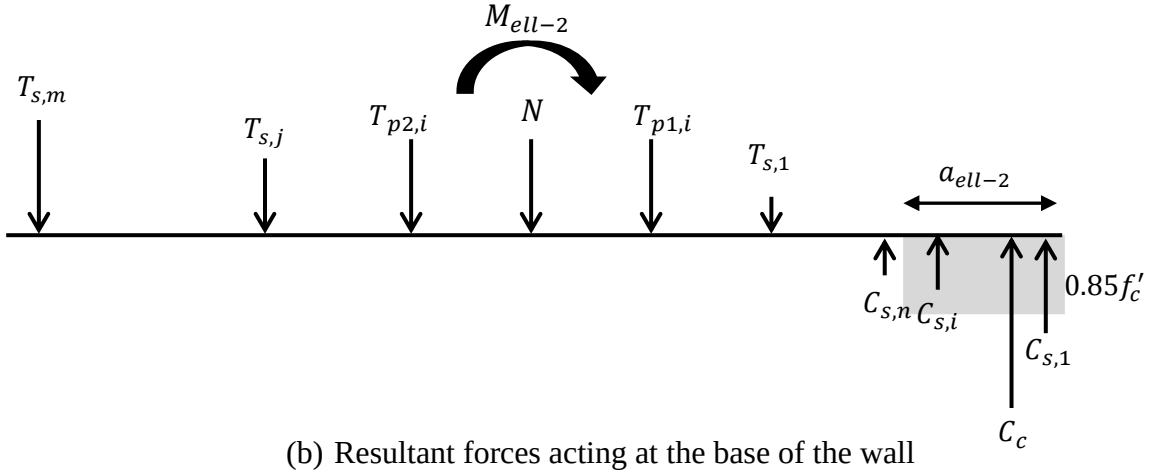

(b) Resultant forces acting at the base of the wall

Figure 3.6: Forces acting at the base of a wall at ELL-2 with concrete softening

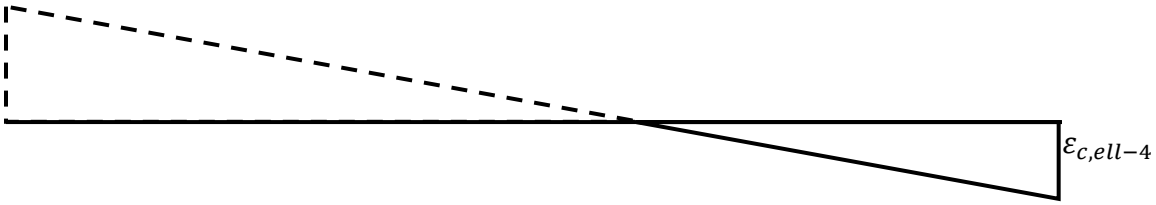

(a) Strain distribution in concrete

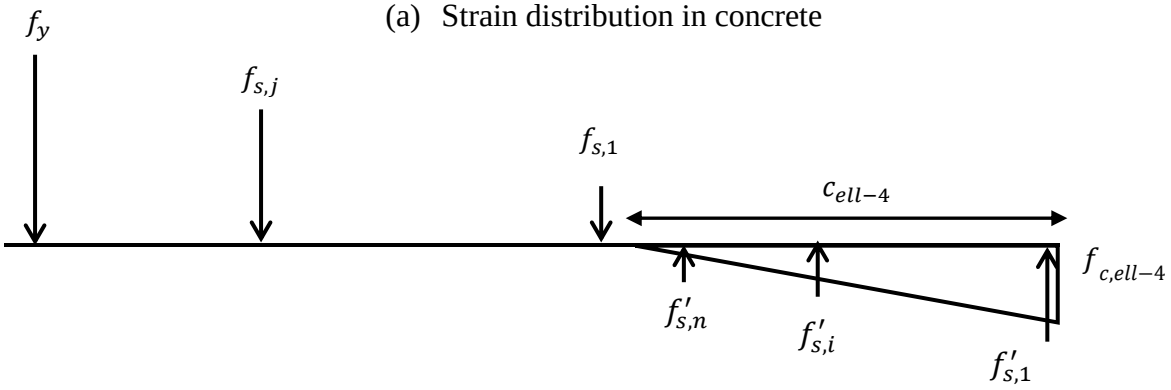

(b) Stress distribution in concrete and reinforcing steel

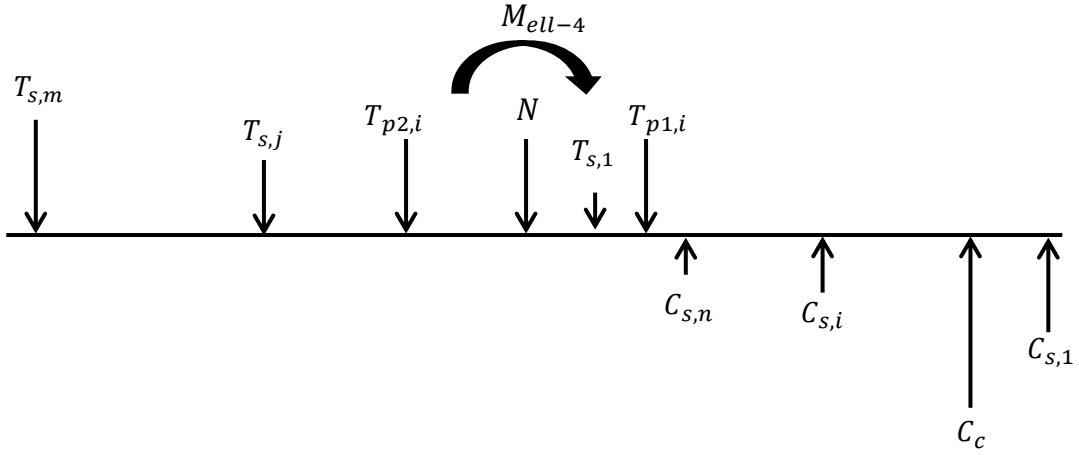

(c) Resultant forces acting at the base of the wall

Figure 3.7: Forces acting at the base of a wall at ELL-4 with yielding of farthest longitudinal reinforcement

(a) Stress distribution in concrete and reinforcing steel

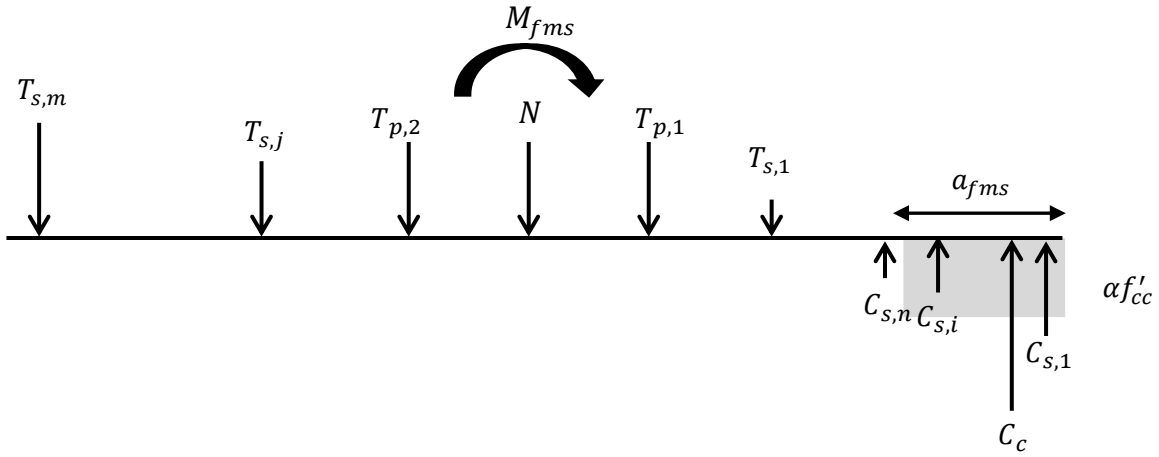

(b) Resultant forces acting at the base of the wall

Figure 3.8: Forces acting at the base of a wall at FMS

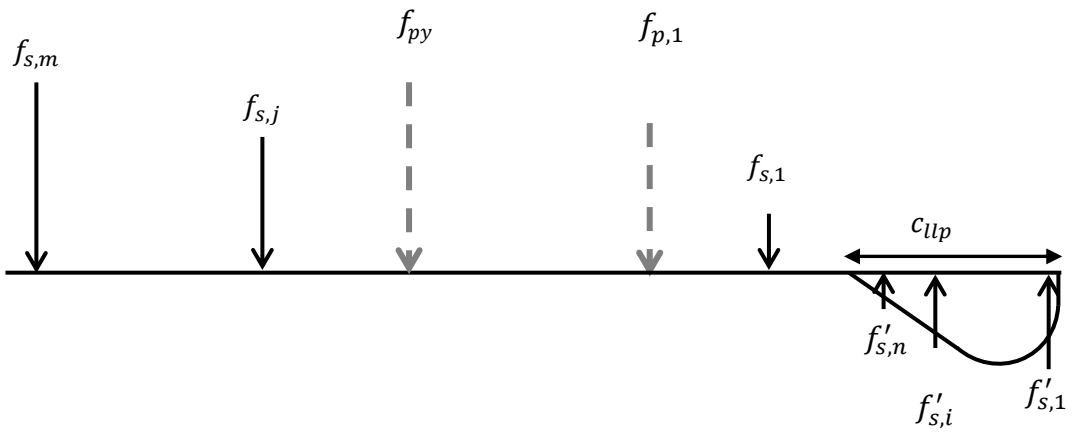

(a) Stress distribution in concrete and reinforcing steel

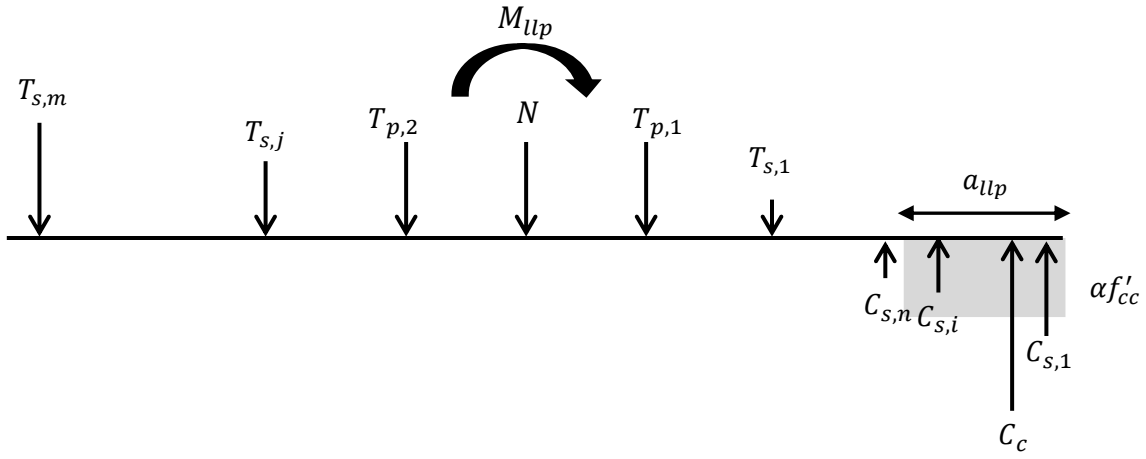

(b) Resultant forces acting at the base of the wall

Figure 3.9: Forces acting at the base of a wall at LLP

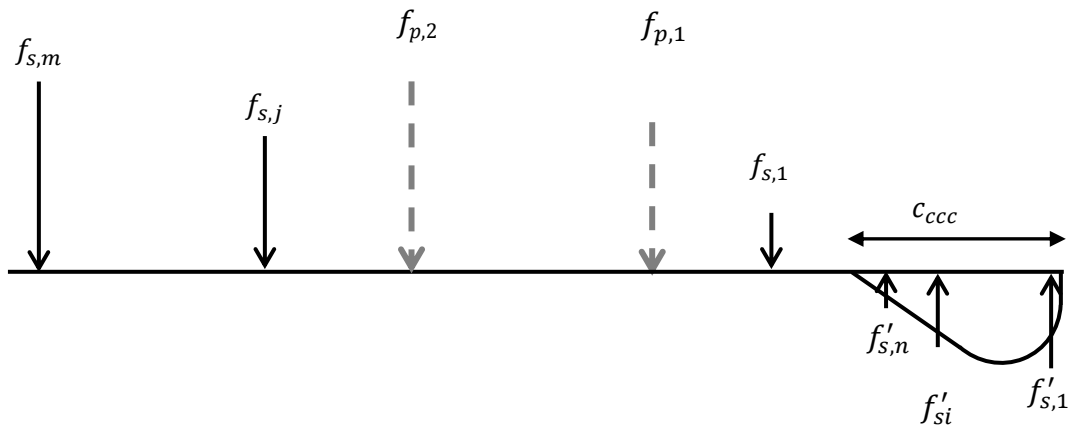

(a) Stress distribution in concrete and reinforcing steel

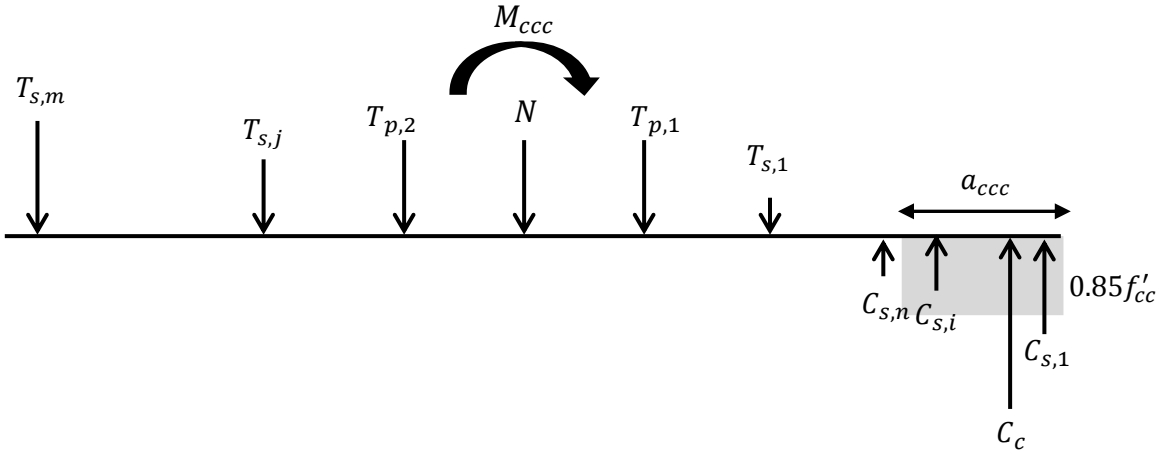

(b) Resultant forces acting at the base of the wall

Figure 3.10: Forces acting at the base of a wall at CCC

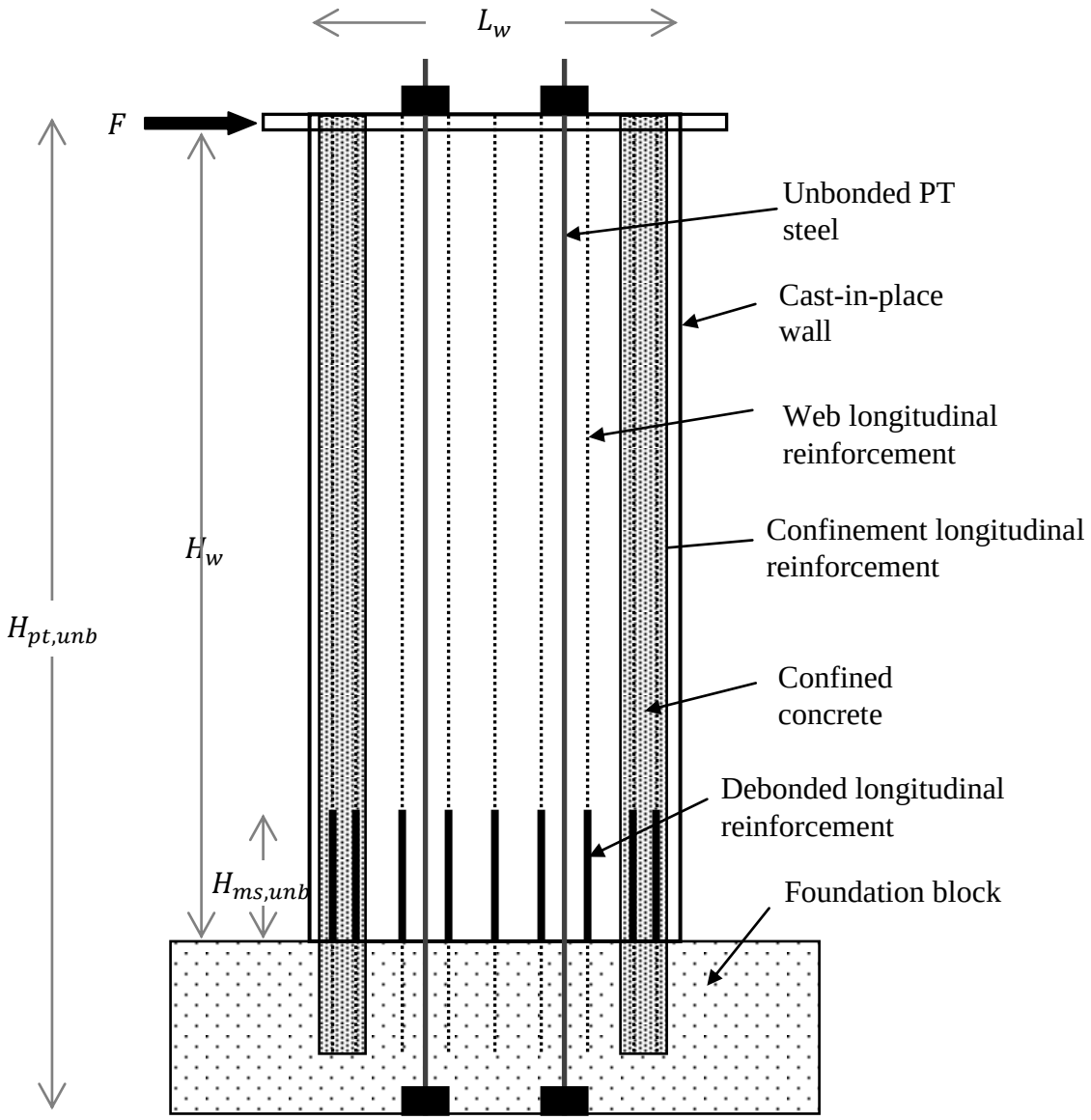

Figure 3.11: Schematic of a cast-in-place special structural wall with unbonded PT steel and debonded longitudinal mild steel reinforcement

CHAPTER 4

DESCRIPTION OF PARAMETRIC BASE WALLS

This chapter discusses properties and detailing of four parametric base walls designed to study the closed-form expressions derived in Chapter 3. Two of the parametric base walls are examples of unbonded post-tensioned cast-in-place concrete walls with bonded longitudinal mild steel reinforcement and two are examples of unbonded post-tensioned cast-in-place concrete walls with longitudinal mild steel reinforcement debonded over a predetermined height at the base of the wall. Section 4.1 gives an overview of the chapter, Section 4.2 describes the reduced scale test walls that have been used as the basis for developing the parametric base walls and Section 4.3 presents detailing of the four parametric base walls.

4.1 OVERVIEW

In order to study the two sets of closed-form expressions (CFE) derived in Chapter 3, four parametric base walls have been selected, two parametric base walls for each set of closed-form expressions. These parametric base walls are based on two reduced scale test walls designed for an experimental program at the ATLSS Research Center at Lehigh University. A number of variations in properties and detailing of walls were studied during the design of the test walls to select suitable properties and detailing. The properties that were varied include initial stress in post-tensioning (PT) steel, area of the PT steel, area of the web longitudinal mild steel reinforcement, spacing of the web longitudinal mild steel reinforcement, length of the concrete confinement region, detailing and configuration of the concrete confinement region. Section 4.2 provides information on dimensions, reinforcement detailing and material properties of the test walls. The parametric base walls have the same dimensions and material properties as the test walls. However, the reinforcement detailing are different for the four parametric base walls and are presented in Section 4.3.

4.2 BASIC PROPERTIES OF THE REDUCED SCALE TEST WALLS

The two test walls are based on a prototype cast-in-place structural wall with post-tensioning steel assumed to be located in a region of high seismicity. The prototype wall is 20 feet long, 150 feet high and 2 feet thick. However, due to limitations on the specimen that can be tested in the ATLSS Laboratory, the test wall dimensions were scaled down to 40% of the prototype wall. Therefore, as summarized in Table 4.1 and shown in Figure 4.1, the test walls and the parametric walls are 6 feet long, 20 feet high and 10 inches thick. The cast-in-place concrete test walls will be constructed monolithically on a 5 feet high, 25 feet long and 2 feet thick foundation block. The earthquake lateral load acting on the walls is simulated as a single point lateral load applied by a hydraulic actuator at a height of 12 feet and 6 inches from the base of the wall, above the foundation block. The PT strands are unbonded over the entire height of the wall and foundation block. Therefore, $H_{pt,unb}$, for the PT steel is 25 feet or 300 in.

4.2.1. ACI 318-11 Requirements

The reduced scale walls to be tested at Lehigh University walls are detailed to meet requirements of Section 21.9 of Chapter 21 of ACI 318-11 which deals with special structural walls designed to resist lateral forces developed by earthquake excitation. The

two test walls have an l_w/t_w aspect ratio of 7.2 which is greater than 6.0, as required by Chapter 21, and an H_w/l_w aspect ratio of 4.17 which is greater than 2.0, as required by Chapter 21. As per section 21.9.6.2, the compression zone should have a boundary element with detailing to confine the concrete that extends over the length of the largest neutral axis depth to confine the concrete. The boundary element transverse reinforcement should comply with section 21.9.6.4 which specifies the transverse reinforcement spacing and the development length of the longitudinal steel into the support or foundation. Therefore, as shown in Figure 4.2, a boundary element length of 13.5 in. on both ends of the test walls is selected. The primary longitudinal steel of the boundary element (eight bars as shown in Figure 4.2) are located within the first 9.5 in. from the ends of the wall. The transverse reinforcement is extended another 4.0 in. to include two longitudinal web reinforcement bars within the confined concrete. The boundary element longitudinal reinforcement is defined as the eight bars as shown in the figure. For the parametric study of Chapter 6 and all other discussions, the two additional web longitudinal reinforcement bars included in the extended boundary element are still considered as part of the web longitudinal reinforcement. The boundary element longitudinal reinforcement detailing varies for the four parametric base walls as discussed in Section 4.3. Rectangular hoops of #3 reinforcement bars with 2.25 in. center-to-center spacing are selected for transverse reinforcement of the boundary element.

The distributed longitudinal and transverse web reinforcement ratios, ρ_l and ρ_t , should be more than 0.25% with a spacing less than 18 in. for a full scale wall per Section 21.9.2.1 in ACI318-11. Therefore, the reduced scale test walls have distributed web reinforcement ratios more than 0.25% with spacing less than 7.2 in. The walls are designed with #3 reinforcement bars for longitudinal and transverse web reinforcement in two layers. The longitudinal reinforcement consists of 16 #3 bars arranged in two layers at a spacing of 7.0 in., with ρ_l of 0.34%. Considering the boundary element transverse reinforcement spacing of 2.25 in., web transverse reinforcement of #3 bars in two layers with a spacing of 4.5 in. center-to-center is selected, with ρ_t of 0.49%.

4.2.2. Material properties

The stress-strain relationship for the unconfined concrete and the confined concrete in compression are presented in Figure 4.3. Table 4.2 lists the important properties of confined and unconfined concrete. The nominal compressive strength of unconfined concrete used for the test walls is 6,000 psi. However, allowing for over strength and based on past experimental results, a factor of 1.3 is used to determine the expected strength of 7,800 psi which is used in designing the walls. For the boundary element, compressive strength of the confined concrete is calculated to be 11,000 psi using equations from Mander et al. (1988a, 1988b).

Figure 4.4 represents the stress-strain behavior of 270 ksi low relaxation post-tensioning steel strands as obtained from an experiment conducted at Lehigh University. The PT strands are 0.6 in. diameter strands with 0.217 in.^{2} area per strand. As listed in Table 4.3, the Young's Modulus for the PT strands, E_p, is 27,500 ksi. The yield stress, f_{py}, is 220 ksi at a strain of 0.008 in./in. and the ultimate strength, f_{pu}, is 270 ksi at 0.045 in./in. strain.

The important properties of reinforcing steel are summarized in Table 4.4. Figure 4.5 presents the stress-strain behavior of ASTM A615 obtained from experiments conducted at Lehigh University is presented in Figure 4.5. The bonded and debonded mild steel reinforcement is assumed to be ASTM A615 Grade 60. To account for over strength of reinforcement steel, an expected yield stress of 1.1 times of the nominal yield stress of mild steel is used in design of the walls and the ultimate strength is assumed to be 1.5 times of the expected yield stress. The ultimate strain for mild steel reinforcement is assumed to be 12% for debonded reinforcement and 7.2% for bonded reinforcement to account for the strain concentration that occurs at flexural shear cracks in the wall. .

4.3 PARAMETRIC WALL BASE CASES

The four parametric base walls are 6 feet long, 20 feet high and 10 inches thick cast-in-place walls with a 5 feet high, 25 feet long and 2 feet thick foundation block. The unbonded length, $H_{pt,unb}$, for PT steel is 25 feet. The earthquake lateral load acts as a single point lateral load at a height of 12 feet and 6 inches from the base of the wall. Material properties of the parametric walls are the same as discussed in Section 4.2.2 and summarized in Tables 4.2 to 4.4.

The boundary elements extend 13.5 in. from the ends of the parametric base walls (Figure 4.2). The boundary element has the eight longitudinal reinforcement bars configuration shown in Figure 4.2. The boundary elements are confined by rectangular hoops of #3 reinforcement bars with 2.25 in. center-to-center spacing. The web of the parametric base walls is reinforced with 16 - #3 reinforcement bars in two layers spaced at 7.0 in in the longitudinal direction and with #3 bars in two layers at a spacing of 4.5 in. in the transverse direction. The boundary reinforcement area and post-tensioning steel area vary for the four parametric walls.

4.3.1 Parametric Base Wall 1 (PW1.0.0)

Figure 4.6 shows detailing of parametric base wall 1, henceforth referred to as PW1.0.0. The reinforcement configuration and prestress force for PW1.0.0 are summarized in Table 4.5. The distinguishing features of this wall are the boundary element which includes eight #7 reinforcement bars in the configuration shown in Figure 4.6 and the number of PT strands. PW1.0.0 has 10 PT strands bundled in two groups of five strands each at an eccentricity of 6.0 in on either side of the section centerline. PW1.0.0 is an example of an unbonded post-tensioned cast-in-place wall with longitudinal mild steel reinforcement bonded, therefore, all longitudinal reinforcement bars are assumed to be completely bonded with the surrounding concrete.

4.3.2 Parametric Base Wall 2 (PW2.0.0)

Figure 4.7 shows detailing of parametric base wall 2, henceforth referred to as PW2.0.0. The reinforcement configuration and prestress force for PW2.0.0 are summarized in Table 4.6. The boundary elements include eight #5 reinforcement bars in the configuration shown in Figure 4.7. There are 19 PT strands divided into three groups, two with seven strands and one with five strands. The group of five strands is located at the section centerline and the two groups of seven strands are located at 9.0 in. on either side of the centerline. All longitudinal reinforcement bars in this parametric wall are completely bonded to the concrete.

4.3.3 Parametric Base Wall 3 (PW3.0.0)

Figure 4.8 and Table 4.7 give the reinforcement detailing of parametric base wall 3, PW3.0.0, which has the same reinforcement configuration as PW1.0.0 with eight #7 bars in the boundary and 10 PT strands. However, PW3.0.0 is an example of unbonded post-tensioned cast-in-place wall with debonded longitudinal reinforcement. Therefore, all the longitudinal reinforcement (in both the web and boundaries) is considered to be debonded over a 24.0 in. height from the base of the wall.

4.3.4 Parametric Base Wall 4 (PW4.0.0)

Table 4.8 summarizes reinforcement configuration and Figure 4.9 shows detailing of parametric base wall 4, PW4.0.0. The reinforcement configuration of this wall is the same as PW2.0.0, with eight #5 bars in the boundary and 19 PT strands in three groups. In PW4.0.0 the longitudinal reinforcement is debonded over a 24.0 in. height from the base of the wall, similar to PW3.0.0.

Table 4.1: Dimensions of the parametric base walls

Wall length	l_w	72 in.
Wall thickness	t_w	10 in.
Wall height	H_w	240 in.
Height of applied equivalent lateral force (actuator force)	H_F	150 in.

Table 4.2: Unconfined and confined concrete properties

Expected unconfined concrete strength	f_c'	7.8 ksi
Expected confined concrete Strength	f_{cc}'	11 ksi
Modulus of elasticity	E_c	5,034 ksi
Expected strain at f_c'	ε_{co}	0.003
Expected strain at f_{cc}'	ε_{cc}	0.006
Ultimate compressive strain	ε_{cu}	0.054

Table 4.3: Post-tensioning steel properties

Expected yield stress	f_{py}	220 ksi
Expected ultimate stress	f_{pu}	270 ksi
Modulus of elasticity	E_p	27,500 ksi
Expected yield strain	ε_{py}	0.008
Expected ultimate strain	ε_{pu}	0.045

Table 4.4: Mild steel properties

Expected yield strength	f_{sy}	66 ksi
Expected ultimate strength	f_{su}	99 ksi
Modulus of elasticity	E_s	29,000 ksi
Expected yield strain	ε_{sy}	0.0023
Expected ultimate strain	ε_{su}	0.0720

Table 4.5: Reinforcement detailing of PW1.0.0 with bonded longitudinal reinforcement

Post-tension	Area of PT steel (two groups)	A_{pt}	1.085+1.085= 2.17in^2
	Eccentricity	e_p	6.0 in.
	Initial prestress in PT steel	$f_{p,i}$	164.7 ksi
	Total initial prestress force	T_p	357.4 kip
	Unbonded height of PT steel	$H_{pt,unb}$	300.0 in.
Reinforcement	Boundary longitudinal reinforcement	$A_{b,l}$	8 - #7 bars (4.80 in.^{2})
	Boundary transverse reinforcement	$A_{b,t}$	#3 @ 2.25 in.
	Web longitudinal reinforcement	$A_{w,l}$	16 - #3 bars (1.76 in.^{2})
	Web transverse reinforcement	$A_{w,t}$	#3 @ 4.5 in.
	Debonded height of reinforcement	$H_{ms,unb}$	0.0 in.

Table 4.6: Reinforcement detailing of PW2.0.0 with bonded longitudinal reinforcement

Post-tension	Area of PT steel (three groups)	A_{pt}	1.519+1.085+1.519 = 4.123 in.^{2}
	Eccentricity	e_p	9.0 in.
	Initial prestress in PT steel	$f_{p,i}$	164.7 ksi
	Total initial prestress force	T_p	679.1 kip
	Unbonded height of PT steel	$H_{pt,unb}$	300.0 in.
Reinforcement	Boundary longitudinal reinforcement	$A_{b,l}$	8 - #5 bars (2.48 in.^{2})
	Boundary transverse reinforcement	$A_{b,t}$	#3 @ 2.25 in.
	Web longitudinal reinforcement	$A_{w,l}$	16 - #3 bars (1.76 in.^{2})
	Web transverse reinforcement	$A_{w,t}$	#3 @ 4.5 in.
	Debonded height of reinforcement	$H_{ms,unb}$	0.0 in.

Table 4.7: Reinforcement detailing of PW3.0.0 with debonded longitudinal reinforcement

Post-tension	Area of PT steel (two groups)	A_{pt}	1.085+1.085= 2.17in.^{2}
	Eccentricity	e_p	6.0 in.
	Initial prestress in PT steel	$f_{p,i}$	164.7 ksi
	Total initial prestress force	T_p	357.4 kip
	Unbonded height of PT steel	$H_{pt,unb}$	300.0 in.
Reinforcement	Boundary longitudinal reinforcement	$A_{b,l}$	8 - #7 bars (4.80 in.^{2})
	Boundary transverse reinforcement	$A_{b,t}$	#3 @ 2.25 in.
	Web longitudinal reinforcement	$A_{w,l}$	16 - #3 bars (1.76 in.^{2})
	Web transverse reinforcement	$A_{w,t}$	#3 @ 4.5 in.
	Debonded height of reinforcement	$H_{ms,unb}$	24.0 in.

Table 4.8: Reinforcement detailing of PW4.0.0 with debonded longitudinal reinforcement

Post-tension	Area of PT steel (three groups)	A_{pt}	1.519+1.085+1.519 = 4.123 in.^{2}
	Eccentricity	e_p	9.0 in.
	Initial prestress in PT steel	$f_{p,i}$	164.7 ksi
	Total initial prestress force	T_p	679.1 kip
	Unbonded height of PT steel	$H_{pt,unb}$	300.0 in.
Reinforcement	Boundary longitudinal reinforcement	$A_{b,l}$	8 - #5 bars (2.48 in.^{2})
	Boundary transverse reinforcement	$A_{b,t}$	#3 @ 2.25 in.
	Web longitudinal reinforcement	$A_{w,l}$	16 - #3 bars (1.76 in.^{2})
	Web transverse reinforcement	$A_{w,t}$	#3 @ 4.5 in.
	Debonded height of reinforcement	$H_{ms,unb}$	24.0 in.

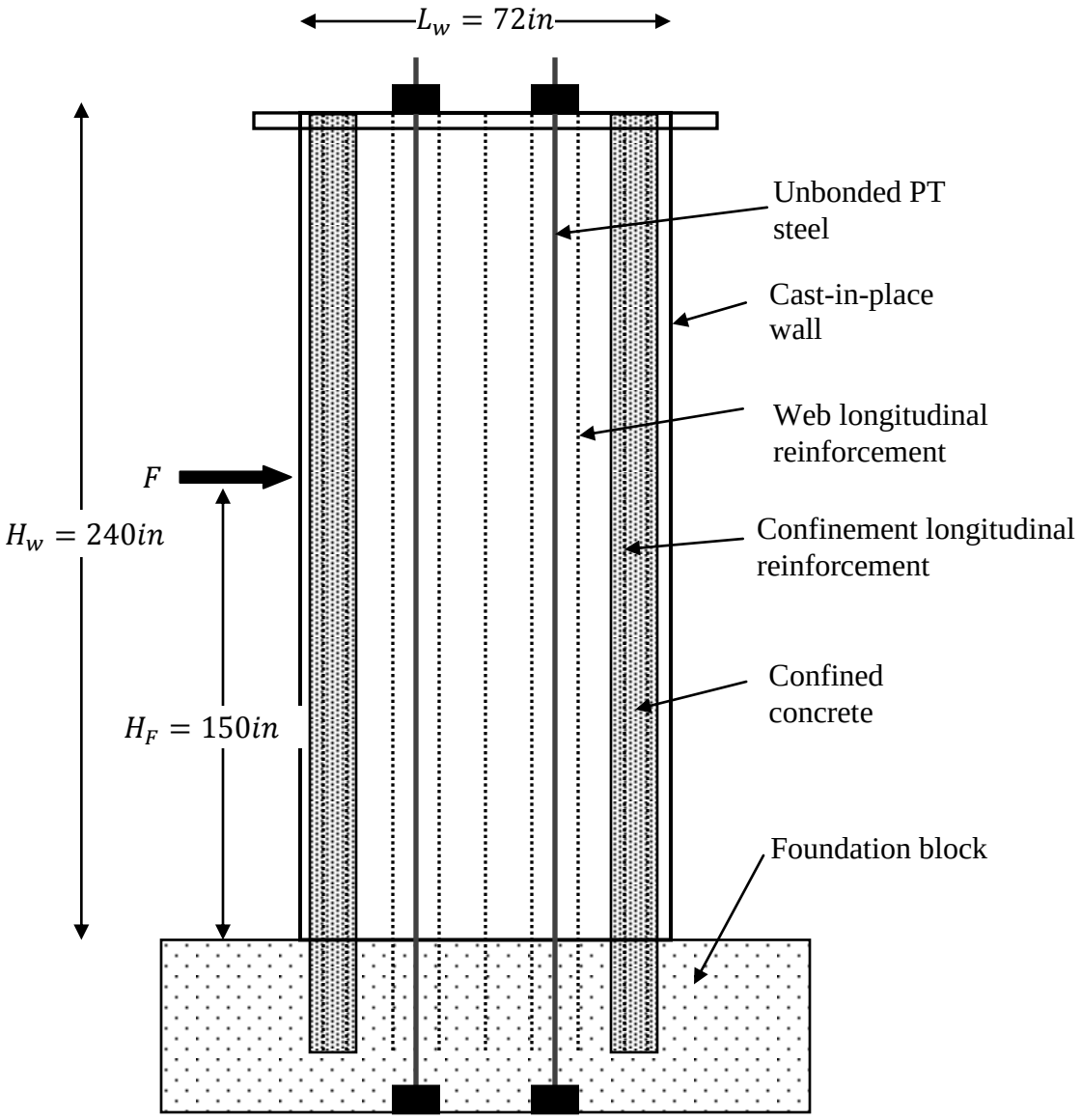

Figure 4.1: Elevation of parametric base wall

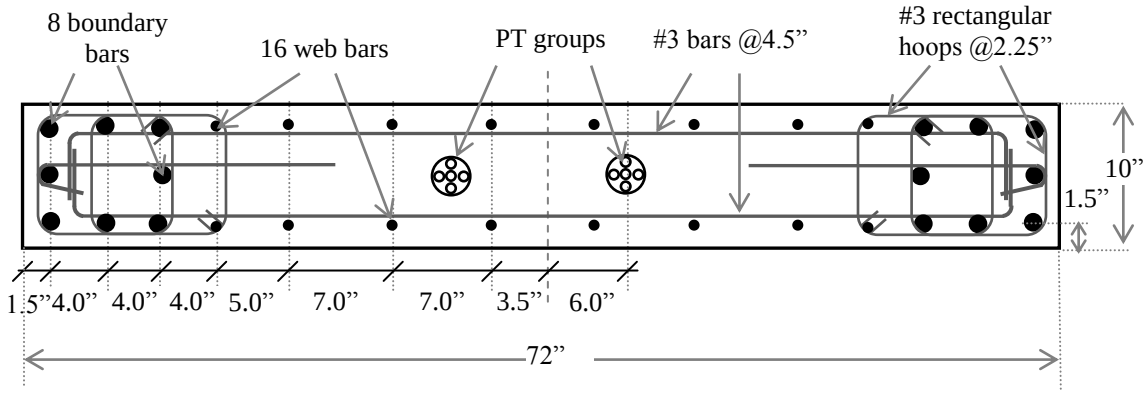

Figure 4.2: Section of a wall with boundary element, longitudinal reinforcement spacing and post-tensioning steel

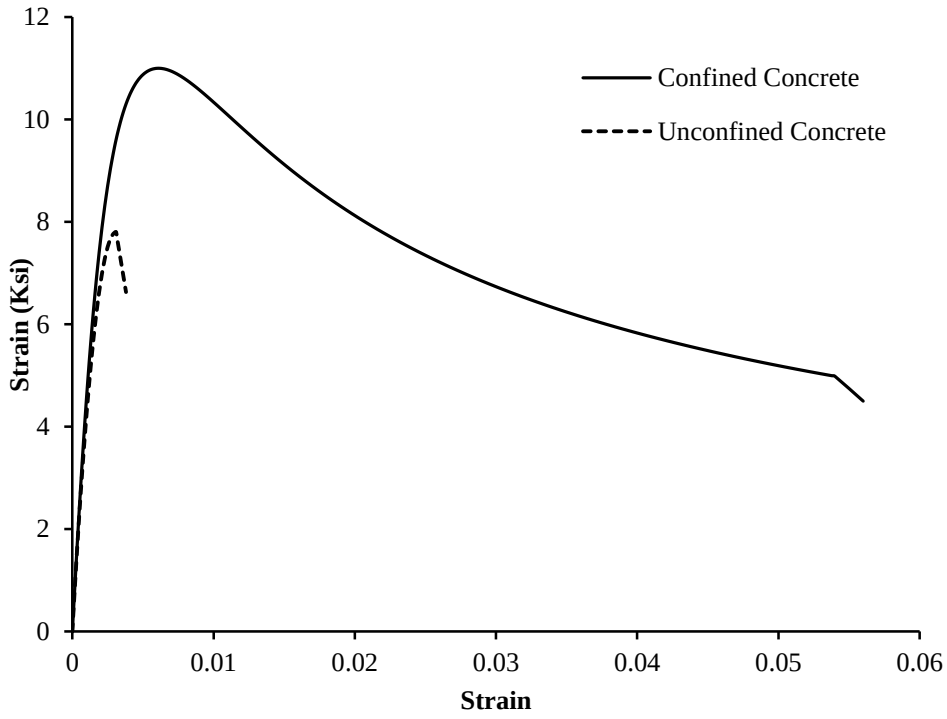

Figure 4.3: Stress-strain behavior of confined and unconfined concrete in compression (stress-strain data derived using equations from Mander 1988a, b)

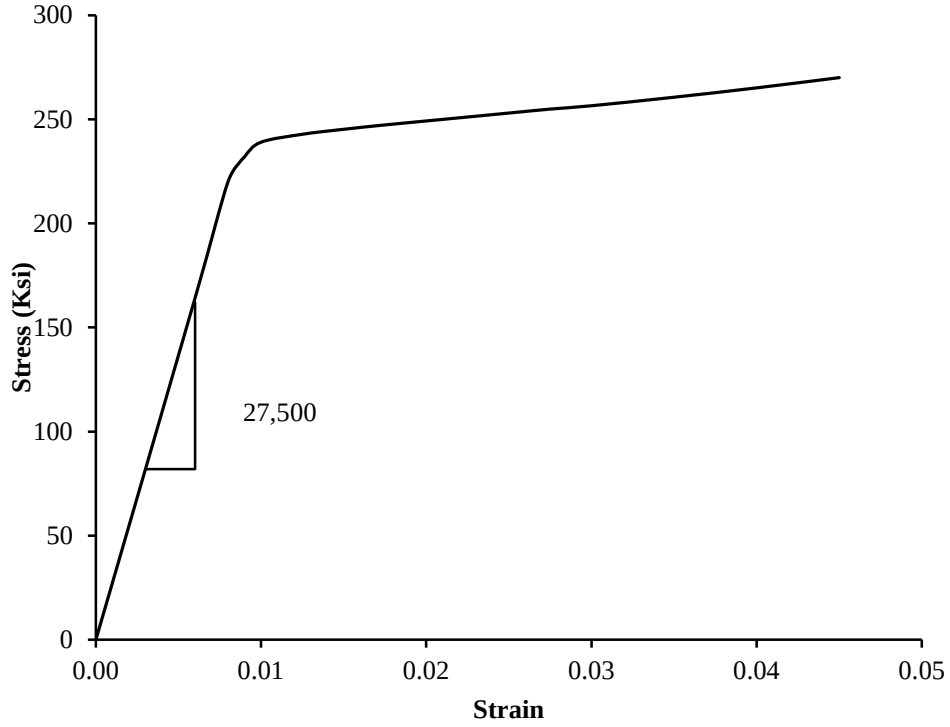

Figure 4.4: Stress-strain behavior of post-tensioning steel from experiments conducted at Lehigh University

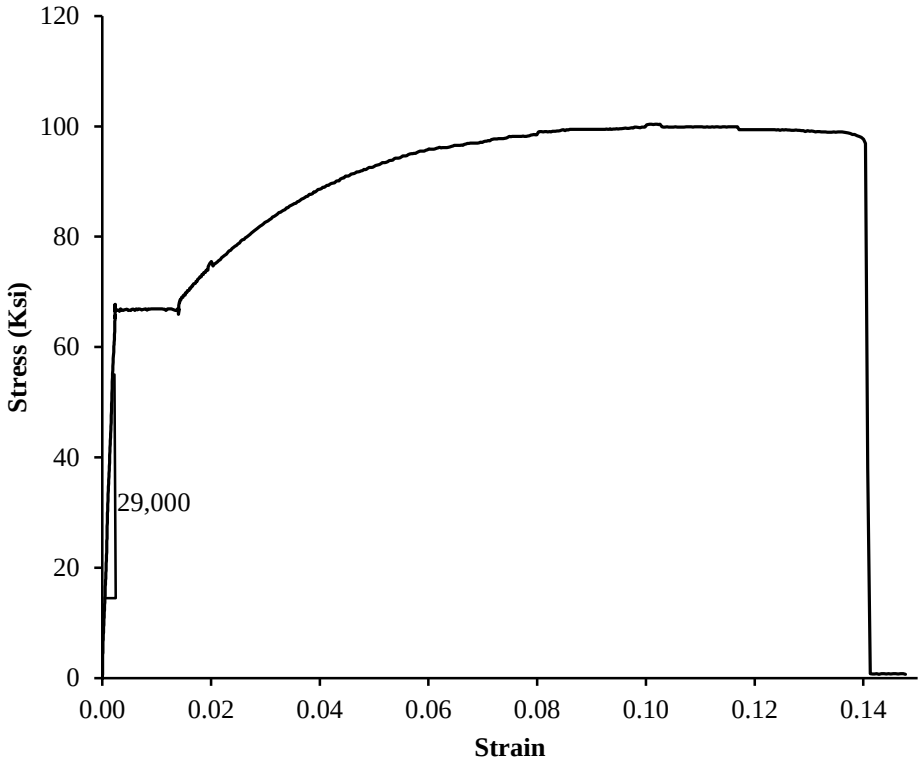

Figure 4.5: Stress-strain behavior of mild steel (ASTM A615) from experiments conducted at Lehigh University

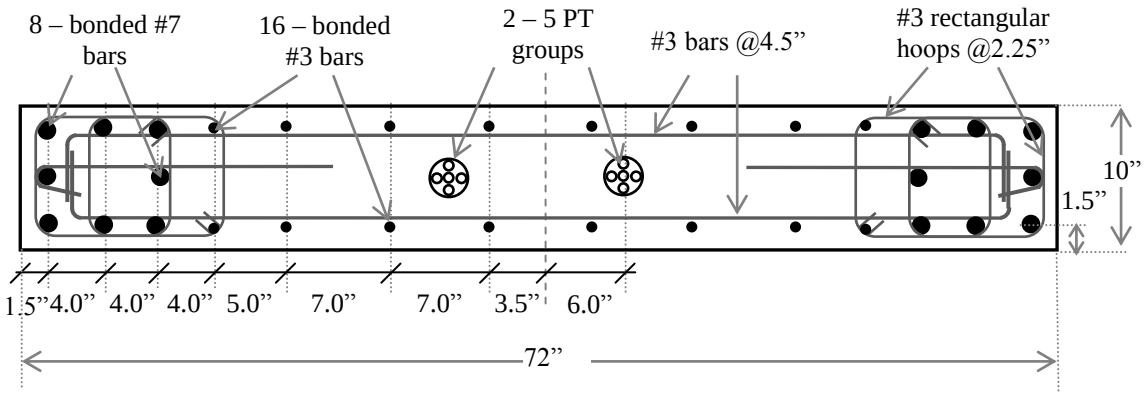

Figure 4.6: Cross-section of PW1.0.0with bonded reinforcement

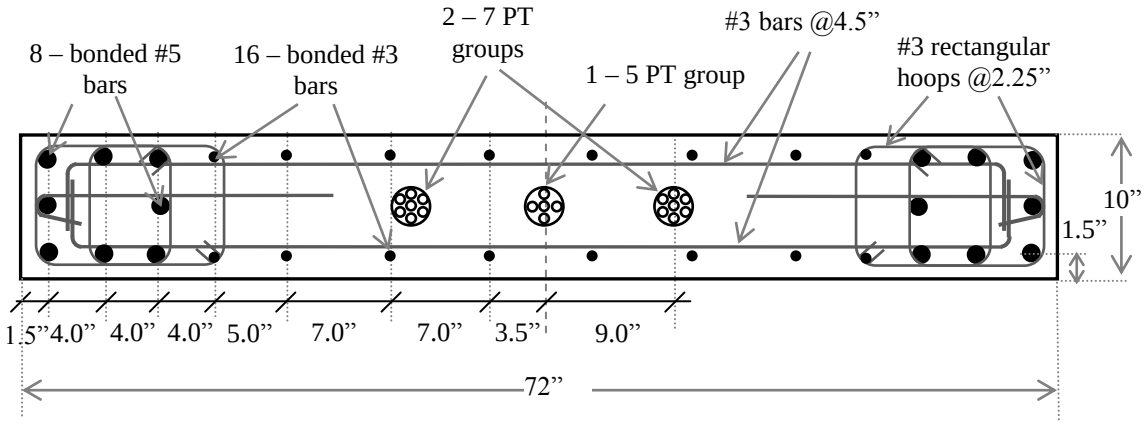

Figure 4.7: Cross-section of PW2.0.0 with bonded reinforcement

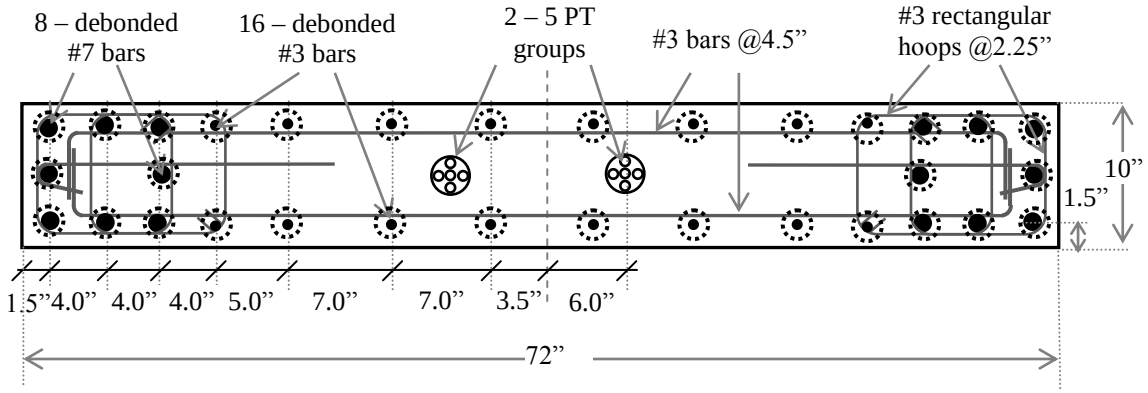

Figure 4.8: Cross-section of PW3.0.0 with debonded reinforcement

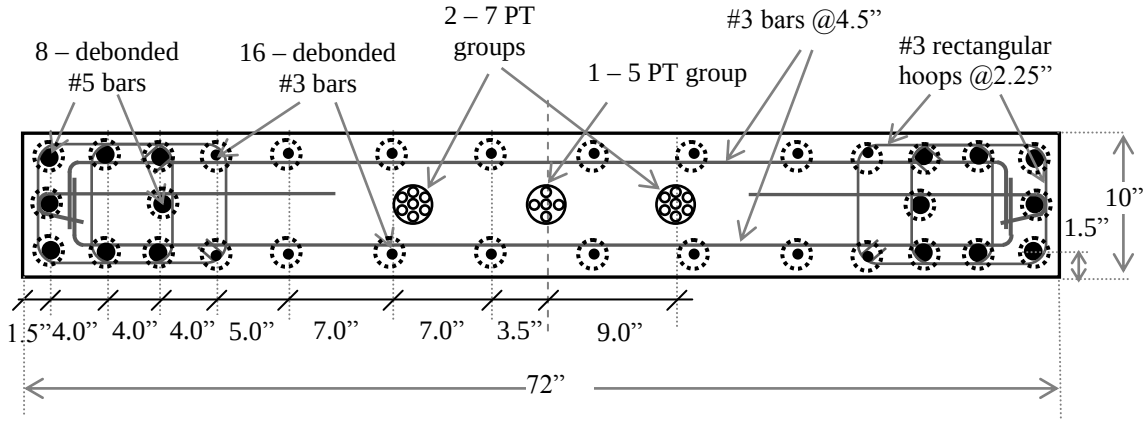

Figure 4.9: Cross-section of PW4.0.0 with debonded reinforcement

CHAPTER 5

ANALYTICAL MODELING OF PARAMETRIC BASE WALLS IN DRAIN-2DX

This chapter discusses the analytical models created to analyze the behavior of the parametric base walls as described in Chapter 4. The analytical models are based on a fiber model approach developed by Kurama et al. (1997) for unbonded post-tensioned precast walls. The DRAIN-2DX program developed by Prakash and Powel (1993) is used in these analyses. The analytical models discussed in this chapter use the fiber beam-column element and truss elements of the program.

A brief description of the fiber model is presented in Section 5.1, followed by modeling assumptions in Section 5.2, and details of the fiber models developed for the four parametric base walls in Section 5.3. Section 5.4 briefly discusses the loads acting on the parametric walls, and Section 5.5 compares the results obtained from the DRAIN-2DX analytical models with results from the closed-form expressions derived in Chapter 3.

5.1 INTRODUCTION TO DRAIN-2DX FIBER MODEL

DRAIN-2DX is a non-linear analysis program which models a structure as a 2-D assemblage of non-linear elements connected at nodes (Prakash and Powel, 1993). The nodes can have three degrees of freedom (DOFs), two translations about X and Y-axes and one rotation about Z-axis. The nodes can be restrained or slaved to limit the DOFs. These nodes are also used for applying any mass or load acting on the structure. The program uses element groups to model components of the structure. The element groups consist of one or more elements of the same type. The program allows a variety of analyses such as gravity analysis, static analysis, cyclic analysis and dynamic analysis. It also has the capability to incorporate P-delta effects.

In the current study, the fiber model developed by Kumara et al. (1997) for non-linear inelastic axial-flexure behavior of unbonded post-tensioned precast walls has been used as a basis to develop analytical models for the four parametric base walls discussed in Chapter 4. Figure 5.1 shows a simplified fiber beam-column element discretization of a cast-in-place concrete wall with unbonded post-tensioning steel. The fiber model uses truss elements to model the uniaxial behavior of the unbonded post-tensioning steel, and fiber beam-column elements to model the axial-flexural behavior of concrete portion of the wall. The fiber beam-column elements are located between two nodes and centered at a longitudinal reference axis as shown in Figure 5.1(b). Figure 5.1(c) shows that the fiber element can be divided into two or more segments. Each segment has a control section, called the fiber slice, at the middle of each segment. The fiber slice has a series of steel and concrete fibers, each identified by three features: uniaxial material stress-strain relationship, area of the fiber, and distance of the fiber from the longitudinal reference axis, as shown in Figure 5.2.

5.2 ANALYSIS AND MODELING ASSUMPTIONS FOR MATERIAL PROPERTIES

In order to model the parametric base walls in DRAIN-2DX some simplifying assumptions were made to address the inherent modeling limitations of the program.

These assumptions may pertain to geometry of the wall, loading on the wall, material properties and response of the wall. The following assumptions were made:

1. The wall is treated as a two-dimensional structure, i.e., it can undergo only in-plane axial, flexural, and shear deformations. Out of plane response of the walls is ignored.
2. The gravity and lateral forces act in the plane of the wall.
3. The PT anchorage is perfect and remains intact throughout the analysis.
4. Bond between longitudinal mild steel reinforcement and surrounding concrete is perfect and no slippage occurs.
5. The foundation of the wall is assumed to be rigid and does not contribute directly towards lateral load response of the walls.

5.2.1 Idealization of PT Steel Stress-Strain Relationship

The PT steel groups are modeled as inelastic truss bar elements in DRAIN-2DX analytical models. The inelastic truss bar element of DRAIN-2DX uses bilinear idealization of the stress-strain relationship, i.e., it requires Young's modulus (E_p), the yield stress (f_{py}), and a strain hardening ratio (E_h/E_p) for modeling the material properties. Figure 5.3 shows the typical stress-strain relationship for grade 270 low relaxation strands with 0.5 in. diameter, area 0.217 in.^{2}, obtained from laboratory test conducted at Lehigh University and the corresponding idealization used in the fiber model. Figure 5.3 indicates that the PT strands do not have a clear yield point, therefore, yielding of the strands is assumed to take place at a yield strain, ε_{py}, of 0.008 with a yield stress, f_{py}, 220 ksi. Young's elastic modulus, E_p, is taken as 27500 ksi. The ultimate strain, ε_{pu}, of the strands is assumed to be 0.045 with constant strain hardening rate up to the ultimate stress f_{pu}, of 270 ksi.

5.2.2 Idealization of Longitudinal Reinforcement Stress-Strain Relationship

The longitudinal mild steel reinforcement is modeled differently in the two cases considered. For walls with bonded reinforcement, it is modeled using fibers in the fiber element. For walls with debonded reinforcement, it is modeled using inelastic truss bar elements.

The parametric walls are assumed to be reinforced with ASTM A615 Grade 60 steel reinforcement bars. Figure 5.4 shows the typical stress-strain relationship of ASTM A615 Grade 60 steel reinforcement bar obtained from a tensile test at Lehigh University and the corresponding idealization used in the fiber model for bonded and debonded longitudinal reinforcement cases. For both the cases, yielding is expected to occur at a yield strain, ε_{sy}, of 0.00227 in./in. with an expected yield stress, f_{sy}, of 66 ksi. However, in the case of bonded longitudinal reinforcement, bonding between concrete and reinforcement causes flexural and shear cracking in the wall which is expected to reduce the ultimate strain capacity of the bonded reinforcement upon load reversal. Therefore, in consideration of strain concentration at the cracks, the ultimate strain, ε_{su}, for bonded longitudinal reinforcement, is reduced to 0.072 in./in. (60% of the typical test value) with an ultimate stress, f_{su}, of 99 ksi. For the debonded longitudinal reinforcement 100% of

the expect ultimate strain of 0.12 in./in. is used with the same ultimate stress, as no stress concentration at cracks is expected.

5.2.3 Idealization of Concrete Stress-Strain Relationship

The fiber element in DRAIN-2DX requires the stress-strain of concrete fibers to be defined using a maximum of five-segment piecewise linear idealization. Figure 5.5 shows the concrete compressive stress-strain relationship for concrete obtained using the Mander model (Mander et al. 1988a, 1988b), for the rectangular hoop confinement geometry shown in Figures 4.6 to 4.9. The corresponding idealization used in the fiber model is also shown in Figure 5.5. The confined concrete compressive strength, f'_{cc}, is calculated to be 11.0 ksi using the expected unconfined concrete strength, f'_c, of 7.8 ksi, and the expected yield stress, f_{sy}, of 66 ksi for the mild steel confining reinforcement. The corresponding ultimate strain capacity ε_{cu} is 0.054 in./in. A different idealization of the descending branch of the unconfined concrete was used for bonded and debonded longitudinal reinforcement cases to achieve convergence of DRAIN-2DX analyses. This difference in descending branch did not give a significant difference in the base moment-drift response of the analytical models, as reported in Perez (2004).

The compressive strain in a concrete fiber can exceed the last specified strain value in the model but the stress remains constant at the last specified stress value, represented as horizontal line segment in Figure 5.5 (Perez 2004). Therefore, in order to determine CCC, crushing of confined concrete, strain in the outermost fiber was computed and compared with ε_{cu} to determine the occurrence of CCC.

5.3 DETAILS OF DRAIN-2DX FIBER WALL MODELS

This section discusses the DRAIN-2DX fiber models developed for the parametric base walls used to study the closed-form expressions derived in Chapter 3 and described in Chapter 4. The models use the elements described in Section 5.1 and the assumptions and material models described in Section 5.2. PW1.0.0 and PW2.0.0 are examples with bonded longitudinal mild steel reinforcement, and PW3.0.0 and PW4.0.0 are examples with debonded longitudinal mild steel reinforcement.

5.3.1 Parametric Base Wall 1 (PW1.0.0)

Figure 5.6(a) shows the reinforcement detailing of PW1.0.0, Figure 5.6(b) shows the elevation of PW1.0.0 and its analytical discretization, and Figure 5.6(c) shows the fiber arrangement of the wall section in the first fiber element. The model consists of six fiber elements centered at longitudinal reference axis and the arranged vertically using seven nodes at 50 in. Each fiber element consists of 14 bonded mild steel fibers, 10 unconfined concrete fibers and eight confined concrete fibers distributed symmetrically about the longitudinal reference axis. The fiber elements are subdivided into four segments. The first segment of the first fiber element is 16.5 in which is the critical confined concrete crushing height (H_{cr}) for PW1.0.0 calculated from the section detailing shown in Figure 5.6(a). The remaining fiber segments are evenly sized. The two PT steel groups are modeled as two truss bar elements connected longitudinally through seven nodes each, with 6 in. eccentricity on either side of the longitudinal reference axis. All the truss bar

element nodes are slaved to the corresponding fiber element nodes to restrain displacement in the horizontal direction, i.e., the horizontal displacement of truss bar element nodes is same as that of the corresponding fiber element nodes. The vertical displacement of the fiber element nodes and the truss bar nodes are different to model unbonded behavior. At the ends of the unbonded height of the PT steel, the vertical displacement of the truss bar elements nodes are fully slaved to the corresponding fiber element nodes to model the anchorage of the PT steel.

5.3.2 Parametric Base Wall 2 (PW2.0.0)

Figure 5.7 shows reinforcement detailing of PW2.0.0, the elevation of PW2.0.0 and its analytical discretization, and the fiber arrangement of the wall section. As for PW1.0.0, this model also consists of six fiber elements, each 50 in. high and containing 14 bonded mild steel fibers, 10 unconfined concrete fibers and eight confined concrete fibers distributed symmetrically about the longitudinal reference axis. The fiber elements are subdivided into four segments. The first segment of the first fiber element is 16 in. which is the critical confined concrete crushing height (H_{cr}) for PW2.0.0 calculated from the section detailing shown in Figure 5.7(a). The remaining fiber segments are evenly sized. The three PT steel groups are modeled as three truss bar elements connected longitudinally through seven nodes each, with two elements at 9 in. eccentricity on either side of the longitudinal reference axis and one centered at the longitudinal reference axis, aligned with the fiber element. All the truss bar element nodes are slaved to the corresponding fiber element nodes as described for PW1.0.0.

5.3.3 Parametric Base Wall 3 (PW3.0.0)

Figure 5.8 shows the reinforcement detailing of PW3.0.0, the elevation of PW3.0.0 and its analytical discretization, and the arrangement of fibers of the wall section in the fiber element. The model consists of seven fiber elements centered at longitudinal reference axis and arranged vertically using eight nodes. The height of the first fiber element is 24 in., i.e. debonded height of the longitudinal mild steel reinforcement, second fiber element is 26 in. and the remaining five are 50 in. each. The first fiber elements is subdivided into two segments, with first segment 16.5 in. high which is the critical confined concrete crushing height (H_{cr}) for PW3.0.0 calculated from the section detailing. The remaining fiber elements are subdivided into four segments of equal size. The first fiber element consists of 10 unconfined concrete fibers and eight confined concrete fibers distributed symmetrically about the longitudinal reference axis, as shown in Figure 5.8(c). The remaining fiber elements consist of 30 fibers, which are same as in case of PW1.0.0. The two PT steel groups are modeled as two truss bar elements connected longitudinally through eight nodes each, with 6 in. eccentricity on either side of the longitudinal reference axis. The 24 in. debonded height of the longitudinal mild steel reinforcement is modeled as truss bar elements with stress-strain properties as discussed earlier. The nodes of the truss bar elements which model the PT steel are slaved as described for PW1.0.0. The nodes of the truss bar elements which model the debonded longitudinal mild steel reinforcement are fully slaved at the ends to the corresponding

fiber element nodes to model bonding of the longitudinal mild steel reinforcement at the ends.

5.3.1 Parametric Base Wall 4 (PW4.0.0)

Figure 5.9 shows the reinforcement detailing of PW4.0.0, the elevation of PW4.0.0, and its analytical discretization, and the arrangement of fibers of the wall section in the first fiber element. Similar to PW3.0.0, the fiber model consists of seven fiber elements centered at the longitudinal reference axis and arranged vertically using eight nodes. The height of the first fiber element is 24 in. which is the debonded height of the longitudinal mild steel reinforcement. The height of the second fiber element is 26 in. and the remaining fiber elements are 50 in. each. The first fiber elements is subdivided into two segments, with first segment 16 in. high which is the critical confined concrete crushing height (H_{cr}) for PW4.0.0 calculated from the section detailing. The remaining fiber elements are subdivided into four segments of equal size. Figure 5.9(c) shows the arrangement of 10 unconfined concrete fibers and eight confined concrete fibers in the first fiber element. The remaining fiber elements consist of 30 fibers, which are the same as in case of PW2.0.0. The three PT steel groups are modeled as three truss bar elements connected longitudinally through eight nodes each, with two elements at 9 in. eccentricity on either side of the longitudinal reference axis and one centered at the longitudinal reference axis, aligned with the fiber element. The 24 in. debonded height of the longitudinal mild steel reinforcement is modeled as truss bar elements with stress-strain properties as discussed earlier. The nodes of the truss bar elements which model the PT steel are slaved as described for PW1.0.0. The nodes of the truss bar elements which model the debonded longitudinal mild steel reinforcement are fully slaved at the ends to the corresponding fiber element nodes to model bonding of the longitudinal mild steel reinforcement at the ends.

5.4 MODELING OF LOADS

There are three types of load acting on the parametric base walls: (i) the post-tensioning forces; (ii) the gravity load due to self-weight; and (iii) the lateral load at 150 in from the base of the wall. In the fiber model, post-tensioning forces are implemented as initial forces in the truss bar elements. The self-weight is calculated to be 18.75 kip, and applied as vertical force acting at the mid-height of the wall. The lateral load is applied as a horizontal force acting at 12 feet and 6 inches from the base of the wall, as shown in Figure 5.10.

5.5 ANALYSES TO VALIDATE CLOSED-FORM EXPRESSIONS

Table 5.1 summarizes the availability of results from fiber model analysis and closed-form expressions lateral load responses for the limit states considered in this research. For each parametric base wall, the moment acting at the base of the wall and the lateral drift of the wall at 12 feet and 6 inches from the base of the wall (the location of the applied lateral load) were estimated for the limit states of DEC, ELL, YMS, FMS, LLP, and CCC using the closed-form expressions derived in Chapter 3 and material properties presented in Chapter 4. The fiber models described in Section 5.3 were used to estimate the values for the limit states of DEC, YMS, FMS, LLP and CCC. Tables 5.2 to 5.5 and Figures

5.11 to 5.14 summarize the results obtained from the two methods. The closed-form expressions results are in good agreement with the fiber model results. The following observations are made:

1. The base moment for ELL1, the effective linear limit state when 25% of the section is in compression, are in close agreement. The ELL1drift values show large differences. These differences are attributed to the simplifying assumption of a triangular stress distribution in concrete made in deriving the closed-form expressions. This assumption may not be accurate depending on the prestressing force, gravity load, and the reinforcement; the concrete may be nonlinear at this limit state. This behavior is incorporated in the fiber model through appropriate material properties.
2. In general, the base moment values from the closed-form expressions are less than those from the fiber model analysis, except for the limit state of yielding of mild steel reinforcement ELL4 (YMS). This difference was observed because derivation of the closed-form expression was based on the assumption that the unconfined concrete is nonlinear at this limit state. However, the fiber model analysis shows that the entire wall section in compression was not in linear elastic. Therefore, locations of the resultant vertical forces were different in the fiber model and the closed-form expressions.
3. The analytical model results for drift at LLP are smaller than those from the closed-form expressions. This is essentially because neutral axis depth is larger for the closed-form expressions. The larger neutral axis depth in closed-form expressions gives a larger rigid body rotation at the base of the wall. Therefore, the total lateral deflection at the roof is larger for the results of closed-form expression at LLP. In the analytical mode, smaller neutral axis depth at LLP is expected as a result of the unconfined concrete model. In closed-form expressions, unconfined concrete is assumed to have spalled at LLP; however, the unconfined concrete does contribute to compressive forces in the analytical models.
4. Debonding the longitudinal mild steel reinforcement significantly increases the drift value of the walls for FMS, LLP and CCC, provided all other parameters remain constant. This can be observed by comparing the results of PW1.0.0 with PW3.0.0 and the results of PW2.0.0 with PW4.0.0.
5. Debonding the longitudinal mild steel reinforcement decreases the base moment values for the limit state of LLP because debonding the mild steel distributes the mild steel deformation over the debonded height. Therefore, the strain in the longitudinal mild steel reinforcement at LLP reduces which in turn reduces the force and moment contribution from the debonded longitudinal mild steel reinforcement. However, the base moment values for the limit states of FMS and CCC are higher for the debonded cases.
6. At CCC difference in base moment values closed-form expressions and analytical models are high for the parametric base walls with debonded longitudinal mild steel reinforcement compared to the bonded longitudinal mild steel reinforcement

cases. This effect is caused by the use of truss bar element in the analytical model for the debonded longitudinal mild steel reinforcement which could not be designed to have zero or constant stress after the ultimate strain was achieved. Therefore, stresses (and hence forces) in the reinforcement bar(s) continued to increase after the limit state of FMS was achieved, leading to large difference between the results.

7. At CCC the fiber model result for drift is larger than the closed-form expression result for PW3.0.0. However, it is smaller than the closed-form expression result for PW4.0.0. This difference may be caused by a combination of factors including total area of PT steel, total initial PT force, area of the longitudinal mild steel reinforcement, and difference in material properties considered for the two cases. In deriving the closed-form expressions, it is assumed that the unconfined concrete cover is spalled which is not the case in analytical models. In analytical models the unconfined concrete cover is still contributing at a constant stress. Also, the debonded mild steel reinforcement is modeled as truss bar element in the analytical model. As explained earlier, stresses in the reinforcement bar(s) continue to increase after the limit state of FMS was achieved. However, according to the material model used in the closed-form expressions, stress remains constant in debonded mild steel after the limit state of FMS.
8. The DRAIN-2DX base moment-roof drift results for PW2.0.0 and PW4.0.0 shows a dip at around 5% drift as in Figures 5.12 and 5.14. This dip can be attributed to two factors; detailing of these walls and stress-strain model of confined concrete used in the fiber models. These two walls have 2.48 $in.^2$ longitudinal reinforcement in the boundary and three groups of 19 PT strands with total PT steel area of 4.123 $in.^2$. Therefore, compared to PW1.0.0 and PW3.0.0, concrete at the toe of these two parametric base walls is under higher strain state at any given limit state because of larger forces exerted by the PT steel. Due to higher strains in PW2.0.0 and PW4.0.0, the confined and unconfined concrete fibers are either located on the descending branch of the stress-strain curve or beyond. As strain in the extreme confined concrete fiber in compression crosses 0.006 (ε_{cc}), the stresses in that fiber starts to decline and hence total base moment starts to decline. Once all the confined concrete fibers at the toe of the wall crosses the end of the descending stress-strain branch and becomes constant, the base moment starts to stabilize which is shown in Figures 5.12 and 5.14.

Table 5.1: Matrix indicating availability of results from fiber model (FM) analysis and closed-form expressions (CFE) for the all limit states

	FM	CFE
DEC	√	√
ELL-1	√	√
ELL-2		√
ELL-3		√
ELL-4 (YMS)	√	√
LLP	√	√
FMS	√	√
CCC	√	√

Table 5.2: Analytical fiber model (FM) and closed-form expressions (CFE) results for PW1.0.0

PW1.0.0	Moment (kip-in)			Drift (%)		
	FM	CFE	Difference	FM	CFE	Difference
DEC	4,917	4,731	-4%	0.02	0.02	-13%
ELL1	34,306	33,309	-3%	0.38	0.25	-34%
ELL2	-	36,431	-	-	0.54	-
ELL3 (2.5DEC)	-	11,828	-	-	0.04	-
ELL4 (YMS)	29,124	31,540	8%	0.25	0.18	-27%
FMS	48,702	46,924	-4%	2.91	2.18	-25%
LLP	45,066	47,151	5%	1.89	2.23	18%
CCC	49,545	49,105	-1%	9.13	6.43	-30%

Table 5.3: Analytical fiber model (FM) and closed-form expressions (CFE) results for PW2.0.0

PW2.0.0	Moment (kip-in)			Drift (%)		
	FM	CFE	Difference	FM	CFE	Difference
DEC	8,754	8,504	-3%	0.04	0.03	-19%
ELL1	35,044	33,691	-4%	0.47	0.29	-38%
ELL2	-	34,155	-	-	0.43	-
ELL3 (2.5DEC)	-	21,259	-	-	0.08	-
ELL4 (YMS)	28,488	31,239	10%	0.24	0.18	-23%
FMS	45,348	42,399	-7%	2.46	2.25	-8%
LLP	43,838	42,566	-3%	1.91	2.31	21%
CCC	43,046	44,207	3%	4.91	4.40	-10%

Table 5.4: Analytical fiber model (FM) and closed-form expressions (CFE) results for PW3.0.0

PW3.0.0	Moment (kip-in)			Drift (%)		
	FM	CFE	Difference	FM	CFE	Difference
DEC	4,916	4,731	-4%	0.02	0.02	-15%
ELL1	34,204	32,945	-4%	0.42	0.28	-34%
ELL2	-	35,676	-	-	0.62	-
ELL3 (2.5DEC)	-	11,828	-	-	0.04	-
YMS	29,137	31,706	9%	0.26	0.21	-19%
FMS	48,768	48,092	-1%	5.26	4.98	-5%
LLP	41,888	41,870	0%	1.92	2.14	11%
CCC	53,886	49,174	-9%	10.07	9.30	-8%

Table 5.5: Analytical fiber model (FM) and closed-form expressions (CFE) results for PW4.0.0

PW4.0.0	Moment (kip-in)			Drift (%)		
	FM	CFE	Difference	FM	CFE	Difference
DEC	8,755	8,504	-2.9%	0.04	0.03	-22%
ELL1	34,379	33,412	-2.8%	0.48	0.33	-31%
ELL2	-	33,916	-	-	0.49	-
ELL3 (2.5DEC)	-	21,259	-	-	0.08	-
YMS	28,512	31,480	10.4%	0.25	0.22	-13%
FMS	45,311	44,652	-1.5%	5.73	5.35	-7%
LLP	42,699	40,401	-5.4%	1.91	2.16	13%
CCC	45,400	44,099	-2.9%	5.80	6.44	11%

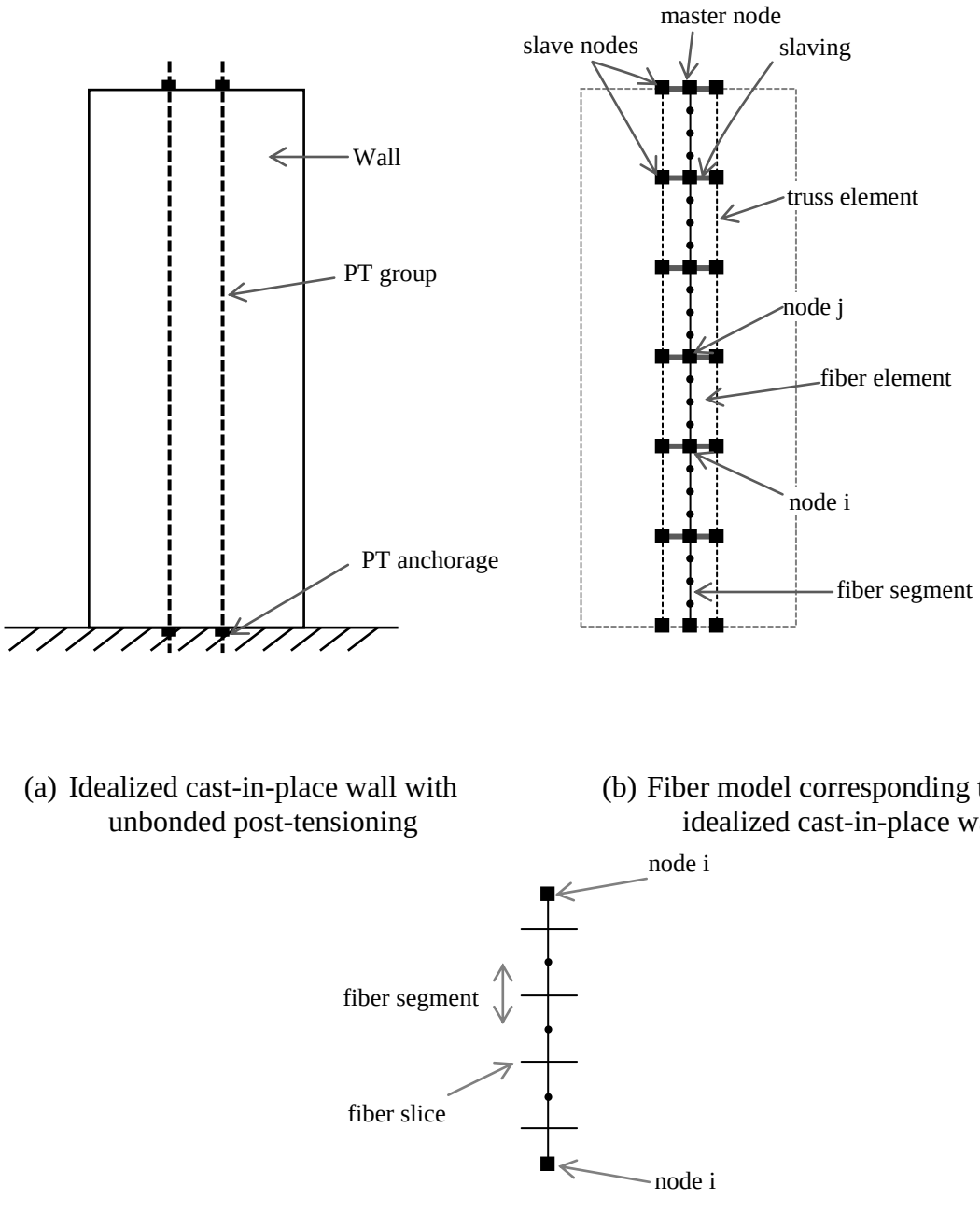

(a) Idealized cast-in-place wall with unbonded post-tensioning

(b) Fiber model corresponding to the idealized cast-in-place wall

(c) Fiber element

Figure 5.1: Typical analytical fiber model

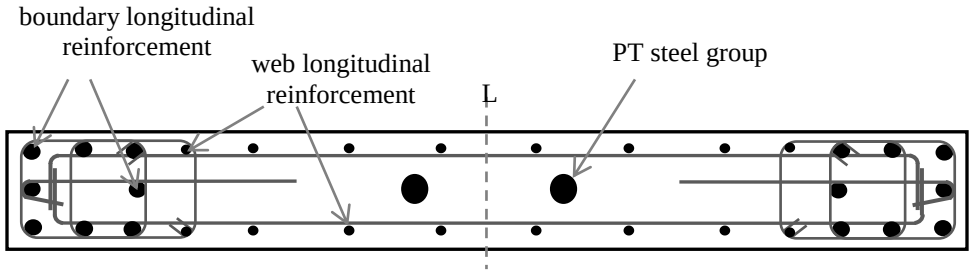

(a) Wall section with longitudinal reinforcement

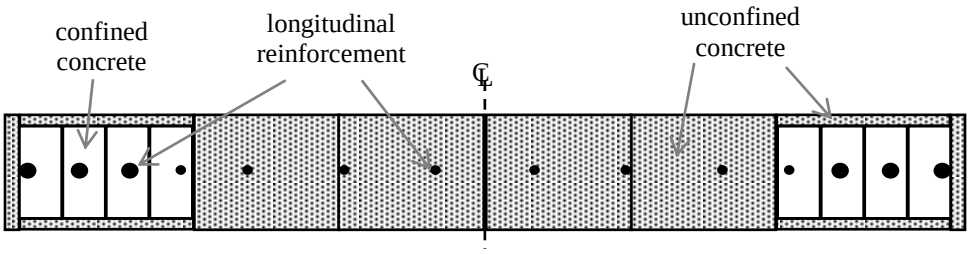

(b) Idealized fiber section

Figure 5.2: Idealization of fiber element section

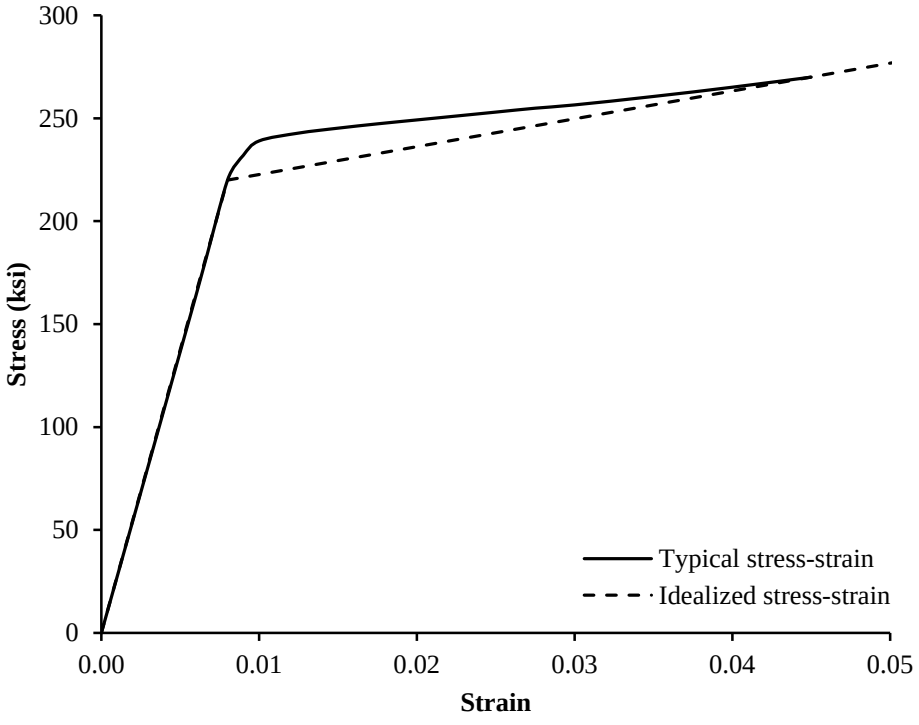

Figure 5.3: Idealized stress-strain relationship for post-tensioning steel

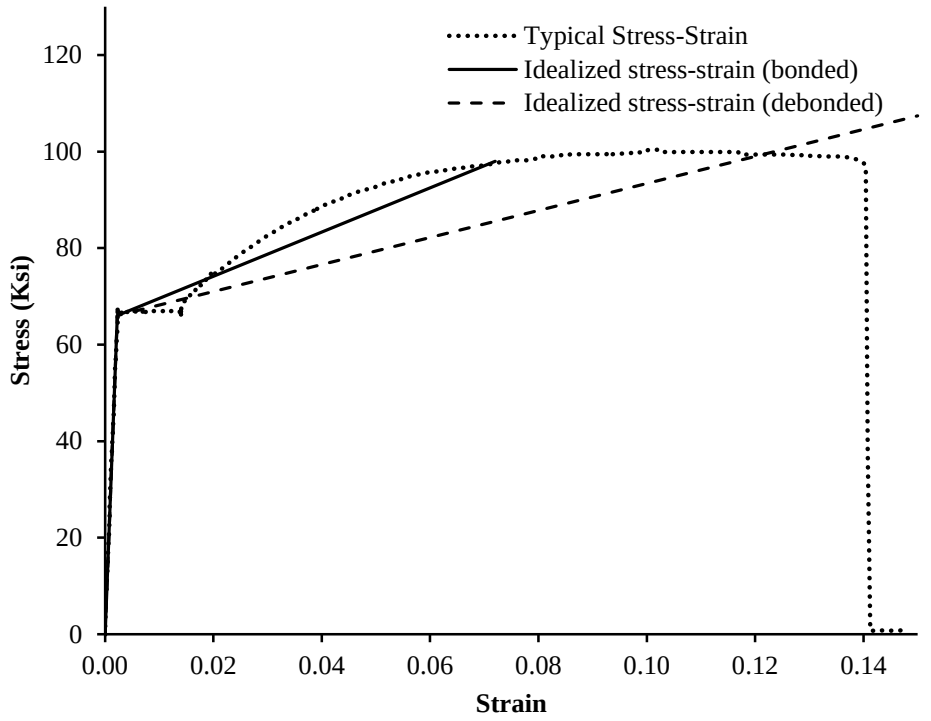

Figure 5.4: Idealized stress-strain relationship for mild reinforcing steel

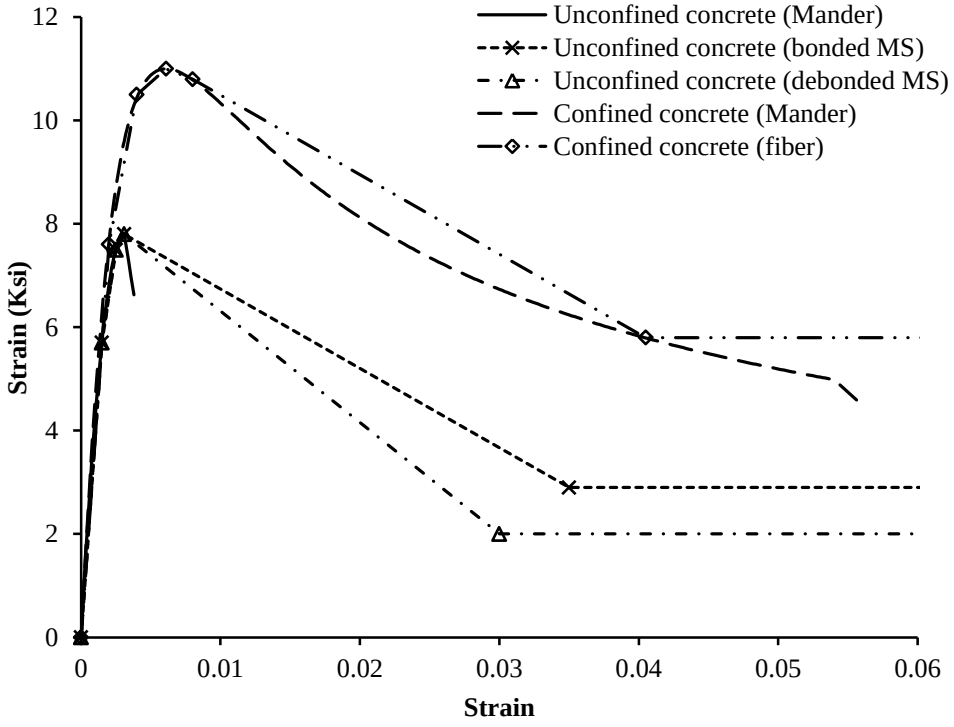

Figure 5.5: Idealized compressive stress-strain relationship for confined and unconfined concrete

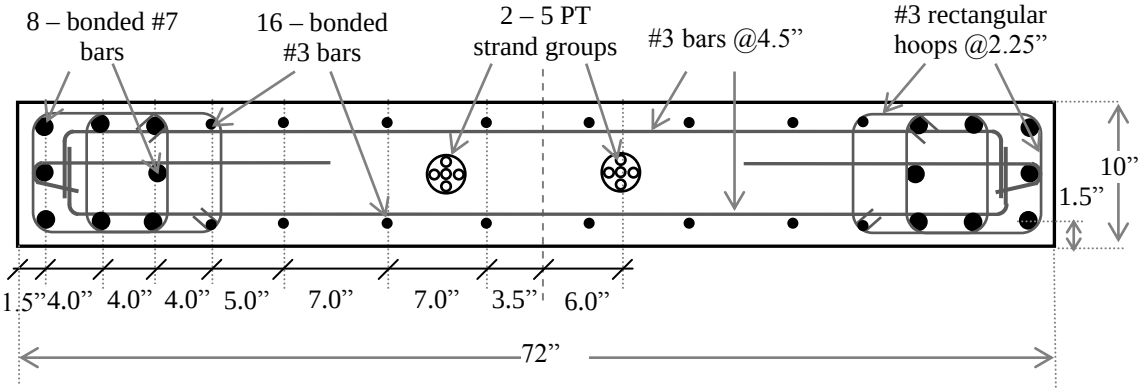

(a) Reinforcement detailing of PW1.0.0

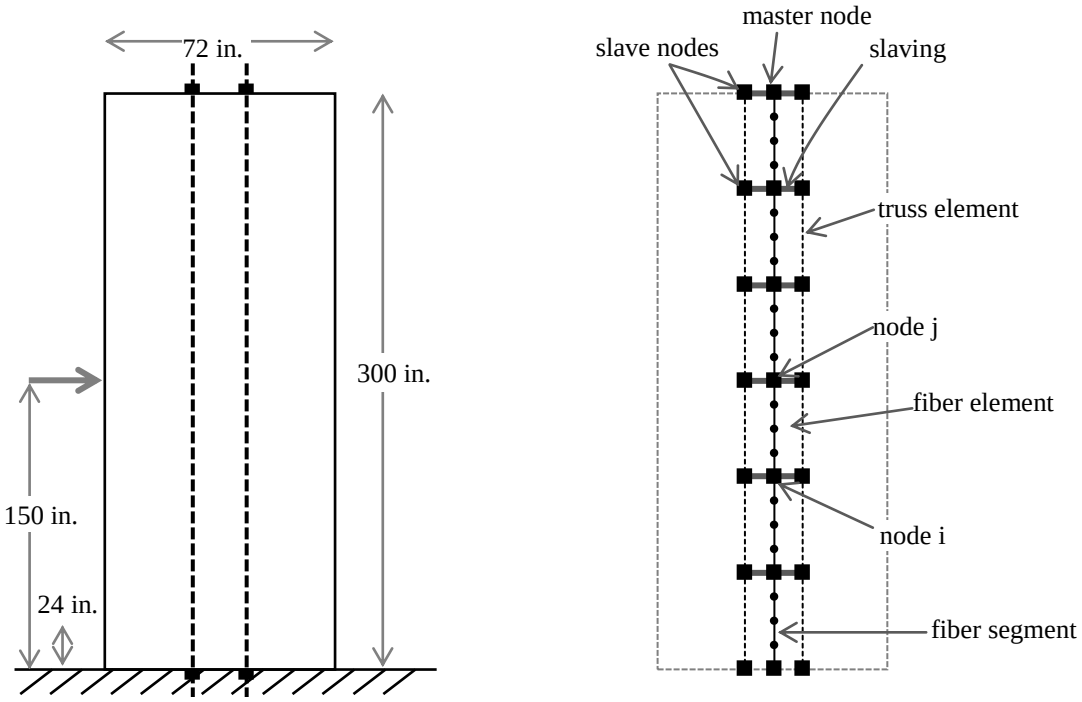

(b) Discretization of PW1.0.0 elevation in analytical model

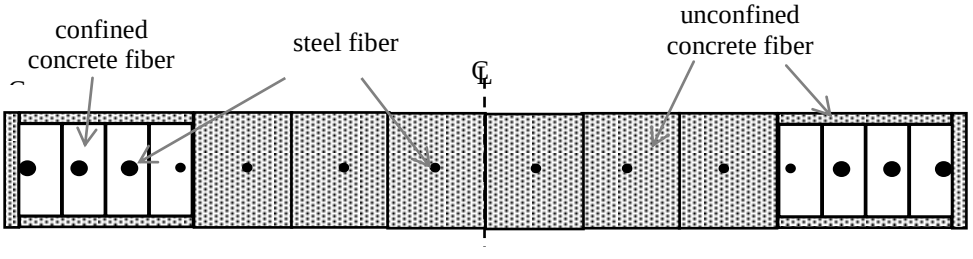

(c) Fiber layout in the wall section

Figure 5.6: Fiber Model for parametric base wall 1 (PW1.0.0)

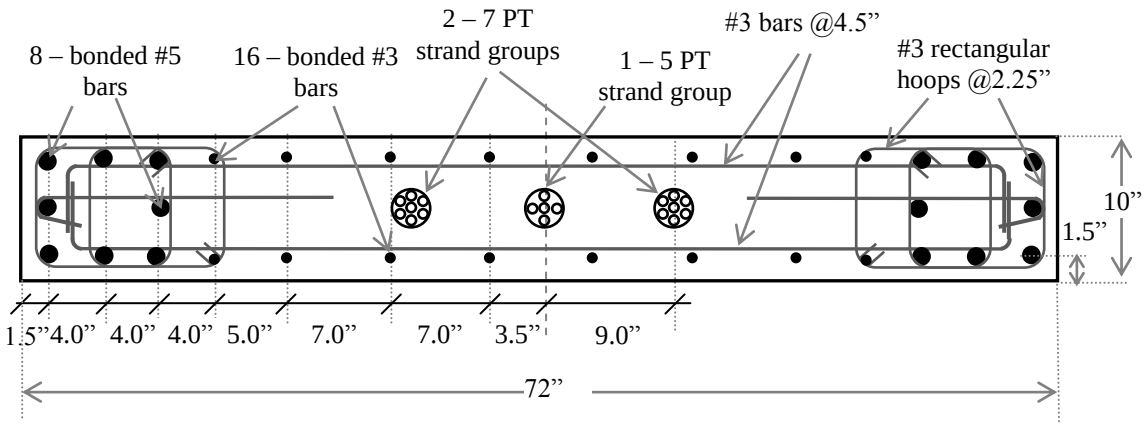

(a) Reinforcement detailing of PW2.0.0

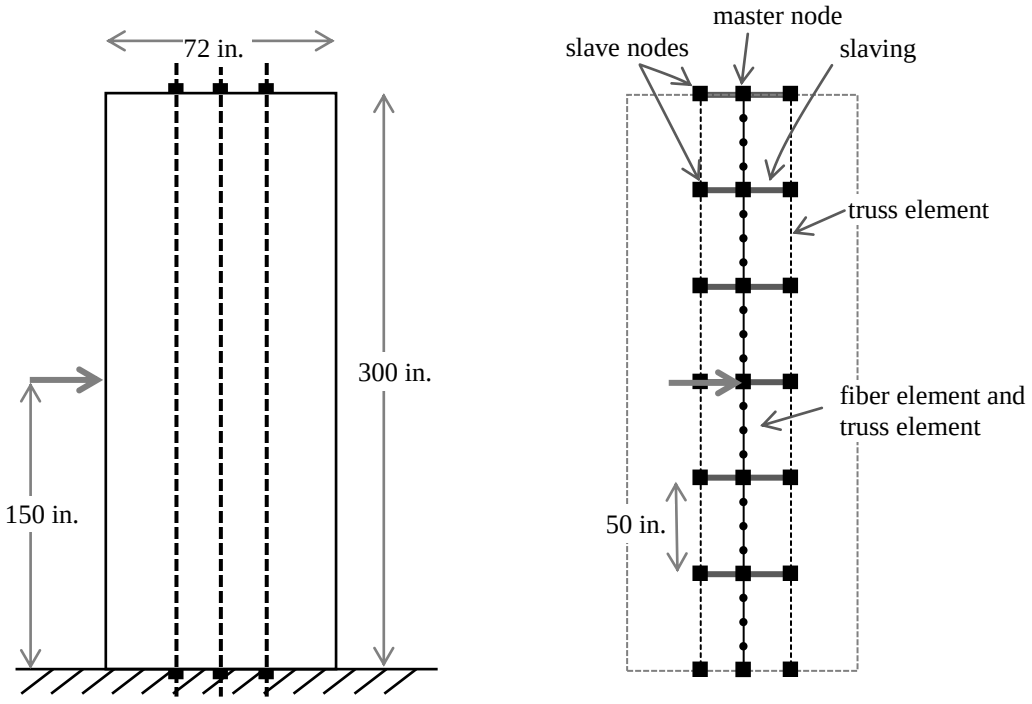

(b) Discretization of PW2.0.0 elevation in analytical model

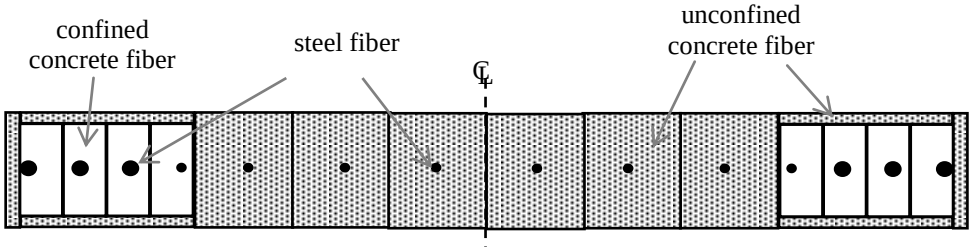

(c) Fiber layout in the wall section

Figure 5.7: Fiber Model for parametric base wall 2 (PW2.0.0)

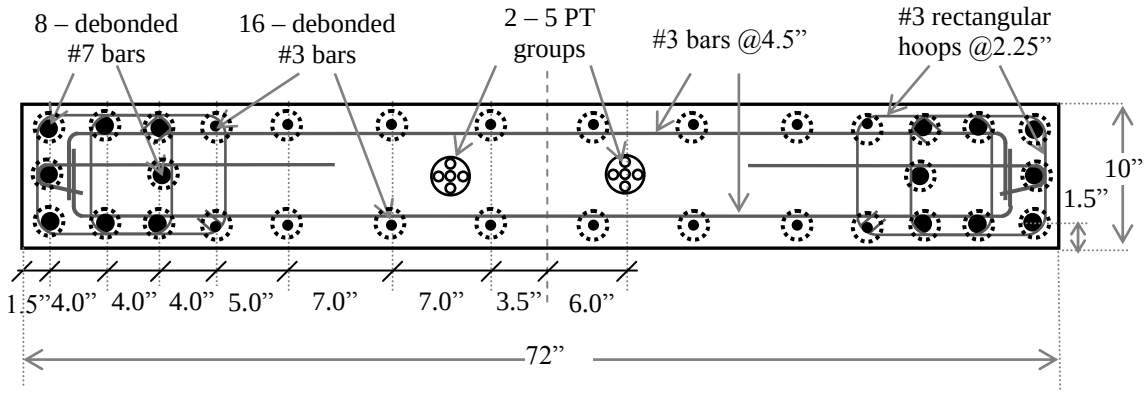

(a) Reinforcement detailing of PW3.0.0

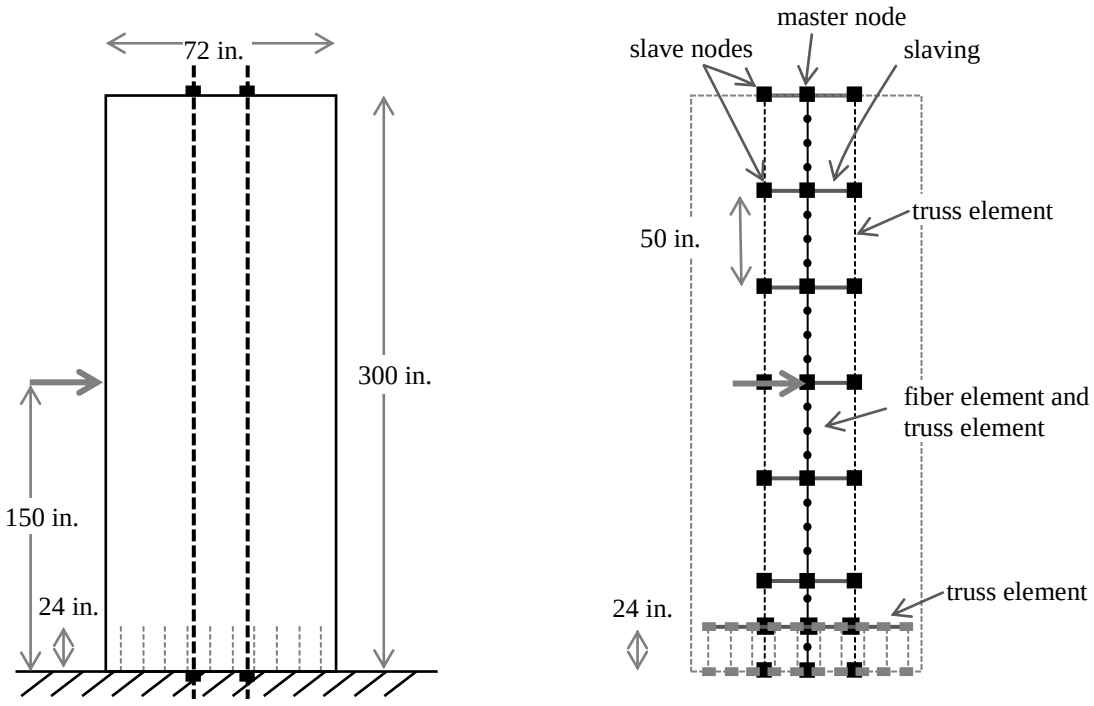

(b) Discretization of PW3.0.0 elevation in analytical model

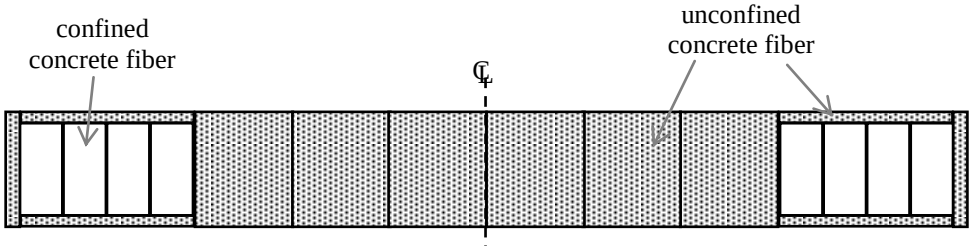

(c) Fiber layout in the first fiber element of wall section

Figure 5.8: Fiber Model for parametric base wall (PW3.0.0)

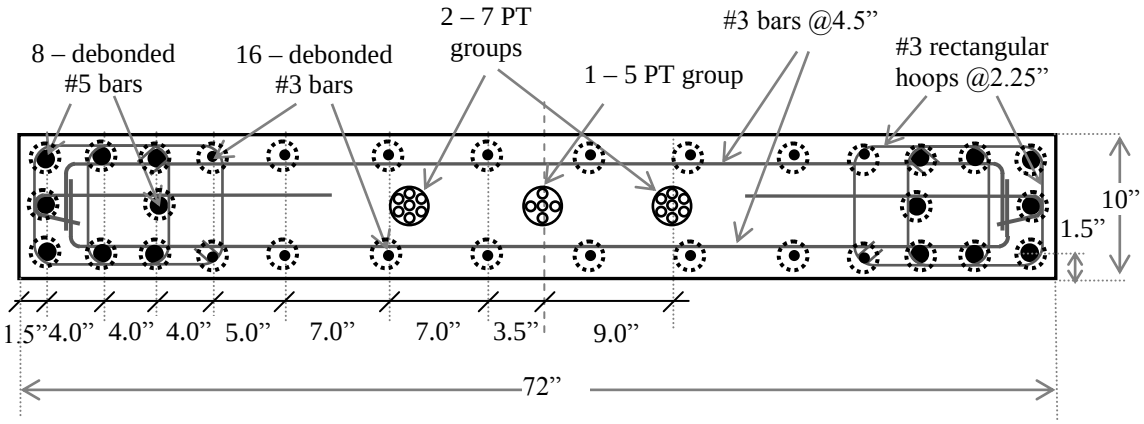

(a) Reinforcement detailing of PW4.0.0

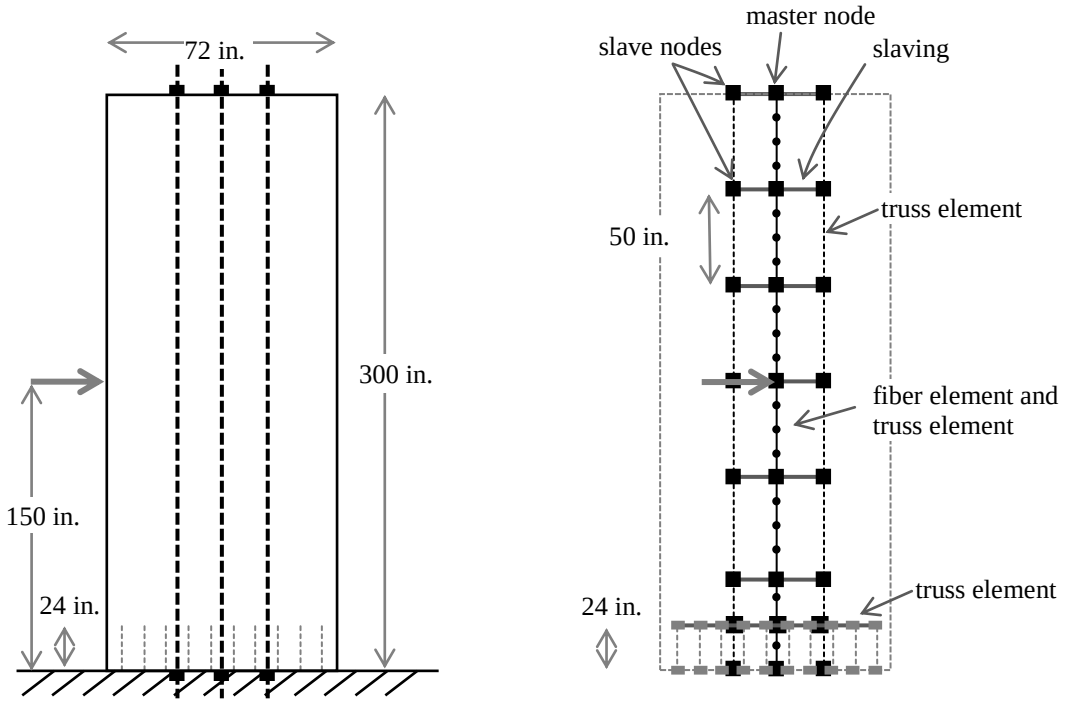

(b) Discretization of PW4.0.0 elevation in analytical model

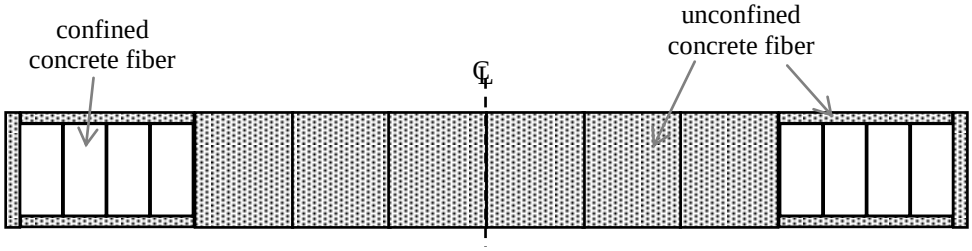

(c) Fiber layout in the first fiber element of wall section

Figure 5.9: Fiber Model for parametric base wall (PW4.0.0)

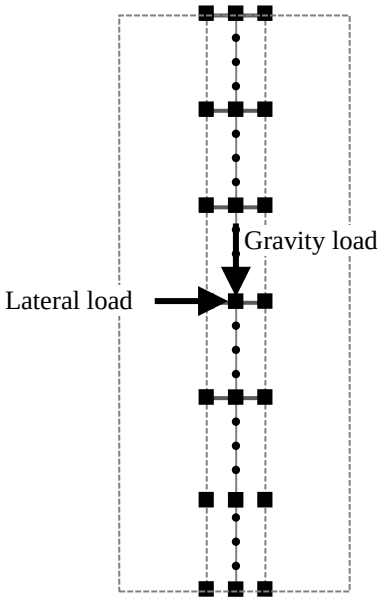

Figure 5.10: Modeling of gravity and lateral seismic loads

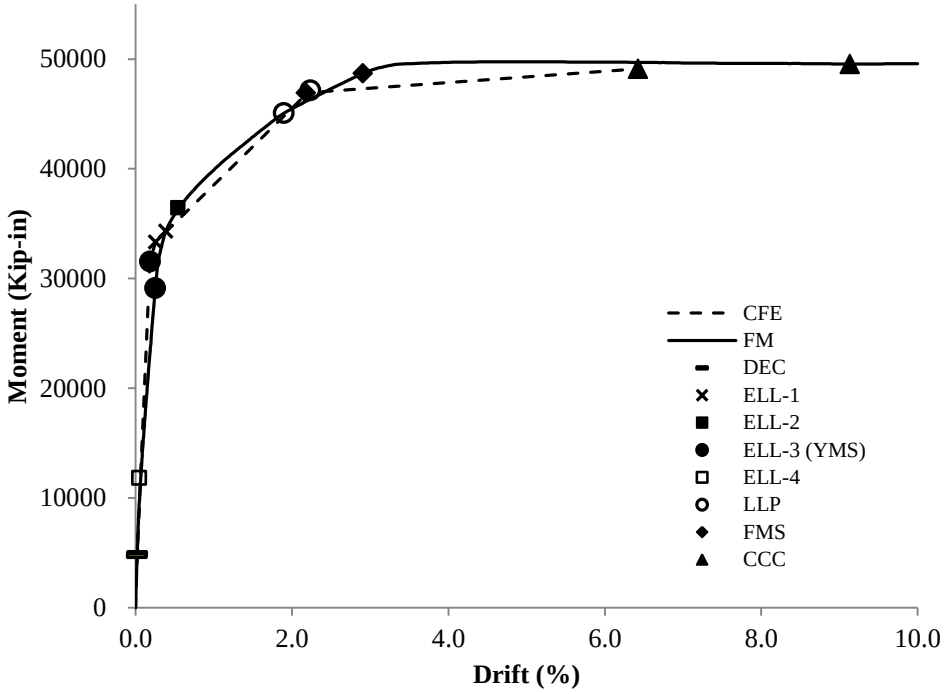

Figure 5.11: Fiber model (FM) analysis and closed-form (CFE) results for PW1.0.0

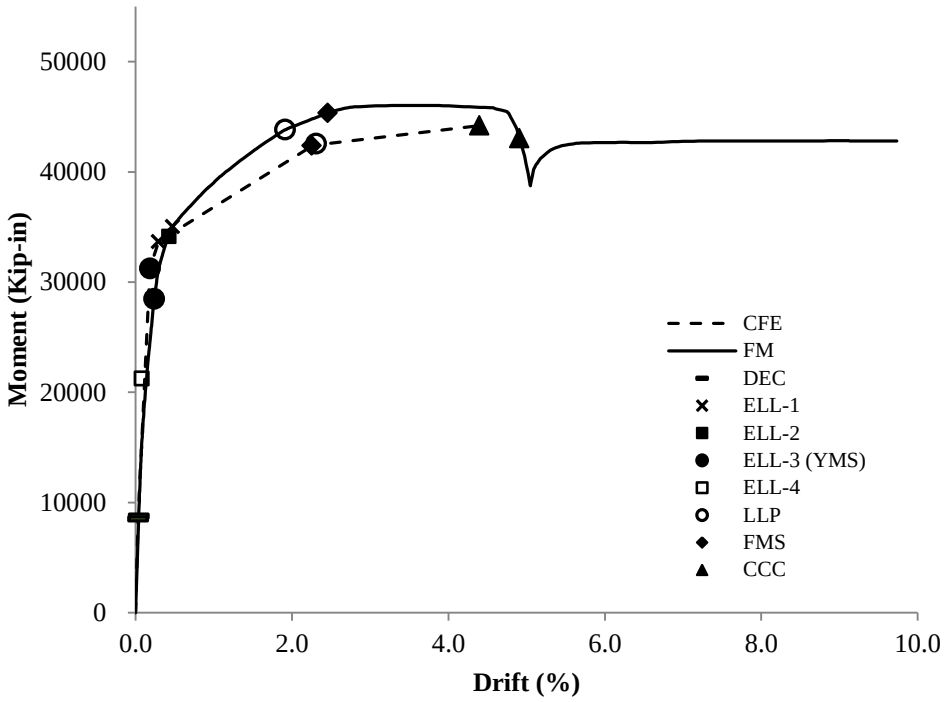

Figure 5.12: Fiber model (FM) analysis and closed-form (CFE) results for PW2.0.0

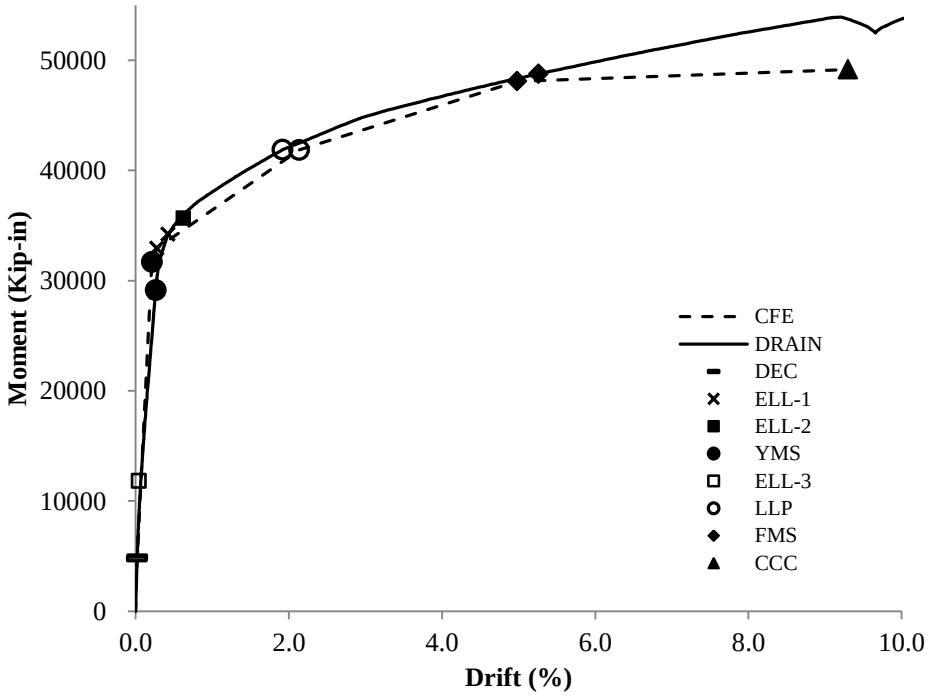

Figure 5.13: Fiber model (FM) analysis and closed-form (CFE) results for PW3.0.0

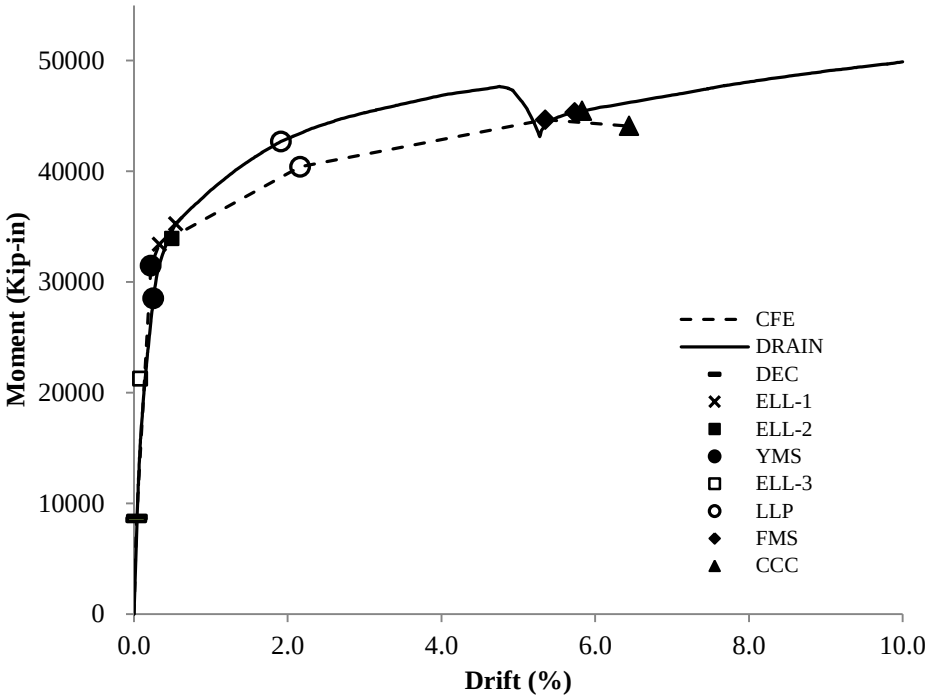

Figure 5.14: Fiber model (FM) analysis and closed-form (CFE) results for PW4.0.0

CHAPTER 6

COMPARATIVE STUDY OF RESULTS OBTAINED FROM CLOSED FORM EXPRESSIONS AND ANALYTICAL MODELING

This chapter discusses results obtained from a series of monotonic lateral load analyses of unbonded post-tensioned cast-in-place concrete walls with longitudinal mild steel reinforcement. A total of 52 walls are studied in this chapter. Four of the walls are the parametric base walls PW1.0.0, PW2.0.0, PW3.0.0, and PW4.0.0, as described in Chapter 4. The remaining 48 walls are systematic variations of the parametric base walls, 12 for each parametric base wall, wherein one or more parameters were varied with respect to the parametric base wall.

Section 6.1 describes the six design parameters investigated in this chapter. The analysis response quantities defined as the lateral load response of the walls are presented in Section 6.2. Finally, Section 6.3 presents and discusses the results of parametric study under monotonic lateral loading.

6.1 DETAILS OF THE PARAMETERS STUDIED

The effect of six design parameters on the static nonlinear lateral load response of unbonded post-tensioned cast-in-place special structural walls with bonded or debonded longitudinal mild steel reinforcement is investigated. The six design parameters are: (1) total area of PT steel with constant initial prestress, (2) initial stress in the post-tensioning steel with constant area of PT steel, (3) variable area of PT steel and initial prestress to produce constant initial prestress force, (4) area of boundary longitudinal mild steel reinforcement with constant spacing, (5) area of web longitudinal mild steel reinforcement with constant spacing, and (6) spacing of web longitudinal mild steel reinforcement with constant area. The study of each design parameter is called a parameter study. The effects of the six parameters are evaluated in terms of the base moment and drift response of 52 walls obtained from two methods: (1) fiber model analysis using DRAIN-2DX program and (2) using closed-form expressions derived in Chapter 3.

6.1.1 Discussion of the Parametric Walls Studied

Tables 6.1 to 6.4 reproduce properties of the four parametric base walls described in Section 4.3, i.e. PW1.0.0, PW2.0.0, PW3.0.0, and PW4.0.0. These four walls are used as the basis for developing 48 more parametric walls, 12 for each parametric base wall.

Table 6.5 lists the 12 parametric walls corresponding to the base case PW1.0.0, two walls for each of the six parameters, and the associated design parameters that have been changed with respect to PW1.0.0. The PT steel area is reduced, from $2.17in^2$, to $1.736in^2$ in PW1.1.1 and increased to $2.604in^2$ in PW1.1.2 with 60% of ultimate strength as initial prestress, leading to change in the total prestress force, all other properties remain unchanged. Similarly, the initial prestress is reduced from 60% to 55% of ultimate strength in PW1.2.1 and increased to 65% in PW1.2.2, with constant PT steel area. For PW1.3.1 and PW1.3.2 the total prestress force is constant at 351.5 kip but initial prestress and total PT area is changed. The area of boundary longitudinal mild steel reinforcement is reduced to $3.0in^2$ in PW1.4.1 and increased to $7.0in^2$ in PW1.4.2 with 8 bar configuration of the parametric base wall. Similarly, the area of web longitudinal mild

steel reinforcement is reduced to 1.0in^2 in PW1.5.1 and increased to 3.0in^2 in PW1.5.2. Lastly, the spacing of web longitudinal mild steel reinforcement is reduced to 4.5in in PW1.6.1 and increased to 9.0in in PW1.6.2 but the area remains unchanged. Similarly, Tables 6.6, 6.7 and 6.8 list detailing of the 12 parametric walls corresponding to PW2.0.0, PW3.0.0 and PW4.0.0, respectively.

6.1.2 Total Area of PT Steel with Constant Initial Prestress

This parameter study is designed to determine the effect of change in the total area of PT steel, with constant initial prestress, on the lateral load response of a post-tensioned cast-in-place special structural wall with bonded or debonded longitudinal reinforcement. The parameter was investigated with the help of four groups of three walls each which are: (i) PW1.1.1, PW1.0.0and PW1.1.2, (ii) PW2.1.1, PW2.0.0 and PW2.1.2, (iii) PW3.1.1, PW3.0.0 and PW3.1.2, and (iv) PW4.1.1, PW4.0.0 and PW4.1.2. Groups (i) and (iii) consist of walls with total PT area of 1.736, 2.17 and 2.604in^2 and groups (ii) and (iv) consist of walls with total PT area of 3.689, 4.123 and 4.557in^2.

6.1.3 Initial Prestress in the PT Steel with Constant PT Steel Area

In the parameter study of initial prestress in PT steel with constant PT steel area, the effect of change in the initial prestress on the lateral load response of a post-tensioned cast-in-place special structural wall with longitudinal reinforcement is studied. As in the previous case, three walls with initial prestress of 55%, 60% and 65% of the ultimate strength of PT steel with total PT steel area as in the four base cases are examined for the four base cases. Therefore, this parameter investigation comprises four groups of three walls: (i) PW1.2.1, PW1.0.0and PW1.2.2, (ii) PW2.2.1, PW2.0.0 and PW2.2.2, (iii) PW3.2.1, PW3.0.0 and PW3.2.2, and (iv) PW4.2.1, PW4.0.0 and PW4.2.2.

6.1.4 Variable Area of PT Steel and Initial Prestress to Produce Constant Initial Prestress Force

This parameter study is examines the effect of change in the total area of PT steel and initial prestress with constant initial prestress force on the lateral load response of a post-tensioned cast-in-place special structural wall with bonded or debonded longitudinal reinforcement. The initial prestress of 55%, 60% and 65% of the ultimate strength of PT steel and the corresponding total PT steel area is used to produce total prestress force of 351.5 kips for base cases of PW1.0.0and PW3.0.0 and 667.9 kips base cases of PW2.0.0 and PW4. Therefore, this parameter investigation comprises four groups of three walls: (i) PW1.3.1, PW1.0.0and PW1.3.2, (ii) PW2.3.1, PW2.0.0 and PW2.3.2, (iii) PW3.3.1, PW3.0.0 and PW3.3.2, and (iv) PW4.3.1, PW4.0.0 and PW4.3.2.

6.1.5 Area of Boundary Longitudinal Mild Steel Reinforcement

This parameter study is designed to analyze the effect of change in the total area of boundary longitudinal mild steel reinforcement on the base moment and drift response of post-tensioned cast-in-place special structural wall with bonded or debonded longitudinal reinforcement. The four groups for this parameter are: (i) PW1.41, PW1.0.0and PW1.4.2, (ii) PW2.4.1, PW2.0.0 and PW2.4.2, (iii) PW3.4.1, PW3.0.0 and PW3.4.2, and (iv) PW4.4.1, PW4.0.0 and PW4.4.2.

6.1.6 Area of Web Longitudinal Mild Steel Reinforcement with Constant Spacing

This parameter study is designed to analyze the effect of change in the total area of web longitudinal mild steel reinforcement on the lateral load response of post-tensioned cast-in-place special structural wall with bonded or debonded longitudinal reinforcement. The four groups for this parameter are: (i) PW1.5.1, PW1.0.0and PW1.5.2, (ii) PW2.5.1, PW2.0.0 and PW2.5.2, (iii) PW3.5.1, PW3.0.0 and PW3.5.2, and (iv) PW4.5.1, PW4.0.0 and PW4.5.2.

6.1.7 Spacing of Web Longitudinal Mild Steel Reinforcement with Constant Area

This parameter study is designed to analyze the effect of change in spacing of web longitudinal mild steel reinforcement with constant area on the base moment and drift response of post-tensioned cast-in-place special structural wall with bonded or debonded longitudinal reinforcement. The spacing of web longitudinal reinforcement used for this parametric study are 4.5, 7.0 and 9.0 in. The four groups for this parameter are: (i) PW1.6.1, PW1.0.0and PW1.6.2, (ii) PW2.6.1, PW2.0.0 and PW2.6.2, (iii) PW3.6.1, PW3.0.0 and PW3.6.2, and (iv) PW4.6.1, PW4.0.0 and PW4.6.2.

6.2 ANALYSIS RESPONSE QUANTITIES STUDIED

The results of the parametric study are presented in terms of the base moment and lateral drift for each of the key structural limit states of the wall discussed in Section 3.1. The moment is at the base of the wall at the lateral drift is at the applied force level. The response quantities of base moment and drift for each of the key structural limit states are obtained from the fiber model analysis and estimated using closed-form expressions of Section 3.2 and 3.3. The analysis response quantities are:

6.2.1 Decompression

The wall structural limit state of decompression for walls with longitudinal mild steel reinforcement is discussed in Section 3.1. The base moment and drift associated with DEC are represented as M_{dec} and Θ_{dec}, respectively. These response quantities are determined from fiber model analysis and estimated using CFEs of Section 3.2.1 for walls with bonded longitudinal mild steel reinforcement and Section 3.3.1 for walls with debonded longitudinal mild steel reinforcement.

6.2.2 Effective Linear Limit

The wall structural limit state of effective linear limit (ELL) for walls with longitudinal mild steel reinforcement is discussed in Section 3.1. These response quantities are estimated using CFEs of Section 3.2.2 for walls with bonded longitudinal mild steel reinforcement and Section 3.3.2 for walls with debonded longitudinal mild steel reinforcement. As explained in Sections 3.2.2 and 3.3.2, ELL indicates a significant reduction in stiffness of the wall may occur due to one of following: (i) significant gap opening at the base of the wall; or (ii) nonlinear behavior of unconfined concrete; or (iii) initiation of yielding in longitudinal mild steel reinforcement. However, all these alternative values of ELL could not be determined from the fiber model analysis. For the bonded mild steel reinforcement cases, the fiber model provided an estimate of effective linear limit with 25% cross-section under compression (ELL1), and effective linear limit with yielding of bonded longitudinal mild steel reinforcement (ELL4).For the debonded

longitudinal mild steel reinforcement case, only the effective linear limit with 25% cross-section under compression (ELL1) was treated.

6.2.3 Yielding of Longitudinal Mild Steel Reinforcement

The wall structural limit state of YMS for walls with debonded longitudinal mild steel reinforcement occurs at the initiation of yielding of the farthest longitudinal reinforcement on the tension side. The base moment and drift associated with YMS are represented as M_{yms} and Θ_{yms}, respectively. These response quantities are determined from fiber model analysis and estimated using CFEs of Section 3.3.3. The corresponding values for bonded mild steel reinforcement cases are the ELL4 values.

6.2.4 Fracture of Longitudinal Reinforcement

The wall structural limit state of FMS for walls with longitudinal mild steel reinforcement occurs when the farthest longitudinal reinforcement on the tension side reaches its ultimate strain. The base moment and drift associated with FMS are represented as M_{fms} and Θ_{fms}, respectively. These response quantities are determined from fiber model analysis and estimated using CFEs of Section 3.2.3 for bonded longitudinal mild steel reinforcement and Section 3.3.4 for debonded longitudinal mild steel reinforcement.

6.2.5 Linear Limit of Post-Tensioning Steel

The wall structural limit state of LLP for walls with longitudinal mild steel reinforcement occurs at the initiation of yielding of the farthest PT group. The base moment and drift associated with FMS are represented as M_{llp} and Θ_{llp}, respectively. These response quantities are determined from fiber model analysis and estimated using CFEs of Section 3.2.4 for bonded longitudinal mild steel reinforcement and Section 3.3.5 for debonded longitudinal mild steel reinforcement.

6.2.6 Crushing of Confined Concrete

The wall structural limit state of Crushing of confined concrete is the limit state at which extreme fiber of the confined concrete fails in compression. The base moment and drift associated with FMS are represented as M_{ccc} and Θ_{ccc}, respectively. These response quantities are determined from fiber model analysis and estimated using CFEs of Section 3.2.5 for bonded longitudinal mild steel reinforcement and Section 3.3.6 for debonded longitudinal mild steel reinforcement.

Tables 6.9 to 6.12 list the results of the base moment and drift, for each of the key structural limit states of the walls, calculated for the 52 walls using fiber model and closed-form expressions. For the parametric walls with bonded longitudinal mild steel reinforcement, the fiber model analyses provided results for the limit state of decompression (DEC), effective linear limit with 25% cross-section under compression (ELL1), effective linear limit with nonlinear behavior of concrete in compression (ELL2), effective linear limit at initiation of yielding of bonded longitudinal mild steel reinforcement (ELL4), linear limit of post-tensioning steel (LLP), fracture of bonded longitudinal mild steel reinforcement (FMS) and crushing of confined concrete in compression (CCC). For the debonded longitudinal mild steel reinforcement case, fiber model analyses provided responses for the limit state of decompression (DEC), effective

linear limit with 25% cross-section under compression (ELL1), effective linear limit with nonlinear behavior of concrete in compression (ELL2), at initiation of yielding of debonded longitudinal mild steel reinforcement (YMS), linear limit (yielding) of post-tensioning steel (LLP), fracture of debonded longitudinal mild steel reinforcement (FMS) and crushing of confined concrete in compression (CCC).

6.3 PRESENTATION AND DISCUSSION OF RESULTS OF THE DESIGN PARAMETER STUDY

This section reports the base moment and drift responses obtained for the 52 wall cases. It also provided a comparative analysis of the responses of the walls for parametric study as discussed in Section 6.2.

The base moments and lateral drifts results obtained from fiber model analyses and closed-form expressions for the parametric walls associated with PW1.0.0 are listed in Tables 6.9(a) and 6.9(b). Similar results are presented in Tables 6.10, 6.11 and 6.12 for PW2.0.0, PW3.0.0 and PW4.0.0.

Figures 6.1(a) to 6.1(m) are the comparative plots of results calculated from the two methods. In general, the closed-form expressions give a conservative estimation of the moment at the base of the wall and lateral drift of the wall compared to the fiber models.

6.3.1 Effect of Area of PT Steel on the Base Moment and Drift Response of Walls

Figure 6.5 compares the analytical model results for the parametric walls to illustrate effect of change in area of post-tensioning steel without any change in the initial prestress. Figures 6.11 shows the effect of change in normalized area of post-tensioning steel on the normalized based moment for all the limit states considered. The area of post-tensioning steel and base moments are normalized with respect to the peak base moment response associated parametric base wall obtained from the fiber model analyses. A similar normalized comparison for lateral drift is shown in Figure 6.12. It can be concluded from the results that an increase in the area of PT steel increases the moment at the base of the wall and decreases the total drift value for all the wall structural limit states. The increase in base moment values is observed because with increase in area of the PT steel total initial prestressing force increases. However, same causes the reduction in lateral drift values for all the limit states because of increased restoring force with increase in PT steel area.

As noted in Section 5.5, the total area of PT steel and total initial PT forces causes larger strains in the confined concrete. This causes the confined concrete fibers to be located on the descending branch of the stress-strain curve or beyond. This phenomenon is reflected in the results as a dip in the base-moment and drift plots of the parametric walls associated with PW2.0.0 and PW4.0.0. It can also be noted from Figures 6.5(b) and (d) that the dip occurs earlier in the parametric walls with larger PT steel area (PW2.1.2 and PW4.1.2 with 21 PT strands) than the parametric walls with smaller PT steel area (PW2.1.1 and PW4.1.1 with 17 PT strands).

6.3.2 Effect of Initial Prestress in PT Steel on the Base Moment and Roof Drift Response of Walls

Figures 6.6, 6.13 and 6.14 illustrate the effect of change in initial prestress without changing the total area of PT steel. Increasing the initial prestress increases the base

moment values for the limit states of decompression and effective linear limits because of increase in downward force with increase in initial prestress but the corresponding drift values were not affected much. The base moment and drift values were less sensitive to the change in initial prestress. However, the limit state of linear limit of post-tensioning steel (LLP) was significantly influenced. Increasing the initial prestress reduced the increase in PT steel force and deformation capacity at LLP. LLP occurs at an earlier lateral deflection of the wall and the forces developed in longitudinal mild steel reinforcement are smaller for higher initial prestress in PT steel. Therefore, both base moment and drift values declined at LLP with increase in initial prestress.

6.3.3 Effect of Constant Prestress Force with Changing Area of PT Steel and Changing Initial Prestress on the Base Moment and Roof Drift Response of Walls

In order to achieve constant initial prestress force, smaller total PT steel area is associated with larger initial prestress. Figures 6.7, 6.15 and 6.16 show the base moment and lateral drift responses of the parametric walls for this parameter. The normalized parameter used in Figures 6.15 and 6.16 is the total area of the PT steel. As observed in Section 6.3.1, increasing the initial prestress in PT steel decreases the base moments at the limit states of LLP, FMS and CCC and decreases the lateral drift response of the wall. This is caused by a combined effect of higher initial prestress and lower total PT steel area. All other limit states were unaffected.

6.3.4 Effect of Area of Boundary Longitudinal Mild Steel Reinforcement on the Base Moment and Roof Drift Response of Walls

Figures 6.8, 6.17 and 6.18 study the effect of change in boundary longitudinal mild steel reinforcement area on the base moment and lateral drift of the walls for all the limit states. Any increase in the area of boundary longitudinal mild steel reinforcement increase the base moment values for all the limit states because the boundary reinforcement sustains higher forces for the same strain values, except for the limit state of decompression. The base moment at DEC decreases nominally with increase in are of boundary longitudinal mild steel reinforcement because the equilibrium between the vertical forces is achieved at a lower concrete strain values as sum of the forces developed in longitudinal reinforcement increases with increase in area of longitudinal reinforcement. As the boundary longitudinal mild steel reinforcement is concentrated towards the ends of the walls, a larger moment arm is available. A similar increase in drift values takes place for all limit states except the limit state of crushing of the confined concrete. This discrepancy is observed because of increase in the forces developed in the boundary longitudinal reinforcement. This increase causes CCC to occur at an earlier later deflection state.

6.3.5 Effect of Area of Web Longitudinal Mild Steel Reinforcement on the Base Moment and Roof Drift Response of Walls

As in the case of area of boundary longitudinal mild steel reinforcement, an increase in the area of web longitudinal reinforcement also increases both base moment and drift responses of the walls for all the limit states with except of base moment at DEC and drift at CCC as shown in Figures 6.8, 6.17 and 6.18.

6.3.6 Effect of Spacing of Web Longitudinal Mild Steel Reinforcement on the Base Moment and Roof Drift Response of Walls

It can be seen in Figures 6.10, 6.20 and 6.22 that changing the spacing of web longitudinal reinforcement, for a constant web longitudinal reinforcement area, did not produce any noticeable change in the base moment and drift responses of the walls. Therefore, it can be concluded that this design parameter is not significant as long as total area of web longitudinal reinforcement is constant.

Table 6.1: Properties of PW1.0.0 with bonded longitudinal reinforcement

Dimensions	Length	l_w	72.0 in.
	Thickness	t_w	10.0 in.
	Height	H_w	300.0 in.
	Height of applied force	H_F	150.0 in.
Post-tension	Area of PT steel	A_{pt}	1.085+1.085 = 2.17in^2
	Eccentricity	e_p	6.0 in.
	Yield strength of PT steel	f_{py}	220 ksi
	Ultimate strength of PT steel	f_{pu}	270 ksi
	Modulus of Elasticity	E_p	27500 ksi
	Initial prestress in PT steel	f_{pi}	$0.60f_{pu}$ = 162.0 ksi
	Prestress force	T_p	351.5 kip
	Unbonded height of PT steel	$H_{pt,unb}$	300.0 in.
Concrete	Unconfined concrete strength	f_c'	7.8 ksi
	Confined concrete Strength	f_{cc}'	11.0 ksi
	Modulus of Elasticity	E_c	5034.1 ksi
Reinforcement	Boundary longitudinal reinforcement	$A_{b,l}$	8 - #7 bars (4.80 in.^{2})
	Boundary transverse reinforcement	$A_{b,t}$	#3 @ 2.25 in.
	Yield strength of reinforcement	f_{sy}	66.0 ksi
	Ultimate strength of reinforcement	f_{su}	99.0 ksi

	Modulus of Elasticity	E_s	29000 ksi
	Web longitudinal reinforcement	$A_{w,l}$	16 - #3 bars (1.76 in.^{2})
	Web transverse reinforcement	$A_{w,t}$	#3 @ 4.5 in.
	Unbonded height of PT steel	$H_{ms,unb}$	0.0 in.

Table 6.2: Properties of PW2.0.0 with bonded longitudinal reinforcement

Dimensions	Length	l_w	72.0 in.
	Thickness	t_w	10.0 in.
	Height	H_w	300.0 in.
	Height of applied force	H_F	150.0 in.
Post-tension	Area of PT steel	A_{pt}	1.519+1.085+1.519 = 4.123in^2
	Eccentricity	e_p	9.0 in.
	Yield strength of PT steel	f_{py}	220 ksi
	Ultimate strength of PT steel	f_{pu}	270 ksi
	Modulus of Elasticity	E_p	27500 ksi
	Initial prestress in PT steel	f_{pi}	0.60f_{pu} = 162.0 ksi
	Prestress force	T_p	667.9 kip
	Unbonded height of PT steel	$H_{pt,unb}$	300.0 in.
Concrete	Unconfined concrete strength	f_c'	7.8 ksi
	Confined concrete Strength	f_{cc}'	11.0 ksi
	Modulus of Elasticity	E_c	5034.1 ksi
Reinforcement	Boundary longitudinal reinforcement	$A_{b,l}$	8 - #5 bars (2.48 in.^{2})
	Boundary transverse reinforcement	$A_{b,t}$	#3 @ 2.25 in.
	Yield strength of reinforcement	f_{sy}	66.0 ksi
	Ultimate strength of reinforcement	f_{su}	99.0 ksi
	Modulus of Elasticity	E_s	29000 ksi
	Web longitudinal reinforcement	$A_{w,l}$	16 - #3 bars (1.76 in.^{2})
	Web transverse reinforcement	$A_{w,t}$	#3 @ 4.5 in.
	Unbonded height of PT steel	$H_{ms,unb}$	0.0 in.

Table 6.3: Properties of PW3.0.0 with debonded longitudinal reinforcement

Dimensions	Length	l_w	72.0 in.
	Thickness	t_w	10.0 in.
	Height	H_w	300.0 in.
	Height of applied force	H_F	150.0 in.
Post-tension	Area of PT steel	A_{pt}	1.085+1.085 = 2.17 in^2
	Eccentricity	e_p	6.0 in.
	Yield strength of PT steel	f_{py}	220 ksi
	Ultimate strength of PT steel	f_{pu}	270 ksi
	Modulus of Elasticity	E_p	27500 ksi
	Initial prestress in PT steel	f_{pi}	$0.60f_{pu}$ = 162.0 ksi
	Prestress force	T_p	351.5 kip
	Unbonded height of PT steel	$H_{pt,unb}$	300.0 in.
Concrete	Unconfined concrete strength	f_c'	7.8 ksi
	Confined concrete Strength	f_{cc}'	11.0 ksi
	Modulus of Elasticity	E_c	5034.1 ksi
Reinforcement	Boundary longitudinal reinforcement	$A_{b,l}$	8 - #7 bars (4.80 in.^{2})
	Boundary transverse reinforcement	$A_{b,t}$	#3 @ 2.25 in.
	Yield strength of reinforcement	f_{sy}	66.0 ksi
	Ultimate strength of reinforcement	f_{su}	99.0 ksi
	Modulus of Elasticity	E_s	29000 ksi
	Web longitudinal reinforcement	$A_{w,l}$	16 - #3 bars (1.76 in.^{2})
	Web transverse reinforcement	$A_{w,t}$	#3 @ 4.5 in.
	Unbonded height of PT steel	$H_{ms,unb}$	24.0 in.

Table 6.4: Properties of PW4.0.0 with debonded longitudinal reinforcement

Dimensions	Length	l_w	72.0 in.
	Thickness	t_w	10.0 in.
	Height	H_w	300.0 in.
	Height of applied force	H_F	150.0 in.
Post-tension	Area of PT steel	A_{pt}	1.519+1.085+1.519 = 4.123 in^2
	Eccentricity	e_p	9.0 in.
	Yield strength of PT steel	f_{py}	220 ksi
	Ultimate strength of PT steel	f_{pu}	270 ksi
	Modulus of Elasticity	E_p	27500 ksi
	Initial prestress in PT steel	f_{pi}	$0.60f_{pu}$ = 162.0 ksi
	Prestress force	T_p	667.9 kip
	Unbonded height of PT steel	$H_{pt,unb}$	300.0 in.
Concrete	Unconfined concrete strength	f_c'	7.8 ksi
	Confined concrete Strength	f_{cc}'	11.0 ksi
	Modulus of Elasticity	E_c	5034.1 ksi
Reinforcement	Boundary longitudinal reinforcement	$A_{b,l}$	8 - #5 bars (2.48 in.^{2})
	Boundary transverse reinforcement	$A_{b,t}$	#3 @ 2.25 in.
	Yield strength of reinforcement	f_{sy}	66.0 ksi
	Ultimate strength of reinforcement	f_{su}	99.0 ksi
	Modulus of Elasticity	E_s	29000 ksi
	Web longitudinal reinforcement	$A_{w,l}$	16 - #3 bars (1.76 in.^{2})
	Web transverse reinforcement	$A_{w,t}$	#3 @ 4.5 in.
	Unbonded height of PT steel	$H_{ms,unb}$	24.0 in.

Table 6.5: Properties of parametric walls associated with PW1.0.0

Parameter 1: A_{pt} with constant initial prestress ($f_{pi} = 0.6f_{pu}$)			
PW1.1.1	Area of PT steel	A_{pt}	0.868+0.868 = 1.736 in^2
	Prestress force	T_p	281.2 kip
PW1.1.2	Area of PT steel	A_{pt}	1.302+1.302 = 2.604 in^2
	Prestress force	T_p	421.8 kip
Parameter 2: f_{pi} with constant PT steel area ($A_{pt} = 2.17in^2$)			
PW1.2.1	Initial prestress in PT steel	f_{pi}	$0.55f_{pu}$ = 148.5 ksi
	Prestress force	T_p	322.1 kip
PW1.2.2	Initial prestress in PT steel	f_{pi}	$0.65f_{pu}$ = 175.5 ksi
	Prestress force	T_p	380.8 kip
Parameter 3: A_{pt} and f_{pi} with constant initial prestress force ($T_p = 351.5\ kip$)			
PW1.3.1	Area of PT steel	A_{pt}	1.184+1.184 = 2.368 in^2
	Initial prestress in PT steel	f_{pi}	$0.55f_{pu}$ = 148.5 ksi
PW1.3.2	Area of PT steel	A_{pt}	1.001+1.001 = 2.002 in^2
	Initial prestress in PT steel	f_{pi}	$0.65f_{pu}$ = 175.5 ksi
Parameter 4: $A_{b,l}$ with constant $A_{w,l}$			
PW1.4.1	Boundary longitudinal reinforcement	$A_{b,l}$	8 bars (3.00 in.^{2})
PW1.4.1	Boundary longitudinal reinforcement	$A_{b,l}$	8 bars (7.00 in.^{2})
Parameter 5: $A_{w,l}$ with constant $A_{b,l}$			
PW1.5.1	Web longitudinal reinforcement area	$A_{w,l}$	16 bars (1.00 in.^{2}) @ 7.0 in.
PW1.5.2	Web longitudinal reinforcement area	$A_{w,l}$	16 bars (3.00 in.^{2}) @ 7.0 in.
Parameter 6: Spacing of web longitudinal mild steel reinforcement			
PW1.6.1	Web longitudinal reinforcement spacing		22 bars (1.76 in.^{2}) @ 4.5 in.
PW1.6.2	Web longitudinal reinforcement spacing		12 bars (1.76 in.^{2}) @ 9.0 in.

Table 6.6: Properties of parametric walls associated with PW2.0.0

Parameter 1: A_{pt} with constant initial prestress ($f_{pi} = 0.6f_{pu}$)			
PW2.1.1	Area of PT steel	A_{pt}	1.302+1.085+1.302 = 3.689 in^2
	Prestress force	T_p	597.6 kip
PW2.1.2	Area of PT steel	A_{pt}	1.736+1.085+1.736 = 4.557 in^2
	Prestress force	T_p	738.2 kip
Parameter 2: f_{pi} with constant PT steel area ($A_{pt} = 4.123in^2$)			
PW2.2.1	Initial prestress in PT steel	f_{pi}	$0.55f_{pu}$ = 148.5 ksi
	Prestress force	T_p	612.3 kip
PW2.2.2	Initial prestress in PT steel	f_{pi}	$0.65f_{pu}$ = 175.5 ksi
	Prestress force	T_p	723.6 kip
Parameter 3: A_{pt} and f_{pi} with constant initial prestress force ($T_p = 667.9\ kip$)			
PW2.3.1	Area of PT steel	A_{pt}	1.657+1.184+1.657 = 4.498 in^2
	Initial prestress in PT steel	f_{pi}	$0.55f_{pu}$ = 148.5 ksi
PW2.3.2	Area of PT steel	A_{pt}	1.402+1.001+1.402 = 3.805 in^2
	Initial prestress in PT steel	f_{pi}	$0.65f_{pu}$ = 175.5 ksi
Parameter 4: $A_{b,l}$ with constant $A_{w,l}$			
PW2.4.1	Boundary longitudinal reinforcement	$A_{b,l}$	8 bars (1.50 in.^{2})
PW2.4.1	Boundary longitudinal reinforcement	$A_{b,l}$	8 bars (3.50 in.^{2})
Parameter 5: $A_{w,l}$ with constant $A_{b,l}$			
PW2.5.1	Web longitudinal reinforcement area	$A_{w,l}$	16 bars (1.00 in.^{2}) @ 7.0 in.
PW2.5.2	Web longitudinal reinforcement area	$A_{w,l}$	16 bars (3.00 in.^{2}) @ 7.0 in.
Parameter 6: Spacing of web longitudinal mild steel reinforcement			
PW2.6.1	Web longitudinal reinforcement spacing		22 bars (1.76 in.^{2}) @ 4.5 in.
PW2.6.2	Web longitudinal reinforcement spacing		12 bars (1.76 in.^{2}) @ 9.0 in.

Table 6.7: Properties of parametric walls associated with PW3.0.0

Parameter 1: A_{pt} with constant initial prestress ($f_{pi} = 0.6f_{pu}$)			
PW3.1.1	Area of PT steel	A_{pt}	0.868+0.868 = 1.736 in^2
	Prestress force	T_p	281.2 kip
PW3.1.2	Area of PT steel	A_{pt}	1.302+1.302 = 2.604 in^2
	Prestress force	T_p	421.8 kip
Parameter 2: f_{pi} with constant PT steel area ($A_{pt} = 2.17in^2$)			
PW3.2.1	Initial prestress in PT steel	f_{pi}	$0.55f_{pu}$ = 148.5 ksi
	Prestress force	T_p	322.1 kip
PW3.2.2	Initial prestress in PT steel	f_{pi}	$0.65f_{pu}$ = 175.5 ksi
	Prestress force	T_p	380.8 kip
Parameter 3: A_{pt} and f_{pi} with constant initial prestress force ($T_p = 351.5\ kip$)			
PW3.3.1	Area of PT steel	A_{pt}	1.184+1.184 = 2.368 in^2
	Initial prestress in PT steel	f_{pi}	$0.55f_{pu}$ = 148.5 ksi
PW3.3.2	Area of PT steel	A_{pt}	1.001+1.001 = 2.002 in^2
	Initial prestress in PT steel	f_{pi}	$0.65f_{pu}$ = 175.5 ksi
Parameter 4: $AA_{b,l}$ with constant $A_{w,l}$			
PW3.4.1	Boundary longitudinal reinforcement	$A_{b,l}$	8 bars (3.00 in.^{2})
PW3.4.1	Boundary longitudinal reinforcement	$A_{b,l}$	8 bars (7.00 in.^{2})
Parameter 5: $A_{w,l}$ with constant $A_{b,l}$			
PW3.5.1	Web longitudinal reinforcement area	$A_{w,l}$	16 bars (1.00 in.^{2}) @ 7.0 in.
PW3.5.2	Web longitudinal reinforcement area	$A_{w,l}$	16 bars (3.00 in.^{2}) @ 7.0 in.
Parameter 6: Spacing of web longitudinal mild steel reinforcement			
PW3.6.1	Web longitudinal reinforcement spacing		22 bars (1.76 in.^{2}) @ 4.5 in.
PW3.6.2	Web longitudinal reinforcement spacing		12 bars (1.76 in.^{2}) @ 9.0 in.

Table 6.8: Properties of parametric walls associated with PW4.0.0

Parameter 1: A_{pt} with constant initial prestress ($f_{pi} = 0.6f_{pu}$)			
PW4.1.1	Area of PT steel	A_{pt}	1.302+1.085+1.302 = 3.689 in^2
	Prestress force	T_p	597.6 kip
PW4.1.2	Area of PT steel	A_{pt}	1.736+1.085+1.736 = 4.557 in^2
	Prestress force	T_p	738.2 kip
Parameter 2: f_{pi} with constant PT steel area ($A_{pt} = 4.123in^2$)			
PW4.2.1	Initial prestress in PT steel	f_{pi}	0.55f_{pu} = 148.5 ksi
	Prestress force	T_p	612.3 kip
PW4.2.2	Initial prestress in PT steel	f_{pi}	0.65f_{pu} = 175.5 ksi
	Prestress force	T_p	723.6 kip
Parameter 3: A_{pt} and f_{pi} with constant initial prestress force ($T_p = 667.9\ kip$)			
PW4.3.1	Area of PT steel	A_{pt}	1.657+1.184+1.657 = 4.498 in^2
	Initial prestress in PT steel	f_{pi}	0.55f_{pu} = 148.5 ksi
PW4.3.2	Area of PT steel	A_{pt}	1.402+1.001+1.402 = 3.805 in^2
	Initial prestress in PT steel	f_{pi}	0.65f_{pu} = 175.5 ksi
Parameter 4: $A_{b,l}$ with constant $A_{w,l}$			
PW4.4.1	Boundary longitudinal reinforcement	$A_{b,l}$	8 bars (1.50 in.^{2})
PW4.4.1	Boundary longitudinal reinforcement	$A_{b,l}$	8 bars (3.50 in.^{2})
Parameter 5: $A_{w,l}$ with constant $A_{b,l}$			
PW4.5.1	Web longitudinal reinforcement area	$A_{w,l}$	16 bars (1.00 in.^{2}) @ 7.0 in.
PW4.5.2	Web longitudinal reinforcement area	$A_{w,l}$	16 bars (3.00 in.^{2}) @ 7.0 in.
Parameter 6: Spacing of web longitudinal mild steel reinforcement			
PW4.6.1	Web longitudinal reinforcement spacing		22 bars (1.76 in.^{2}) @ 4.5 in.
PW4.6.2	Web longitudinal reinforcement spacing		12 bars (1.76 in.^{2}) @ 9.0 in.

Table 6.9(a): Moment at the base of parametric walls associated with PW1.0.0

Base Moment (kip-in)		DEC	ELL1	ELL2	ELL3	ELL4	LLP	FMS	CCC
PW1.0.0	Fiber Model	4,917	34,306	-	-	29,124	45,066	48,702	49,545
	CFE	4,731	33,309	36,431	11,828	31,540	47,151	46,924	49,105
PW1.1.1	Fiber Model	3,981	31,906	-	-	27,323	42,271	46,138	46,978
	CFE	3,833	31,010	34,766	9,582	29,717	44,743	44,610	46,736
PW1.1.2	Fiber Model	5,849	36,641	-	-	30,850	47,779	51,190	-
	CFE	5,630	35,561	38,082	14,074	33,305	49,457	49,082	51,348
PW1.2.1	Fiber Model	4,526	33,341	-	-	28,387	46,216	48,372	49,516
	CFE	4,357	32,351	35,738	10,892	30,788	47,732	46,186	49,071
PW1.2.2	Fiber Model	5,304	35,233	-	-	29,862	43,670	48,793	49,583
	CFE	5,106	34,254	37,121	12,764	32,282	45,043	47,277	49,140
PW1.3.1	Fiber Model	4,915	34,337	-	-	29,145	47,466	49,470	-
	CFE	4,731	33,309	36,431	11,828	31,540	48,746	47,162	50,107
PW1.3.2	Fiber Model	4,915	34,275	-	-	29,113	42,620	47,777	48,594
	CFE	4,731	33,309	36,431	11,828	31,540	44,106	46,361	48,240
PW1.4.1	Fiber Model	4,763	26,715	-	-	22,790	35,791	38,174	38,993
	CFE	4,619	25,788	28,857	11,547	25,183	36,697	36,569	38,474
PW1.4.2	Fiber Model	5,091	43,561	-	-	36,791	56,383	61,402	61,434
	CFE	4,862	42,484	45,578	12,155	39,175	59,929	59,530	62,085
PW1.5.1	Fiber Model	4,931	32,938	-	-	28,533	43,277	46,927	47,584
	CFE	4,742	32,111	35,204	11,856	30,824	45,464	45,301	47,318
PW1.5.2	Fiber Model	4,891	36,482	-	-	30,050	47,724	51,552	51,643
	CFE	4,714	35,311	38,383	11,784	32,684	49,794	49,409	51,874
PW1.6.1	Fiber Model	4,912	34,278	-	-	29,048	45,056	48,664	49,555
	CFE	4,728	33,260	36,436	11,819	31,476	47,119	46,892	49,104
PW1.6.2	Fiber Model	4,918	34,307	-	-	29,133	45,066	48,702	49,555
	CFE	4,732	33,302	36,458	11,829	31,545	47,154	46,927	49,115

Table 6.9(b): Lateral Drift of parametric walls associated with PW1.0.0

Drift (%)		DEC	ELL1	ELL2	ELL3	ELL4	LLP	FMS	CCC
PW1.0.0	Fiber Model	0.02	0.38	-	-	0.25	1.89	2.91	9.13
	CFE	0.02	0.25	0.54	0.04	0.18	2.23	2.18	6.43
PW1.1.1	Fiber Model	0.02	0.36	-	-	0.25	1.85	2.96	9.60
	CFE	0.01	0.23	0.57	0.04	0.18	2.18	2.15	7.21
PW1.1.2	Fiber Model	0.02	0.41	-	-	0.25	1.94	2.86	-
	CFE	0.02	0.27	0.52	0.05	0.19	2.32	2.22	5.80
PW1.2.1	Fiber Model	0.02	0.37	-	-	0.25	2.29	2.91	9.18
	CFE	0.02	0.24	0.55	0.04	0.18	2.72	2.17	6.44
PW1.2.2	Fiber Model	0.02	0.39	-	-	0.25	1.49	2.90	9.13
	CFE	0.02	0.26	0.53	0.05	0.19	1.74	2.18	6.42
PW1.3.1	Fiber Model	0.02	0.38	-	-	0.25	2.32	2.89	-
	CFE	0.02	0.25	0.54	0.04	0.18	2.76	2.18	6.14
PW1.3.2	Fiber Model	0.02	0.38	-	-	0.25	1.48	2.92	9.30
	CFE	0.02	0.25	0.54	0.04	0.18	1.73	2.17	6.70
PW1.4.1	Fiber Model	0.02	0.35	-	-	0.23	1.87	2.72	7.87
	CFE	0.02	0.21	0.55	0.04	0.16	2.16	2.13	6.71
PW1.4.2	Fiber Model	0.02	0.41	-	-	0.27	1.93	3.04	7.71
	CFE	0.02	0.30	0.55	0.05	0.21	2.33	2.25	6.13
PW1.5.1	Fiber Model	0.02	0.37	-	-	0.25	1.88	2.88	9.38
	CFE	0.02	0.24	0.56	0.04	0.18	2.20	2.16	6.97
PW1.5.2	Fiber Model	0.02	0.41	-	-	0.25	1.92	2.95	7.48
	CFE	0.02	0.27	0.52	0.04	0.19	2.32	2.22	5.74
PW1.6.1	Fiber Model	0.02	0.38	-	-	0.25	1.89	2.90	9.13
	CFE	0.02	0.25	0.54	0.04	0.18	2.23	2.18	6.42
PW1.6.2	Fiber Model	0.02	0.38	-	-	0.25	1.89	2.90	9.13
	CFE	0.02	0.25	0.54	0.04	0.18	2.23	2.18	6.43

Table 6.10(a): Moment at the base of parametric walls associated with PW2.0.0

Base Moment (kip-in)		DEC	ELL1	ELL2	ELL3	ELL4	LLP	FMS	CCC
PW2.0.0	Fiber Model	8,754	35,044	-	-	28,488	43,838	45,348	43,046
	CFE	8,504	33,691	34,155	21,259	31,239	42,566	42,399	44,207
PW2.1.1	Fiber Model	7,856	32,734	-	-	26,880	41,438	43,353	43,229
	CFE	7,633	31,475	32,571	19,082	29,592	40,622	40,570	42,476
PW2.1.2	Fiber Model	9,648	37,278	-	-	30,076	46,044	47,301	44,678
	CFE	9,374	35,879	35,697	23,436	32,823	44,404	44,104	45,840
PW2.2.1	Fiber Model	8,046	33,248	-	-	27,238	44,277	44,653	43,523
	CFE	7,814	31,937	32,904	19,536	29,940	42,782	41,294	43,985
PW2.2.2	Fiber Model	9,463	36,724	-	-	29,721	43,155	45,815	41,610
	CFE	9,193	35,425	35,379	22,982	32,498	41,674	42,988	44,425
PW2.3.1	Fiber Model	8,756	35,127	-	-	28,510	46,177	46,323	41,869
	CFE	8,504	33,691	34,155	21,259	31,239	44,315	42,725	45,393
PW2.3.2	Fiber Model	8,753	34,923	-	-	28,466	41,475	44,328	43,731
	CFE	8,504	33,691	34,155	21,259	31,239	40,240	41,639	43,151
PW2.4.1	Fiber Model	8,586	30,855	-	-	25,087	38,807	39,703	38,227
	CFE	8,385	29,607	30,151	20,962	27,914	37,004	36,888	38,529
PW2.4.2	Fiber Model	8,920	39,334	-	-	31,994	49,011	51,194	47,296
	CFE	8,624	37,945	38,309	21,561	34,678	48,363	48,129	50,114
PW2.5.1	Fiber Model	8,781	33,483	-	-	27,986	42,412	44,007	44,187
	CFE	8,523	32,417	33,039	21,308	30,606	41,190	41,088	42,822
PW2.5.2	Fiber Model	8,709	37,297	-	-	29,284	46,185	47,927	45,694
	CFE	8,472	35,797	35,911	21,180	32,249	44,754	44,466	46,394
PW2.6.1	Fiber Model	8,749	35,051	-	-	28,426	43,952	45,378	42,000
	CFE	8,497	33,674	34,145	21,242	31,171	42,517	42,340	44,145
PW2.6.2	Fiber Model	8,760	35,058	-	-	28,511	43,972	45,415	42,070
	CFE	8,504	33,709	34,174	21,260	31,245	42,586	42,431	44,254

Table 6.10(b): Lateral Drift of parametric walls associated with PW2.0.0

Drift (%)		DEC	ELL1	ELL2	ELL3	ELL4	LLP	FMS	CCC
PW2.0.0	Fiber Model	0.04	0.47	-	-	0.24	1.91	2.46	4.91
	CFE	0.03	0.29	0.43	0.08	0.18	2.31	2.25	4.40
PW2.1.1	Fiber Model	0.04	0.44	-	-	0.24	1.85	2.50	6.07
	CFE	0.03	0.27	0.44	0.07	0.18	2.22	2.21	4.72
PW2.1.2	Fiber Model	0.04	0.51	-	-	0.24	1.97	2.41	4.25
	CFE	0.04	0.31	0.41	0.09	0.19	2.40	2.30	4.12
PW2.2.1	Fiber Model	0.04	0.44	-	-	0.24	2.33	2.47	5.14
	CFE	0.03	0.27	0.44	0.07	0.18	2.80	2.22	4.47
PW2.2.2	Fiber Model	0.04	0.50	-	-	0.24	1.49	2.44	4.66
	CFE	0.03	0.31	0.41	0.09	0.19	1.80	2.27	4.33
PW2.3.1	Fiber Model	0.04	0.47	-	-	0.24	2.38	2.43	4.36
	CFE	0.03	0.29	0.43	0.08	0.18	2.89	2.26	4.23
PW2.3.2	Fiber Model	0.04	0.47	-	-	0.24	1.47	2.48	5.73
	CFE	0.03	0.29	0.43	0.08	0.18	1.75	2.24	4.56
PW2.4.1	Fiber Model	0.04	0.45	-	-	0.22	1.91	2.32	5.10
	CFE	0.03	0.27	0.42	0.08	0.17	2.26	2.22	4.44
PW2.4.2	Fiber Model	0.04	0.49	-	-	0.25	1.92	2.58	4.71
	CFE	0.03	0.31	0.43	0.08	0.20	2.35	2.29	4.35
PW2.5.1	Fiber Model	0.04	0.43	-	-	0.24	1.88	2.44	6.07
	CFE	0.03	0.28	0.43	0.08	0.18	2.26	2.23	4.57
PW2.5.2	Fiber Model	0.04	0.52	-	-	0.24	1.94	2.52	4.67
	CFE	0.03	0.31	0.42	0.08	0.19	2.39	2.30	4.14
PW2.6.1	Fiber Model	0.04	0.47	-	-	0.24	1.91	2.44	4.73
	CFE	0.03	0.29	0.42	0.08	0.18	2.31	2.26	4.37
PW2.6.2	Fiber Model	0.04	0.47	-	-	0.24	1.91	2.44	4.82
	CFE	0.03	0.29	0.43	0.08	0.18	2.30	2.25	4.43

Table 6.11(a): Moment at the base of parametric walls associated with PW3.0.0

Base Moment (kip-in)		DEC	ELL1	ELL2	ELL3	YMS	LLP	FMS	CCC
PW3.0.0	Fiber Model	4,916	34,204	-	-	29,137	41,888	48,768	53,886
	CFE	4,731	32,945	35,676	11,828	31,706	41,870	48,092	49,174
PW3.1.1	Fiber Model	3,981	31,815	-	-	27,327	39,238	46,176	-
	CFE	3,833	30,630	33,882	9,582	29,854	39,417	45,579	46,693
PW3.1.2	Fiber Model	5,849	36,526	-	-	30,870	44,513	51,238	55,923
	CFE	5,630	35,194	37,444	14,074	33,499	44,277	50,523	51,430
PW3.2.1	Fiber Model	4,526	33,240	-	-	28,397	42,662	48,711	53,892
	CFE	4,357	31,984	34,931	10,892	30,951	42,687	48,066	49,140
PW3.2.2	Fiber Model	5,304	35,120	-	-	29,870	41,000	48,810	53,910
	CFE	5,106	33,882	36,416	12,764	32,451	41,052	48,139	49,208
PW3.3.1	Fiber Model	4,912	34,241	-	-	29,151	43,836	49,855	54,835
	CFE	4,731	32,945	35,676	11,828	31,716	43,779	49,183	50,177
PW3.3.2	Fiber Model	4,915	34,167	-	-	29,121	40,002	47,781	52,426
	CFE	4,731	32,945	35,676	11,828	31,716	43,779	49,183	50,177
PW3.4.1	Fiber Model	4,761	26,677	-	-	22,803	33,479	38,358	-
	CFE	4,619	25,447	28,270	11,547	25,330	33,338	37,691	38,607
PW3.4.2	Fiber Model	5,090	43,346	-	-	36,800	52,157	61,392	68,462
	CFE	4,862	42,036	44,673	12,155	39,384	52,301	60,791	62,017
PW3.5.1	Fiber Model	4,931	32,881	-	-	28,572	40,362	47,058	-
	CFE	4,742	31,850	34,404	11,856	30,988	40,386	45,433	47,427
PW3.5.2	Fiber Model	4,891	36,341	-	-	30,056	44,375	51,553	56,655
	CFE	4,714	34,782	37,698	11,784	32,854	44,260	50,728	51,752
PW3.6.1	Fiber Model	4,912	34,178	-	-	29,055	41,878	48,739	53,832
	CFE	4,728	32,868	35,685	11,819	31,642	41,857	48,073	49,142
PW3.6.2	Fiber Model	4,917	34,194	-	-	29,141	41,878	48,681	53,857
	CFE	4,732	32,919	35,697	11,829	31,711	41,871	48,104	49,167

Table 6.11(b): Lateral Drift of parametric walls associated with PW3.0.0

Drift (%)		DEC	ELL1	ELL2	ELL3	YMS	LLP	FMS	CCC
PW3.0.0	Fiber Model	0.02	0.42	-	-	0.26	1.92	5.26	10.07
	CFE	0.02	0.28	0.62	0.04	0.21	2.14	4.98	9.30
PW3.1.1	Fiber Model	0.02	0.39	-	-	0.26	1.88	5.33	-
	CFE	0.01	0.25	0.66	0.04	0.20	2.08	4.93	8.79
PW3.1.2	Fiber Model	0.03	0.45	-	-	0.27	1.96	5.16	9.47
	CFE	0.02	0.30	0.59	0.05	0.22	2.19	5.07	8.39
PW3.2.1	Fiber Model	0.02	0.41	-	-	0.26	2.32	5.24	10.10
	CFE	0.02	0.27	0.64	0.04	0.21	2.60	4.98	9.32
PW3.2.2	Fiber Model	0.02	0.43	-	-	0.26	1.50	5.27	10.04
	CFE	0.02	0.29	0.61	0.05	0.22	1.67	4.98	9.29
PW3.3.1	Fiber Model	0.02	0.42	-	-	0.26	2.31	5.20	9.78
	CFE	0.02	0.28	0.62	0.04	0.21	2.63	5.02	8.88
PW3.3.2	Fiber Model	0.02	0.42	-	-	0.26	1.48	5.27	10.98
	CFE	0.02	0.28	0.62	0.04	0.21	2.63	5.02	8.88
PW3.4.1	Fiber Model	0.02	0.38	-	-	0.24	1.88	5.07	-
	CFE	0.02	0.23	0.63	0.04	0.19	2.07	4.91	9.74
PW3.4.2	Fiber Model	0.02	0.46	-	-	0.28	1.96	5.40	10.07
	CFE	0.02	0.33	0.63	0.05	0.25	2.20	5.08	8.72
PW3.5.1	Fiber Model	0.02	0.40	-	-	0.26	1.90	5.20	-
	CFE	0.02	0.27	0.65	0.04	0.21	2.10	5.01	9.80
PW3.5.2	Fiber Model	0.02	0.45	-	-	0.27	1.94	5.26	9.68
	CFE	0.02	0.29	0.59	0.04	0.22	2.19	5.08	8.35
PW3.6.1	Fiber Model	0.02	0.42	-	-	0.26	1.92	5.20	10.20
	CFE	0.02	0.28	0.62	0.04	0.21	2.14	4.98	9.30
PW3.6.2	Fiber Model	0.02	0.42	-	-	0.26	1.92	5.20	10.07
	CFE	0.02	0.28	0.62	0.04	0.21	2.14	4.98	9.30

Table 6.12(a): Moment at the base of parametric walls associated with PW4.0.0

Base Moment (kip-in)		DEC	ELL1	ELL2	ELL3	YMS	LLP	FMS	CCC
PW4.0.0	Fiber Model	8,755	35,248	-	-	28,512	42,699	45,311	45,452
	CFE	8,504	33,412	33,916	21,259	31,480	40,401	44,652	44,099
PW4.1.1	Fiber Model	8,756	35,170	-	-	28,504	38,321	46,722	44,411
	CFE	7,633	31,219	32,273	19,082	29,815	38,316	42,580	42,515
PW4.1.2	Fiber Model	9,655	37,666	-	-	30,125	45,145	47,460	47,525
	CFE	9,374	35,599	35,485	23,436	33,084	42,398	46,546	45,562
PW4.2.1	Fiber Model	8,046	33,501	-	-	27,267	43,141	44,828	44,862
	CFE	7,814	31,681	32,619	19,536	30,185	40,613	44,375	43,924
PW4.2.2	Fiber Model	9,464	37,003	-	-	29,745	42,229	49,212	44,881
	CFE	9,193	35,143	35,166	22,982	32,740	40,189	44,722	44,197
PW4.3.1	Fiber Model	8,757	35,344	-	-	28,534	44,956	46,614	46,678
	CFE	8,504	33,412	33,916	21,259	31,499	42,312	46,016	45,189
PW4.3.2	Fiber Model	8,754	35,124	-	-	28,487	40,502	47,477	45,349
	CFE	8,504	33,412	33,916	21,259	31,467	38,658	43,208	43,007
PW4.4.1	Fiber Model	8,590	31,022	-	-	25,121	37,995	42,698	-
	CFE	8,385	29,388	29,967	20,962	28,140	35,829	39,114	38,789
PW4.4.2	Fiber Model	8,920	39,557	-	-	32,039	47,762	52,873	53,267
	CFE	8,624	37,607	38,020	21,561	34,944	45,161	50,406	49,563
PW4.5.1	Fiber Model	8,783	33,807	-	-	28,014	41,387	47,762	47,453
	CFE	8,523	32,218	32,799	21,308	30,849	39,145	43,279	42,985
PW4.5.2	Fiber Model	8,709	37,573	-	-	29,311	45,041	48,580	48,632
	CFE	8,472	35,403	35,657	21,180	32,491	42,403	46,794	45,843
PW4.6.1	Fiber Model	8,751	35,274	-	-	28,446	42,845	45,321	45,406
	CFE	8,497	33,389	33,906	21,242	31,413	40,388	44,600	44,013
PW4.6.2	Fiber Model	8,757	35,202	-	-	28,513	42,716	44,824	45,161
	CFE	8,497	33,389	33,906	21,242	31,413	40,388	44,600	44,013

Table 6.12(b): Lateral Drift of parametric walls associated with PW4.0.0

Drift (%)		DEC	ELL1	ELL2	ELL3	YMS	LLP	FMS	CCC
PW4.0.0	Fiber Model	0.04	0.54	-	-	0.25	1.91	5.73	5.83
	CFE	0.03	0.33	0.49	0.08	0.22	2.16	5.35	6.44
PW4.1.1	Fiber Model	0.04	0.54	-	-	0.25	1.03	5.60	7.16
	CFE	0.03	0.31	0.52	0.07	0.21	2.09	5.25	6.86
PW4.1.2	Fiber Model	0.04	0.60	-	-	0.26	1.96	5.53	5.60
	CFE	0.04	0.35	0.47	0.09	0.23	2.24	5.46	6.05
PW4.2.1	Fiber Model	0.04	0.51	-	-	0.25	2.31	5.87	5.88
	CFE	0.03	0.31	0.51	0.07	0.21	2.62	5.33	6.54
PW4.2.2	Fiber Model	0.04	0.59	-	-	0.26	1.48	5.47	6.20
	CFE	0.03	0.35	0.48	0.09	0.23	1.70	5.34	6.39
PW4.3.1	Fiber Model	0.04	0.54	-	-	0.25	2.36	5.60	5.67
	CFE	0.03	0.33	0.49	0.08	0.22	2.70	5.42	6.20
PW4.3.2	Fiber Model	0.04	0.54	-	-	0.25	1.45	5.60	7.07
	CFE	0.03	0.33	0.49	0.08	0.22	1.66	5.28	6.72
PW4.4.1	Fiber Model	0.04	0.51	-	-	0.24	1.88	5.26	-
	CFE	0.03	0.31	0.48	0.08	0.21	2.14	5.30	6.52
PW4.4.2	Fiber Model	0.04	0.56	-	-	0.26	1.91	6.41	6.53
	CFE	0.03	0.35	0.50	0.08	0.23	2.19	5.40	6.36
PW4.5.1	Fiber Model	0.04	0.51	-	-	0.25	1.87	5.60	7.81
	CFE	0.03	0.32	0.50	0.08	0.22	2.12	5.30	6.64
PW4.5.2	Fiber Model	0.04	0.60	-	-	0.26	1.94	5.73	5.80
	CFE	0.03	0.35	0.48	0.08	0.22	2.22	5.44	6.13
PW4.6.1	Fiber Model	0.04	0.54	-	-	0.25	1.91	5.73	5.80
	CFE	0.03	0.33	0.49	0.08	0.22	2.16	5.36	6.41
PW4.6.2	Fiber Model	0.04	0.54	-	-	0.25	1.90	5.87	5.93
	CFE	0.03	0.33	0.49	0.08	0.22	2.16	5.36	6.41

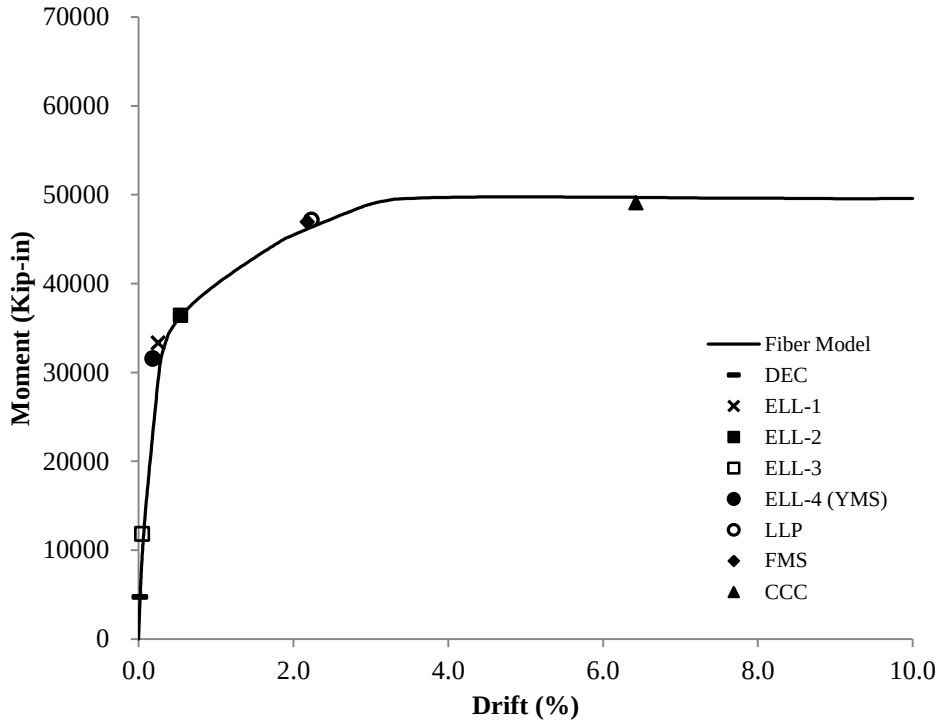

Figure 6.1(a): Base moment and roof drift response of PW1.0.0 with wall limit states

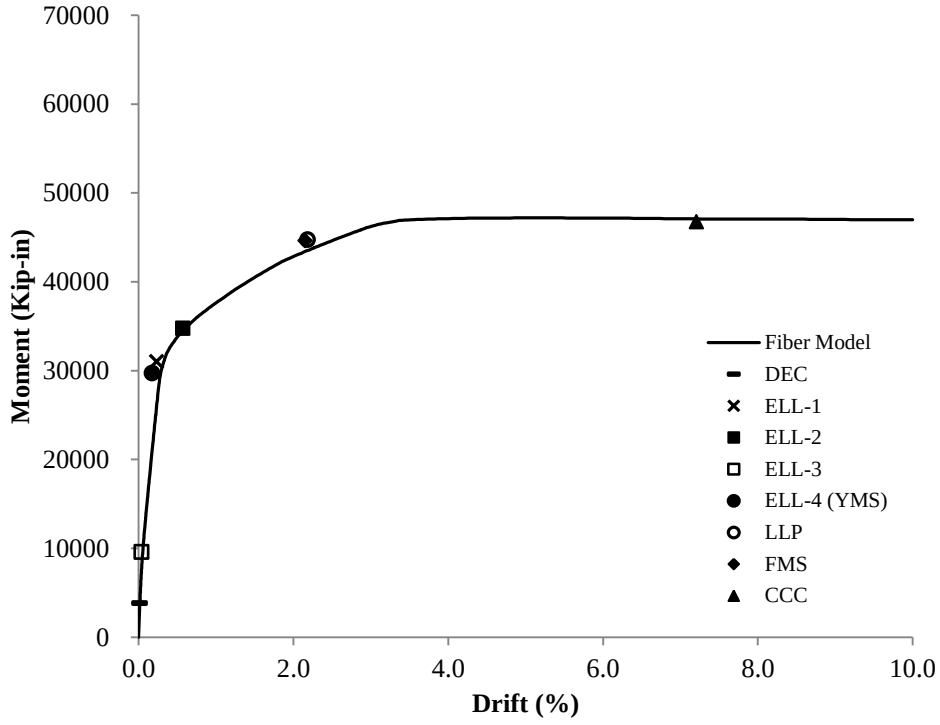

Figure 6.1(b): Base moment and roof drift response of PW1.1.1 with wall limit states

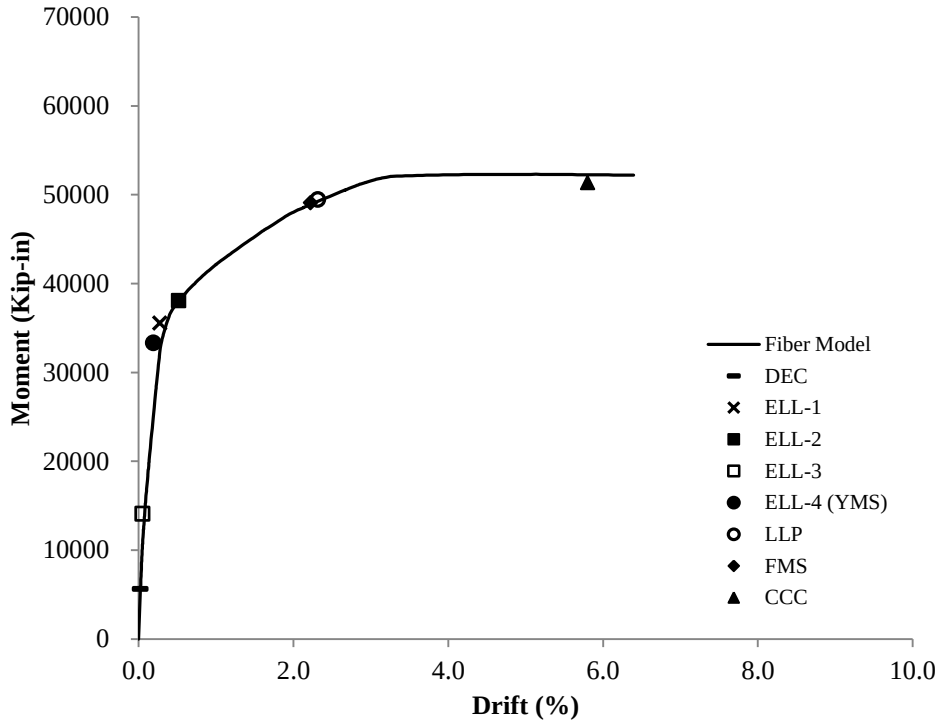

Figure 6.1(c): Base moment and roof drift response of PW1.1.2 with wall limit states

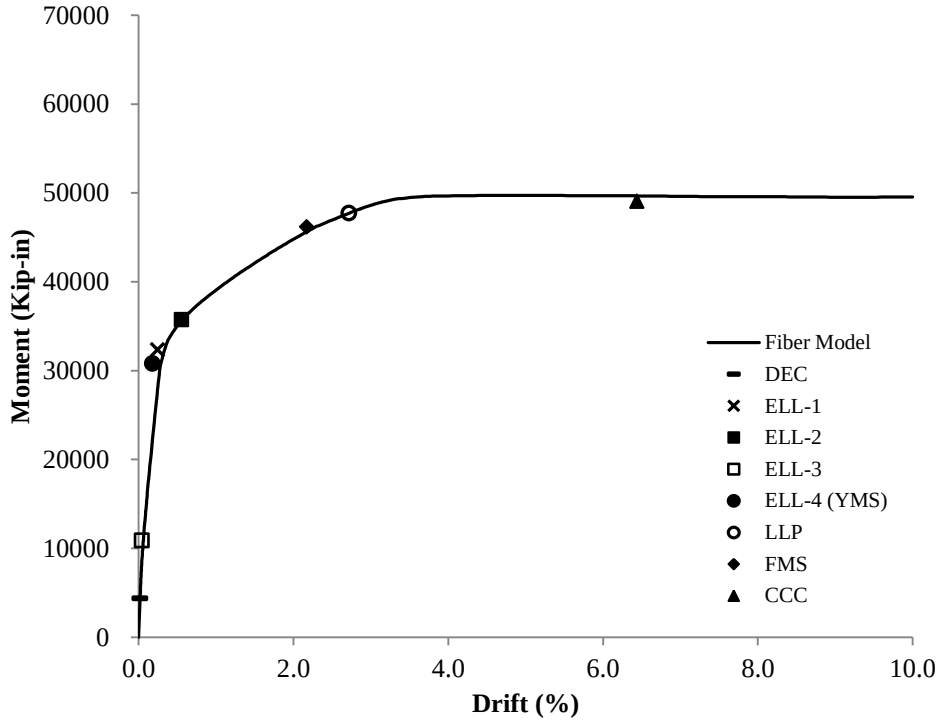

Figure 6.1(d): Base moment and roof drift response of PW1.2.1 with wall limit states

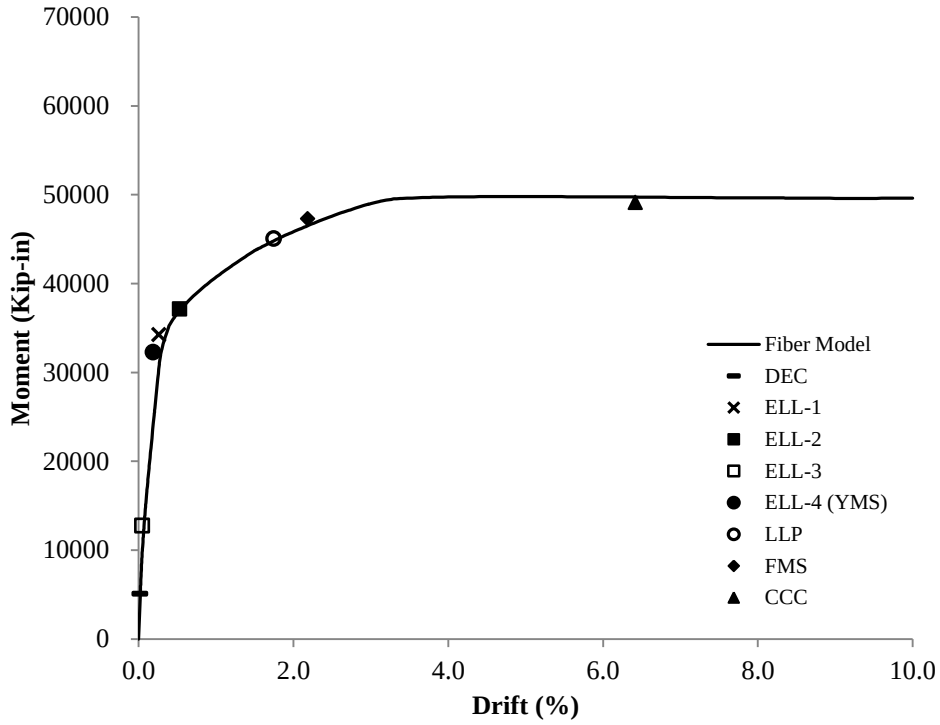

Figure 6.1(e): Base moment and roof drift response of PW1.2.2 with wall limit states

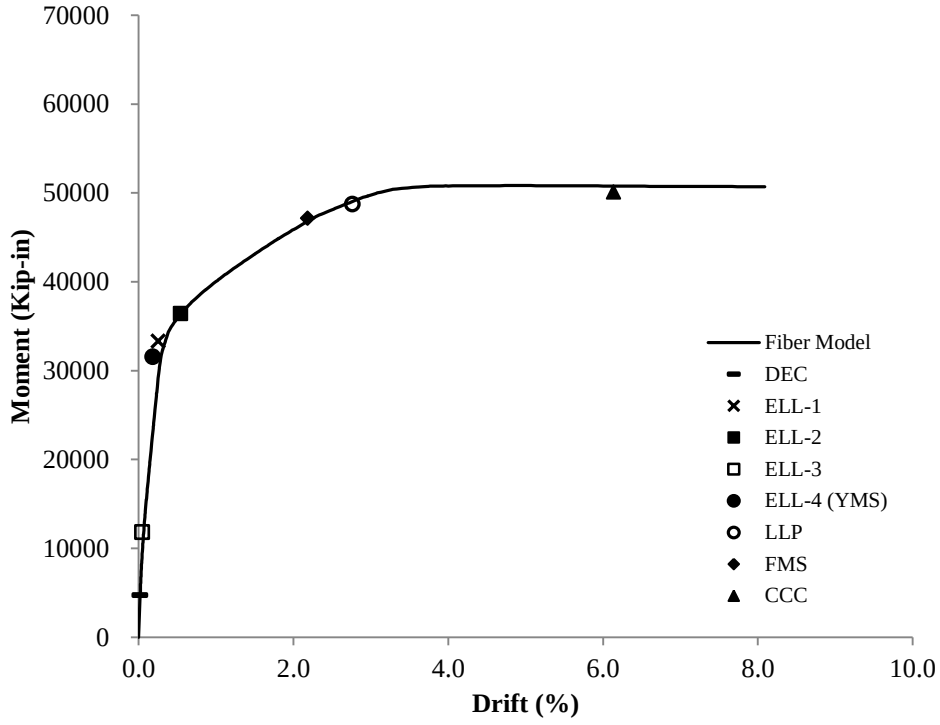

Figure 6.1(f): Base moment and roof drift response of PW1.3.1 with wall limit states

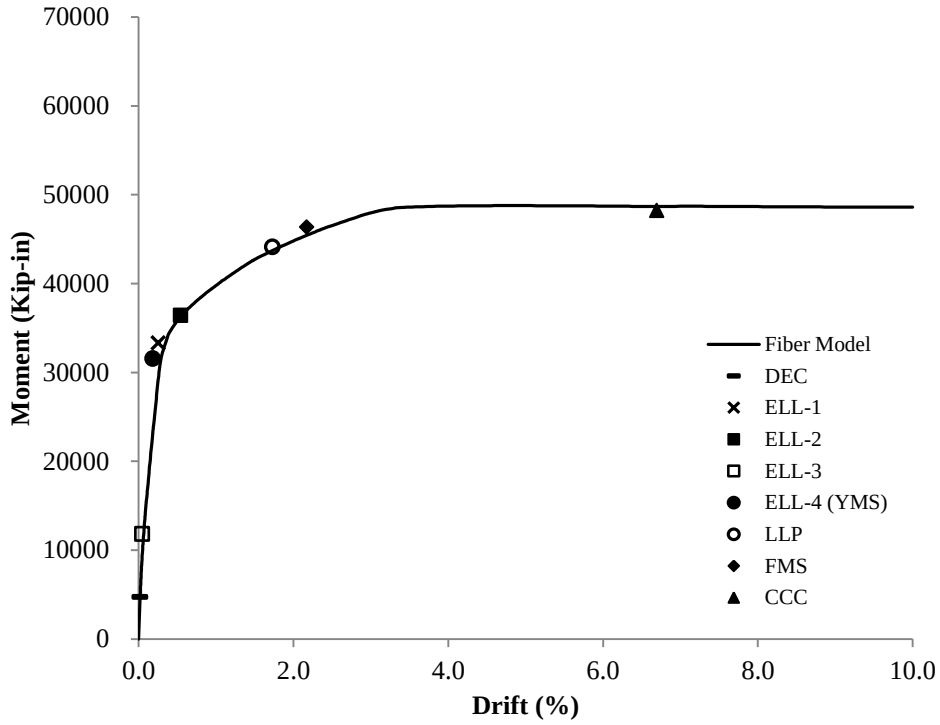

Figure 6.1(g): Base moment and roof drift response of PW1.3.2 with wall limit states

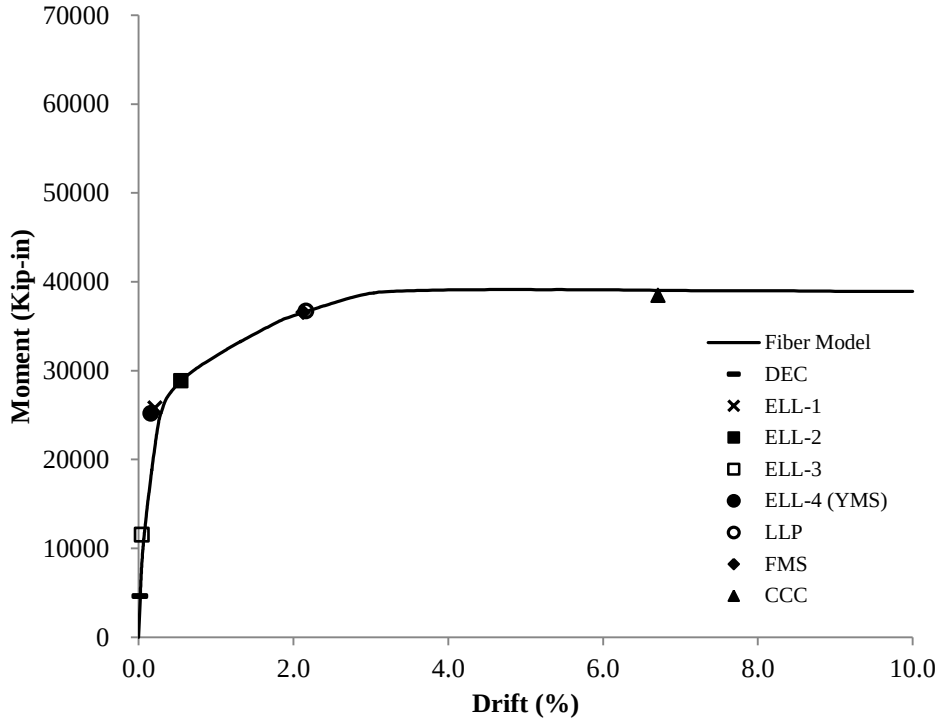

Figure 6.1(h): Base moment and roof drift response of PW1.4.1 with wall limit states

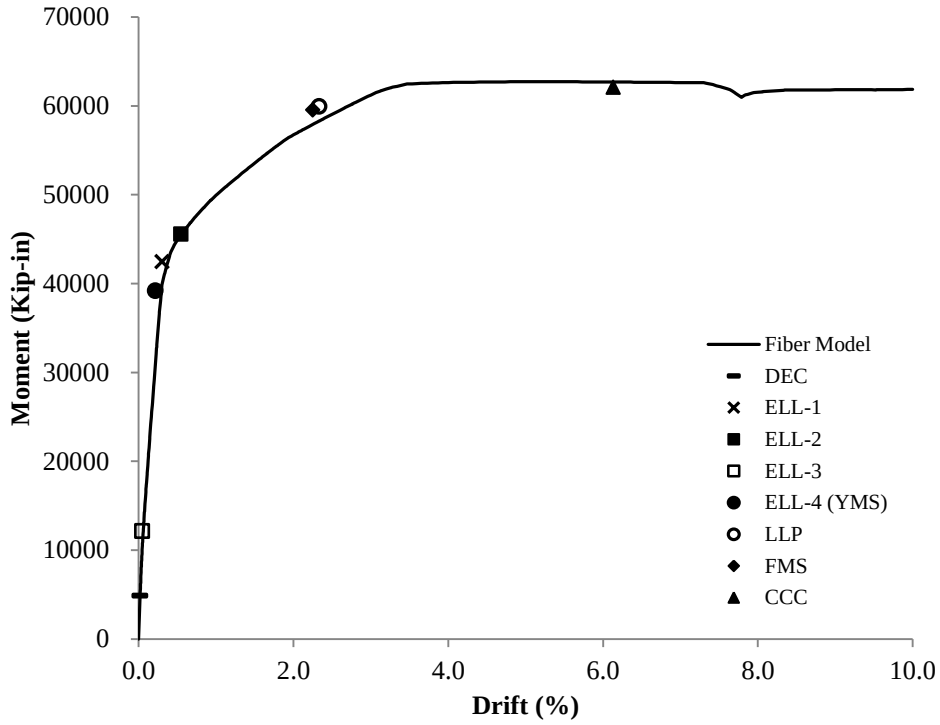

Figure 6.1(i): Base moment and roof drift response of PW1.4.2 with wall limit states

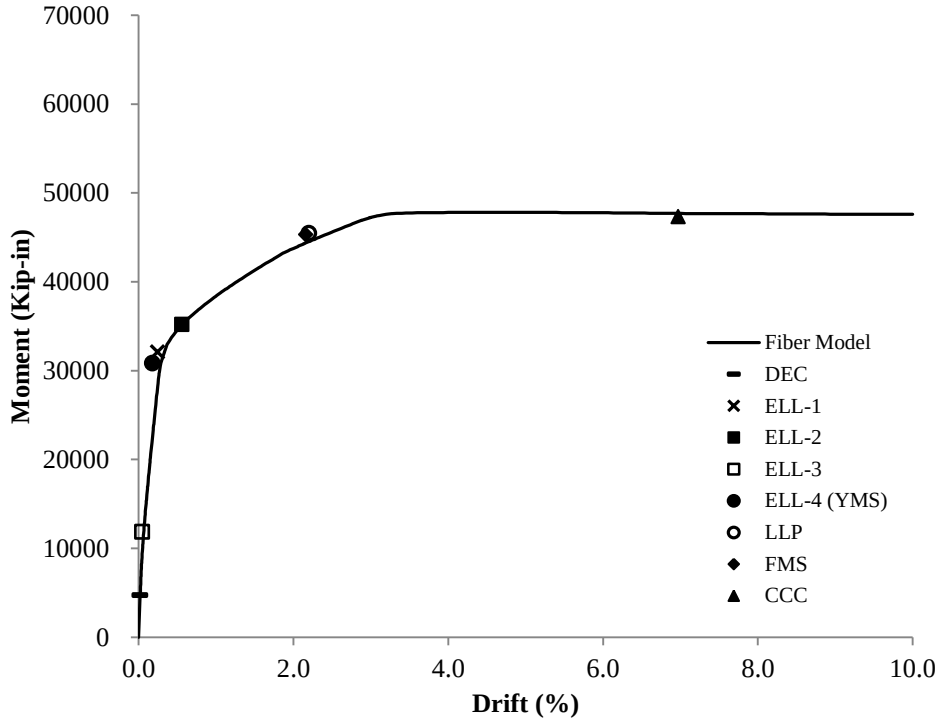

Figure 6.1(j): Base moment and roof drift response of PW1.5.1 with wall limit states

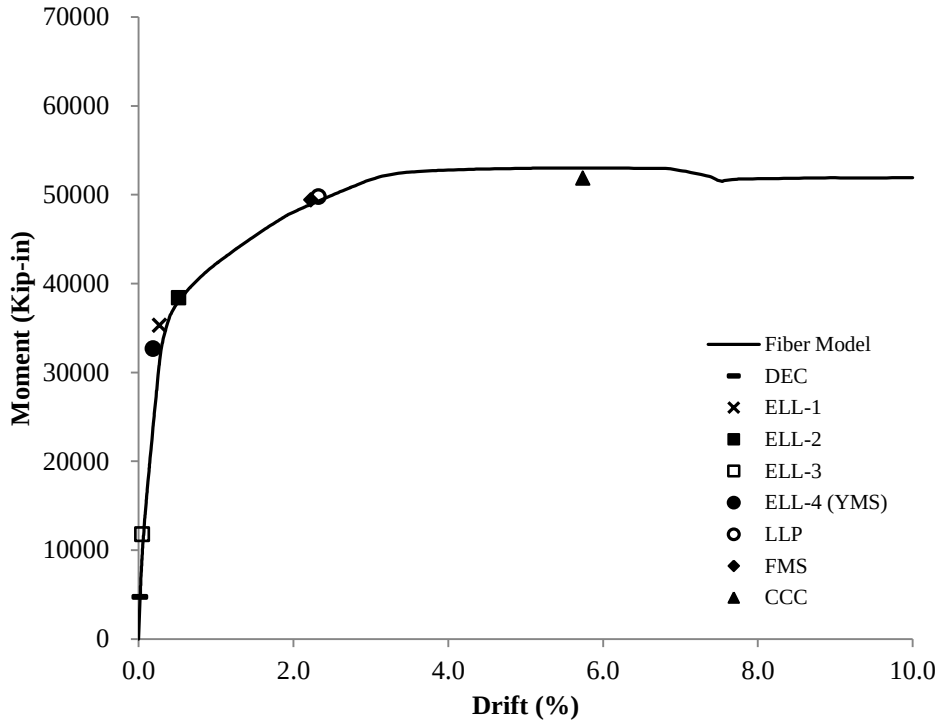

Figure 6.1(k): Base moment and roof drift response of PW1.5.2 with wall limit states

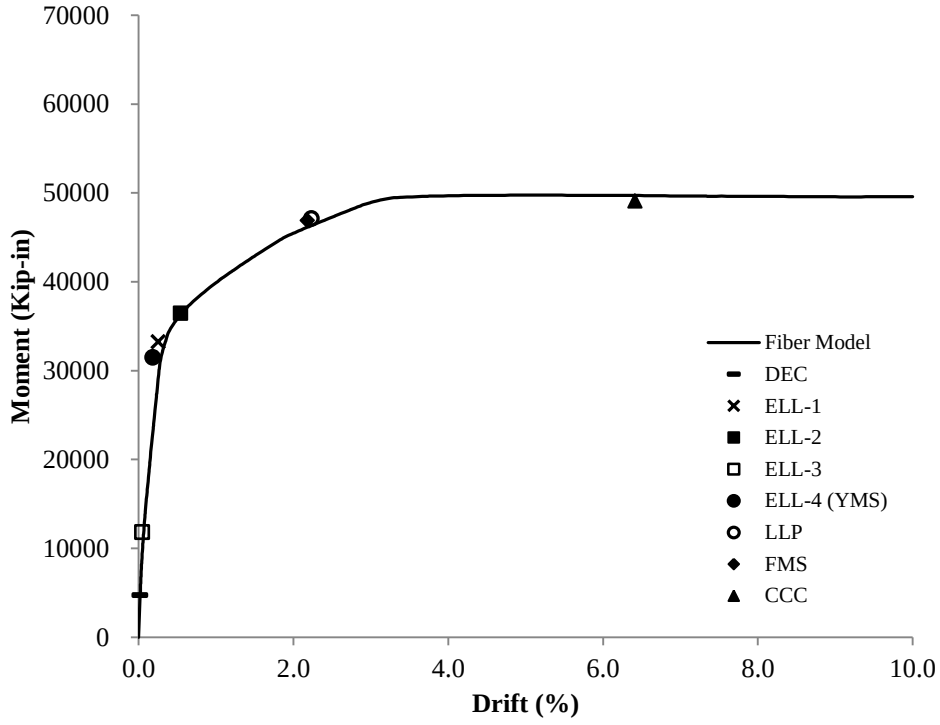

Figure 6.1(l): Base moment and roof drift response of PW1.6.1 with wall limit states

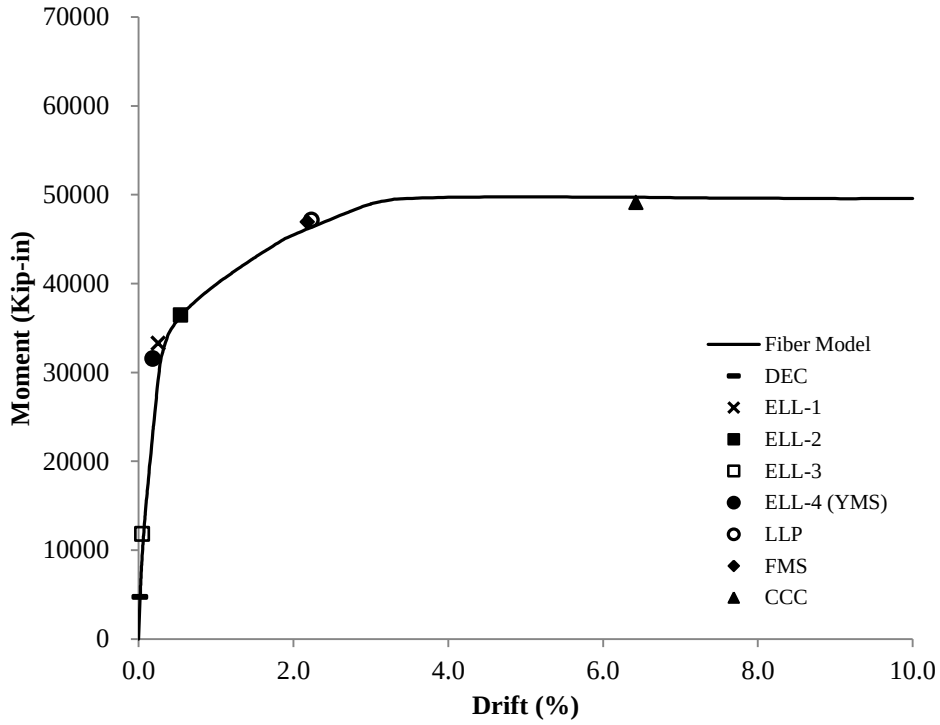

Figure 6.1(m): Base moment and roof drift response of PW1.6.2 with wall limit states

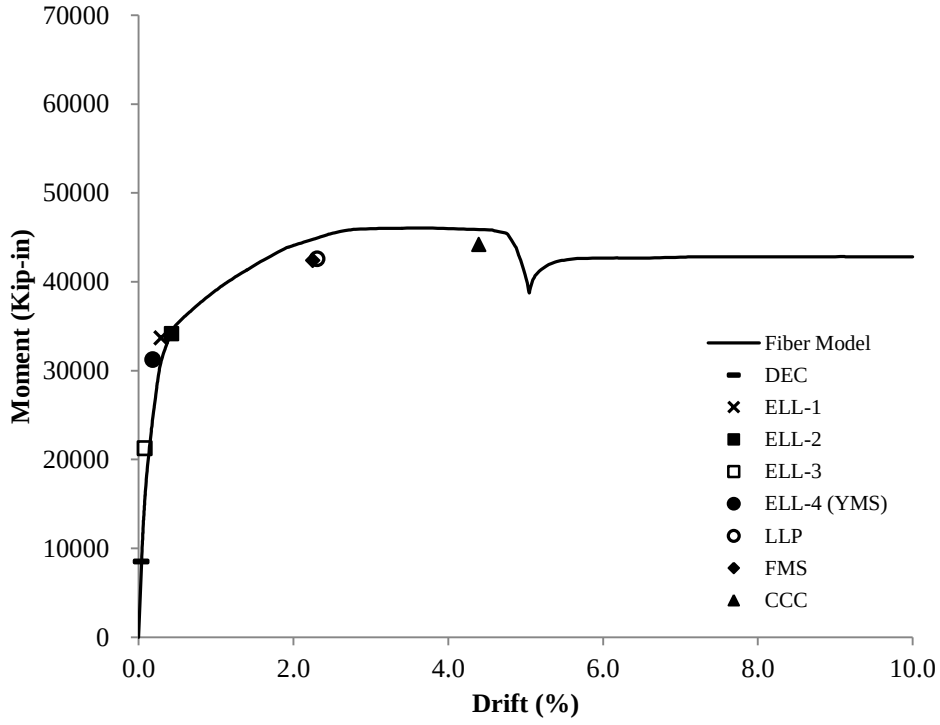

Figure 6.2(a): Base moment and roof drift response of PW2.0.0 with wall limit states

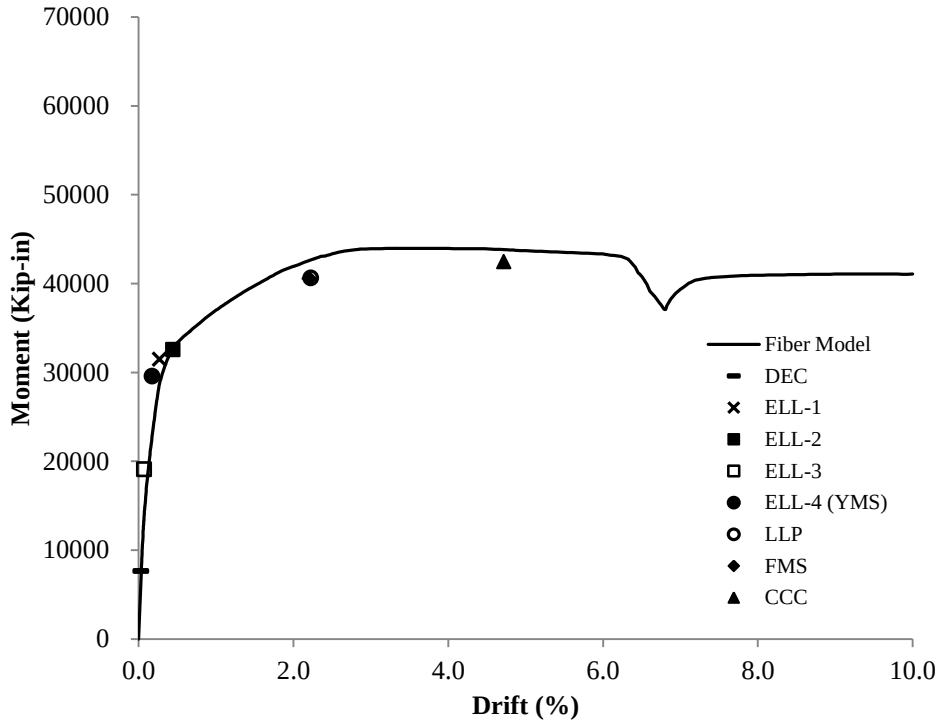

Figure 6.2(b): Base moment and roof drift response of PW2.1.1 with wall limit states

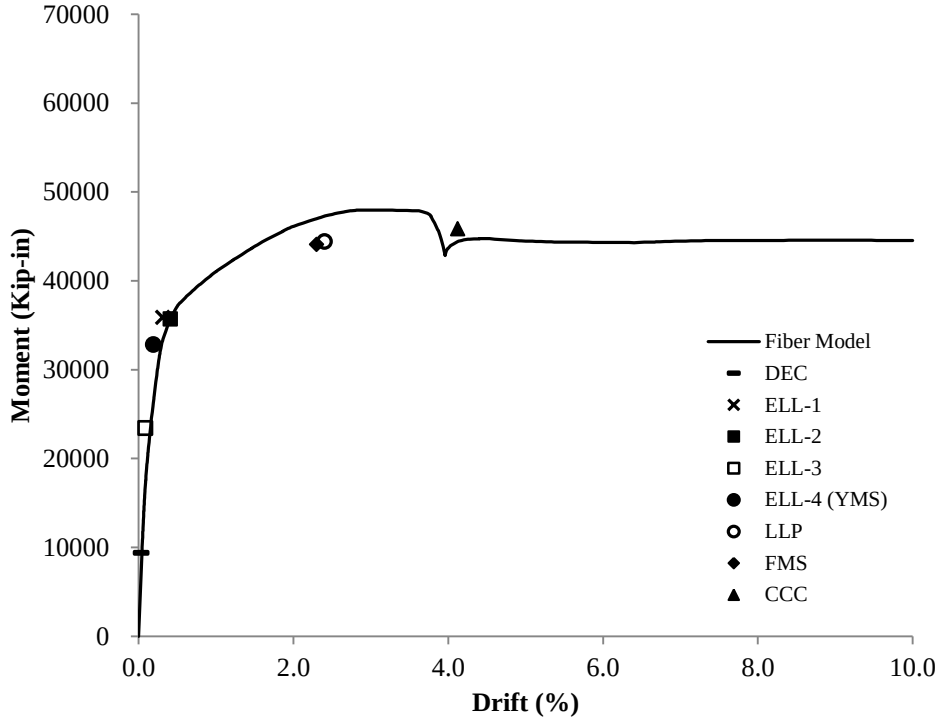

Figure 6.2(c): Base moment and roof drift response of PW2.1.2 with wall limit states

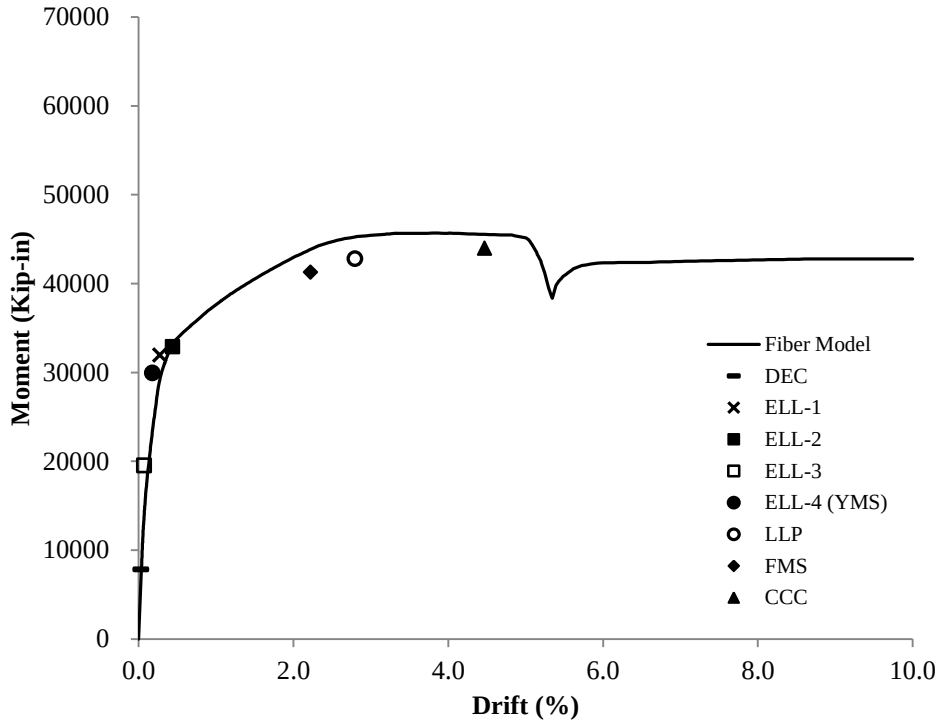

Figure 6.2(d): Base moment and roof drift response of PW2.2.1 with wall limit states

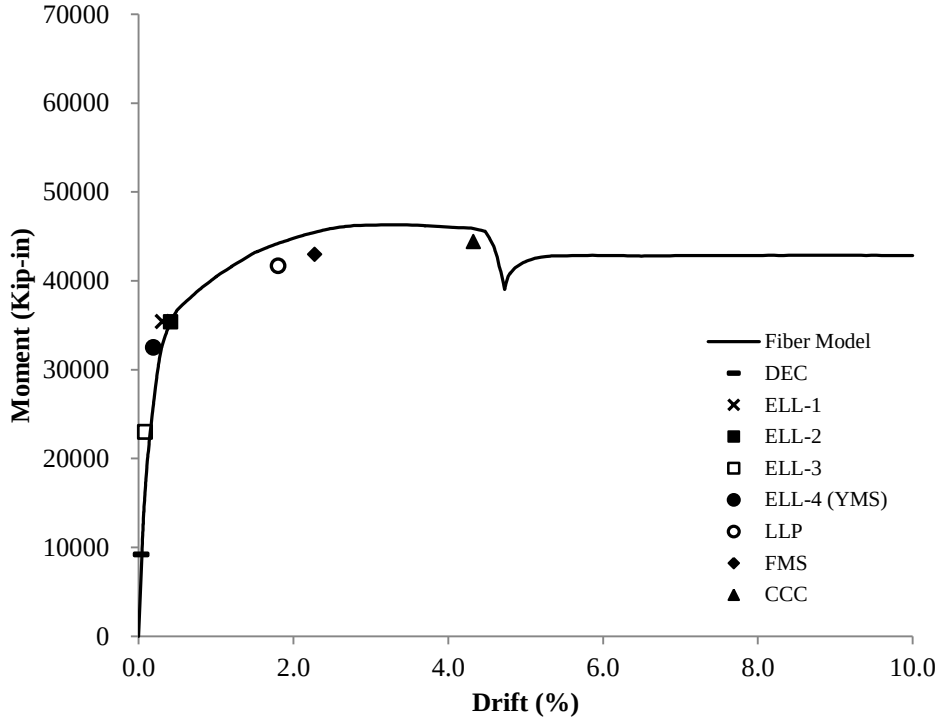

Figure 6.2(e): Base moment and roof drift response of PW2.2.2 with wall limit states

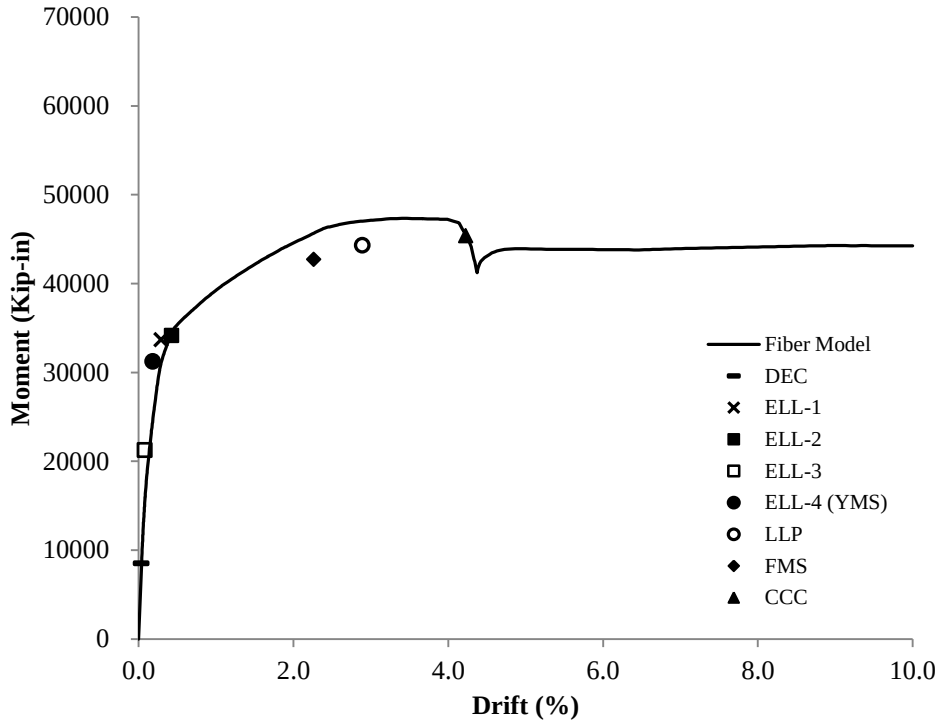

Figure 6.2(f): Base moment and roof drift response of PW2.3.1 with wall limit states

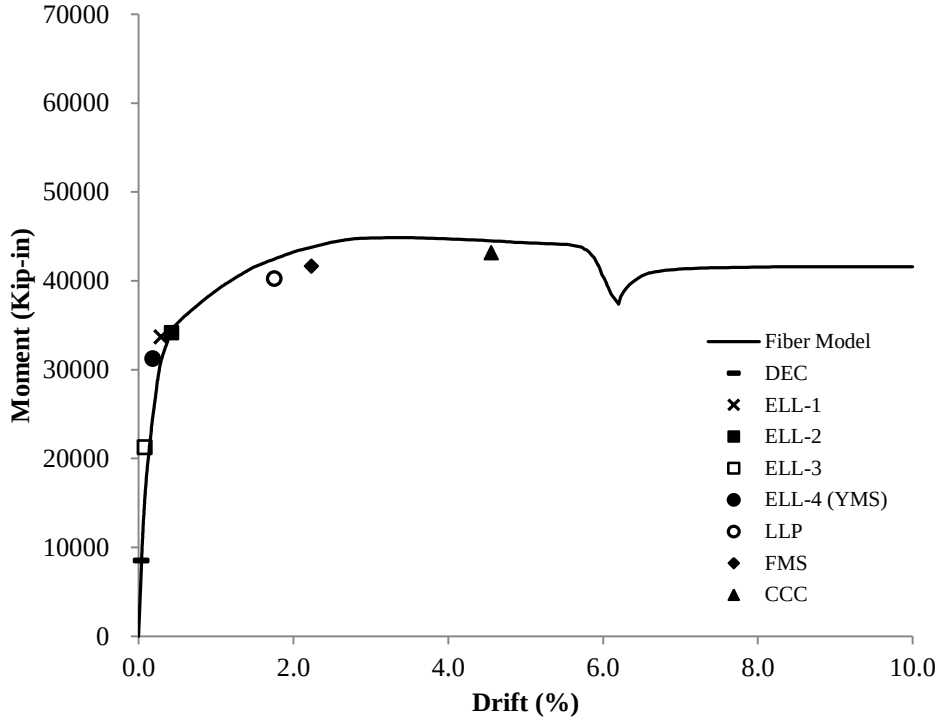

Figure 6.2(g): Base moment and roof drift response of PW2.3.2 with wall limit states

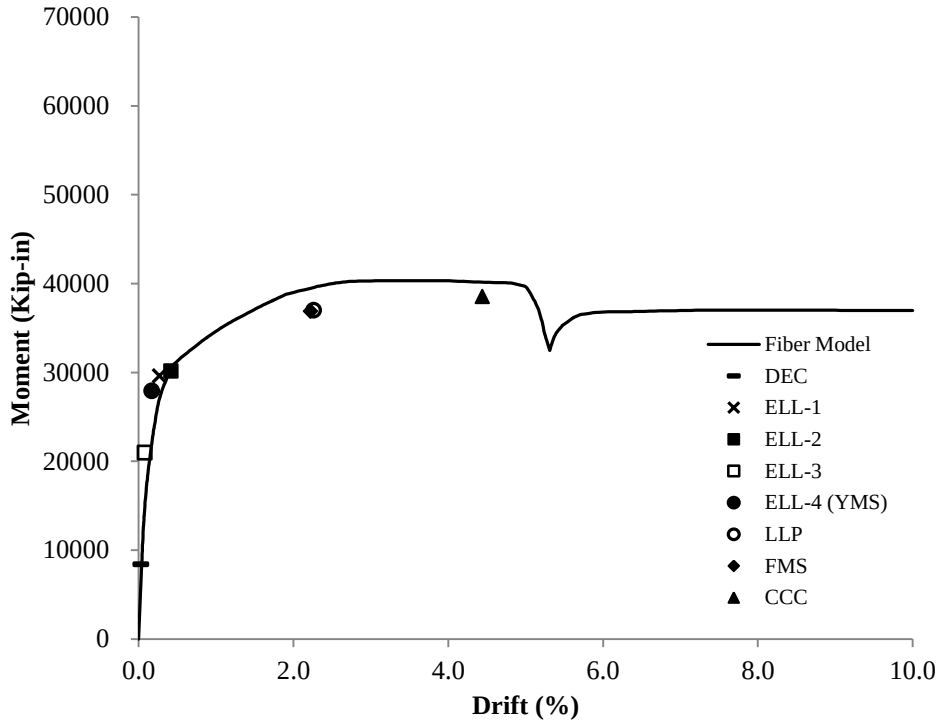

Figure 6.2(h): Base moment and roof drift response of PW2.4.1 with wall limit states

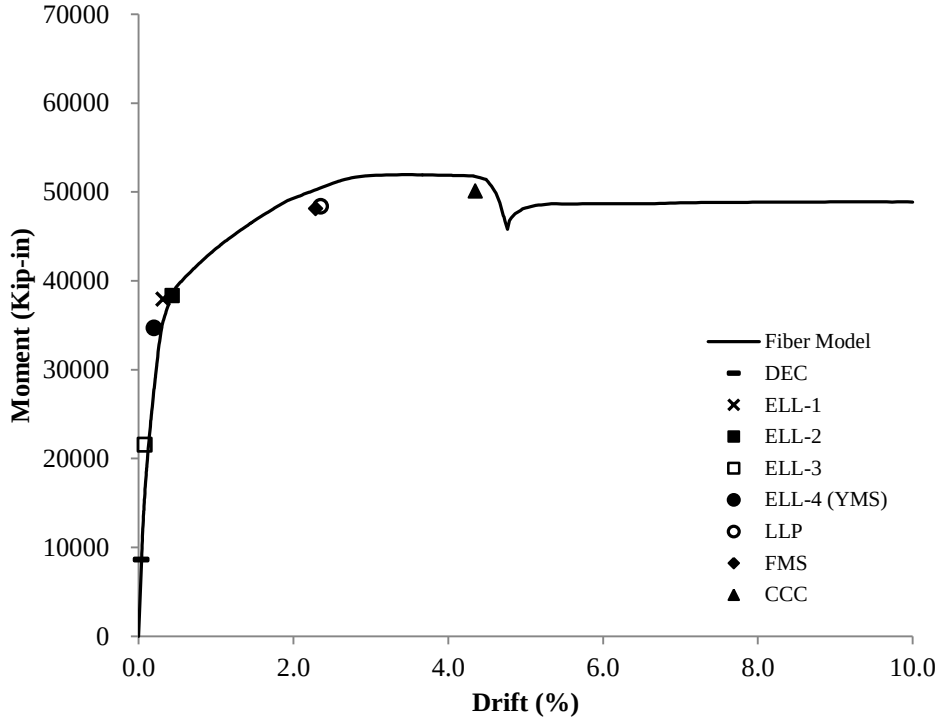

Figure 6.2(i): Base moment and roof drift response of PW2.4.2 with wall limit states

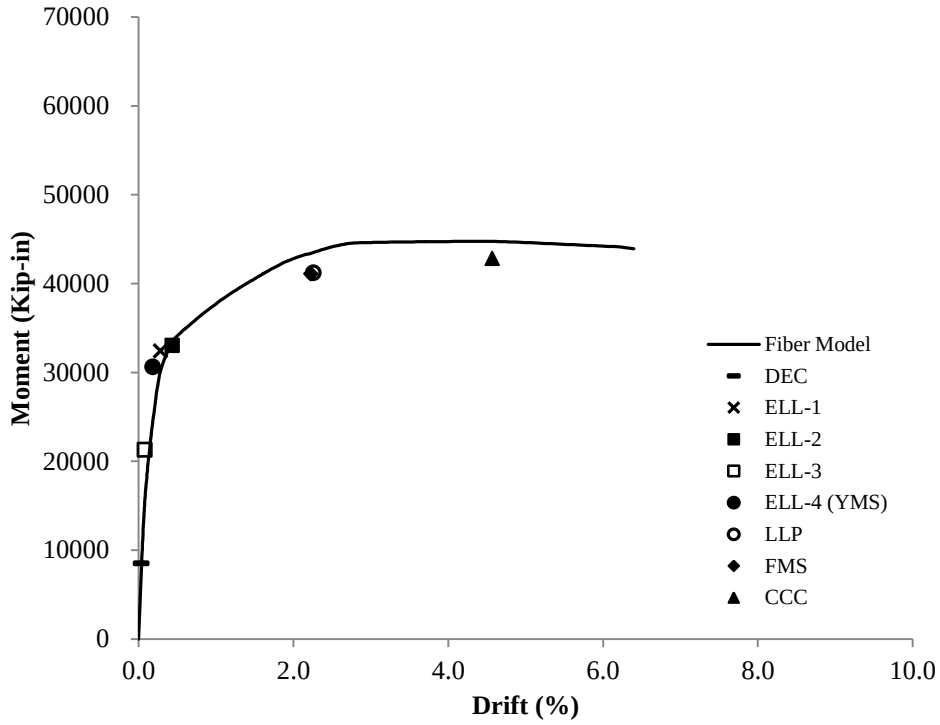

Figure 6.2(j): Base moment and roof drift response of PW2.5.1 with wall limit states

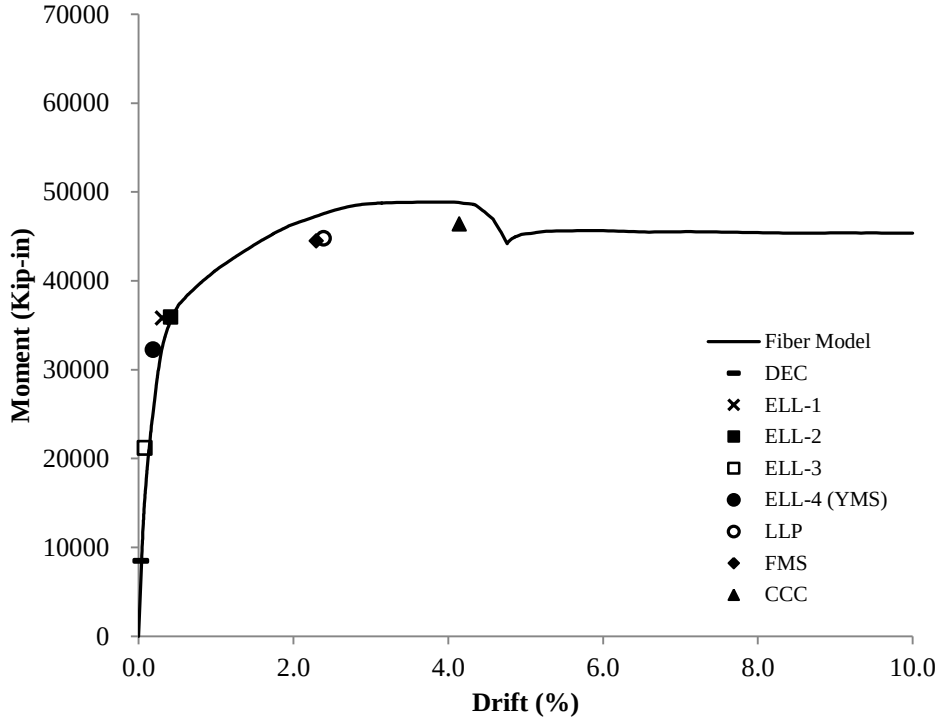

Figure 6.2(k): Base moment and roof drift response of PW2.5.2 with wall limit states

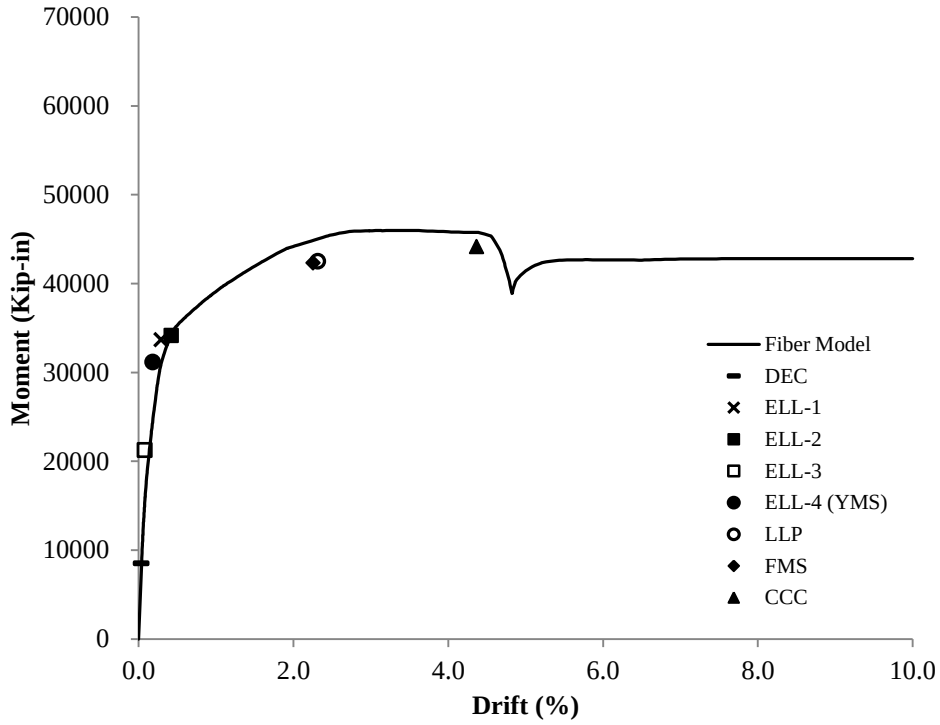

Figure 6.2(l): Base moment and roof drift response of PW2.6.1 with wall limit states

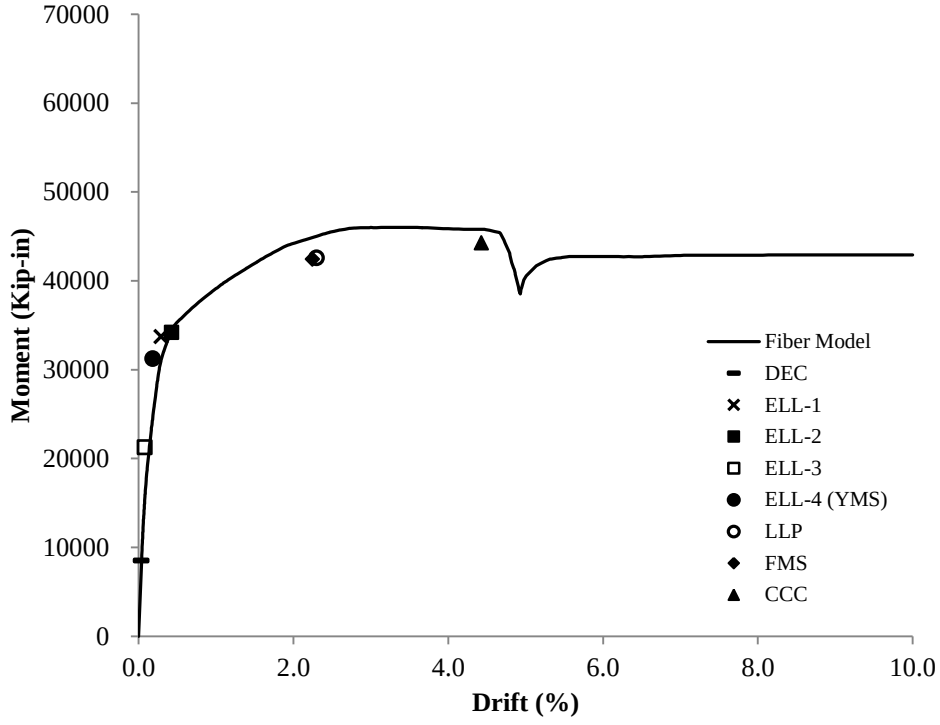

Figure 6.2(m): Base moment and roof drift response of PW2.6.2 with wall limit states

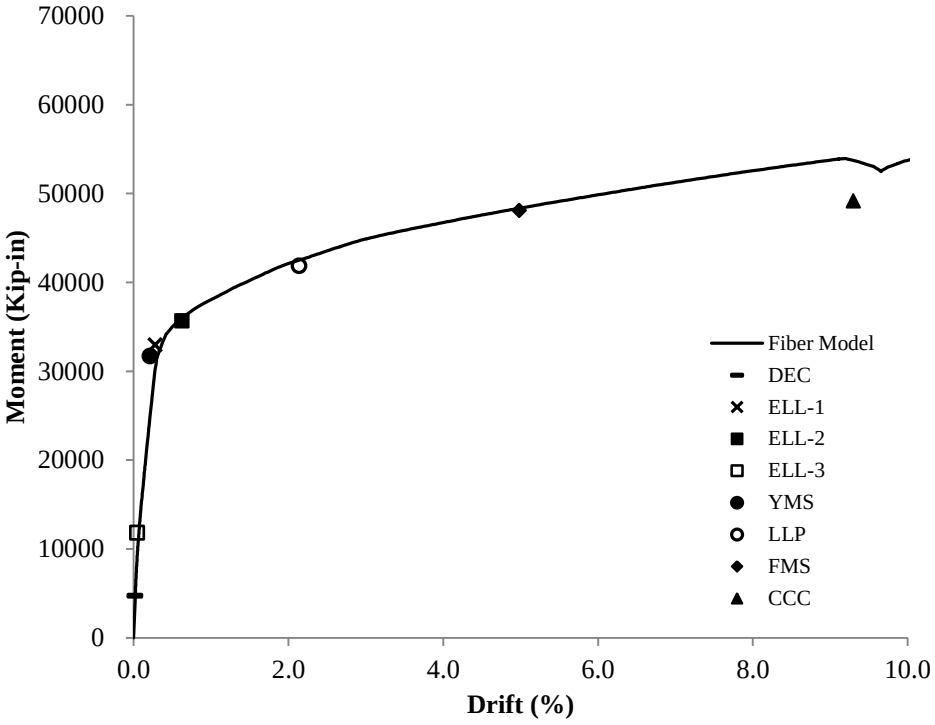

Figure 6.3(a): Base moment and roof drift response of PW3.0.0 with wall limit states

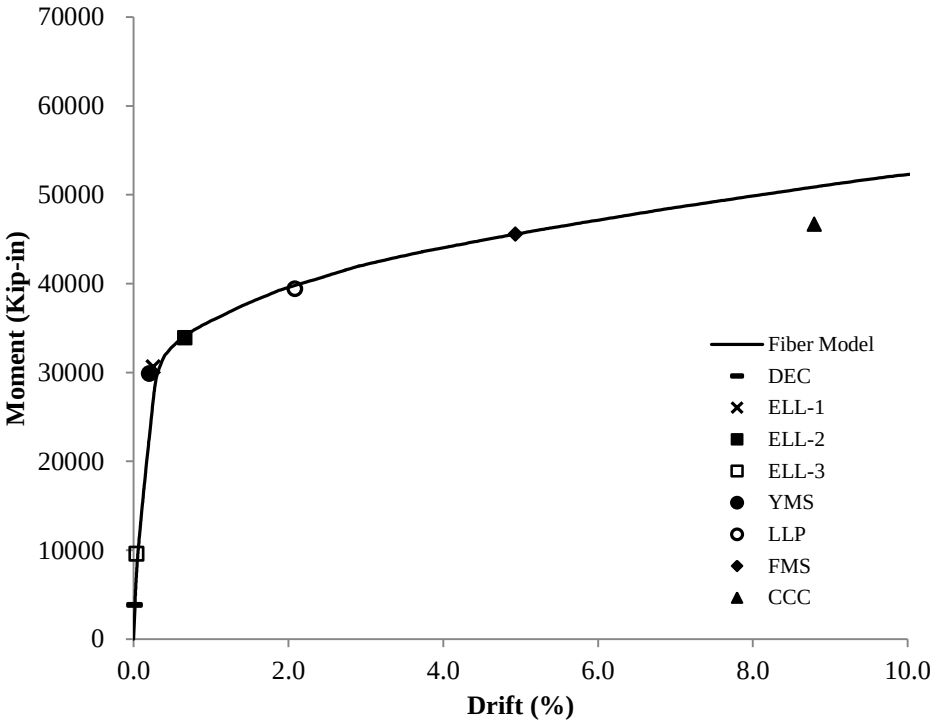

Figure 6.3(b): Base moment and roof drift response of PW3.1.1 with wall limit states

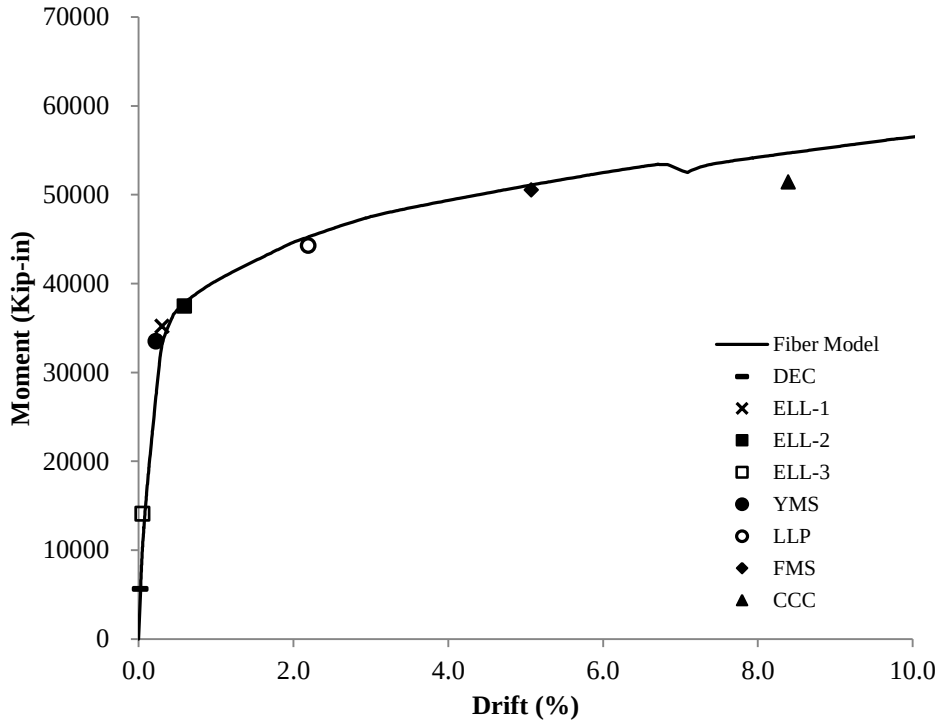

Figure 6.3(c): Base moment and roof drift response of PW3.1.2 with wall limit states

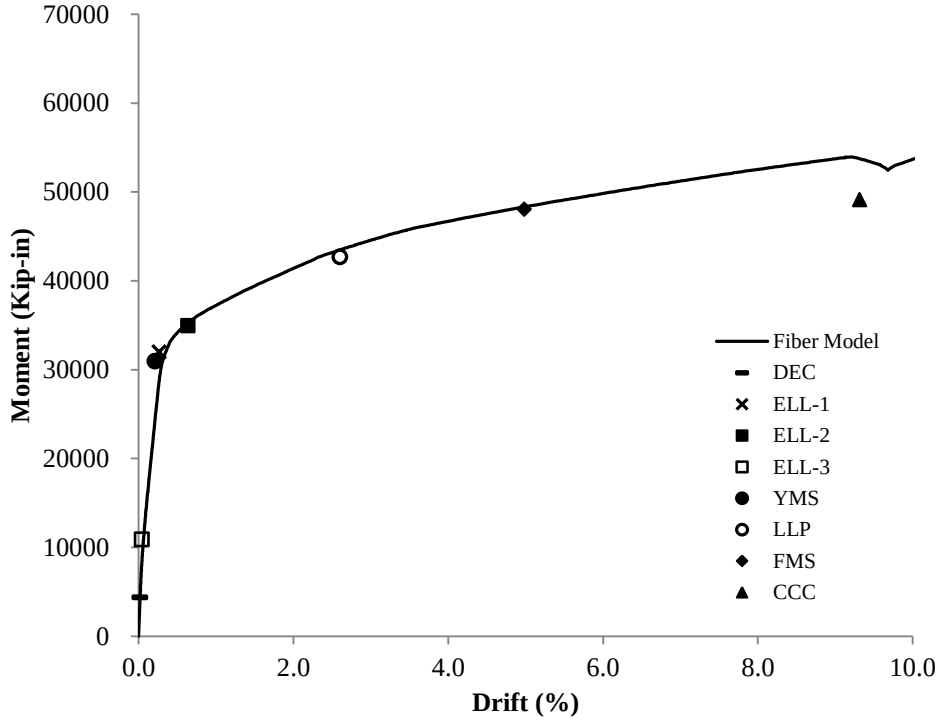

Figure 6.3(d): Base moment and roof drift response of PW3.2.1 with wall limit states

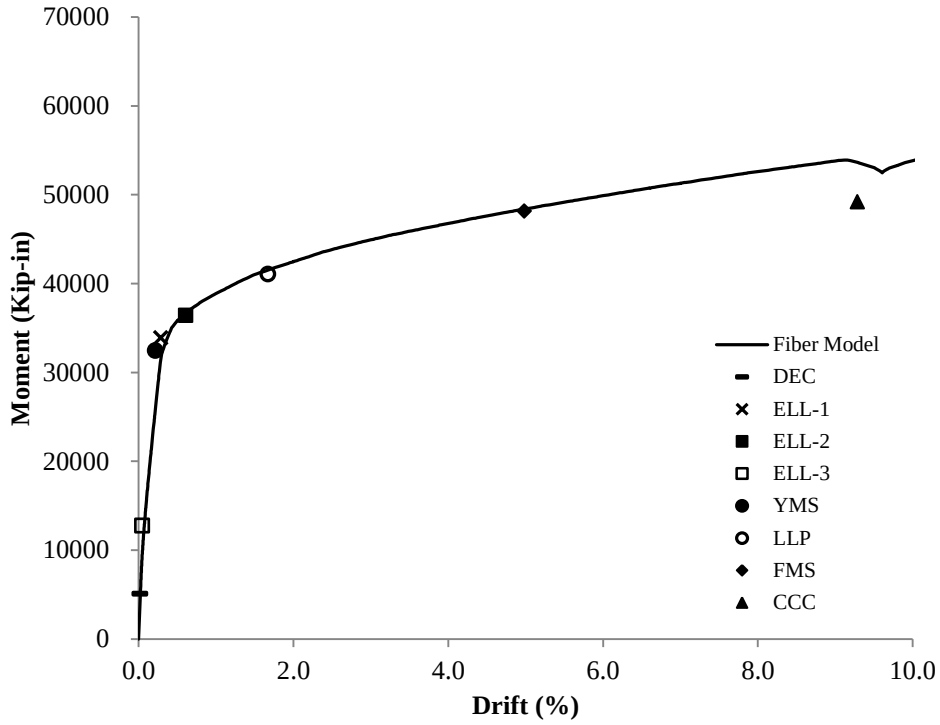

Figure 6.3(e): Base moment and roof drift response of PW3.2.2 with wall limit states

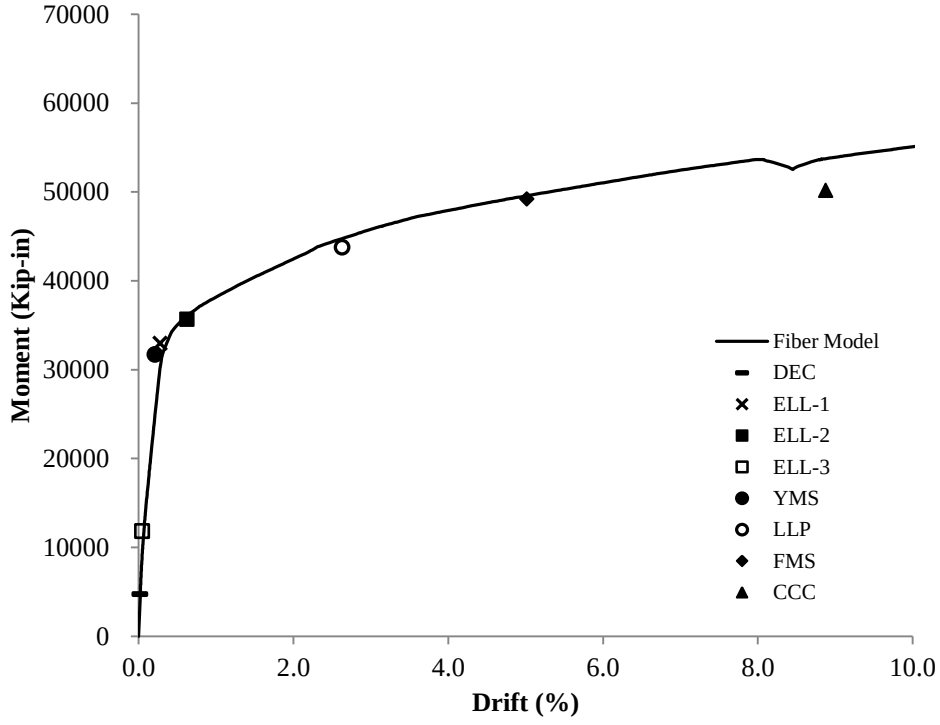

Figure 6.3(f): Base moment and roof drift response of PW3.3.1 with wall limit states

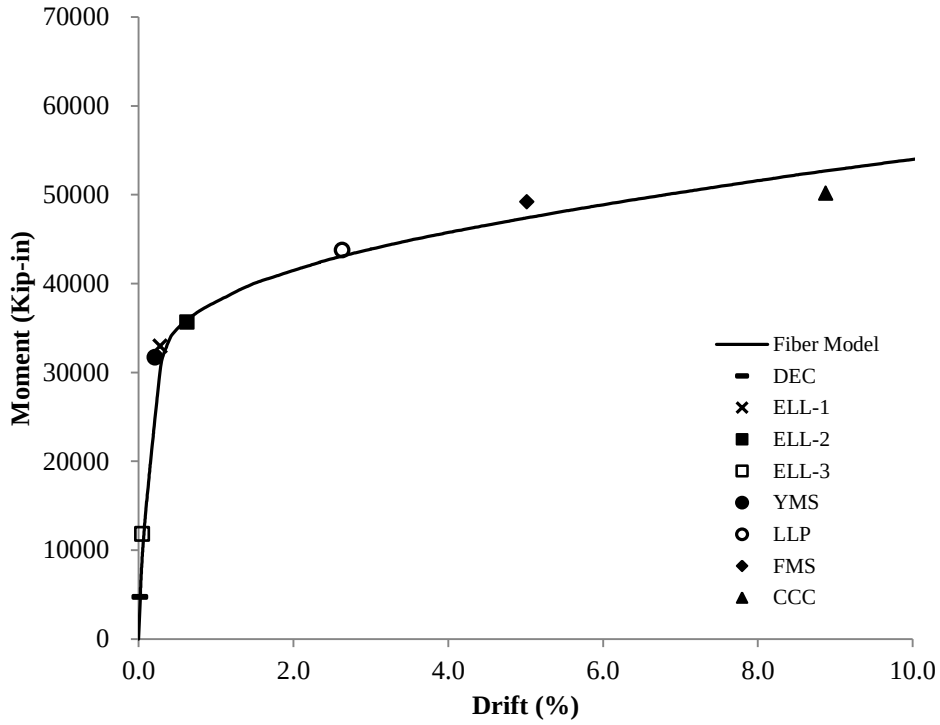

Figure 6.3(g): Base moment and roof drift response of PW3.3.2 with wall limit states

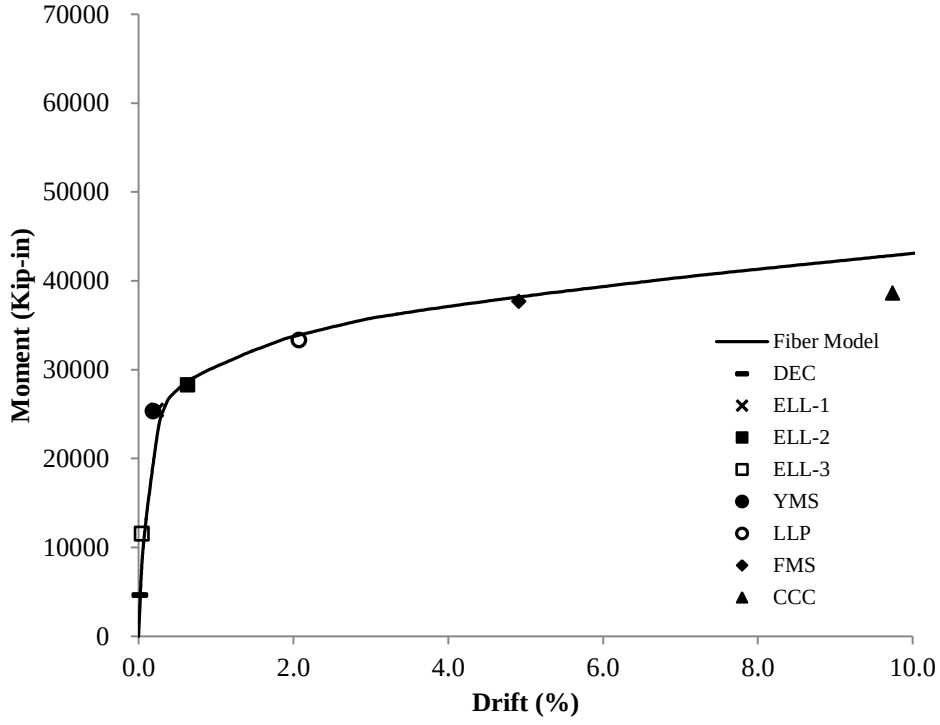

Figure 6.3(h): Base moment and roof drift response of PW3.4.1 with wall limit states

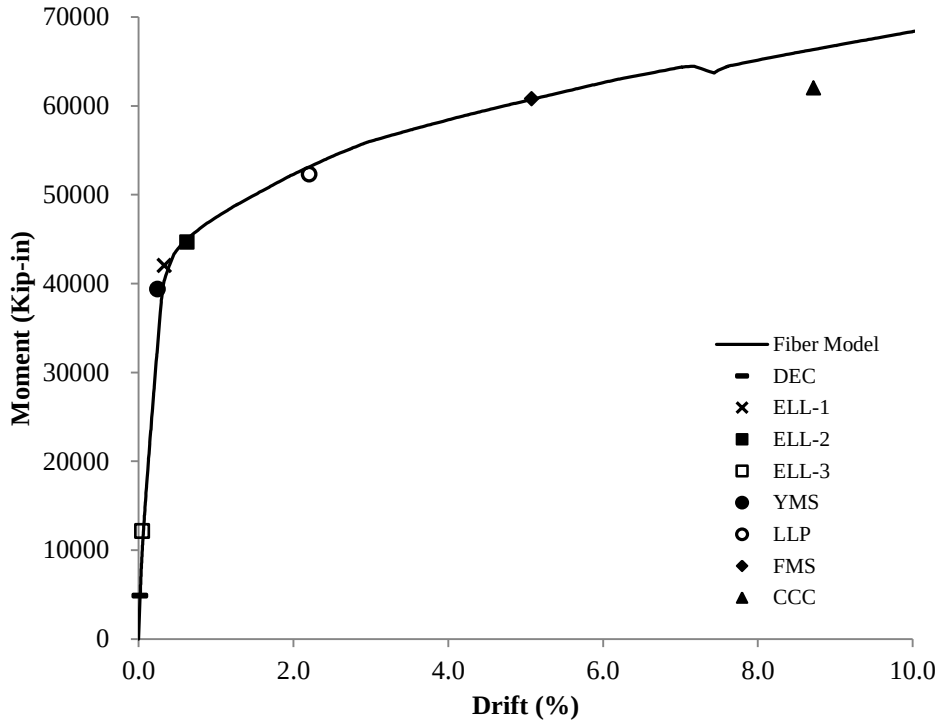

Figure 6.3(i): Base moment and roof drift response of PW3.4.2 with wall limit states

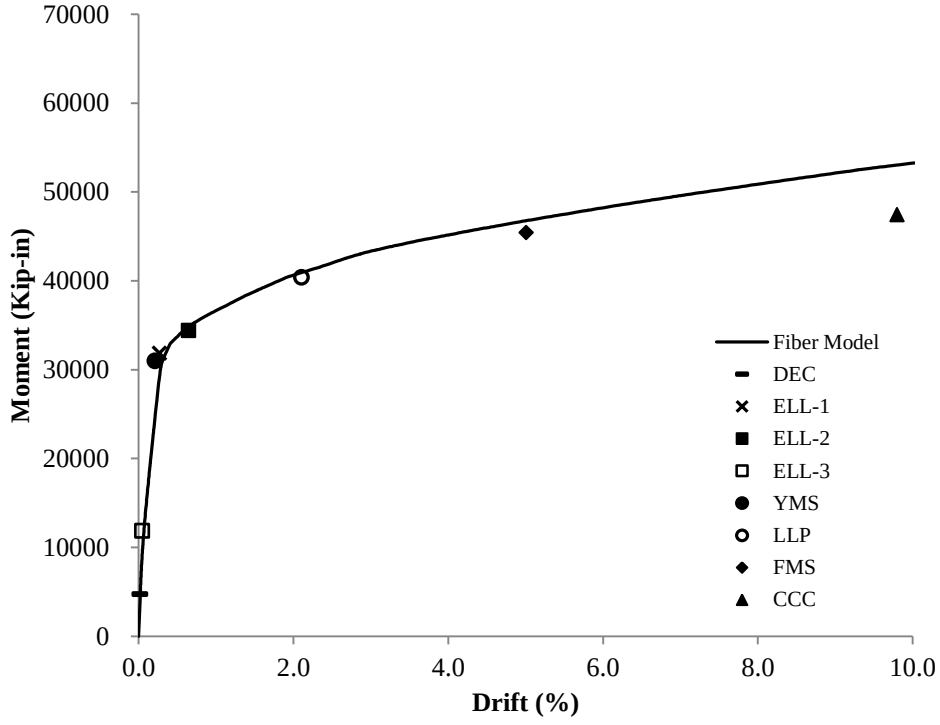

Figure 6.3(j): Base moment and roof drift response of PW3.5.1 with wall limit states

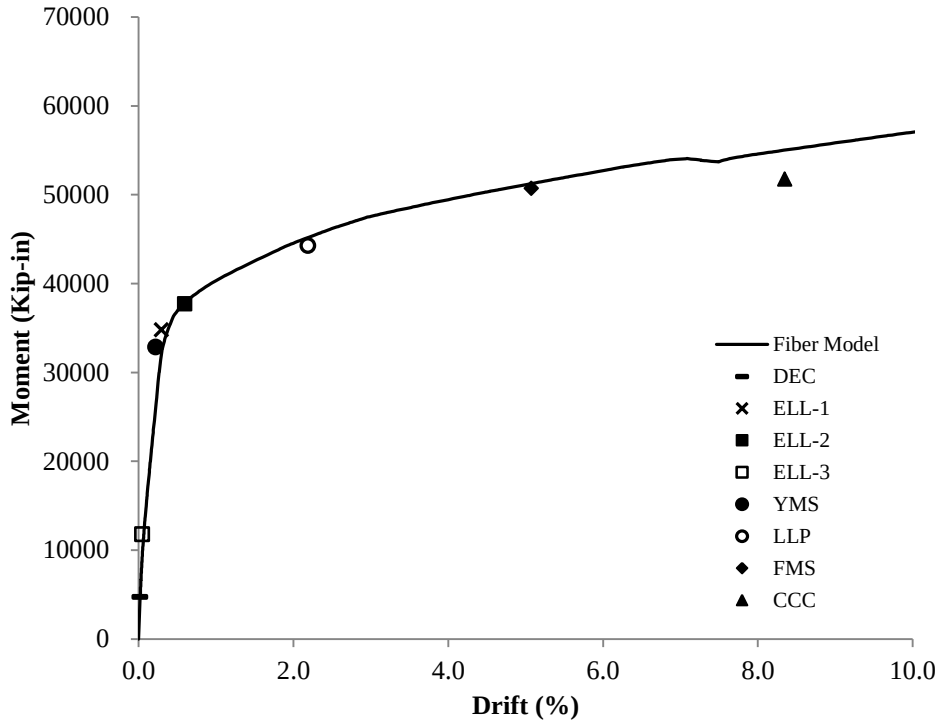

Figure 6.3(k): Base moment and roof drift response of PW3.5.2 with wall limit states

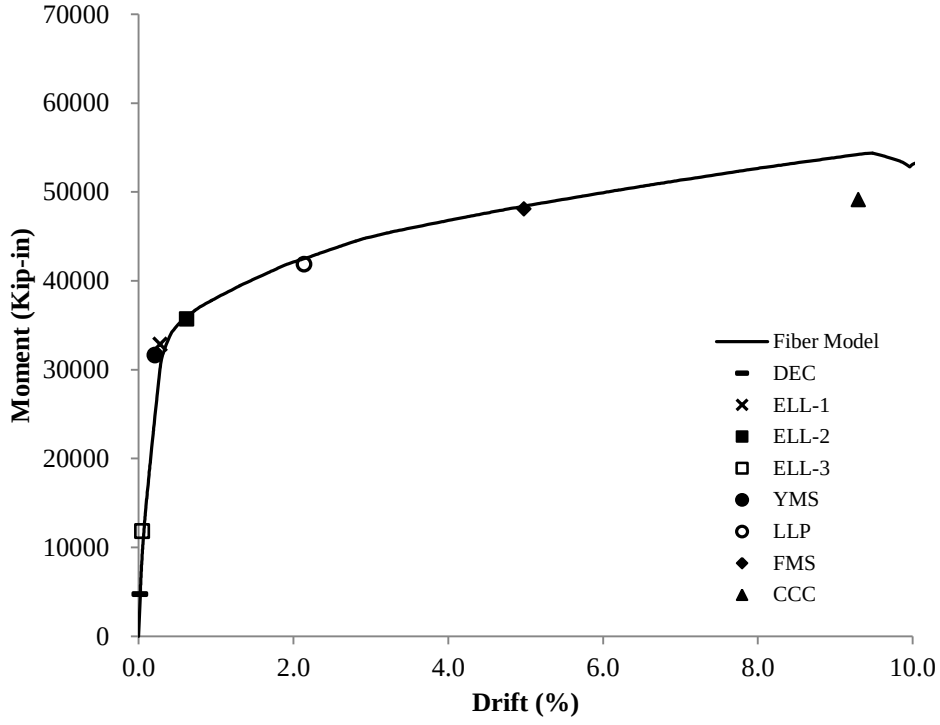

Figure 6.3(l): Base moment and roof drift response of PW3.6.1 with wall limit states

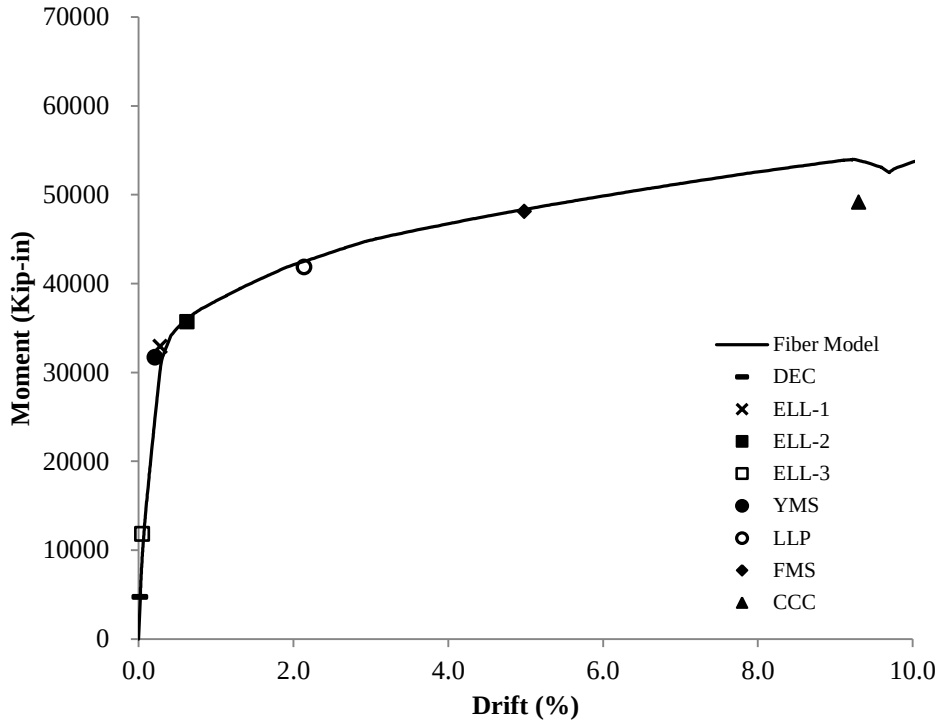

Figure 6.3(m): Base moment and roof drift response of PW3.6.2 with wall limit states

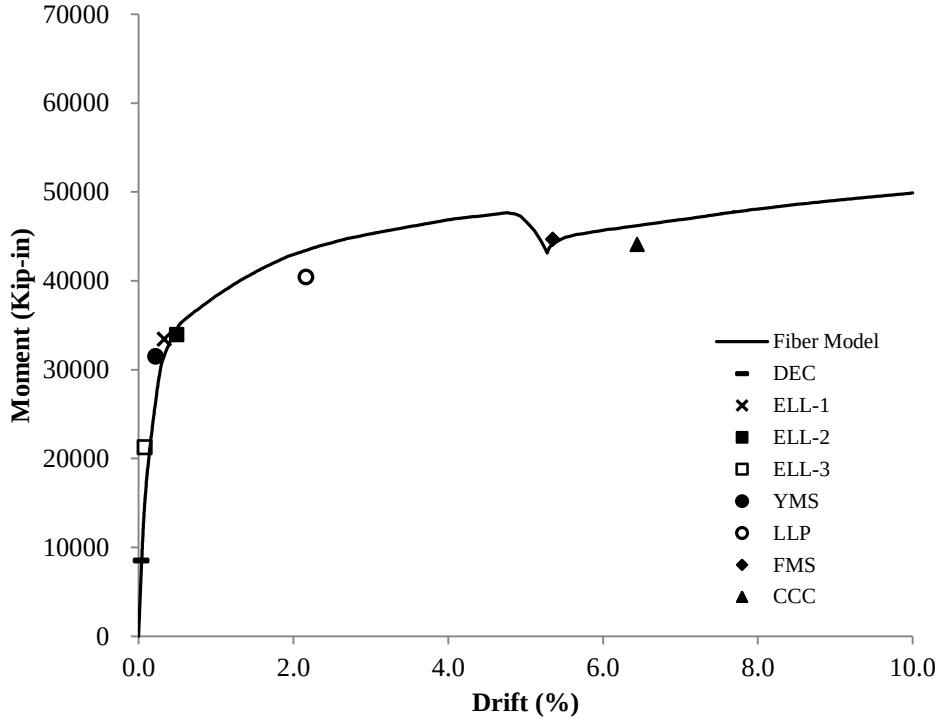

Figure 6.4(a): Base moment and roof drift response of PW4.0.0 with wall limit states

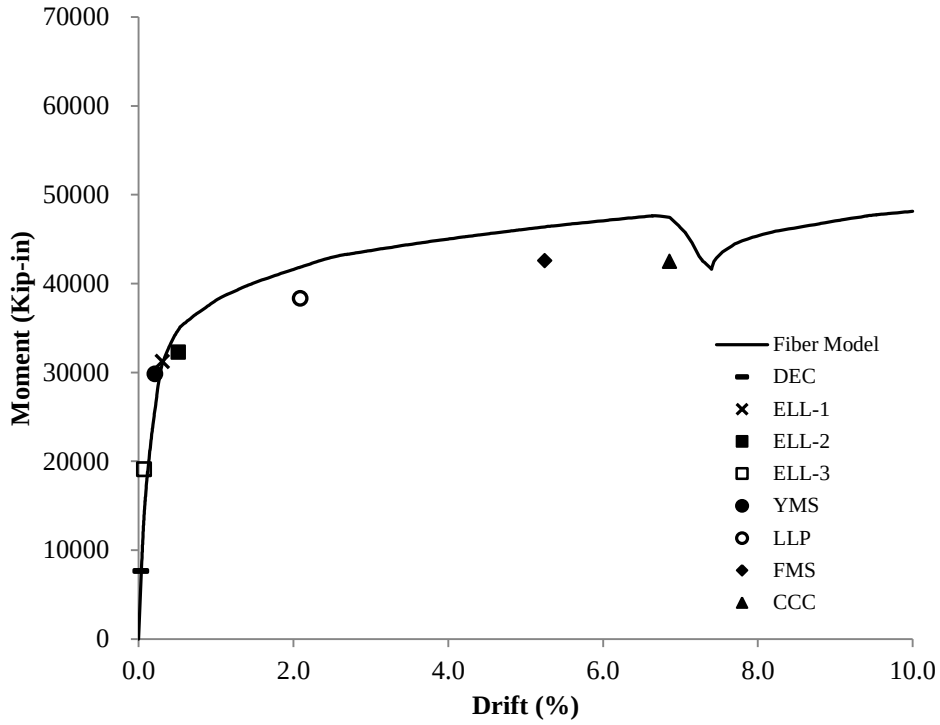

Figure 6.4(b): Base moment and roof drift response of PW4.1.1 with wall limit states

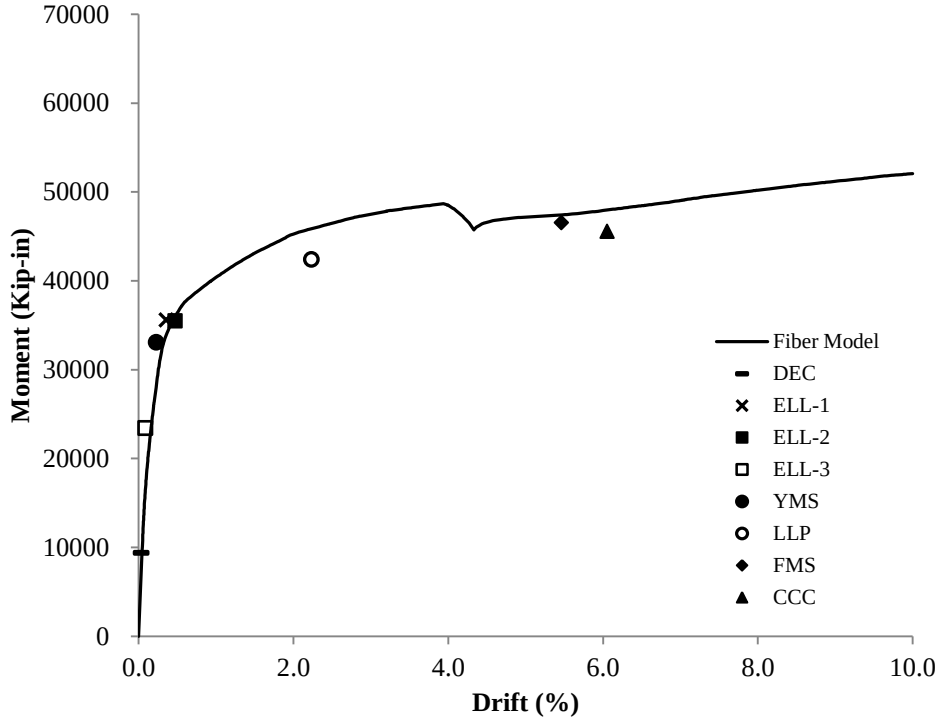

Figure 6.4(c): Base moment and roof drift response of PW4.1.2 with wall limit states

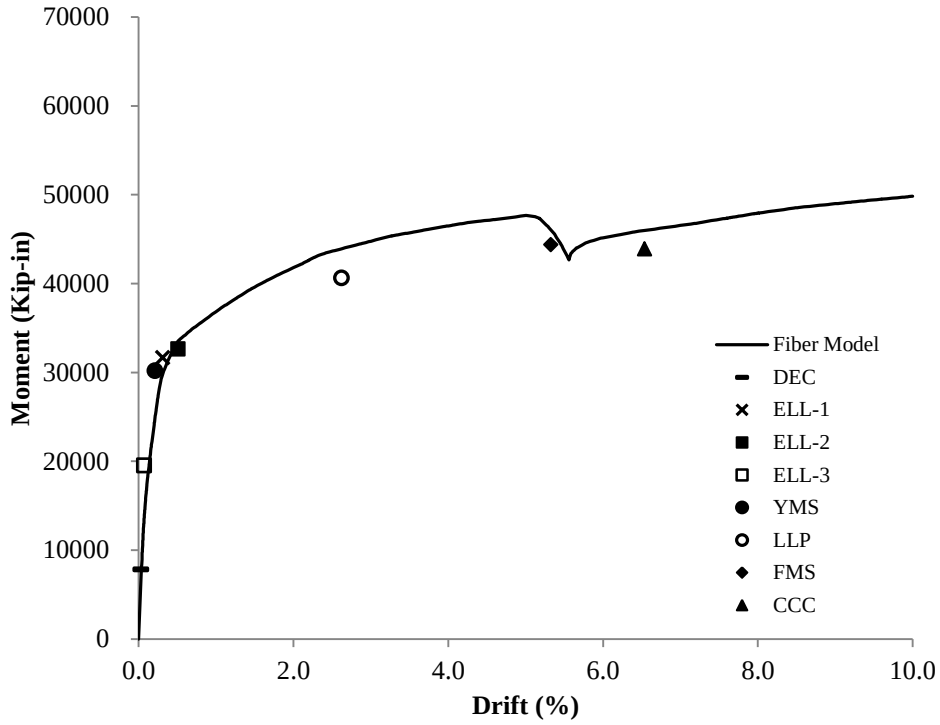

Figure 6.4(d): Base moment and roof drift response of PW4.2.1 with wall limit states

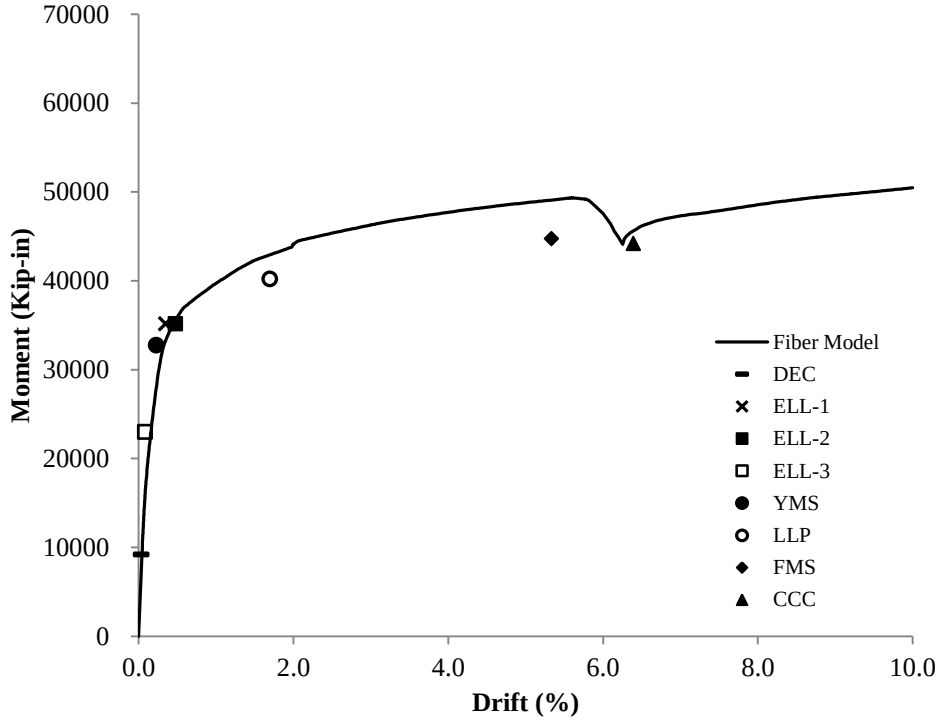

Figure 6.4(e): Base moment and roof drift response of PW4.2.2 with wall limit states

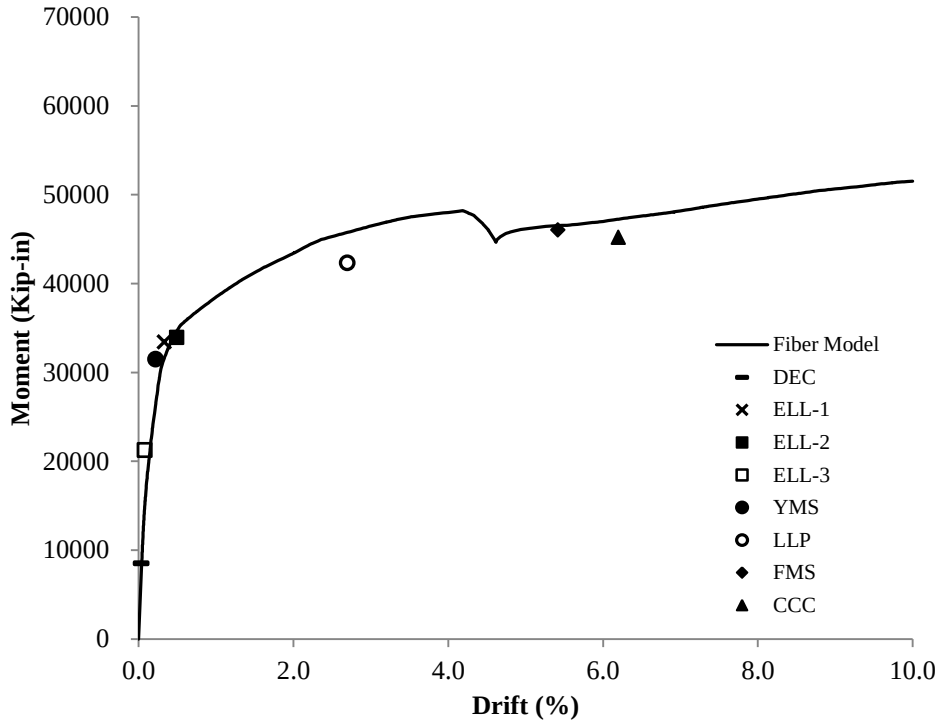

Figure 6.4(f): Base moment and roof drift response of PW4.3.1 with wall limit states

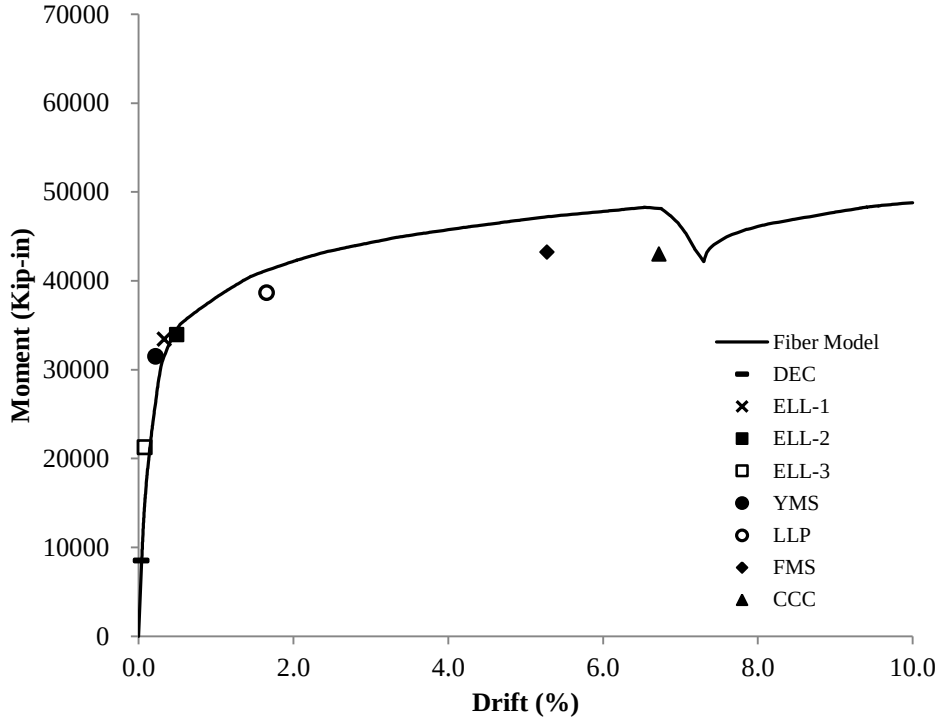

Figure 6.4(g): Base moment and roof drift response of PW4.3.2 with wall limit states

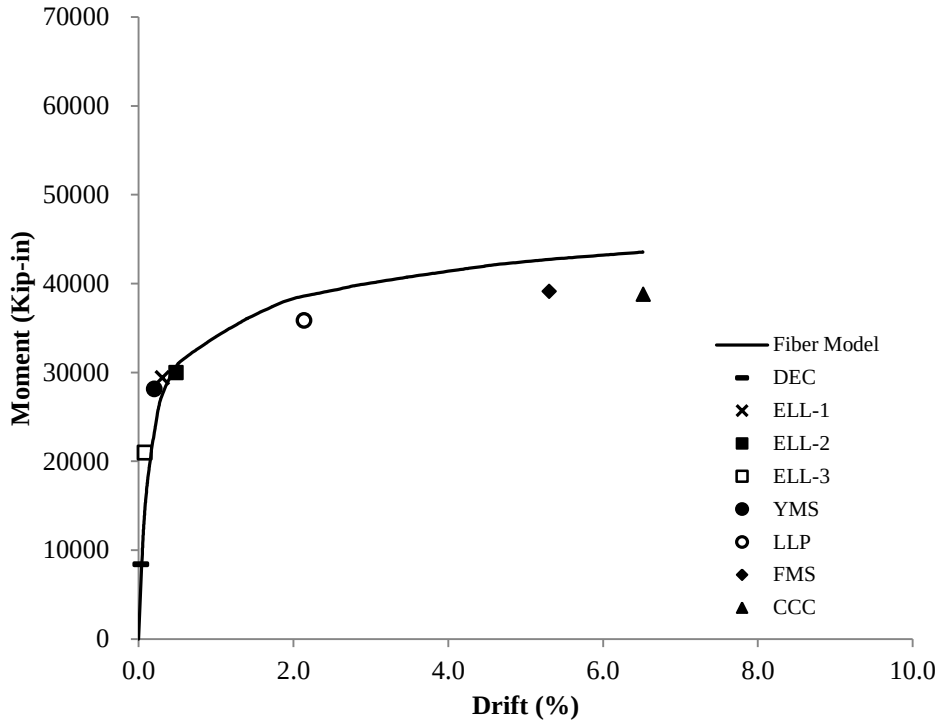

Figure 6.4(h): Base moment and roof drift response of PW4.4.1 with wall limit states

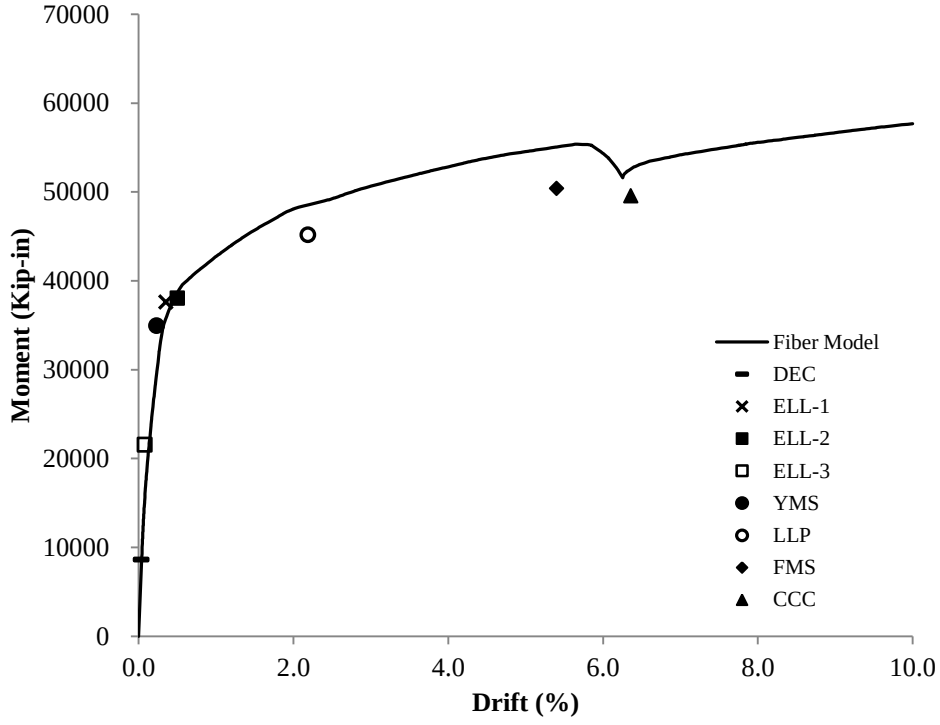

Figure 6.4(i): Base moment and roof drift response of PW4.4.2 with wall limit states

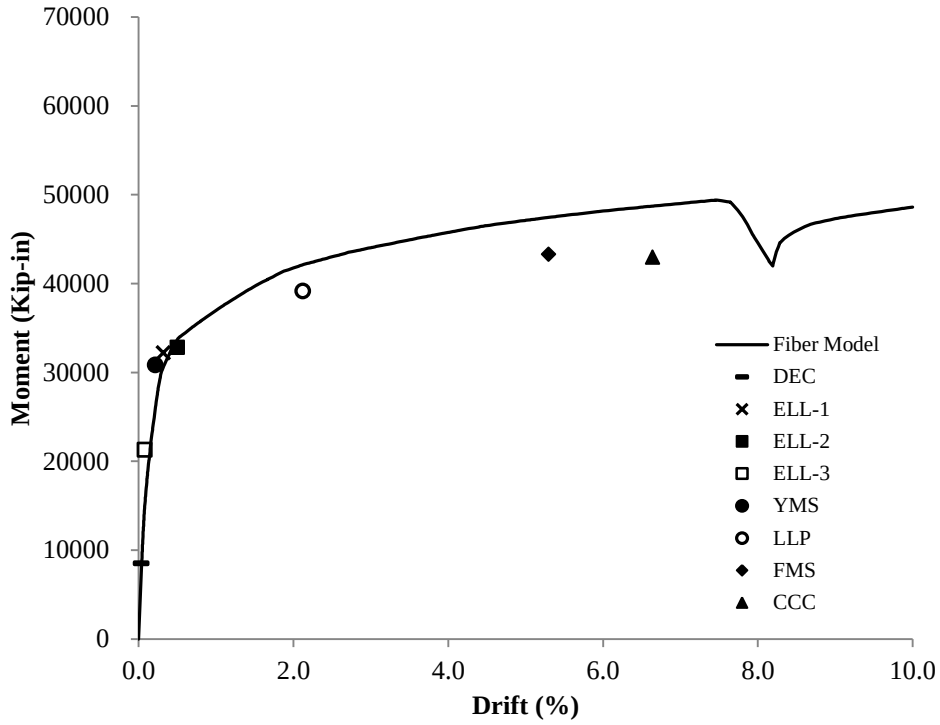

Figure 6.4(j): Base moment and roof drift response of PW4.5.1 with wall limit states

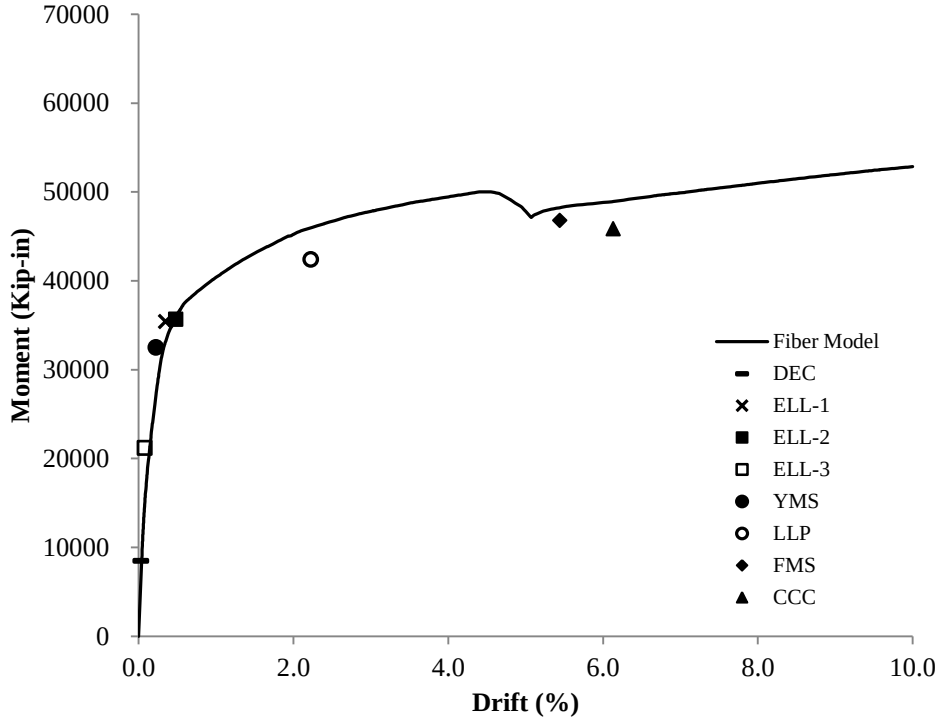

Figure 6.4(k): Base moment and roof drift response of PW4.5.2 with wall limit states

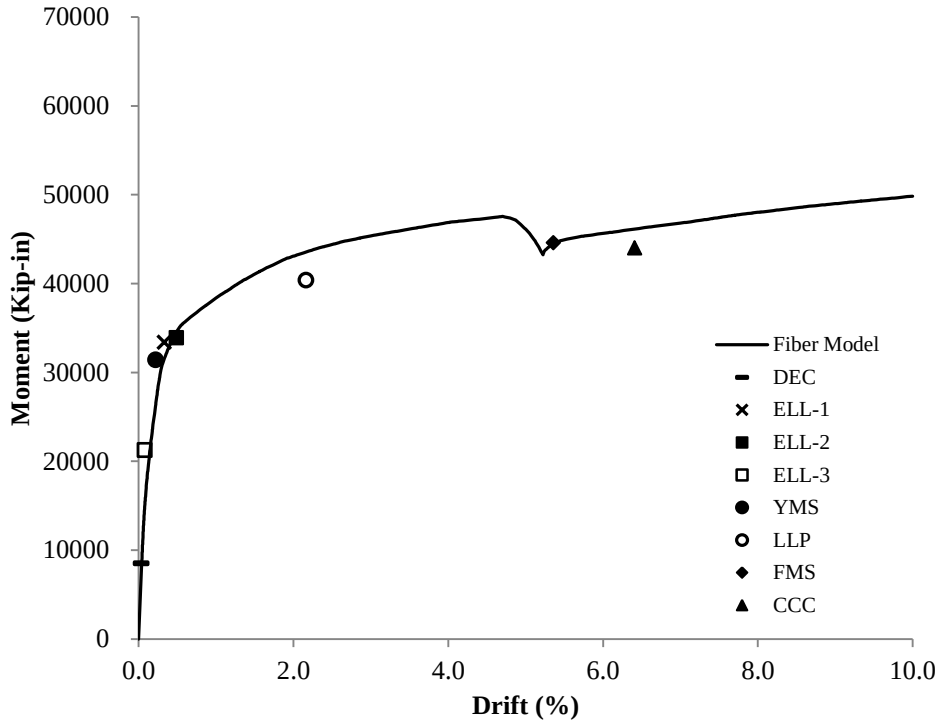

Figure 6.4(l): Base moment and roof drift response of PW4.6.1 with wall limit states

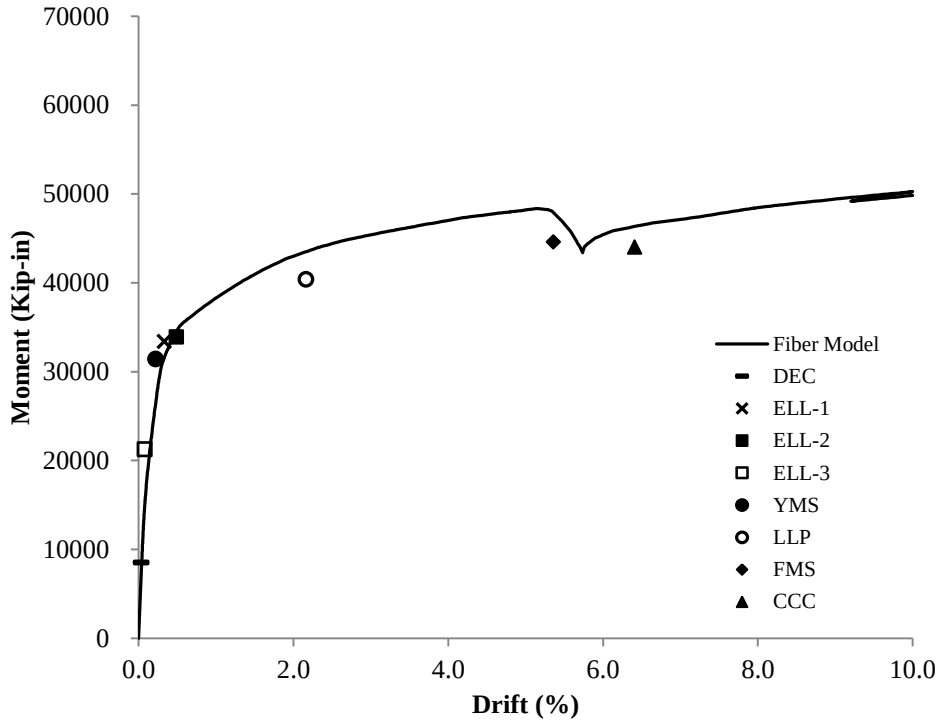

Figure 6.4(m): Base moment and roof drift response of PW4.6.2 with wall limit states

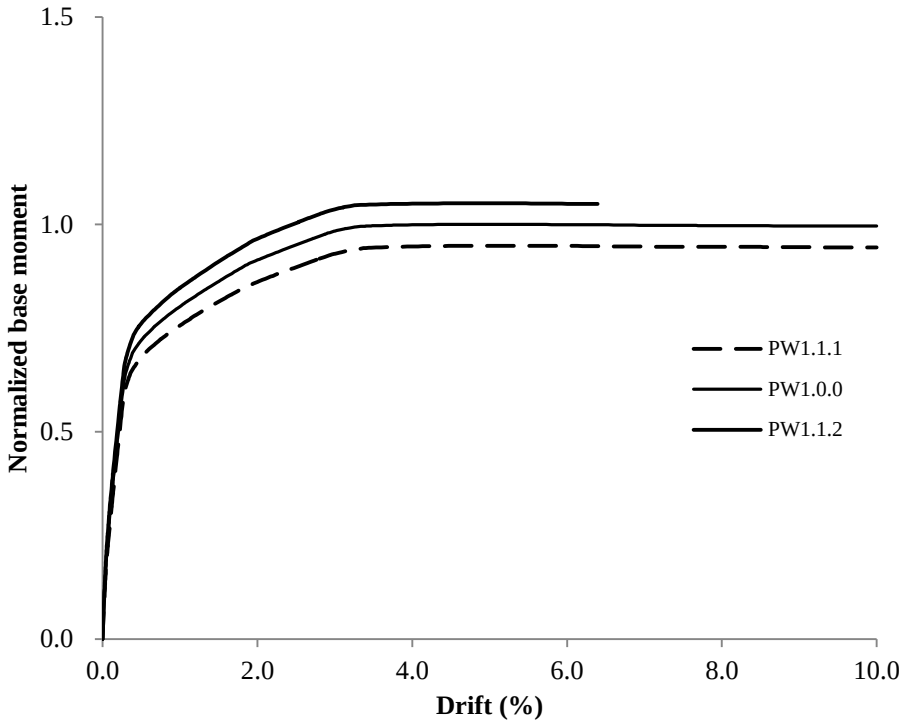

Figure 6.5(a): Parametric wall 1 with varying area of PT steel

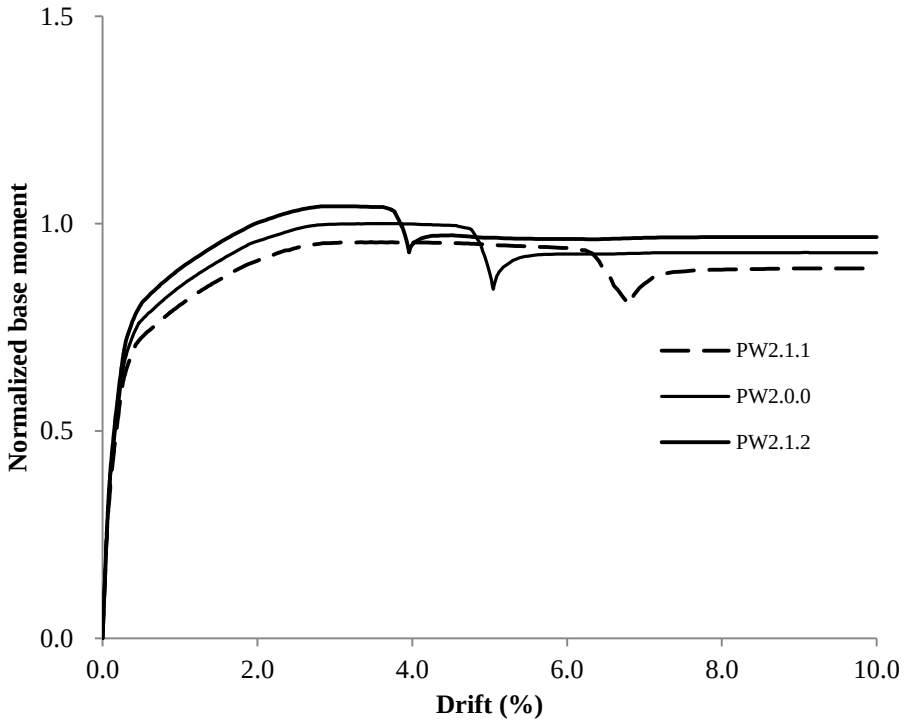

Figure 6.5(b): Parametric wall 2 with varying area of PT steel

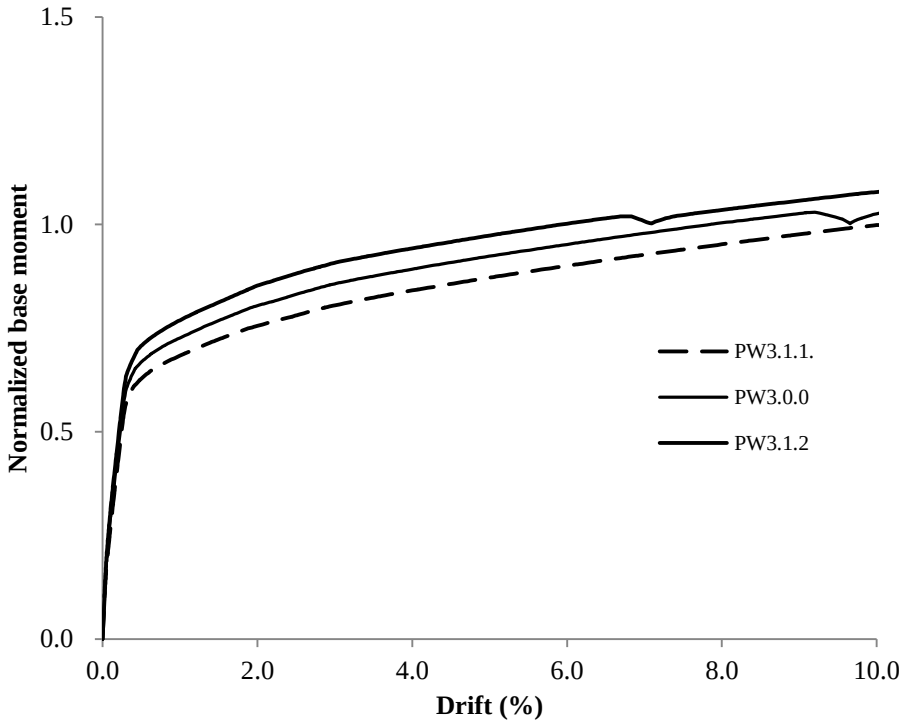

Figure 6.5(c): Parametric wall 3 with varying area of PT steel

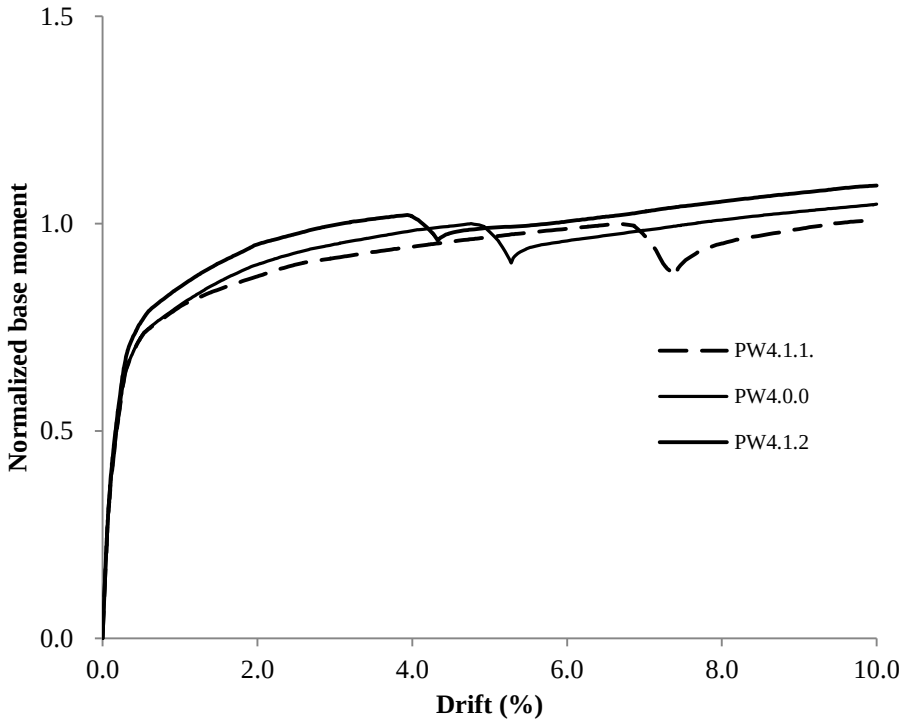

Figure 6.5(d): Parametric wall 4 with varying area of PT steel

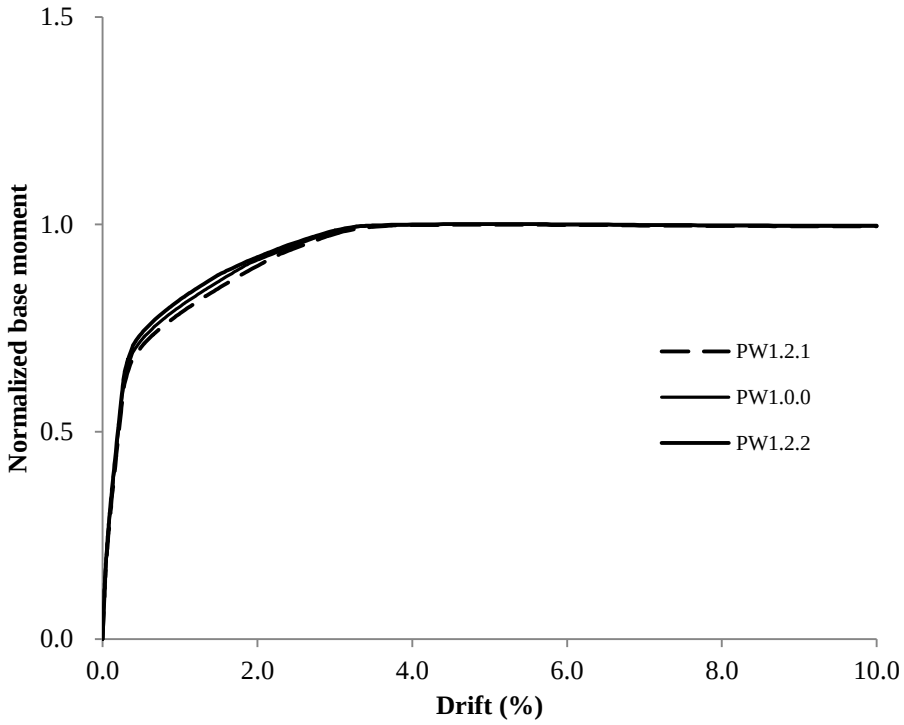

Figure 6.6(a): Parametric wall 1 with varying initial PT stress

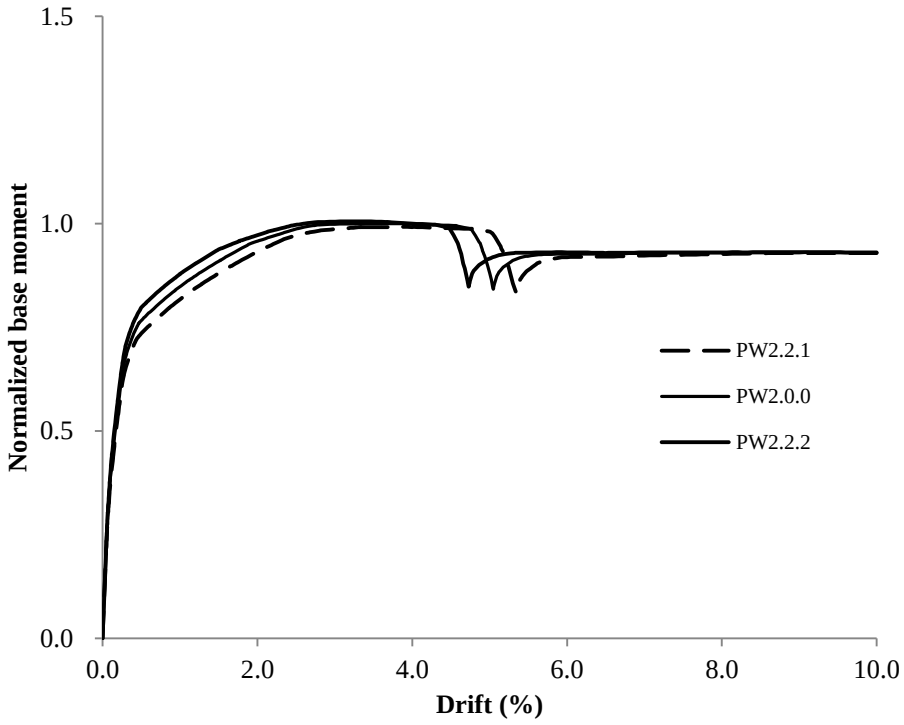

Figure 6.6(b): Parametric wall 2 with varying initial PT stress

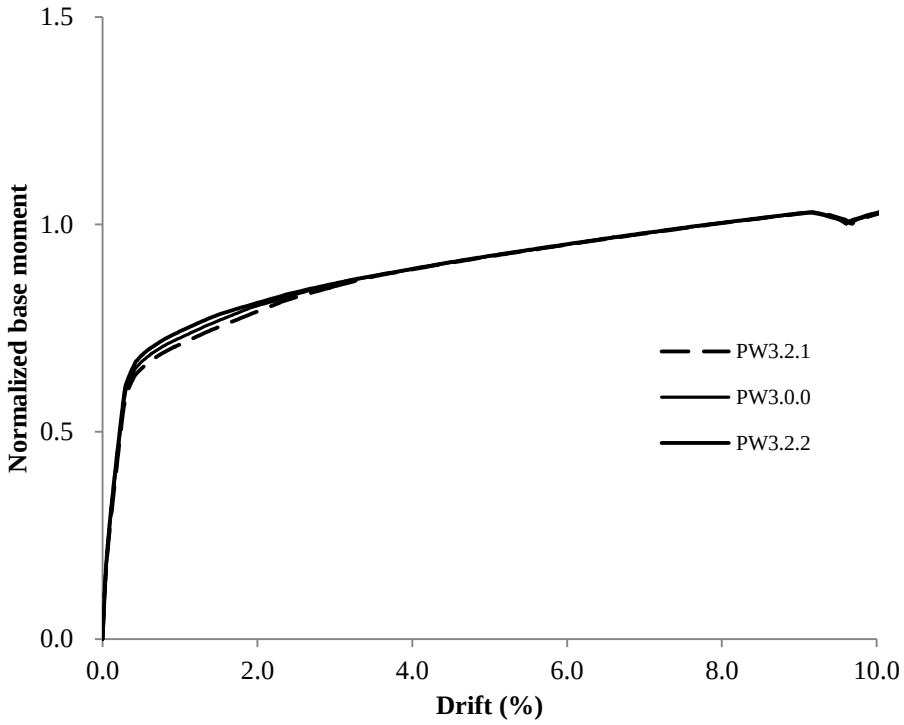

Figure 6.6(c): Parametric wall 3 with varying initial PT stress

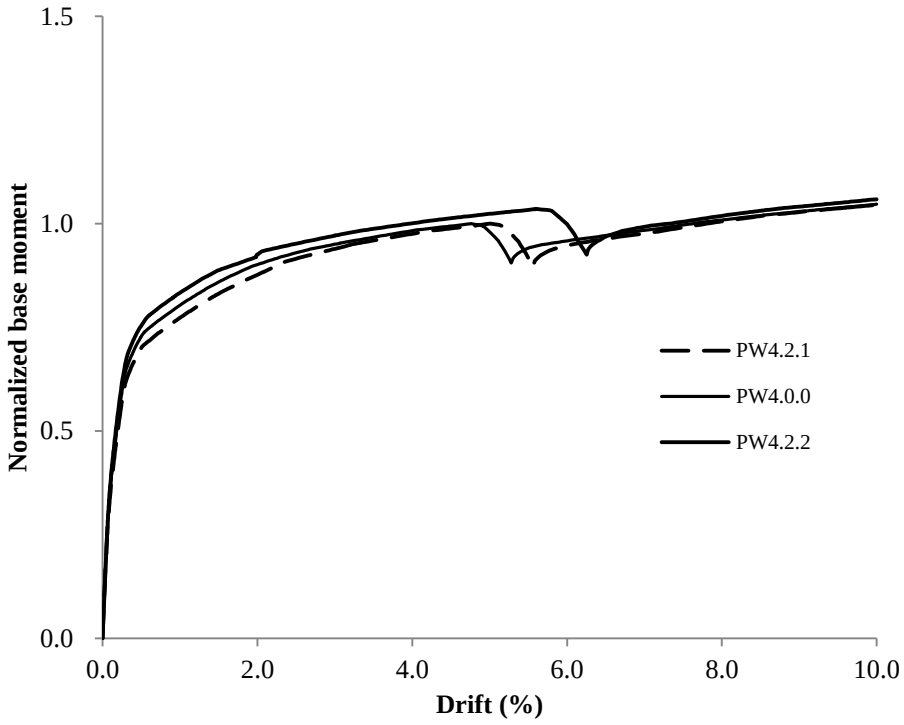

Figure 6.6(d): Parametric wall 4 with varying initial PT stress

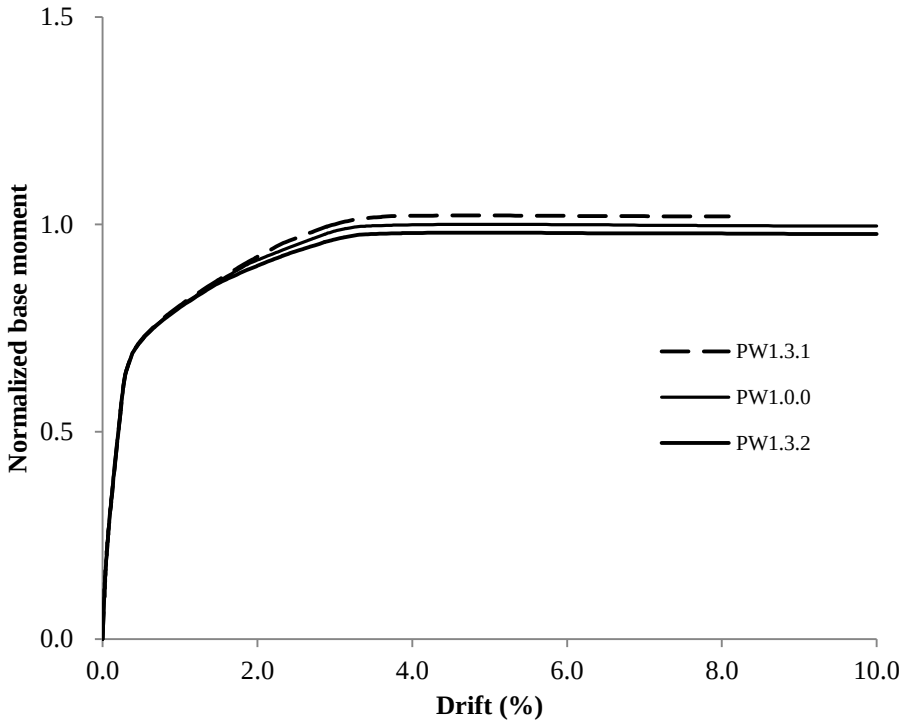

Figure 6.7(a): Parametric wall 1 with constant initial PT force

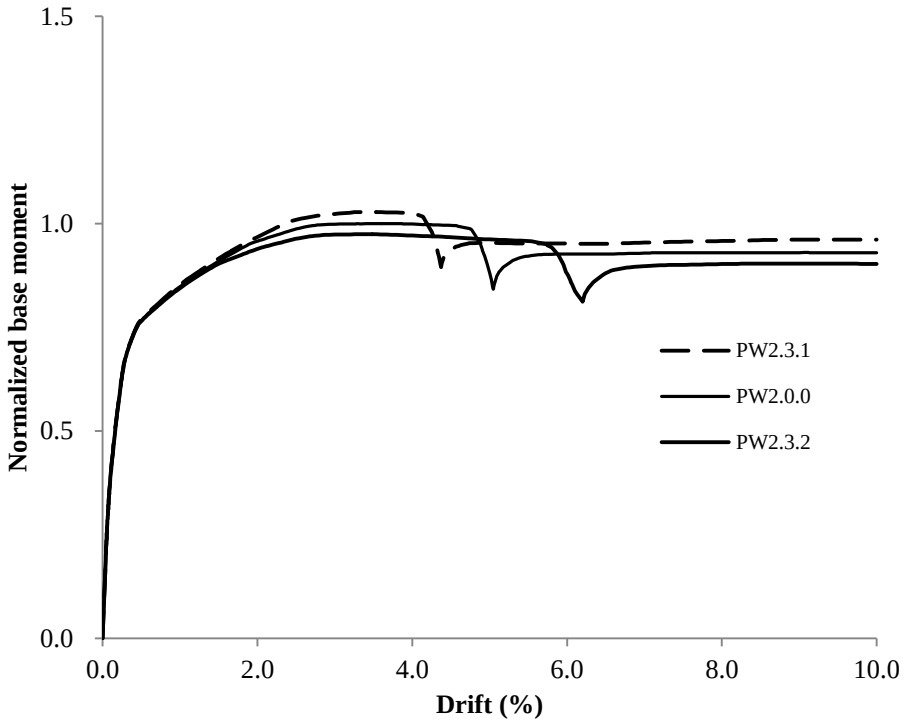

Figure 6.7(b): Parametric wall 2 with constant initial PT force

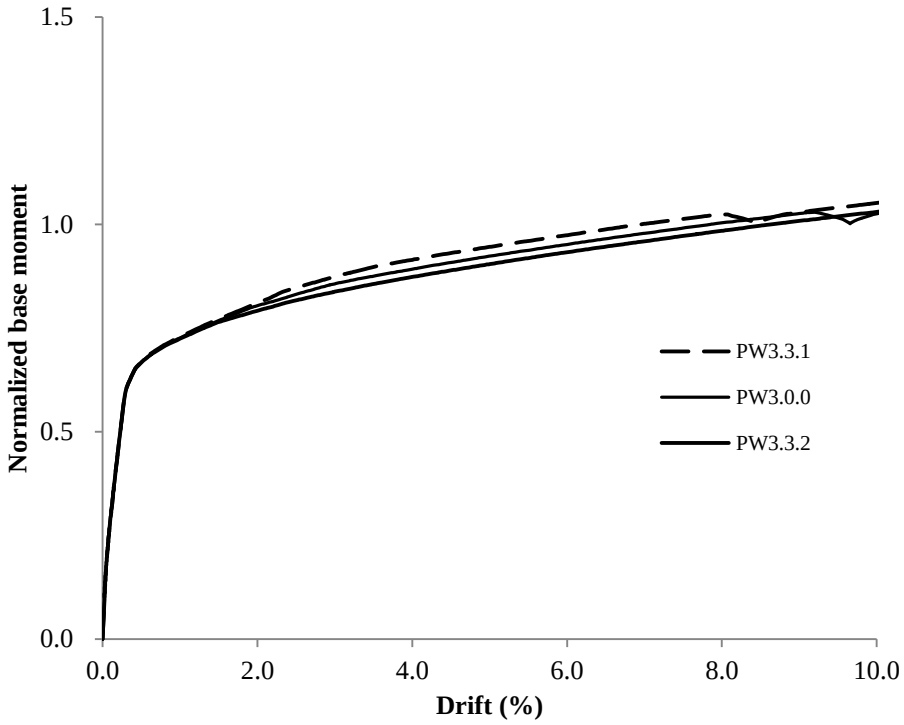

Figure 6.7(c): Parametric wall 3 with constant initial PT force

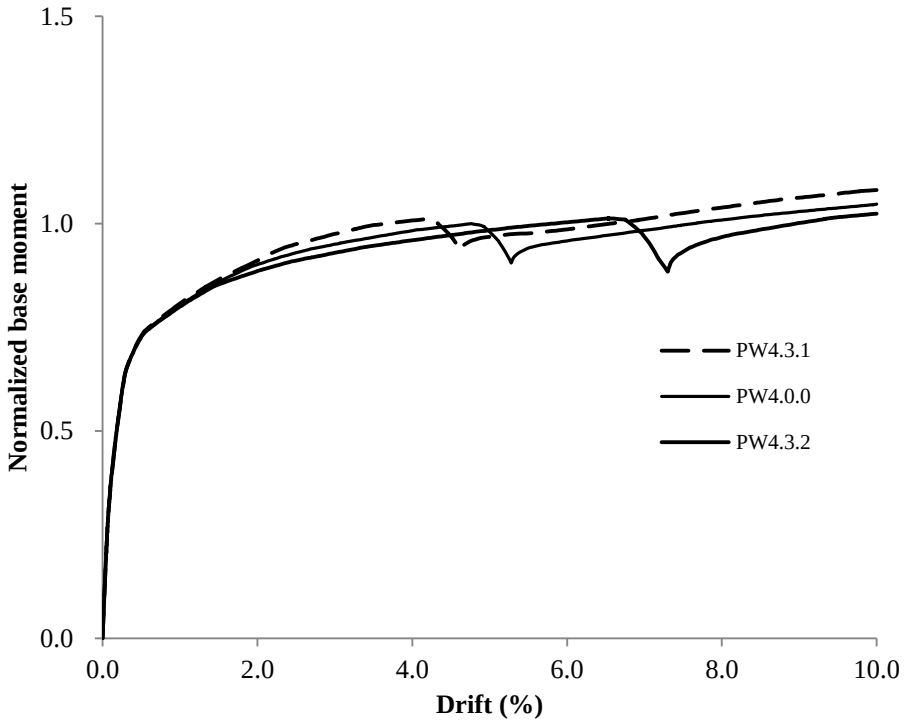

Figure 6.7(d): Parametric wall 4 with constant initial PT force

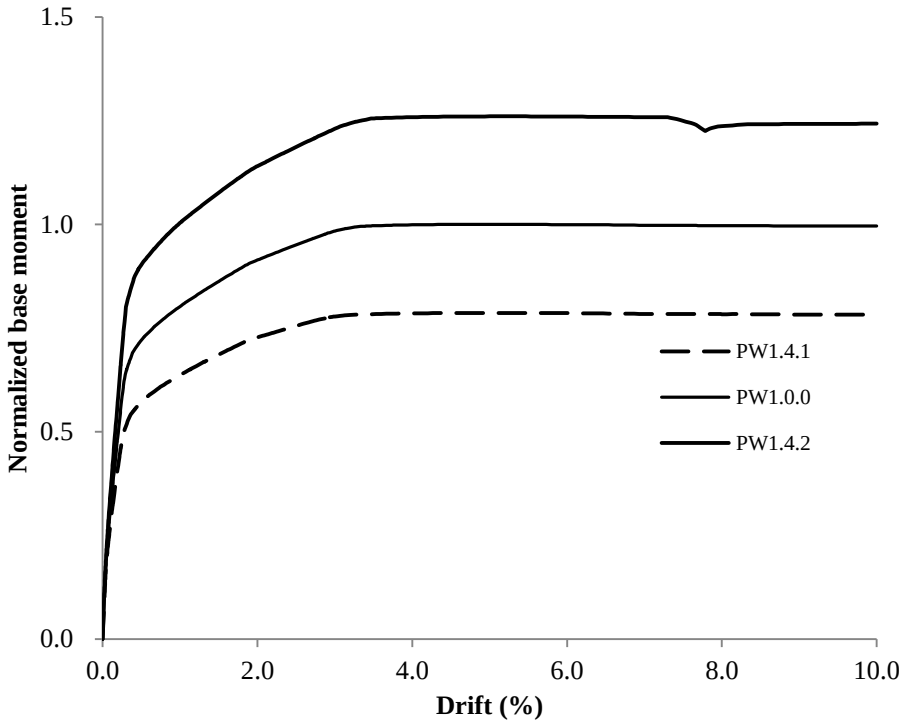

Figure 6.8(a): Parametric wall 1 with varying area of boundary longitudinal reinforcement

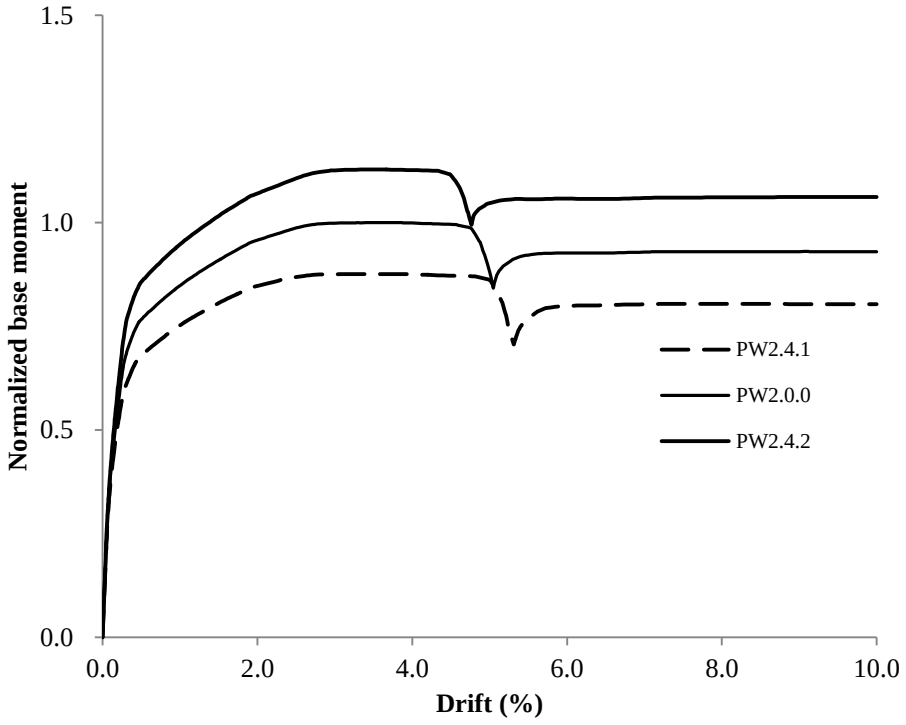

Figure 6.8(b): Parametric wall 2 with varying area of boundary longitudinal reinforcement

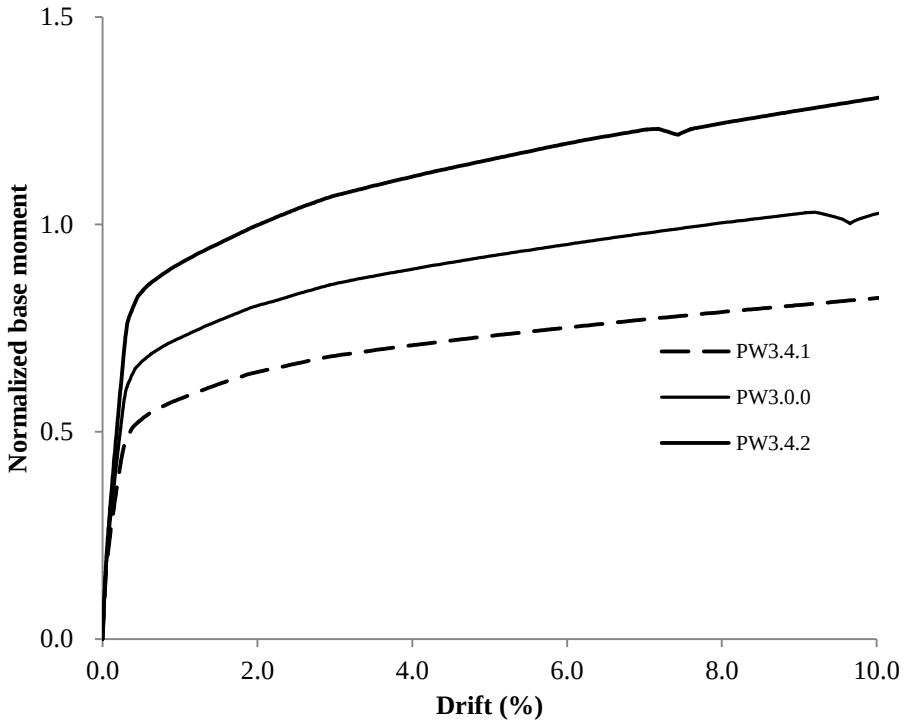

Figure 6.8(c): Parametric wall 3 with varying area of boundary longitudinal reinforcement

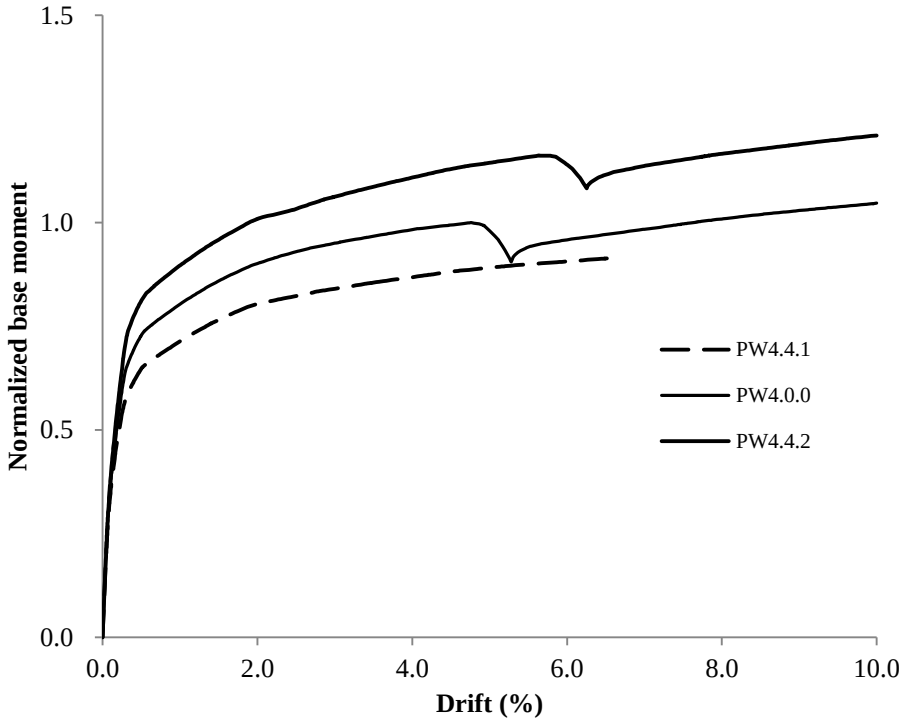

Figure 6.8(d): Parametric wall 4 with varying area of boundary longitudinal reinforcement

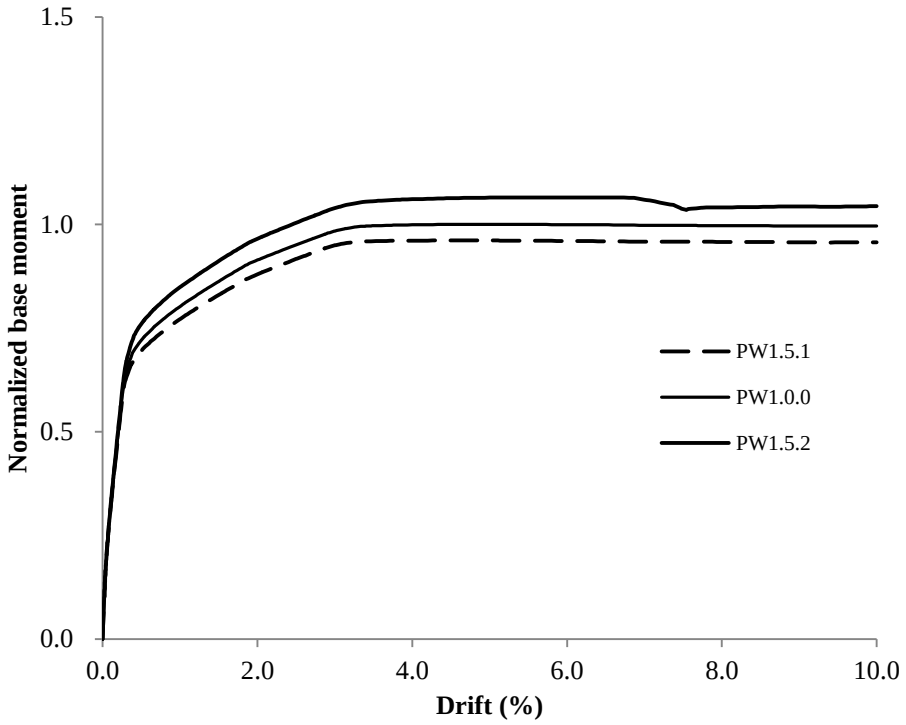

Figure 6.9(a): Parametric wall 1 with varying area of web longitudinal reinforcement

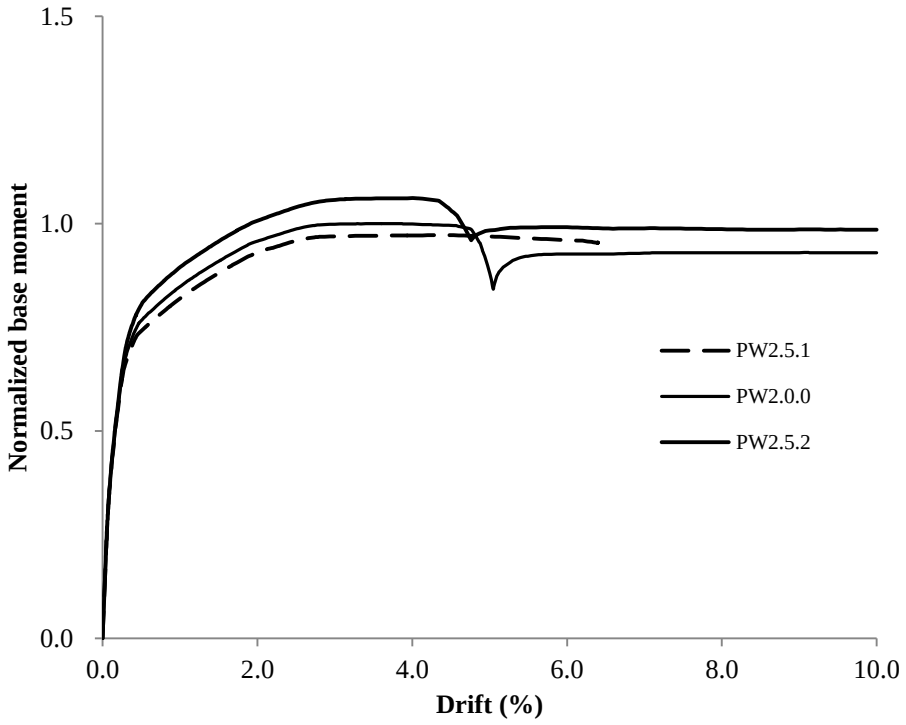

Figure 6.9(b): Parametric wall 2 with varying area of web longitudinal reinforcement

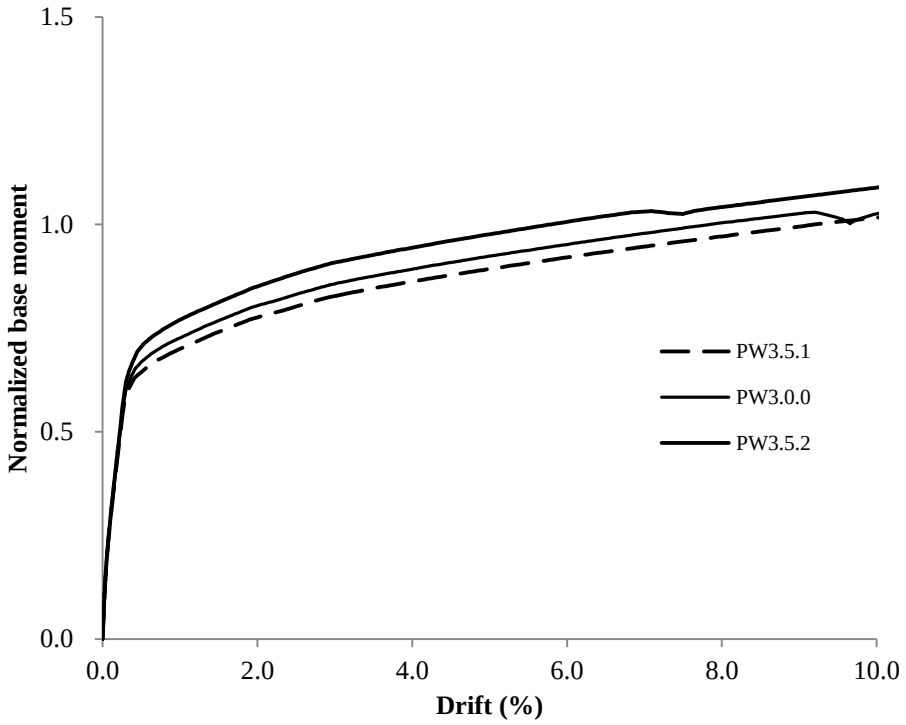

Figure 6.9(c): Parametric wall 3 with varying area of web longitudinal reinforcement

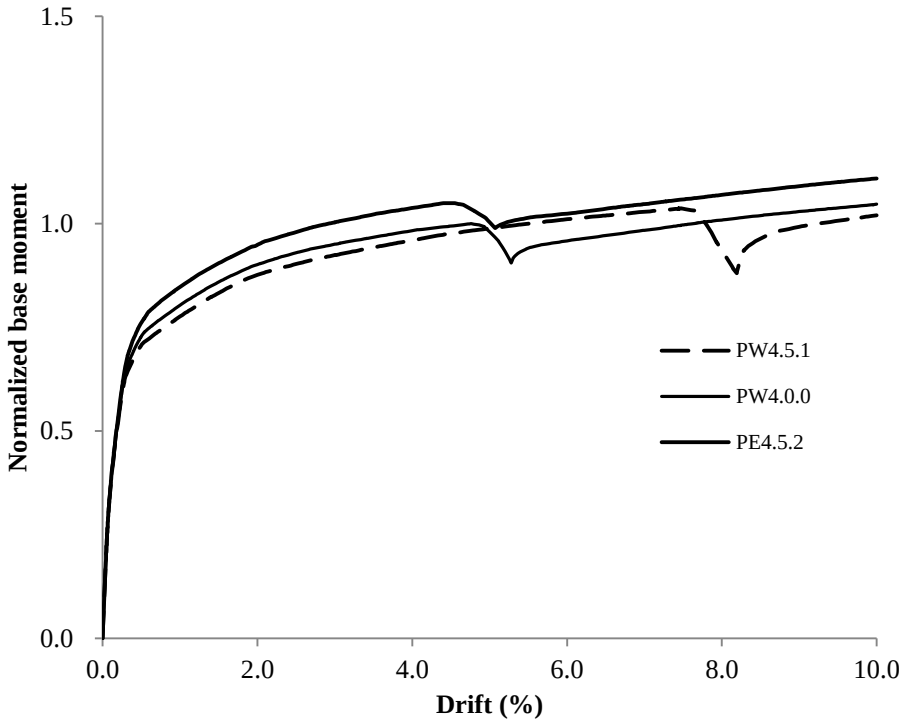

Figure 6.9(d): Parametric wall 4 with varying area of web longitudinal reinforcement

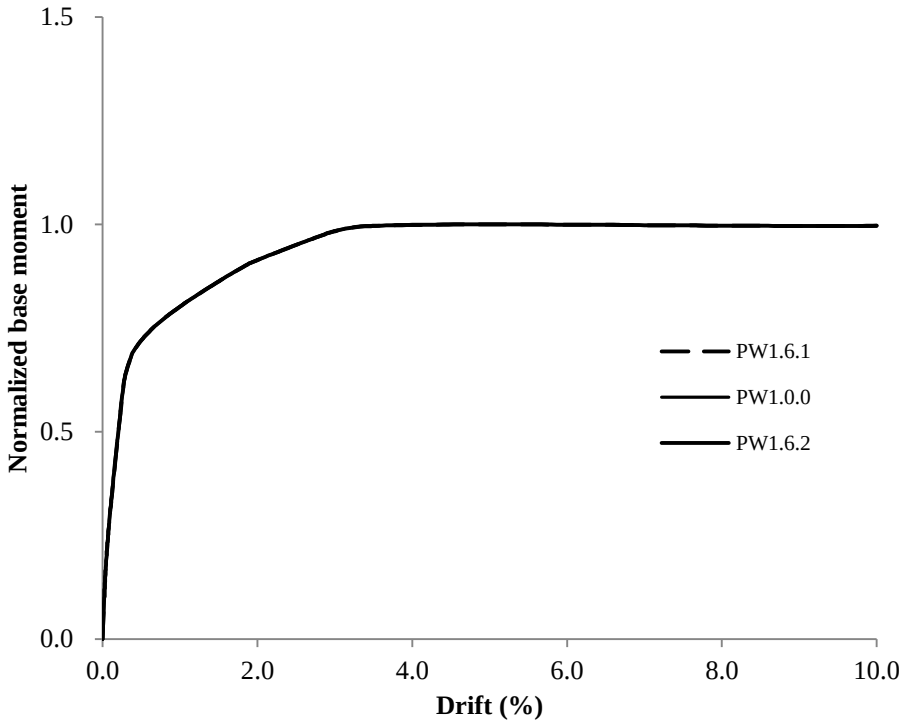

Figure 6.10(a): Parametric wall 1 with varying spacing of web longitudinal reinforcement

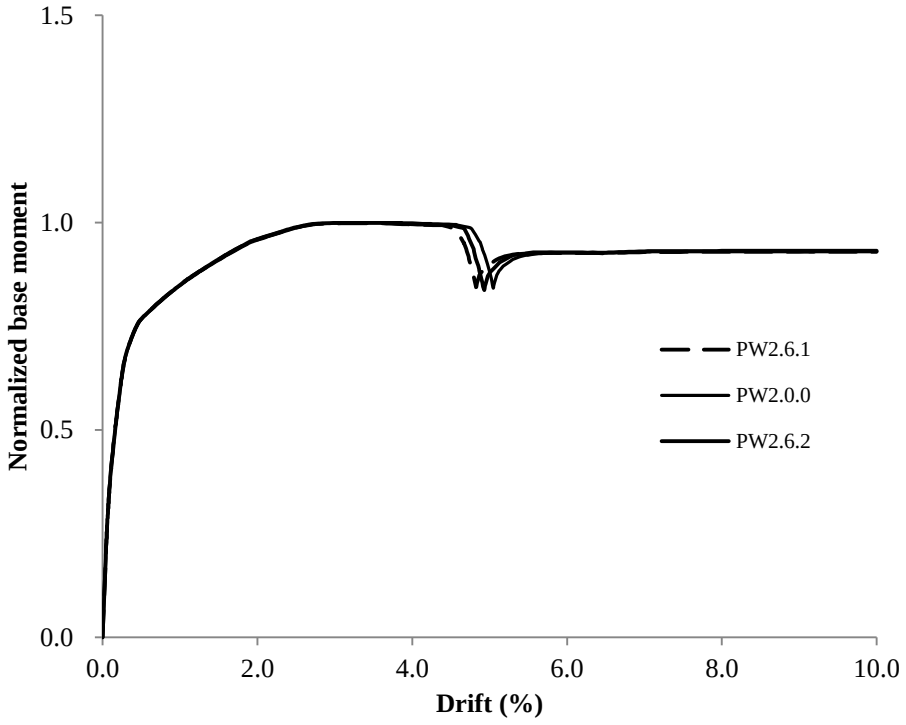

Figure 6.10(b): Parametric wall 2 with varying spacing of web longitudinal reinforcement

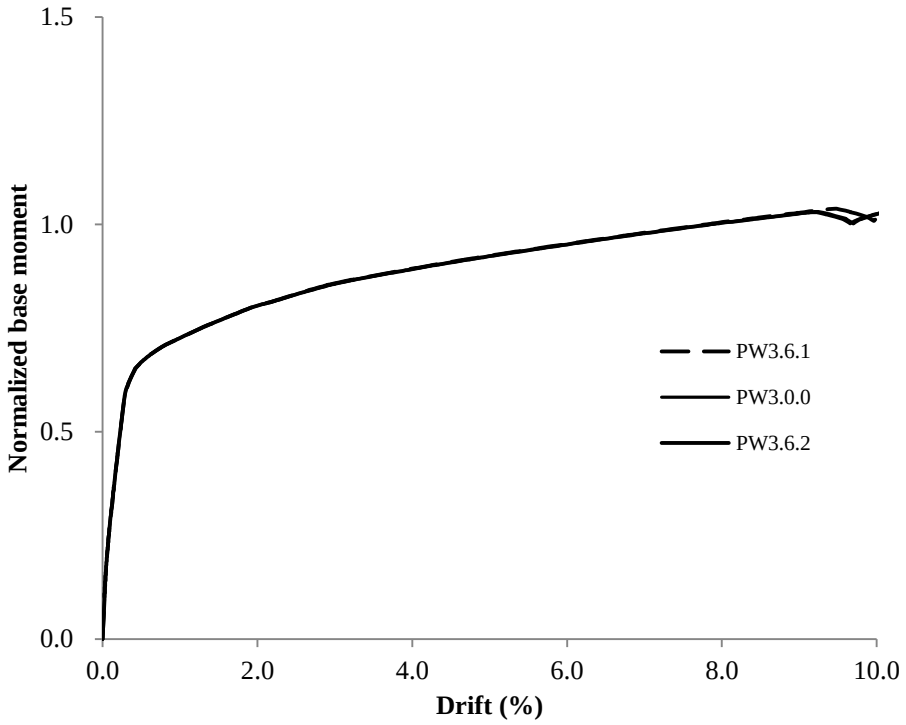

Figure 6.10(c): Parametric wall 3 with varying spacing of web longitudinal reinforcement

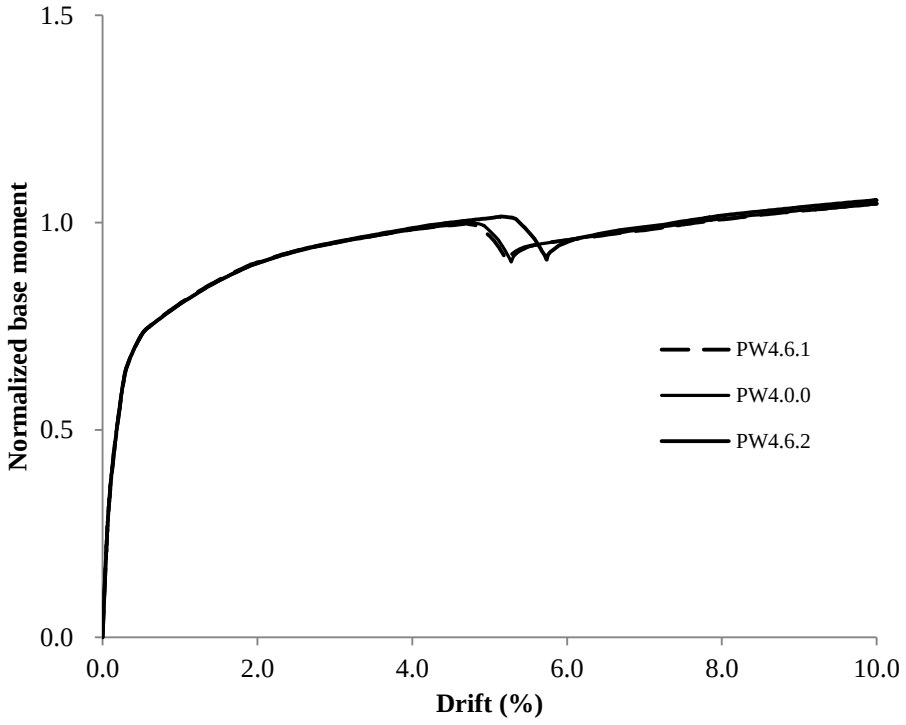

Figure 6.10(d): Parametric wall 4 with varying spacing of web longitudinal reinforcement

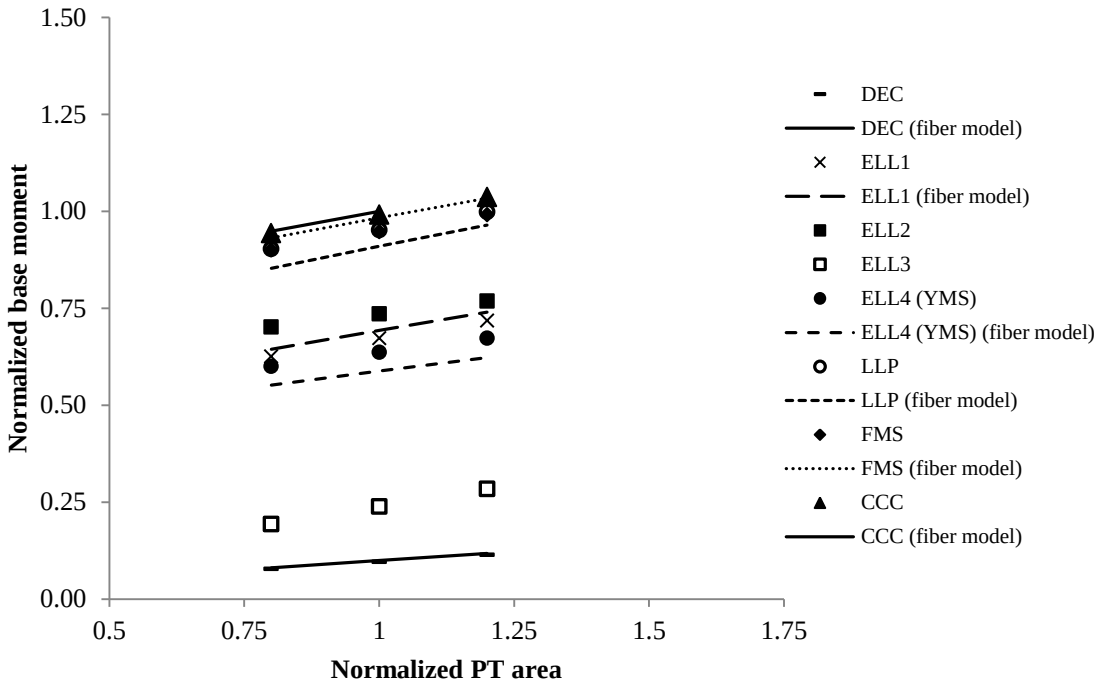

Figure 6.11(a): Effect of change in area of PT steel on base moment of parametric wall 1

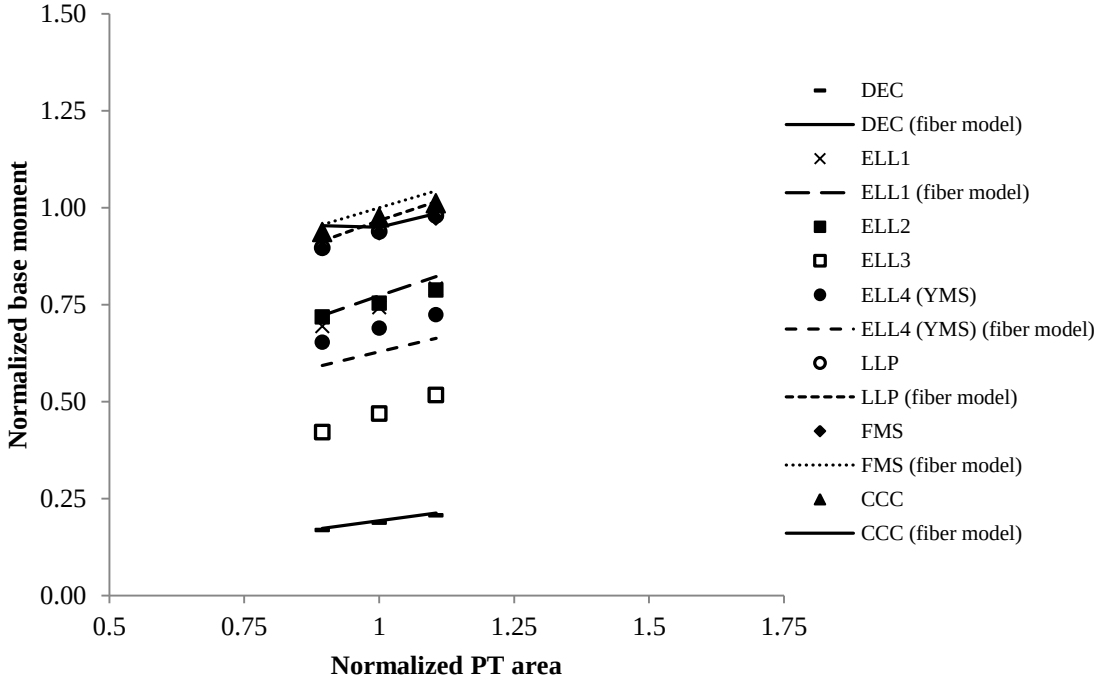

Figure 6.11(b): Effect of change in area of PT steel on base moment of parametric wall 2

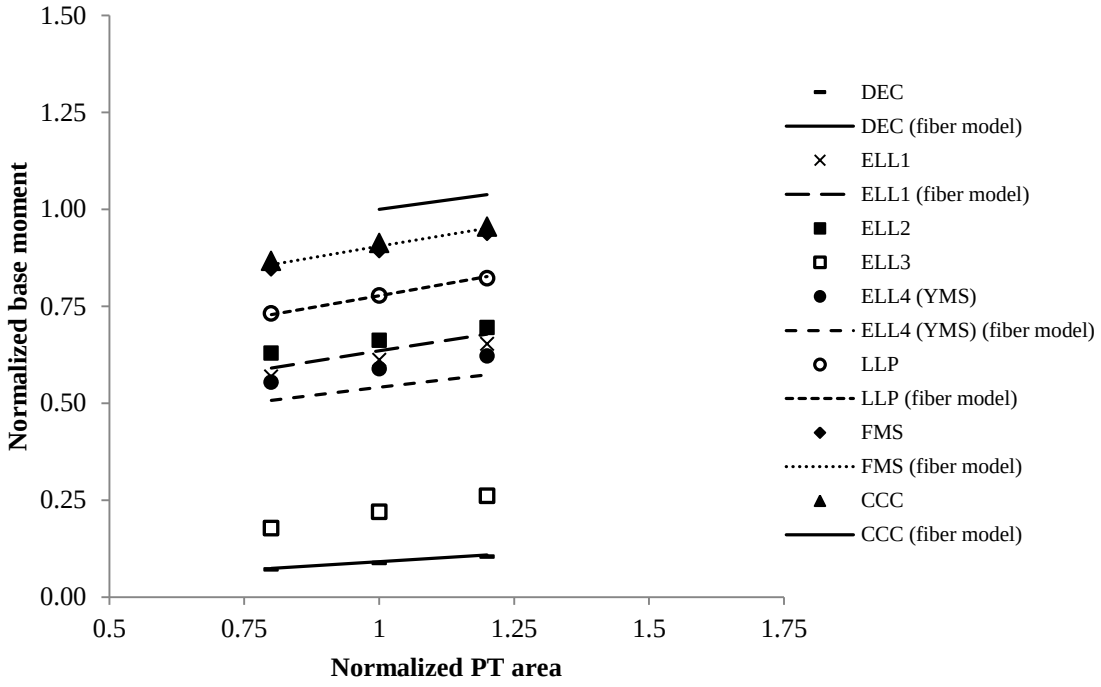

Figure 6.11(c): Effect of change in area of PT steel on base moment of parametric wall 3

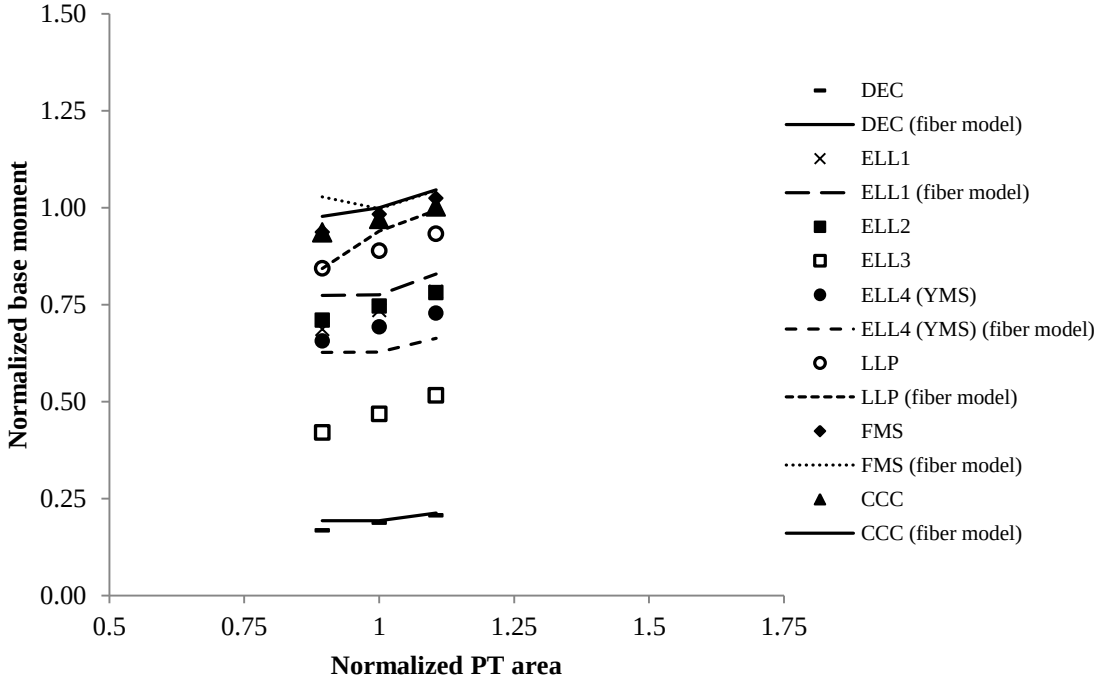

Figure 6.11(d): Effect of change in area of PT steel on base moment of parametric wall 4

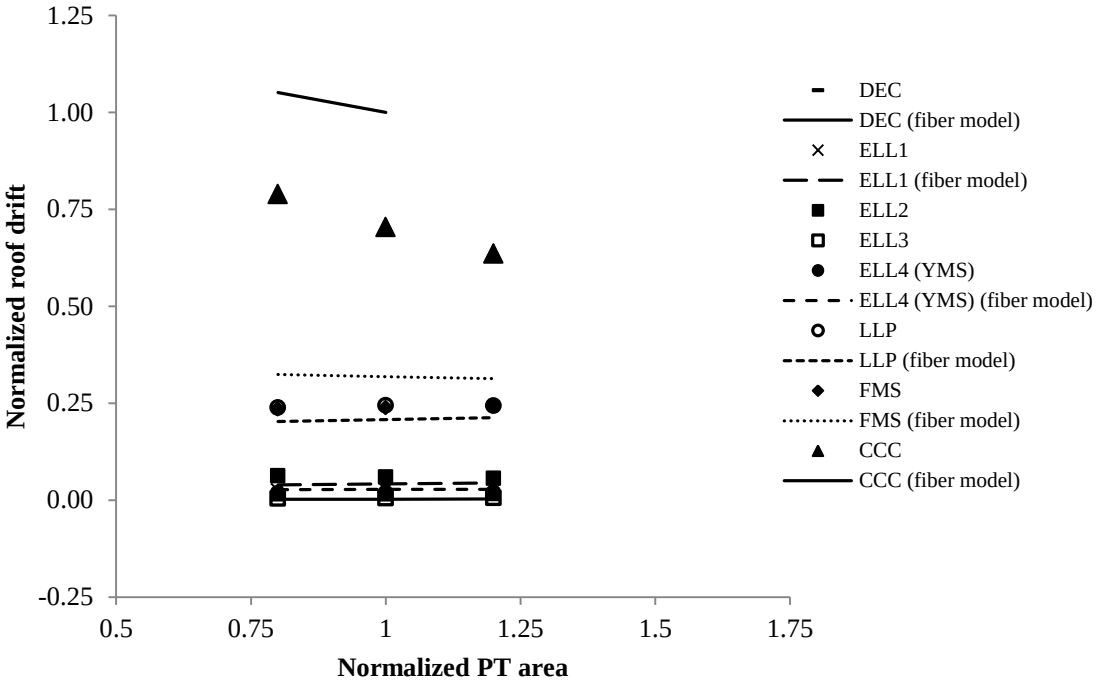

Figure 6.12(a): Effect of change in area of PT steel on drift of parametric wall 1

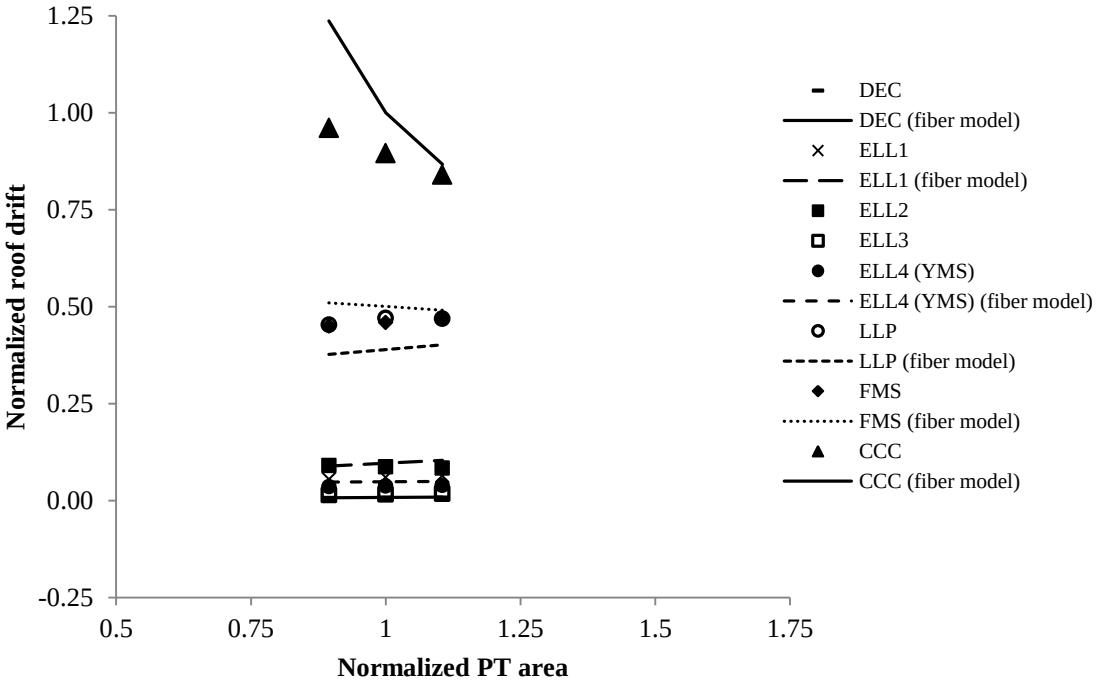

Figure 6.12(b): Effect of change in area of PT steel on drift of parametric wall 2

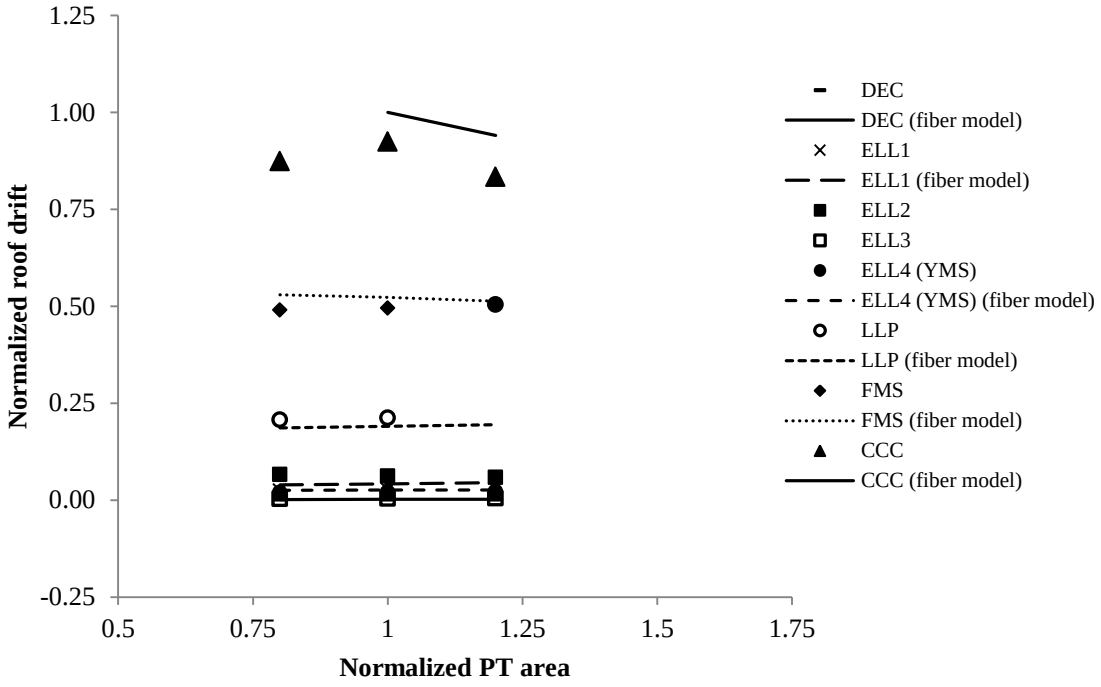

Figure 6.12(c): Effect of change in area of PT steel on drift of parametric wall 3

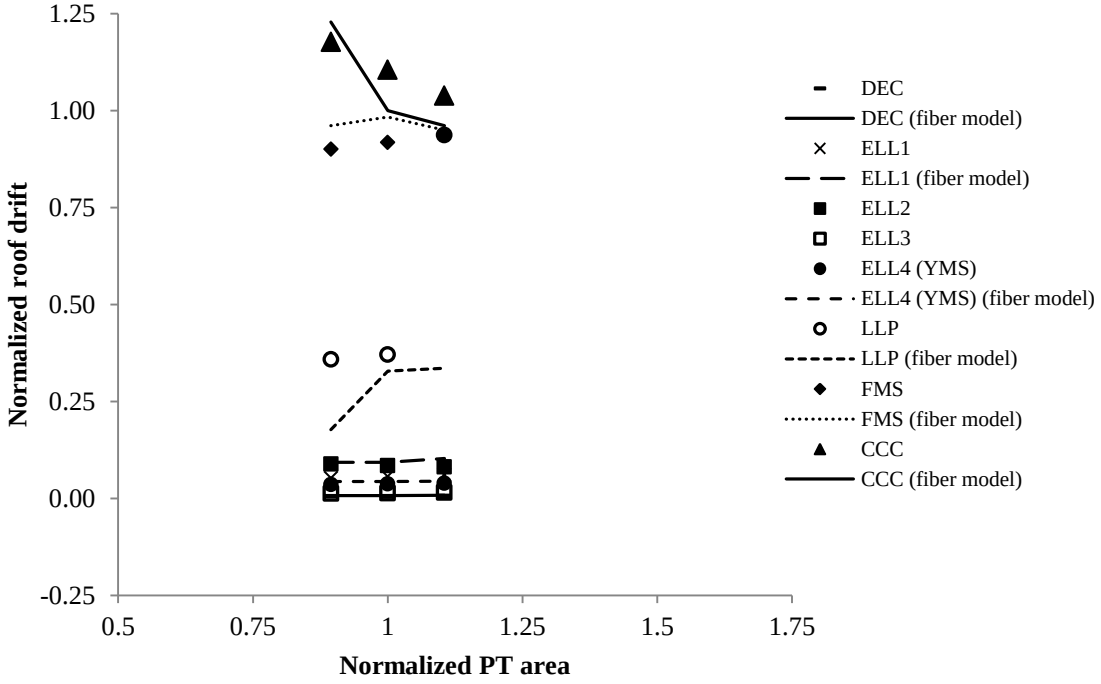

Figure 6.12(d): Effect of change in area of PT steel on drift of parametric wall 4

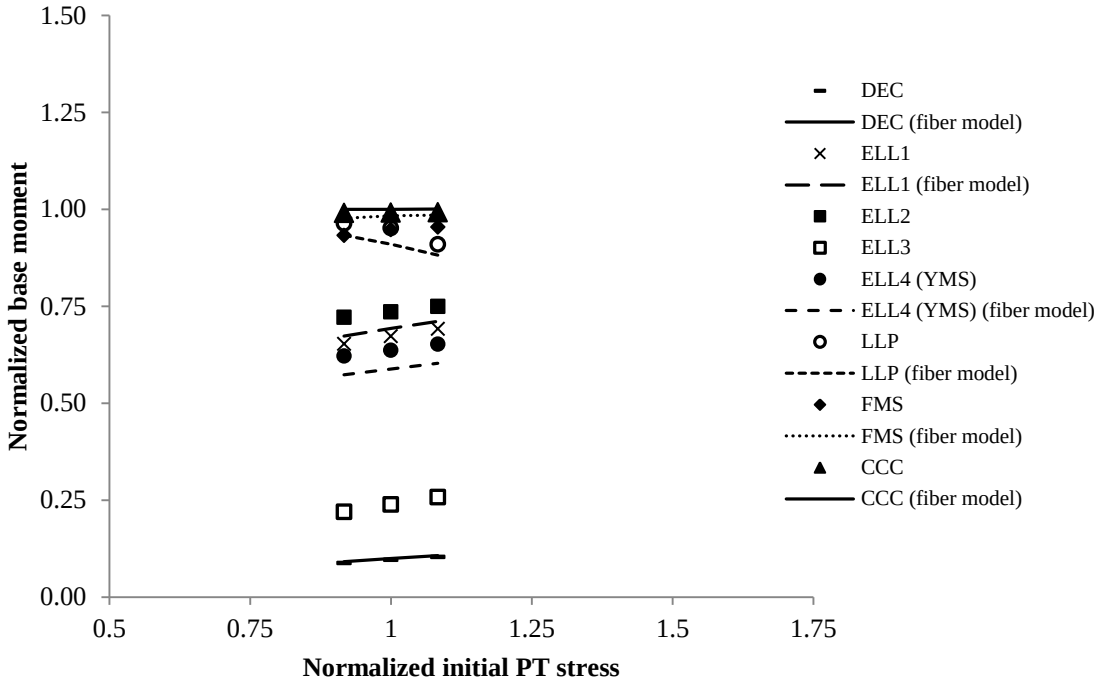

Figure 6.13(a): Effect of change in initial prestress of PT steel on base moment of parametric wall 1

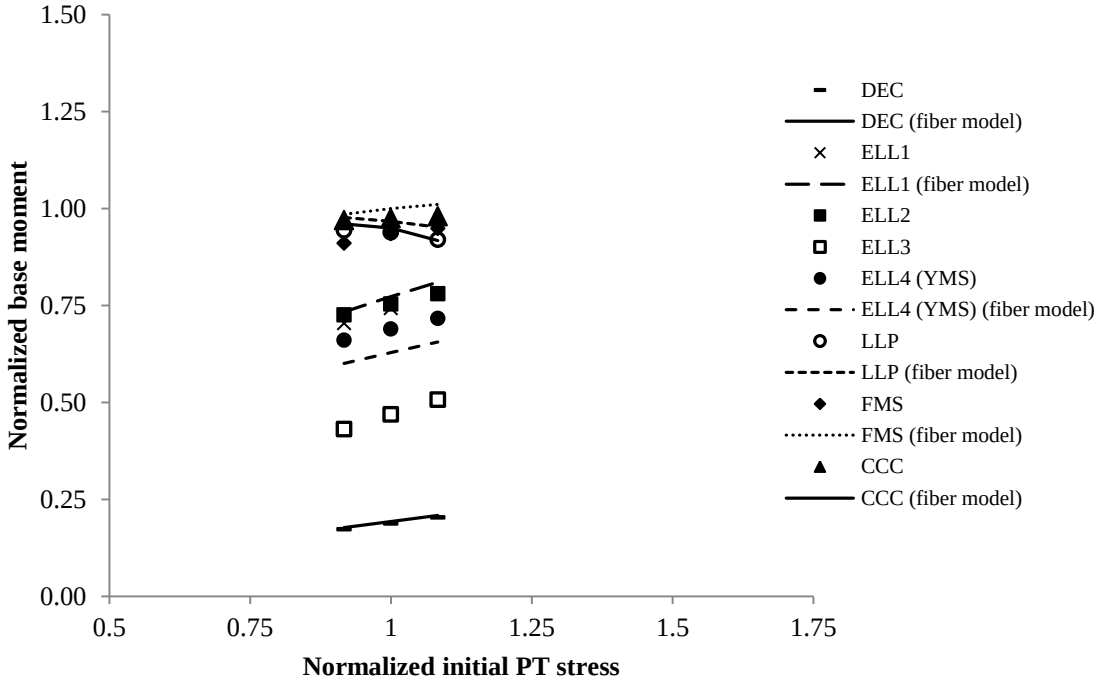

Figure 6.13(b): Effect of change in initial prestress of PT steel on base moment of parametric wall 2

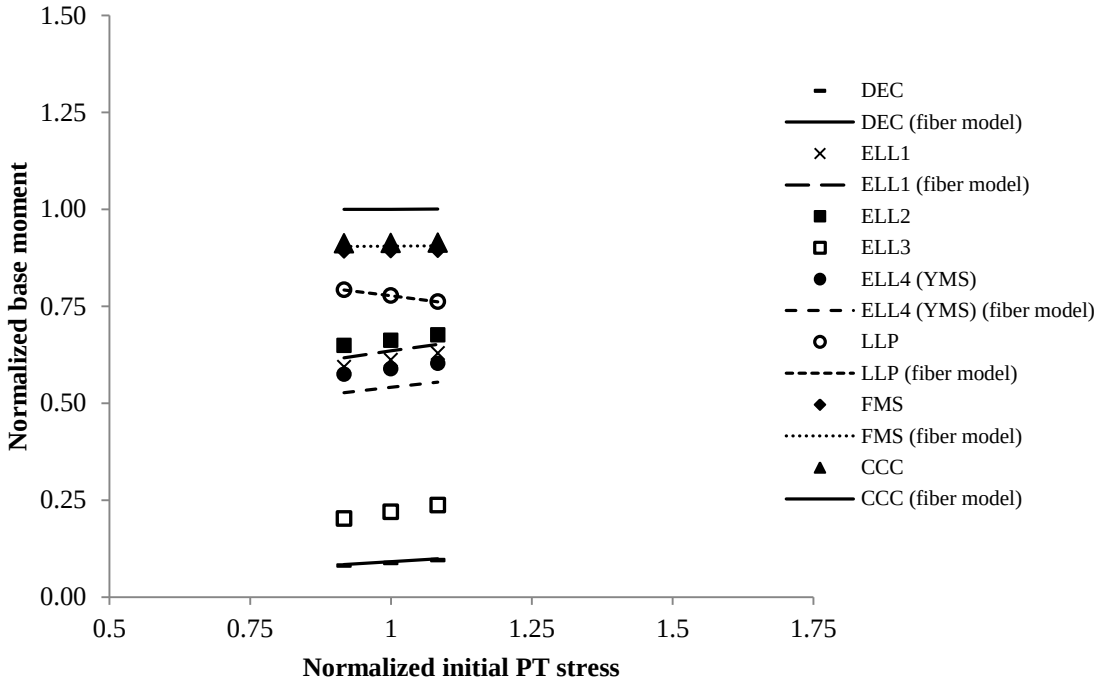

Figure 6.13(c): Effect of change in initial prestress of PT steel on base moment of parametric wall 3

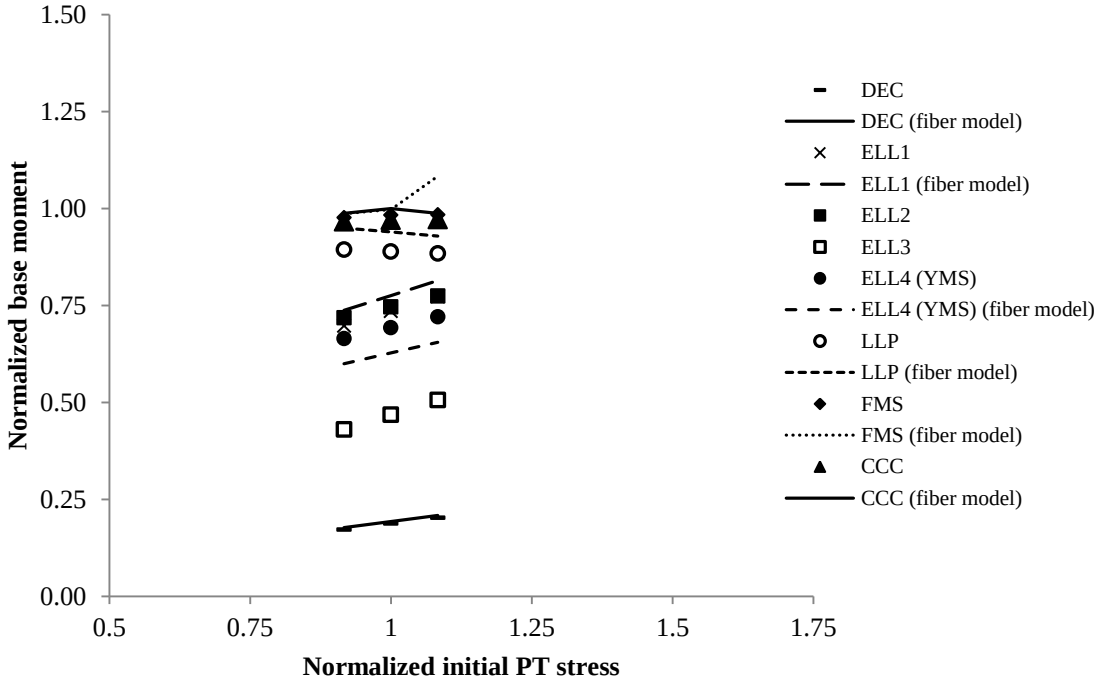

Figure 6.13(d): Effect of change in initial prestress of PT steel on base moment of parametric wall 4

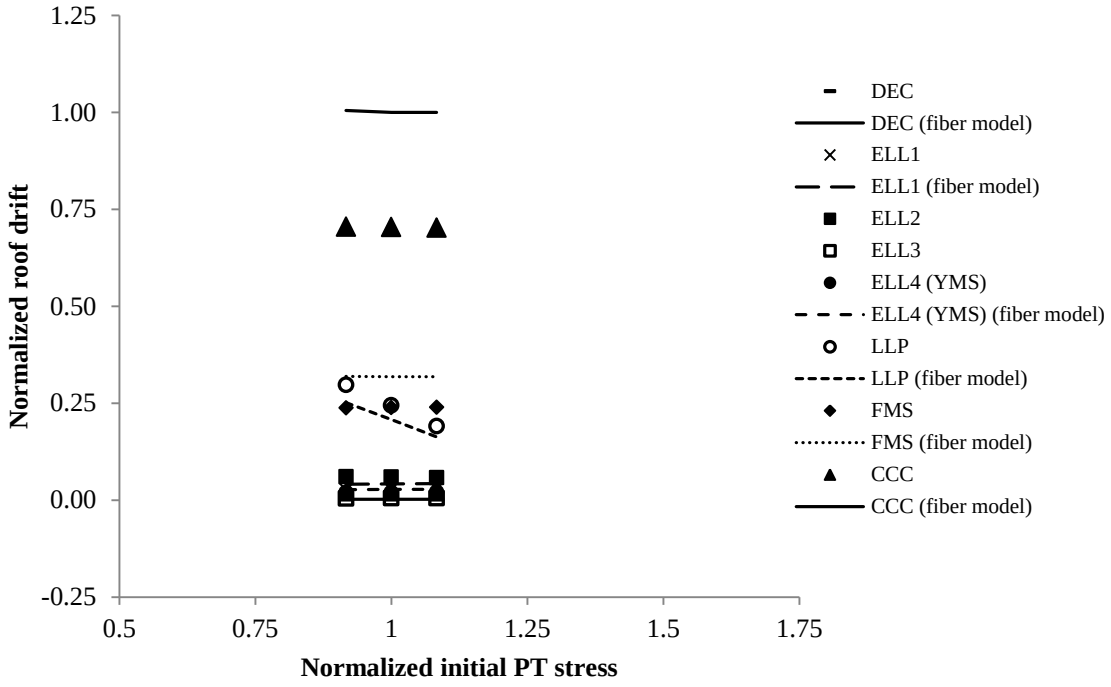

Figure 6.14(a): Effect of change in initial prestress of PT steel on drift of parametric base wall 1

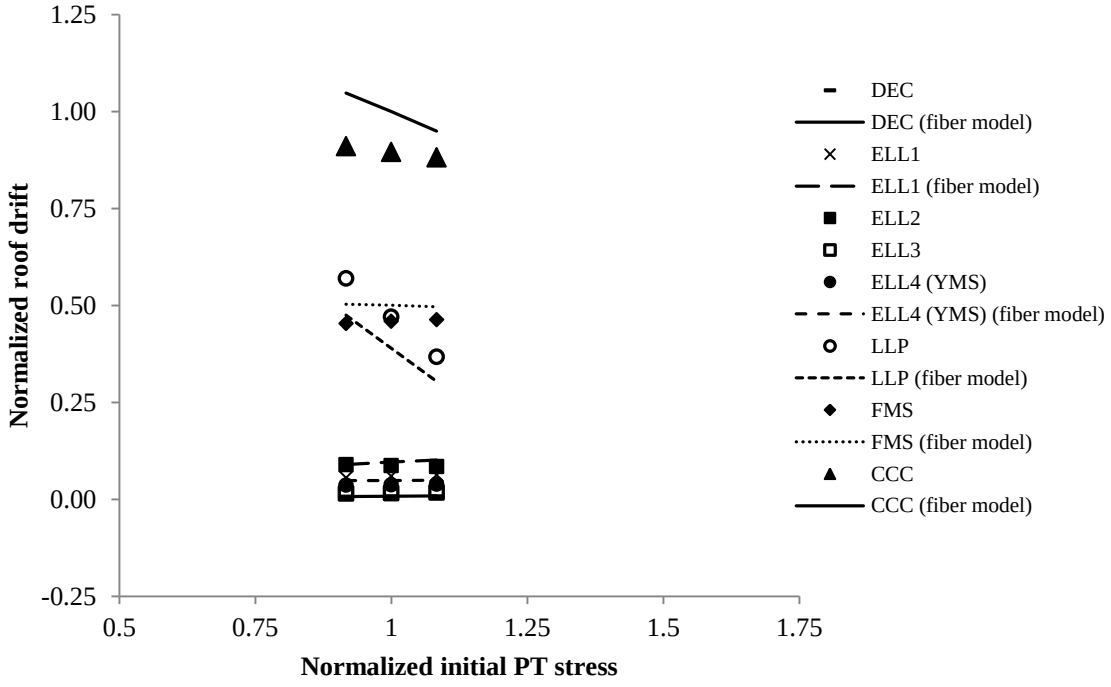

Figure 6.14(b): Effect of change in initial prestress of PT steel on drift of parametric base wall 2

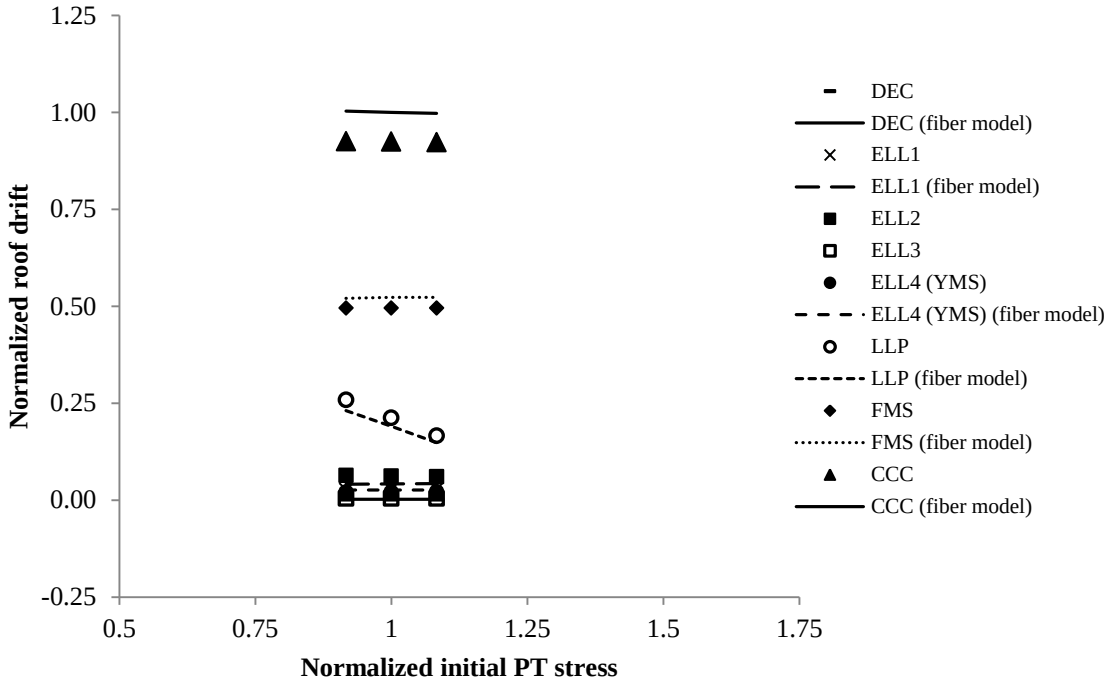

Figure 6.14(c): Effect of change in initial prestress of PT steel on drift of parametric base wall 3

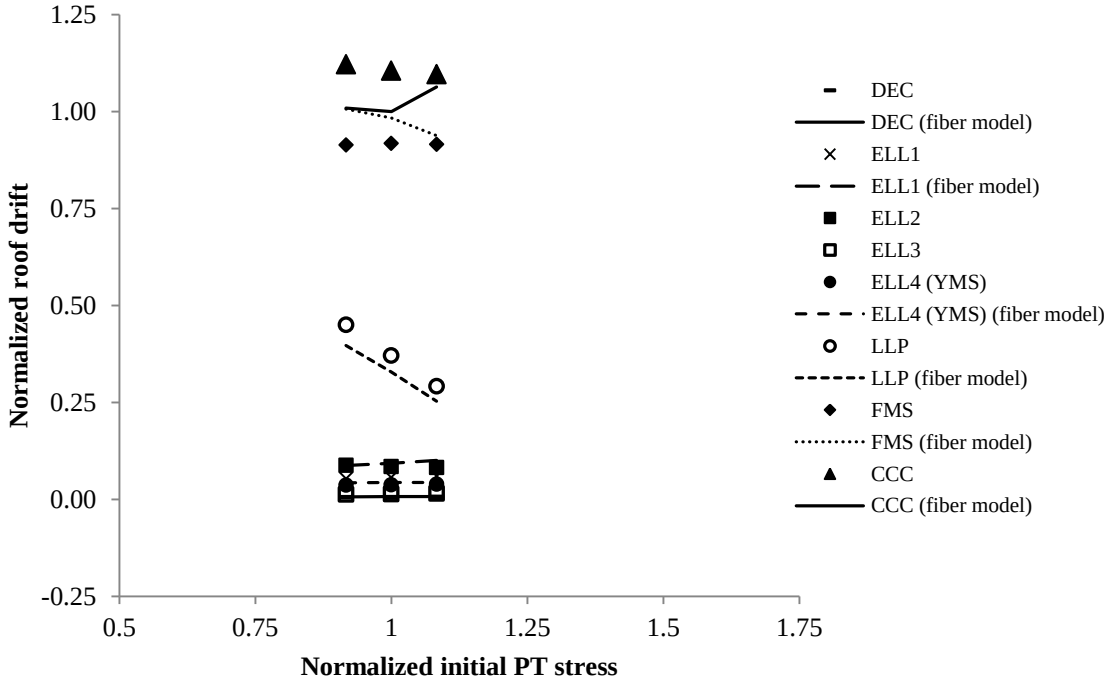

Figure 6.14(d): Effect of change in initial prestress of PT steel on drift of parametric base wall 4

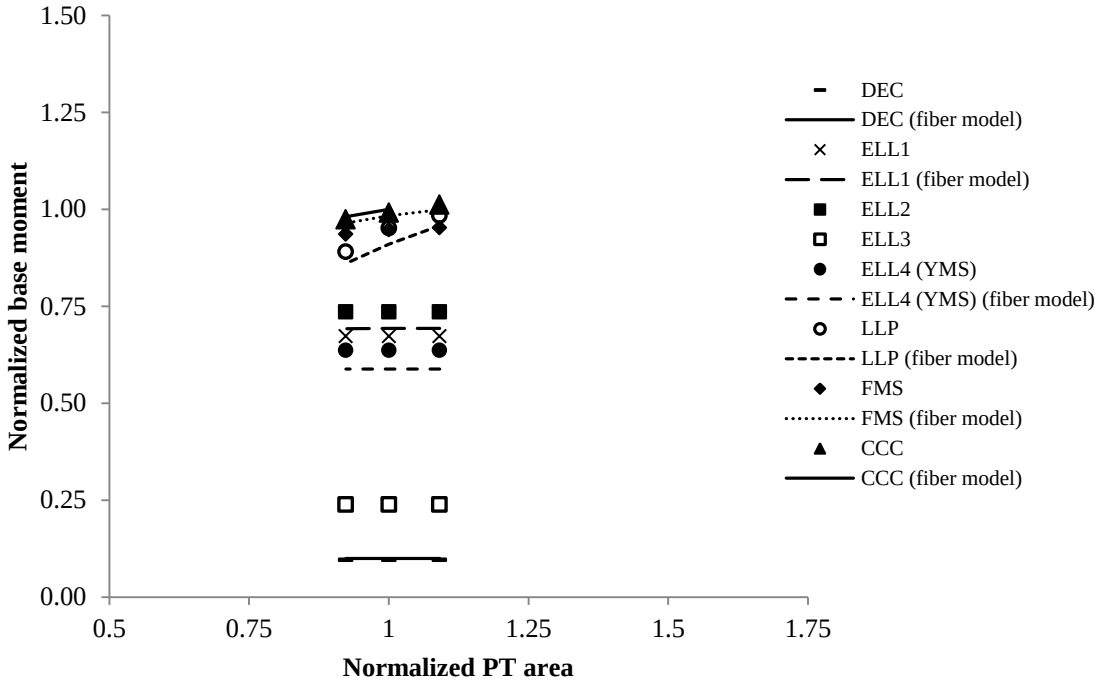

Figure 6.15(a): Effect of change in area of PT steel but with constant initial prestress on base moment of parametric base wall 1

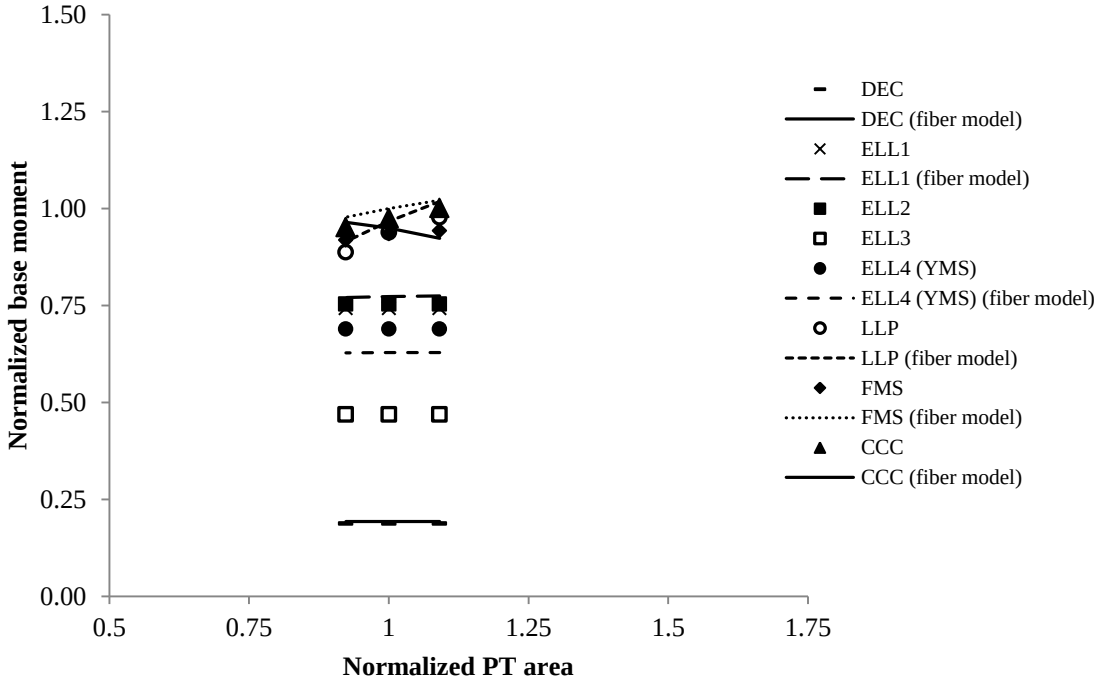

Figure 6.15(b): Effect of change in area of PT steel but with constant initial prestress on base moment of parametric base wall 2

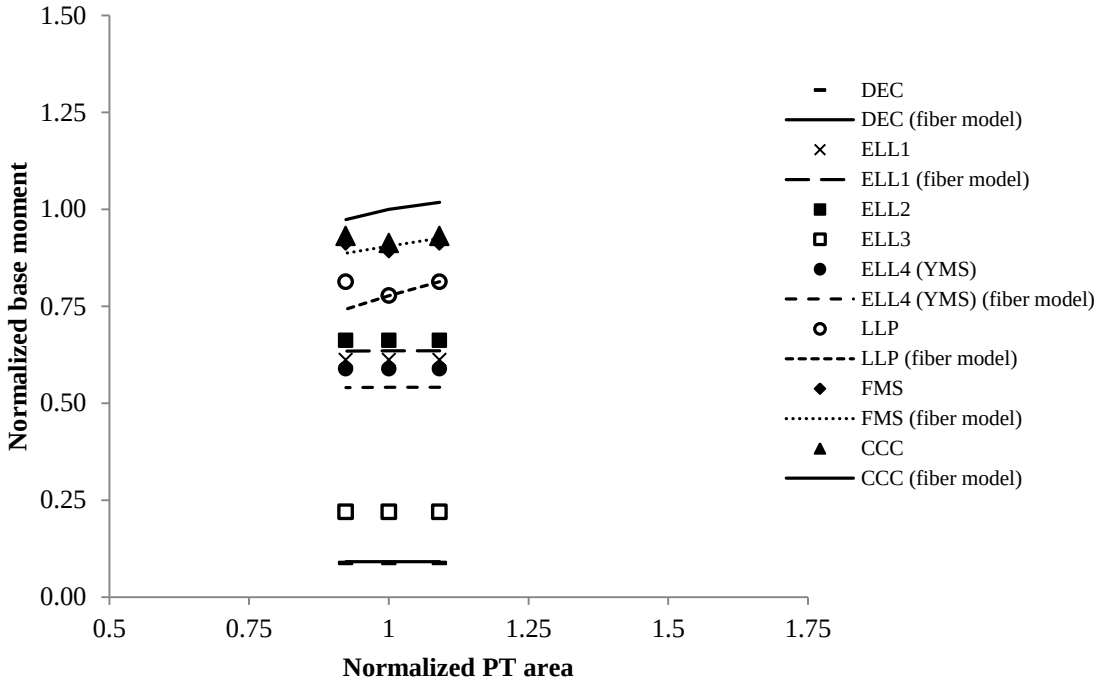

Figure 6.15(c): Effect of change in area of PT steel but with constant initial prestress on base moment of parametric base wall 3

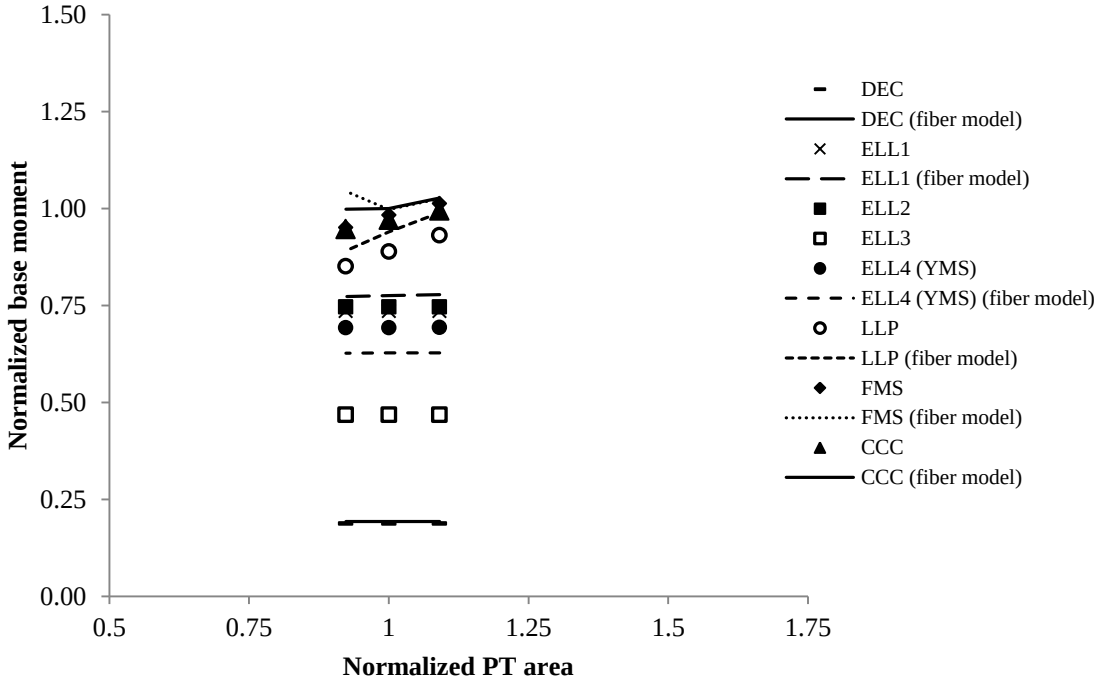

Figure 6.15(d): Effect of change in area of PT steel but with constant initial prestress on base moment of parametric base wall 4

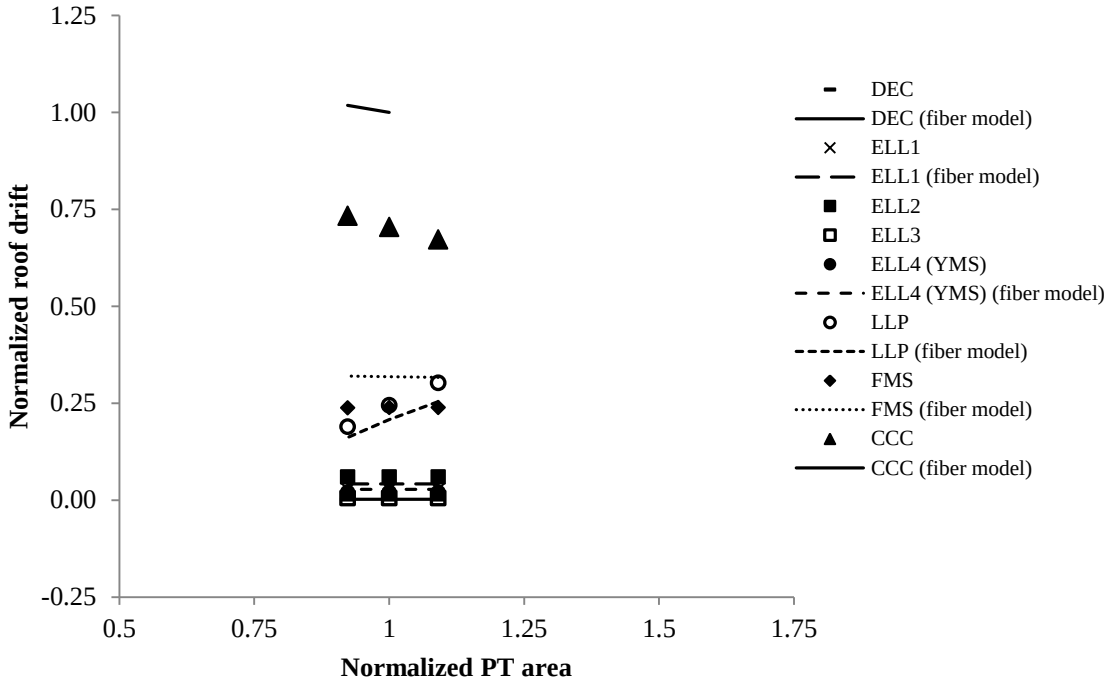

Figure 6.16(a): Effect of change in area of PT steel but with constant initial prestress on drift of parametric base wall 1

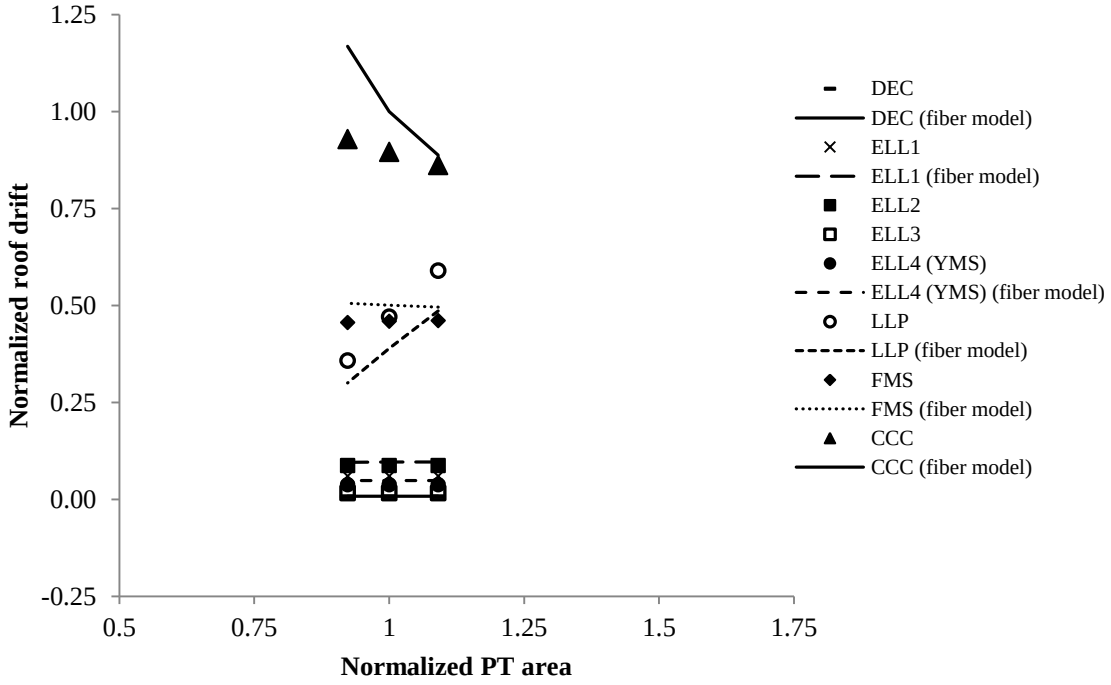

Figure 6.16(b): Effect of change in area of PT steel but with constant initial prestress on drift of parametric base wall 2

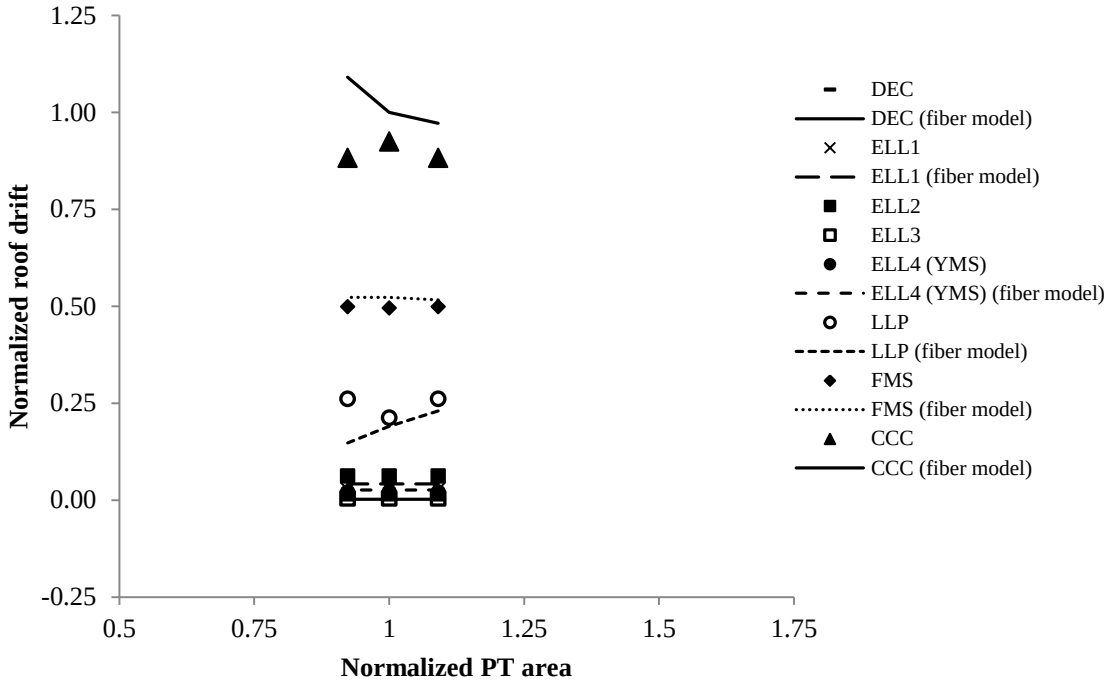

Figure 6.16(c): Effect of change in area of PT steel but with constant initial prestress on drift of parametric base wall 3

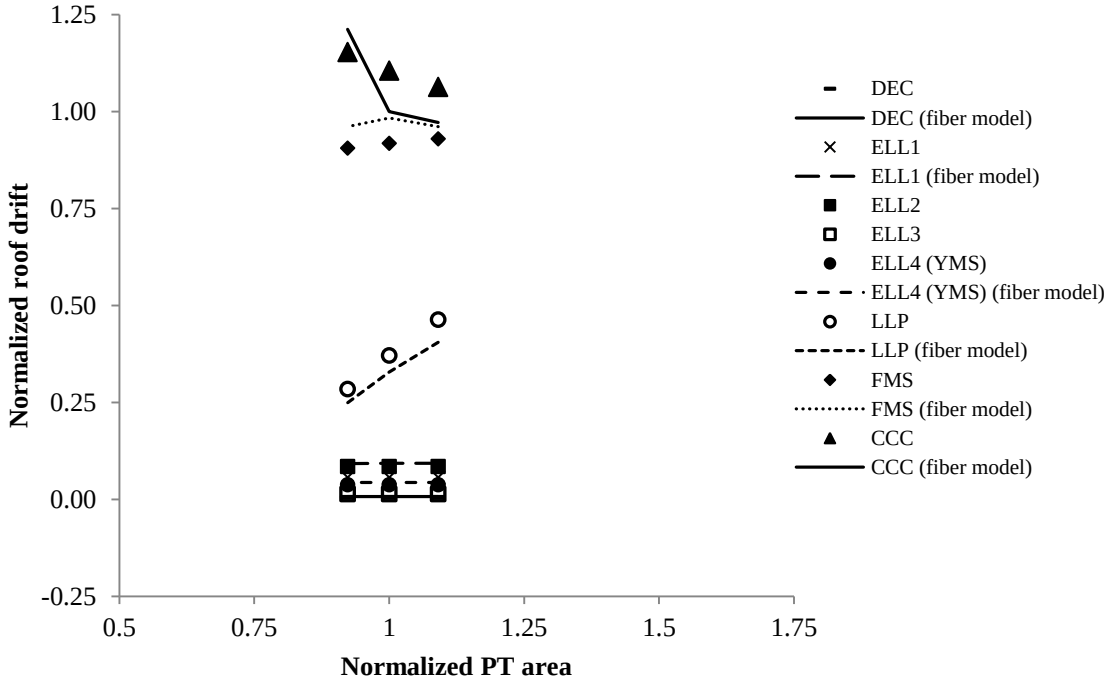

Figure 6.16(d): Effect of change in area of PT steel but with constant initial prestress on drift of parametric base wall 4

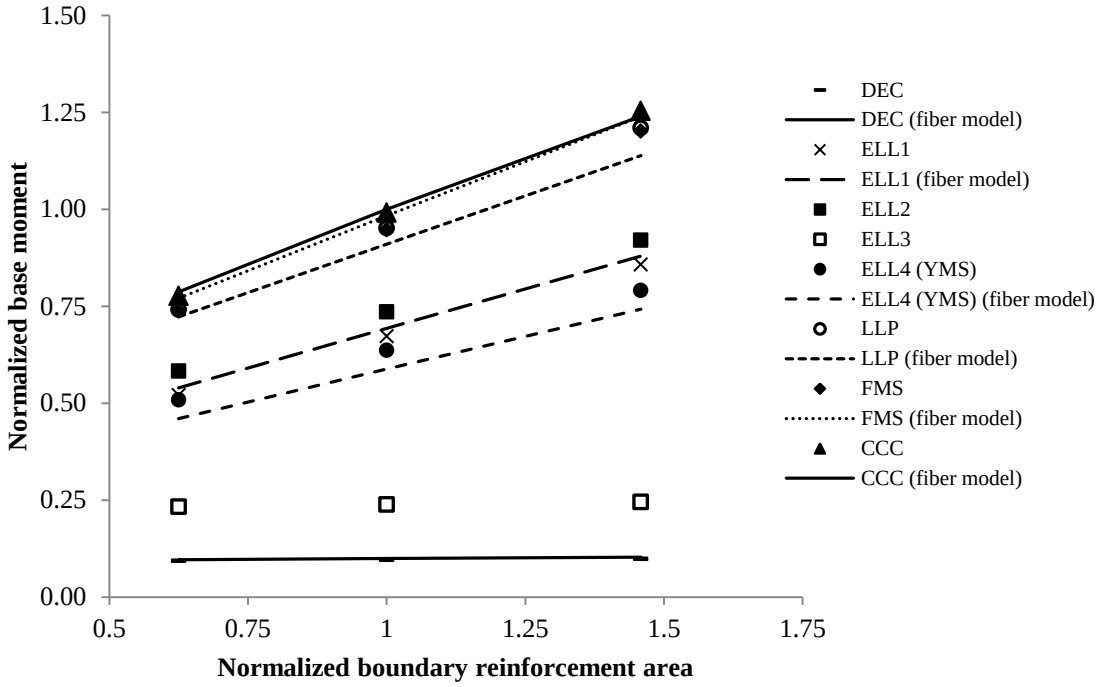

Figure 6.17(a): Effect of change in area of boundary longitudinal reinforcement on base moment of parametric base wall 1

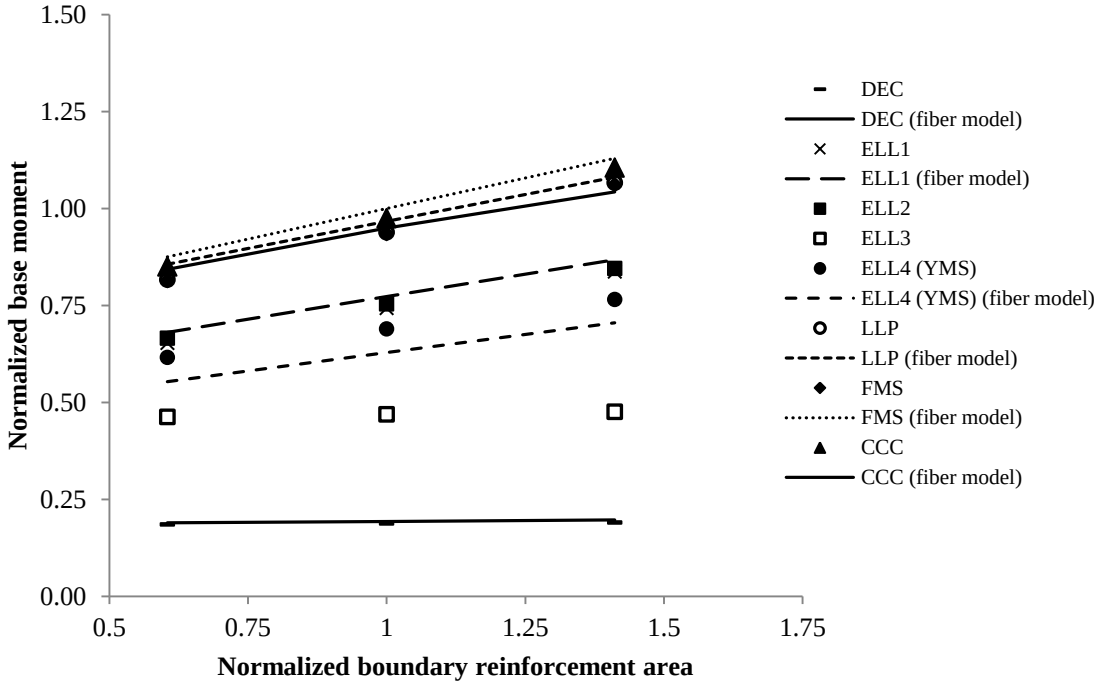

Figure 6.17(b): Effect of change in area of boundary longitudinal reinforcement on base moment of parametric base wall 2

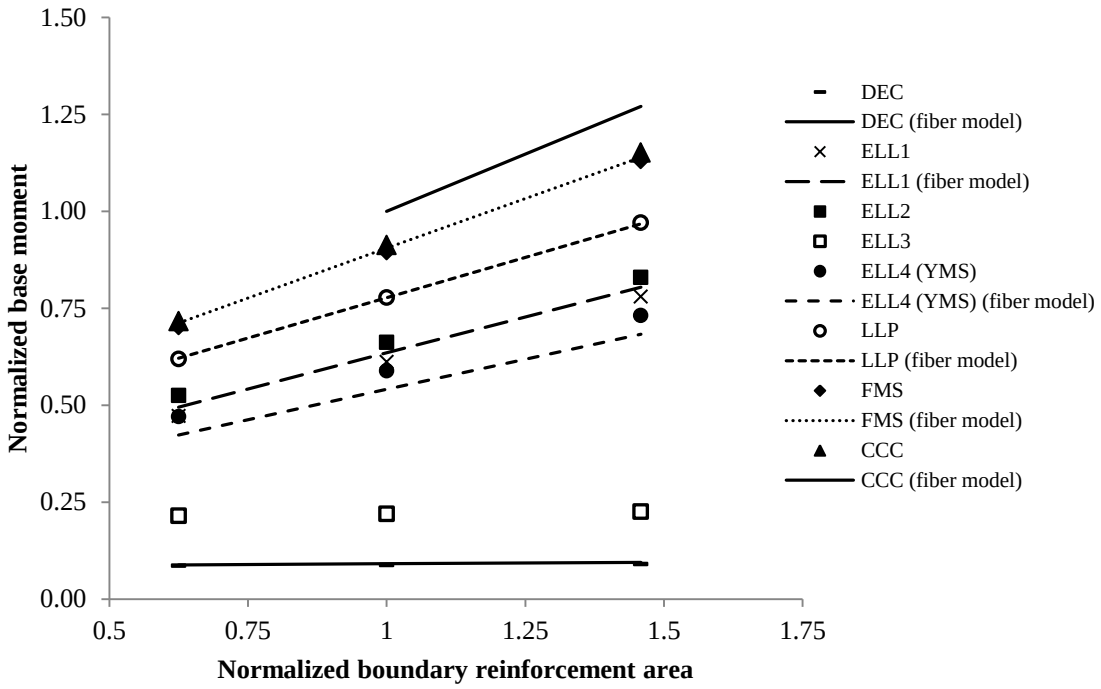

Figure 6.17(c): Effect of change in area of boundary longitudinal reinforcement on base moment of parametric base wall 3

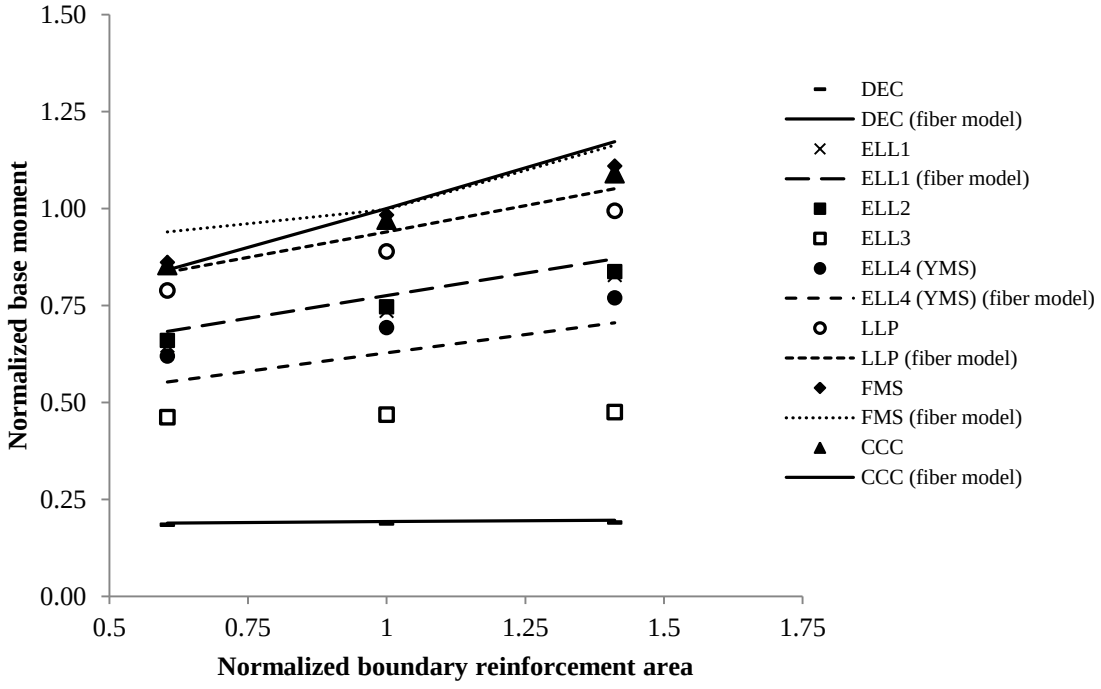

Figure 6.17(d): Effect of change in area of boundary longitudinal reinforcement on base moment of parametric base wall 4

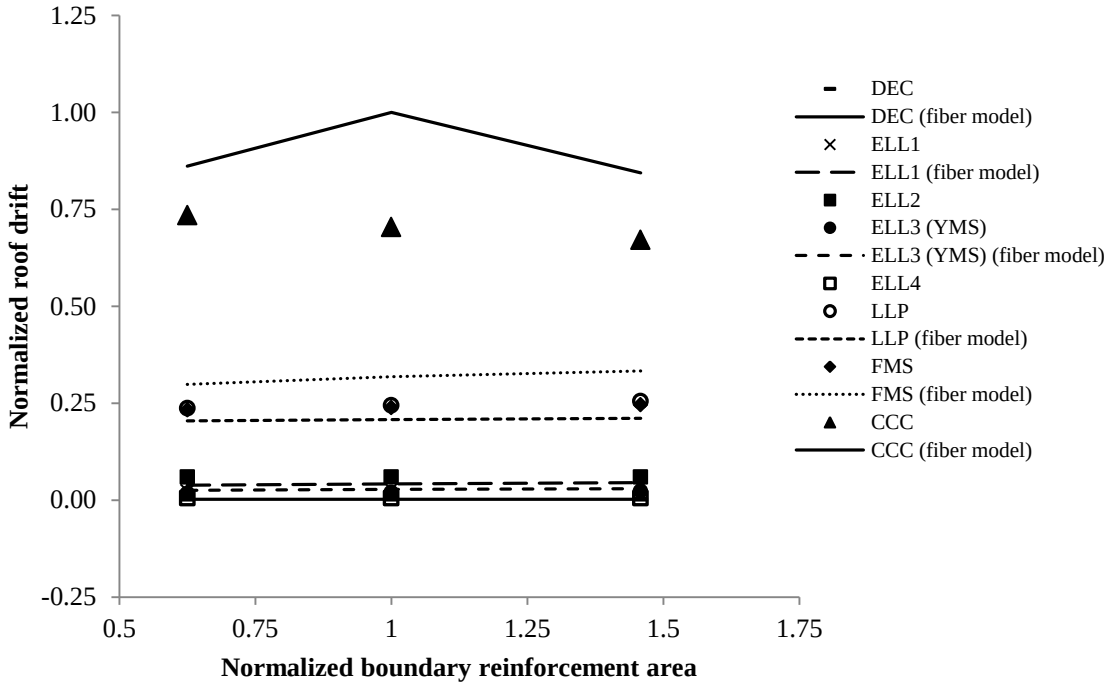

Figure 6.18(a): Effect of change in area of boundary longitudinal reinforcement on drift of moment of parametric base wall 1

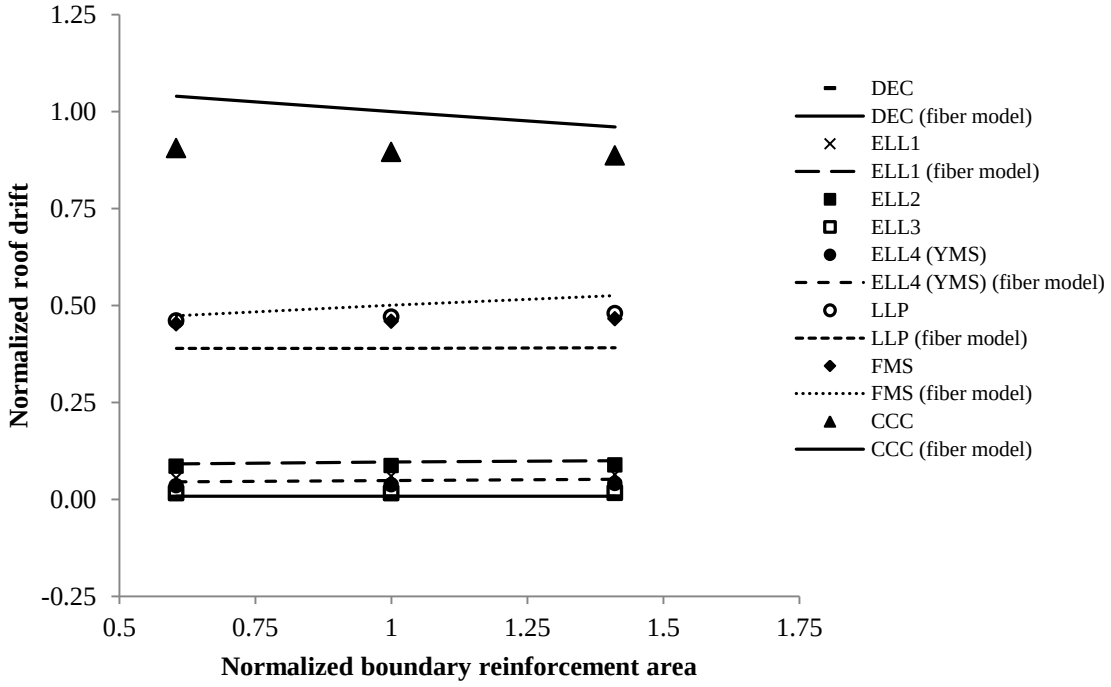

Figure 6.18(b): Effect of change in area of boundary longitudinal reinforcement on drift of parametric base wall 2

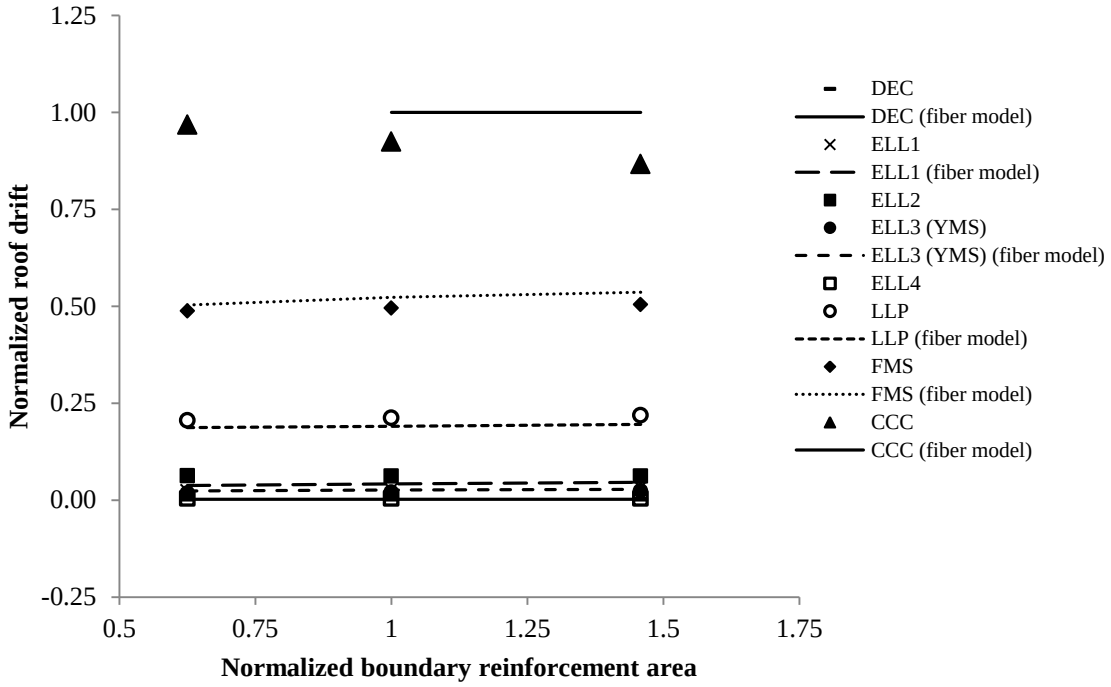

Figure 6.18(c): Effect of change in area of boundary longitudinal reinforcement on drift of parametric wall 3

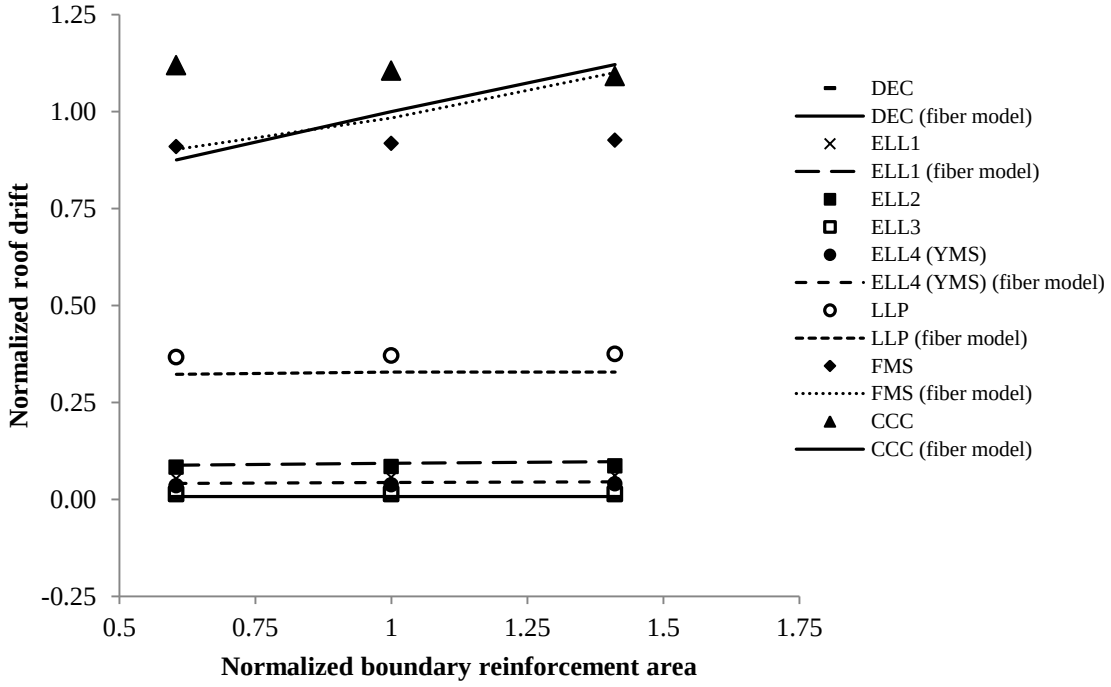

Figure 6.18(d): Effect of change in area of boundary longitudinal reinforcement on drift of parametric wall 4

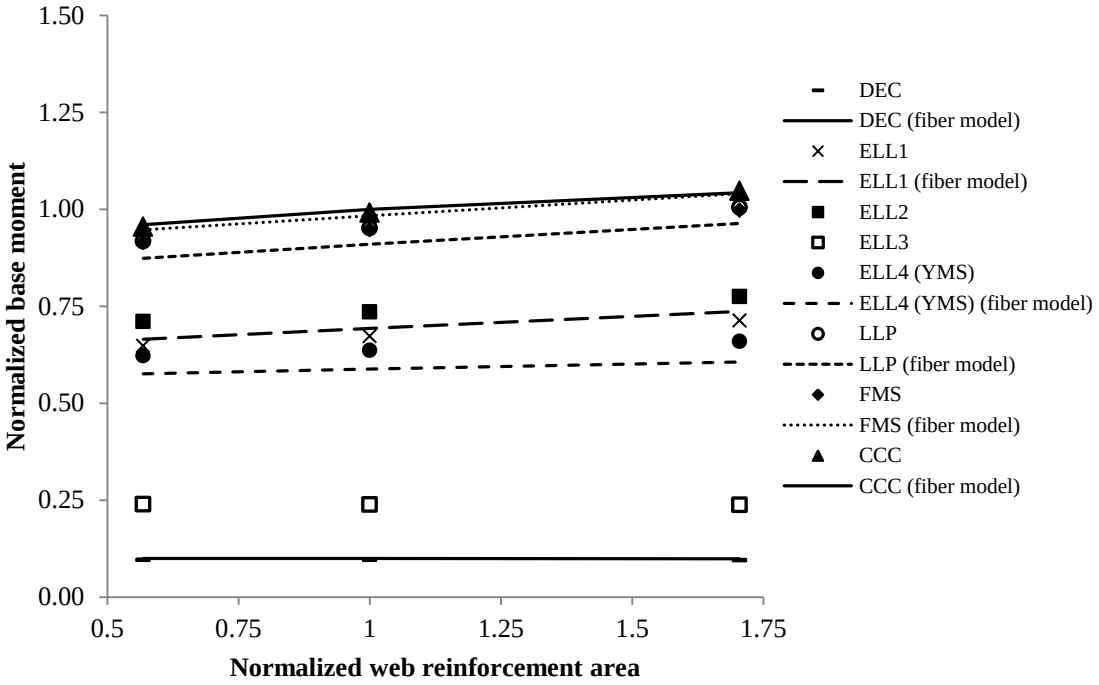

Figure 6.19(a): Effect of change in area of web longitudinal reinforcement on base moment of parametric base wall 1

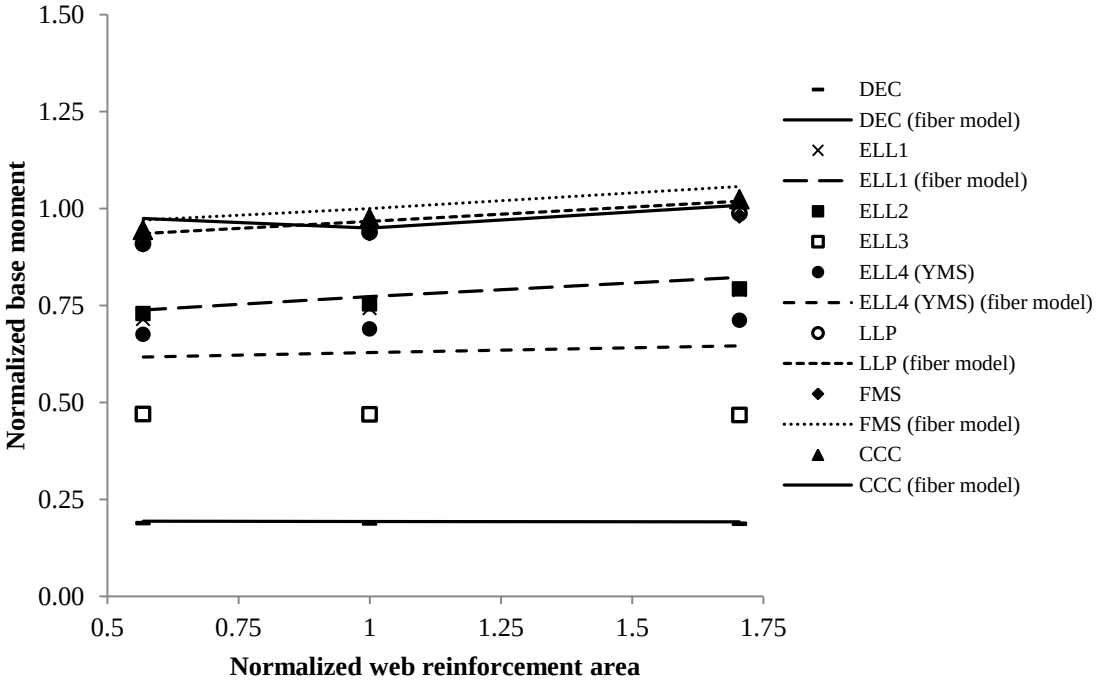

Figure 6.19(b): Effect of change in area of web longitudinal reinforcement on base moment of parametric base wall 2

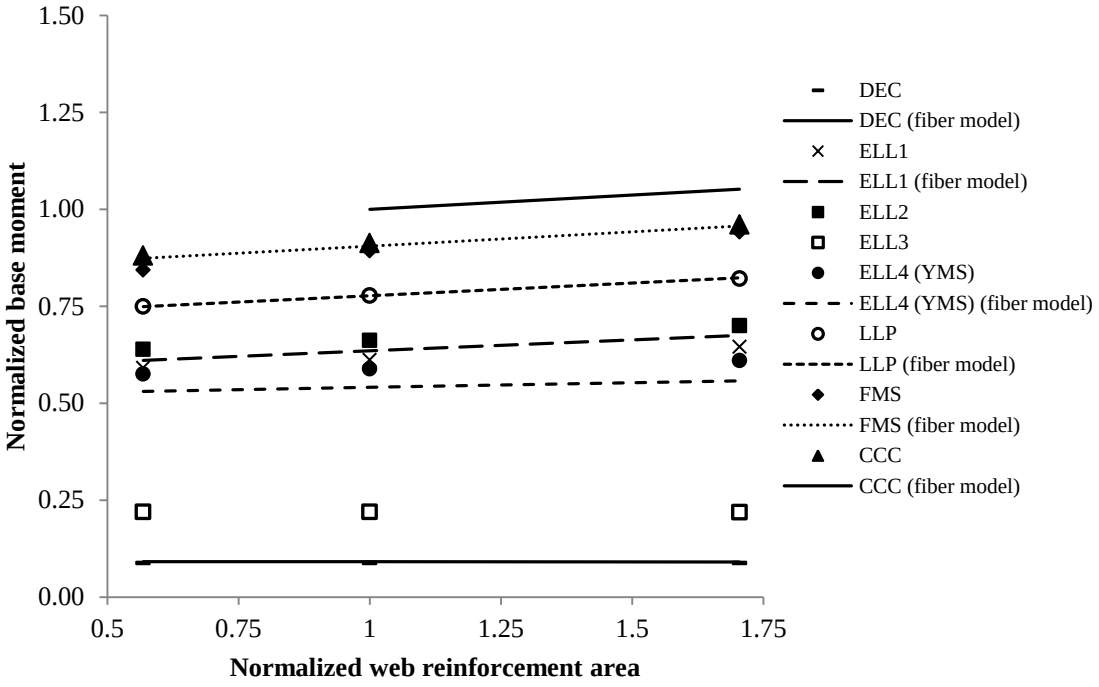

Figure 6.19(c): Effect of change in area of web longitudinal reinforcement on base moment of parametric base wall 3

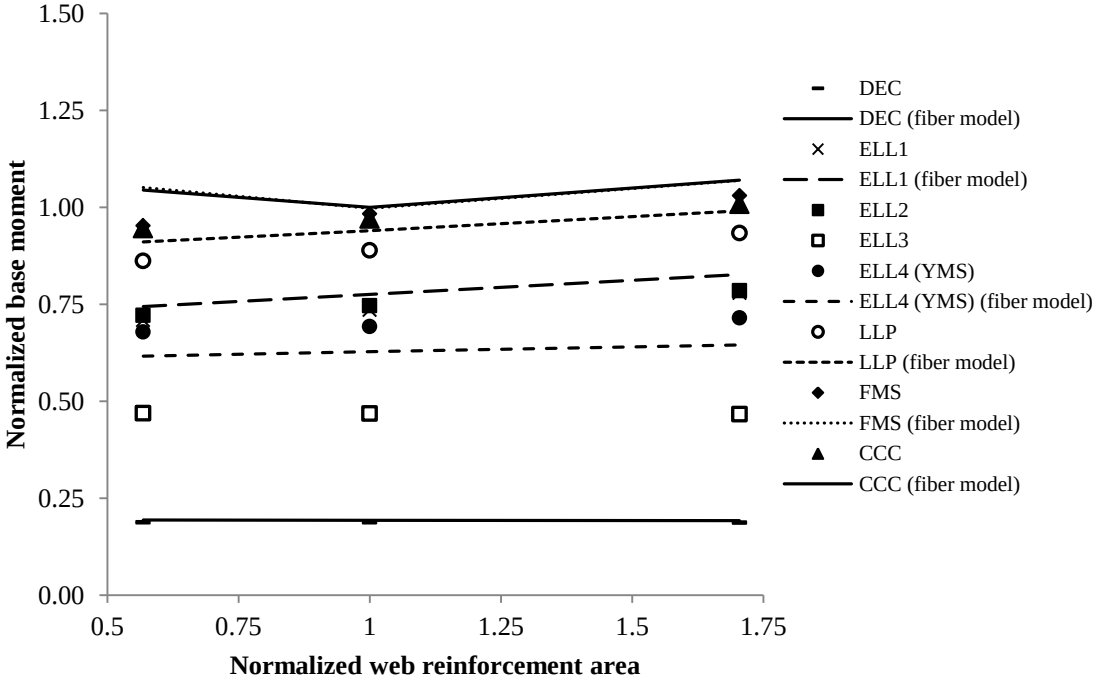

Figure 6.19(d): Effect of change in area of web longitudinal reinforcement on base moment of parametric base wall 4

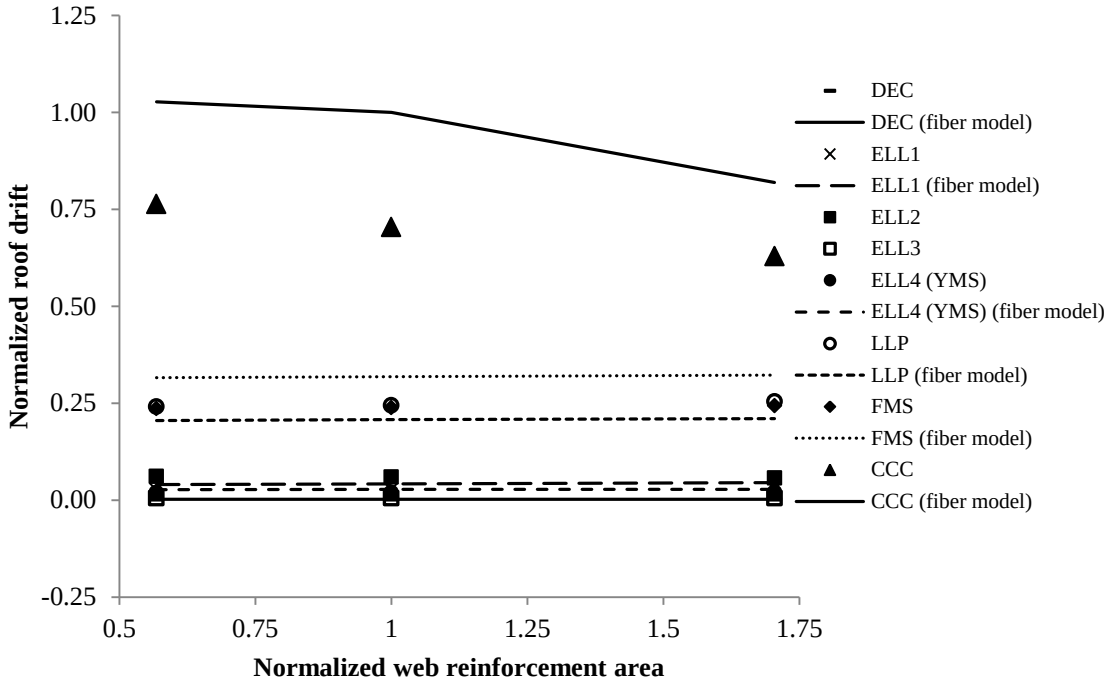

Figure 6.20(a): Effect of change in area of web longitudinal reinforcement on drift of parametric base wall 1

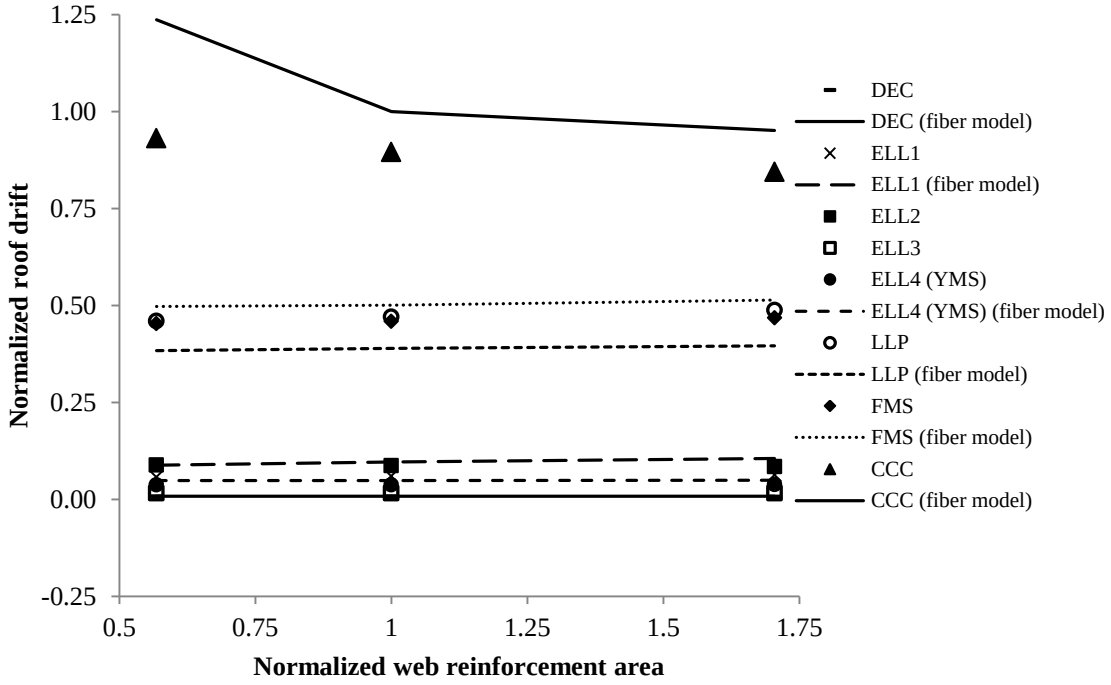

Figure 6.20(b): Effect of change in area of web longitudinal reinforcement on drift of parametric base wall 2

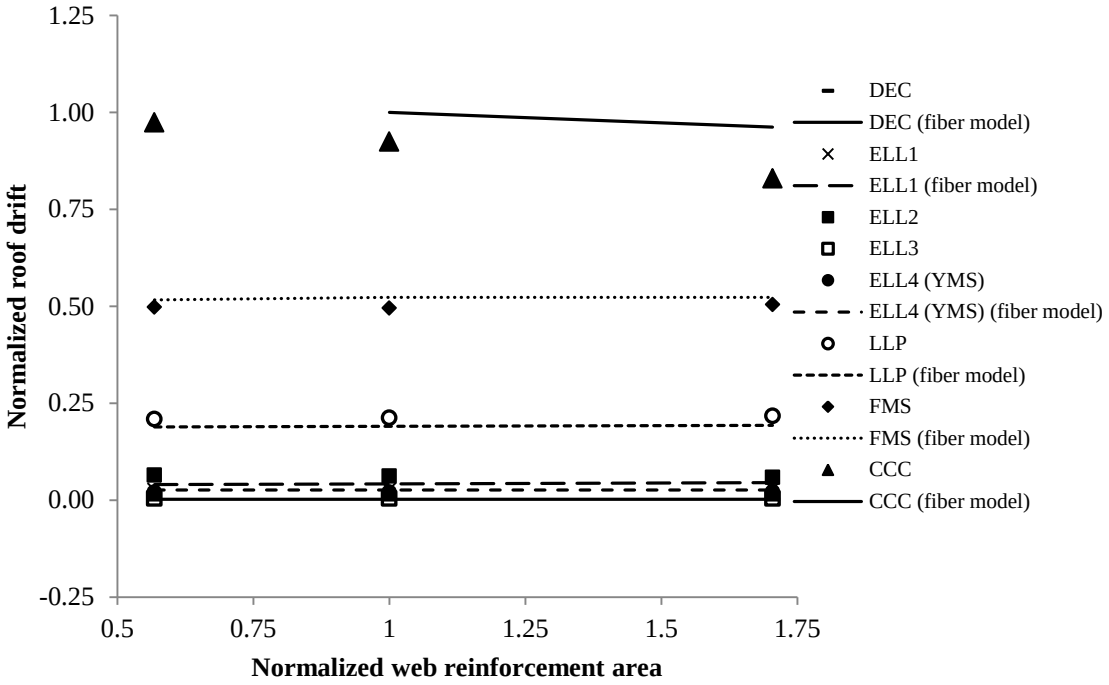

Figure 6.20(c): Effect of change in area of web longitudinal reinforcement on drift of parametric base wall 3

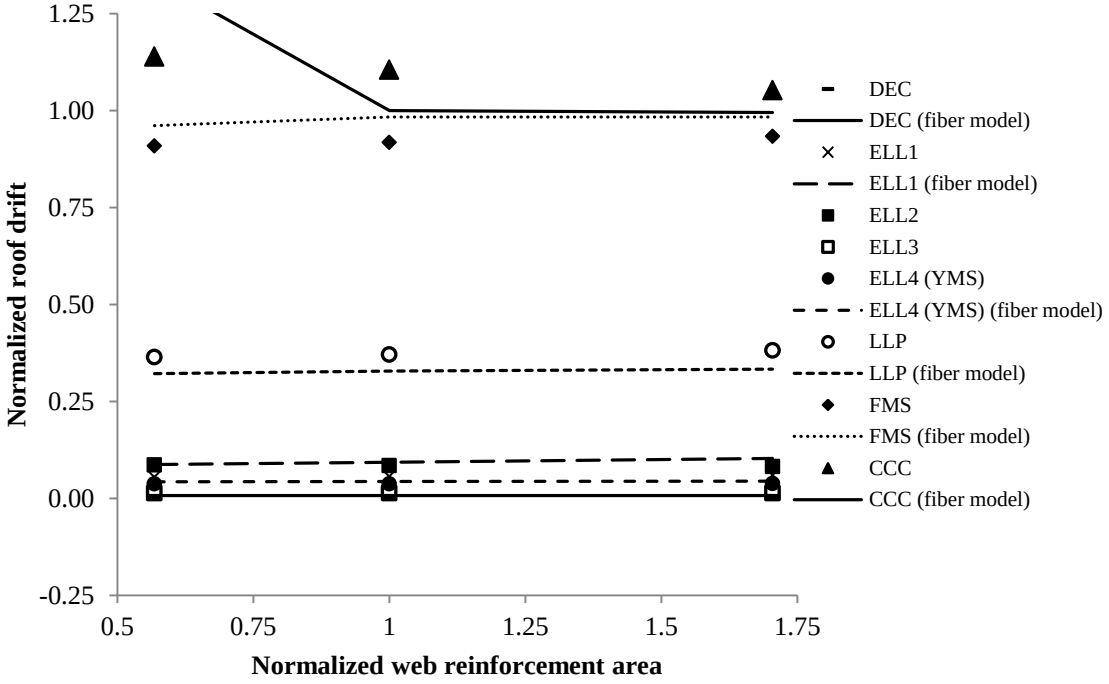

Figure 6.20(d): Effect of change in area of web longitudinal reinforcement on drift of parametric base wall 4

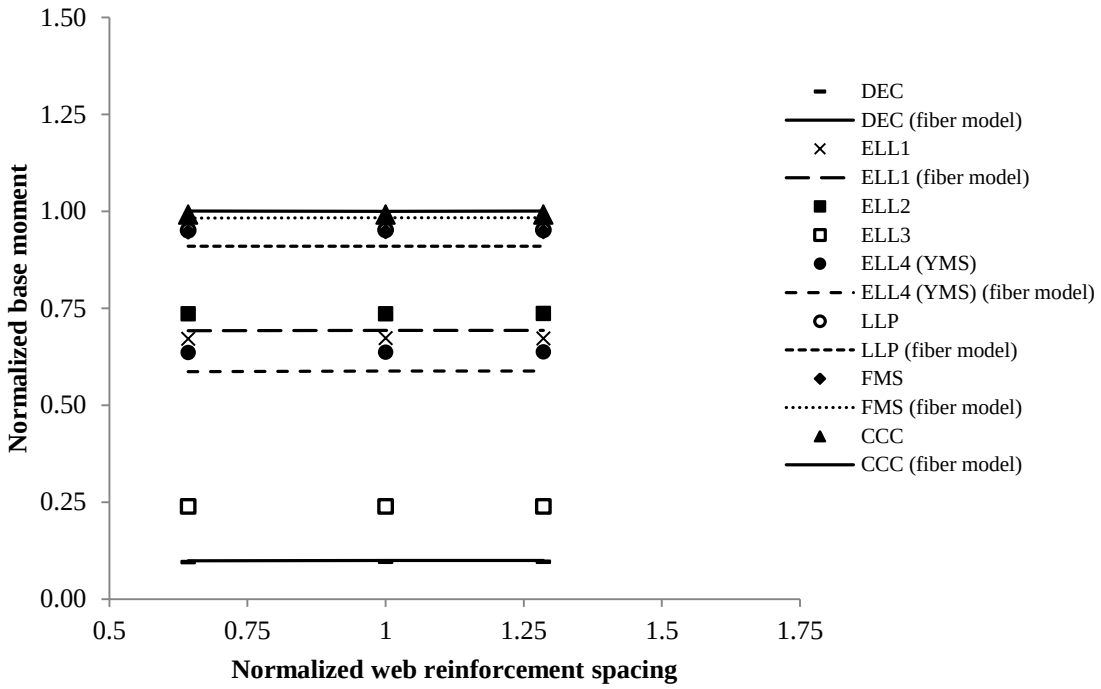

Figure 6.21(a): Effect of change in spacing of web longitudinal reinforcement on base moment of parametric base wall 1

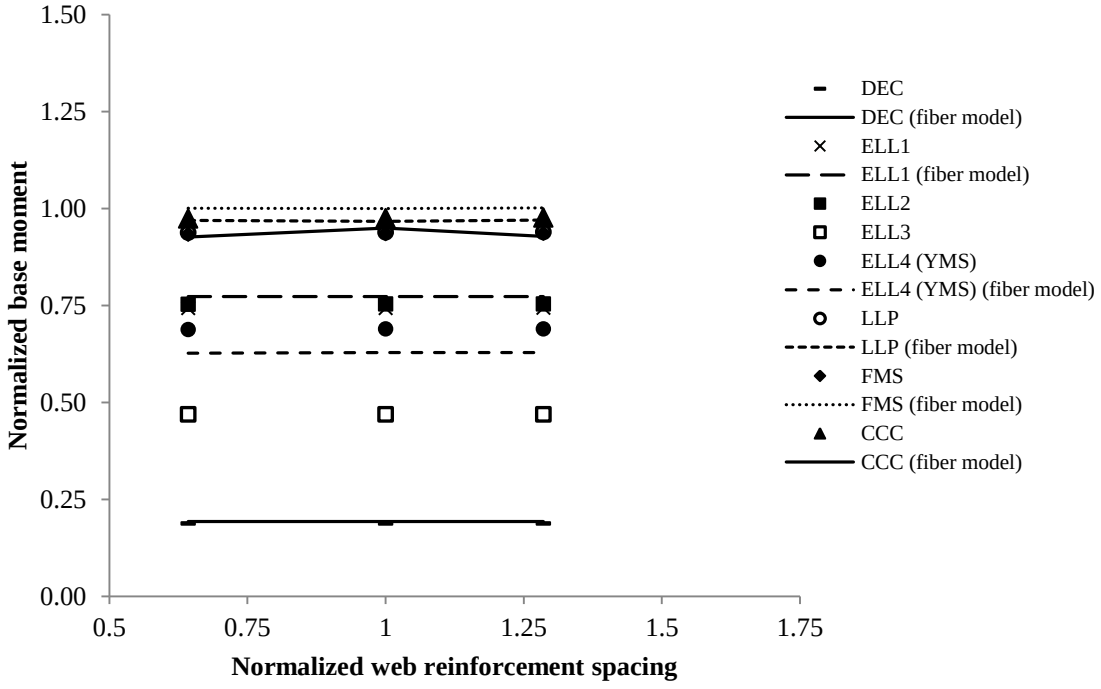

Figure 6.21(b): Effect of change in spacing of web longitudinal reinforcement on base moment of parametric base wall 2

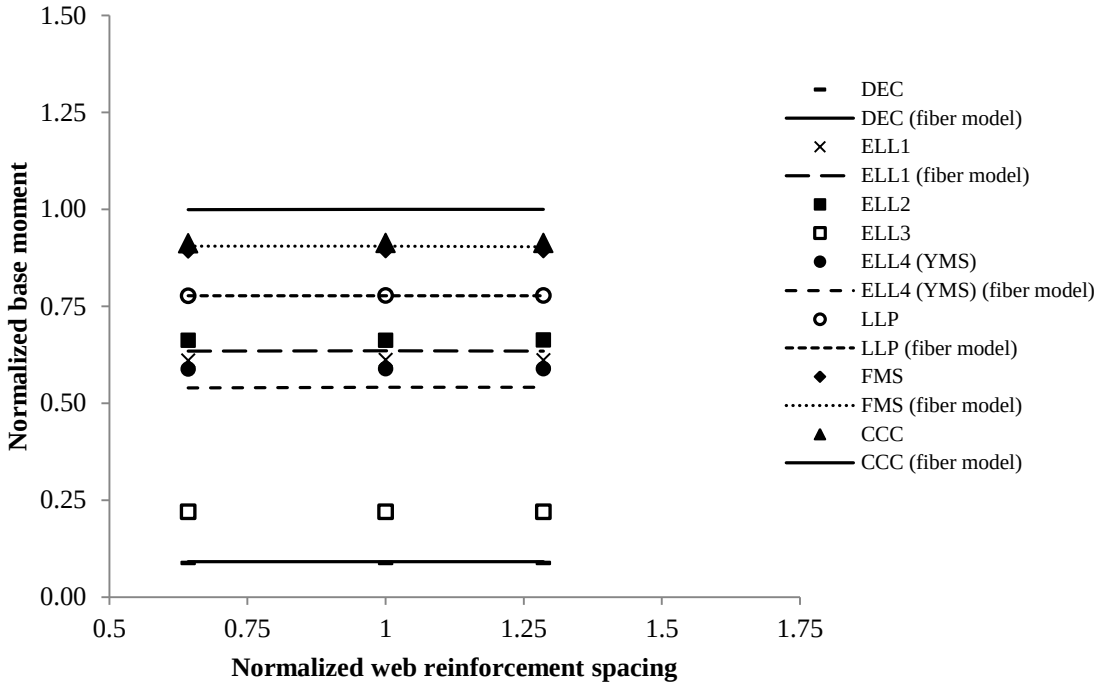

Figure 6.21(c): Effect of change in spacing of web longitudinal reinforcement on base moment of parametric base wall 3

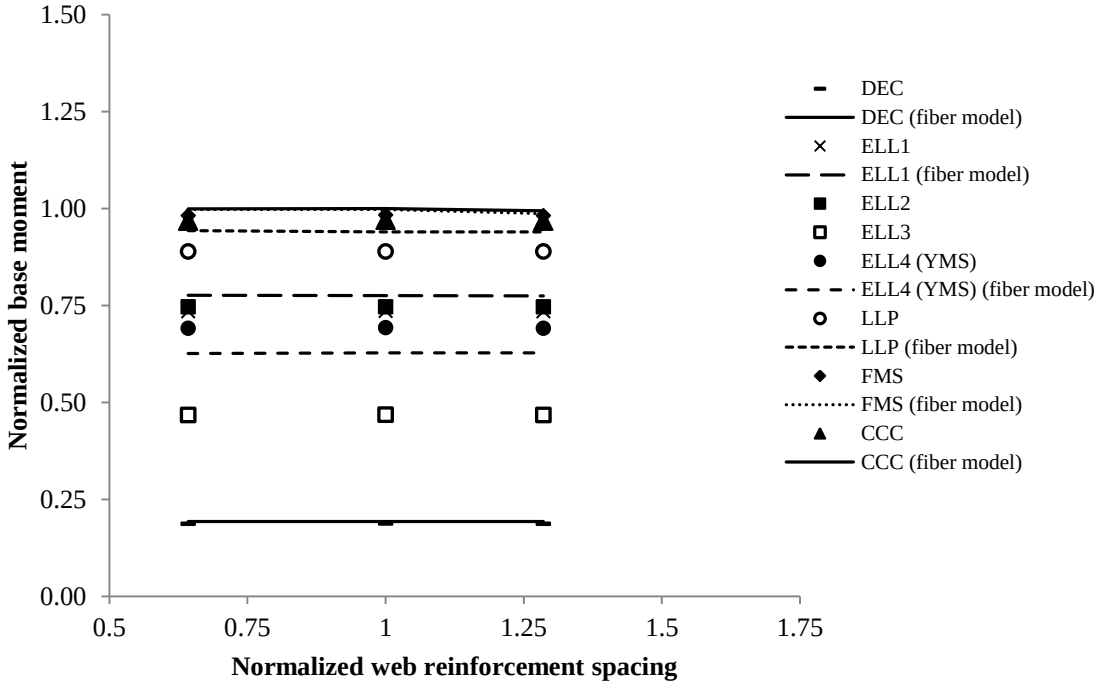

Figure 6.21(d): Effect of change in spacing of web longitudinal reinforcement on base moment of parametric base wall 4

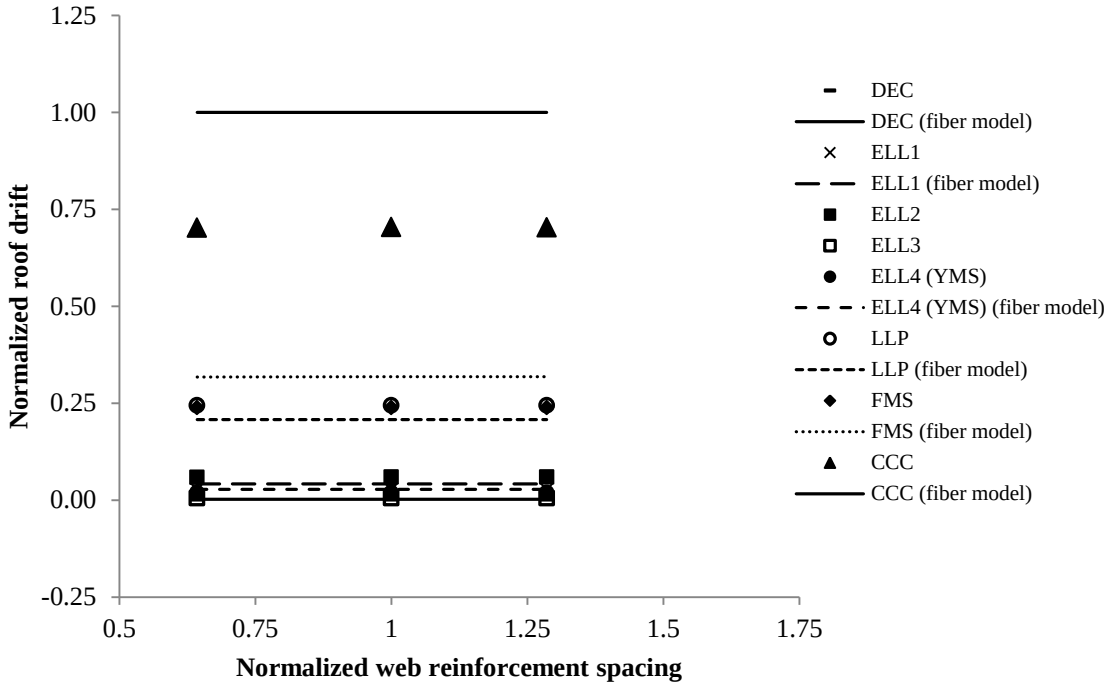

Figure 6.22(a): Effect of change in spacing of web longitudinal reinforcement on drift of parametric base wall 1

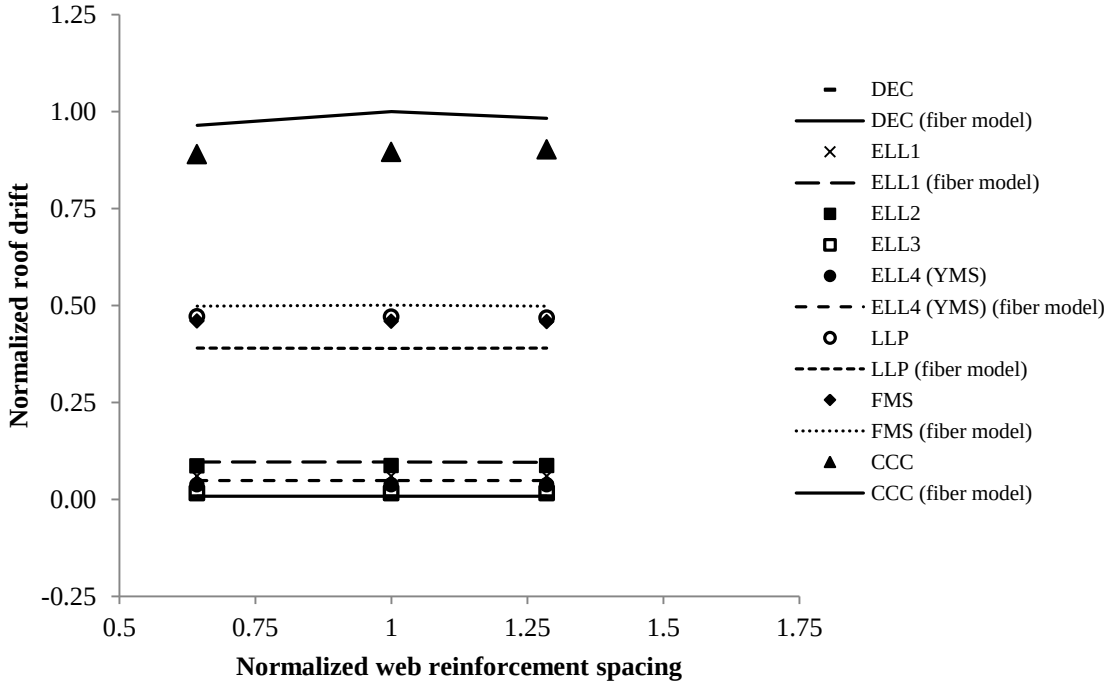

Figure 6.22(b): Effect of change in spacing of web longitudinal reinforcement on drift of parametric base wall 2

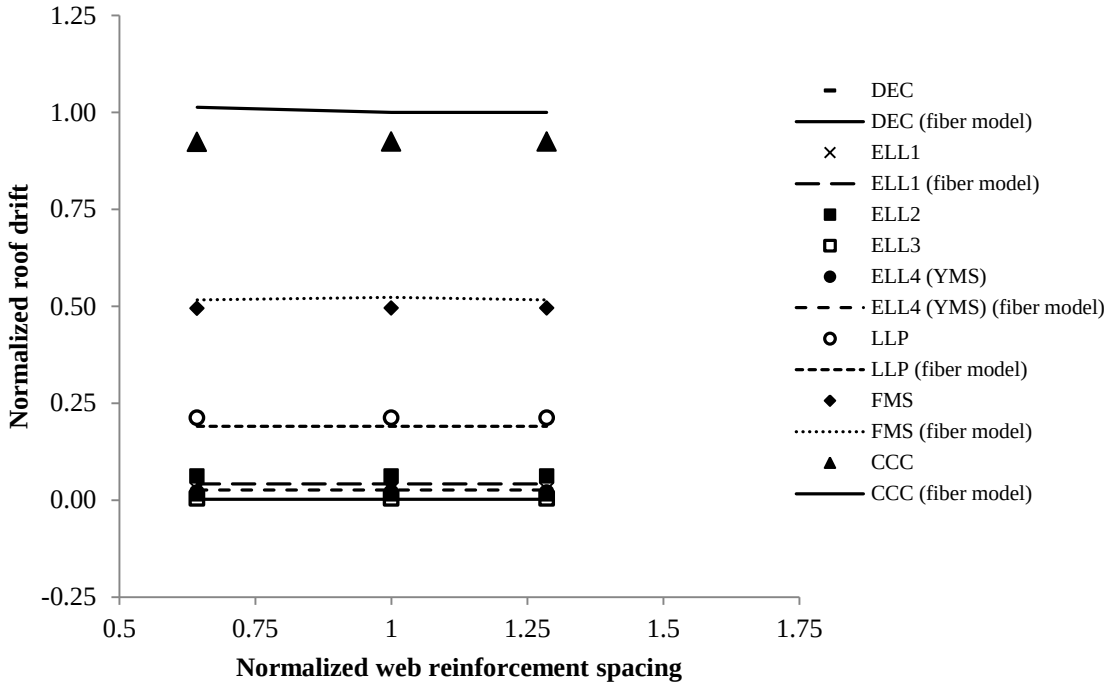

Figure 6.22(c): Effect of change in spacing of web longitudinal reinforcement on drift of parametric base wall 3

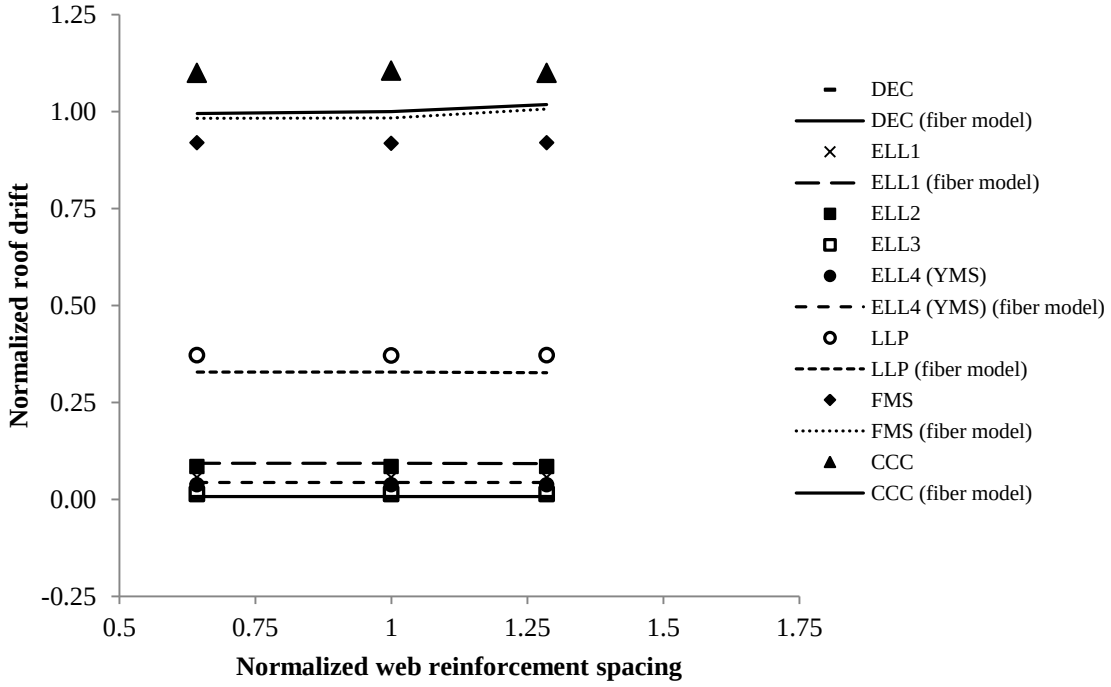

Figure 6.22(d): Effect of change in spacing of web longitudinal reinforcement on drift of parametric base wall 4

CHAPTER 7

SUMMARY, CONCLUSIONS AND FUTURE WORK

This chapter presents a summary of the results and conclusions of the research, and briefly outlines potential topics for future research.

7.1 SUMMARY

This research investigates the lateral load response of unbonded post-tensioned cast-in-place special structural walls with bonded or debonded longitudinal mild steel reinforcement. The report includes derivation of closed-form expressions for calculating expected lateral load responses, moment at the base and lateral drift, of the walls under monotonic lateral load; establishing accuracy of the calculated lateral load response using analytical models; and conducting a design parameter study to assess effects of certain design parameters on the lateral load response of the walls.

Chapter 2 presents a review of the background information on the analytical and experimental work associated with the lateral load response of unbonded post-tensioned precast walls with and without energy dissipaters. This chapter also identifies the research focus of this study, namely, unbonded post-tensioned cast-in-place special structural walls with longitudinal mild steel reinforcement.

In Chapter 3, two sets of closed-form expressions are derived for determining the expected lateral load response of a special structural cast-in-place concrete wall with unbonded post-tensioning and longitudinal mild steel reinforcement for energy dissipation. One set of closed-form expressions is for walls in which the longitudinal mild steel reinforcement is bonded with the surrounding concrete whereas the other one is for walls in which a predetermined length of the longitudinal mild steel reinforcement is debonded at the base of the wall. The key limit states considered for deriving the closed-form expressions are:

1. Decompression of the wall: when one end of the wall reached zero stress under the action of lateral load;
2. Effective linear limit: when significant reduction in the stiffness of the wall takes place which causes beginning of inelastic behavior;
3. Yielding of longitudinal mild steel reinforcement: when farthest longitudinal reinforcement bar(s) starts yielding in tension;
4. Fracture of longitudinal mild steel reinforcement: when farthest longitudinal reinforcement bar(s) reaches its ultimate strain capacity;
5. Linear limit of post tensioning: when the post-tensioning steel starts yielding in tension; and
6. Crushing of confined concrete: when concrete at the toe of the walls fails in compression.

Chapter 4 describes general properties of two reduced scale experimental walls, to be tested at Lehigh University, and four parametric walls which are used in Chapter 5 for verifying accuracy of the closed-form expressions. The four parametric walls are suitable adaptation of the two reduced scale experimental walls. The four parametric walls and their variations are further used in Chapter 6 for parametric study.

Chapter 5 discusses the analytical modeling of the four parametric unbonded post-tensioned cast-in-place special structural walls with longitudinal mild steel reinforcement discussed in Chapter 4. The analytical models are developed using fiber beam-column elements and truss elements of DRAIN-2DX program to represent the axial-flexural behavior of walls. The chapter explains the analysis and modeling assumptions made to model the lateral load response of the parametric walls. The analytical models use fiber beam-column element for modeling confined concrete, unconfined concrete and the bonded longitudinal reinforcement. The unbonded post-tensioning steel and debonded segment of the longitudinal reinforcement is modeled using truss bar elements. Results obtained from these models are compared with lateral load response estimated from the closed-form expressions to verify the accuracy of the closed-form expressions.

Chapter 6 investigates the effect of six design parameters on the lateral load responses, base moment and lateral drift, of the parametric walls. A total of 52 walls, four parametric walls discussed in Chapter 4 and 12 variations of each of the four parametric walls are studied in this chapter. The six design parameters investigated in this chapter are:

1. Area of post-tensioning steel with constant initial prestress;
2. Initial prestress with constant area of post-tensioning steel;
3. Constant initial prestress force in post-tensioning steel by varying initial prestress and area of post-tensioning steel;
4. Area of longitudinal mild steel reinforcement in the boundary region of the walls;
5. Area of longitudinal mild steel reinforcement in the web region of the walls; and
6. Spacing of longitudinal mild steel reinforcement in the web region of the walls.

7.2 CONCLUSIONS

The important conclusion drawn from the study of expected lateral load response of unbonded post-tensioned cast-in-place concrete walls are summarized below:

Validation of the lateral load responses estimated using closed-form expressions:

1. The lateral load responses of the parametric walls estimated from the closed-form expressions and analytical models are in good agreement.
2. In general, the closed-form expressions gave a conservative estimation of the moment at the base of the wall and lateral drift of the wall compared to the analytical models.
3. The roof drift response estimated at the limit state of effective linear limit with 25% section in compression shows large difference between the results of close-form expressions and results of analytical models. In deriving the closed-form expression, a simplifying assumption of triangular stress distribution in concrete was made but the material properties in analytical model also accounts for nonlinear behavior which lead to this difference. The assumption of triangular stress distribution may be applicable to walls with small prestressing force but may not be valid for walls with large prestressing force. Also, it was observed that this assumption can lead to higher stresses than the expected strength of unconfined concrete and/or confined concrete.

4. The accuracy of the limit state of effective linear limit with non-linear behavior of unconfined concrete (ELL-2) could not be established as lateral load responses for this limit state could not be obtained from the analytical model.
5. The closed-form expressions overestimate the moment at the base calculated for the limit state of yielding of longitudinal mild steel reinforcement (ELL-4 for the bonded mild steel case and YMS for the debonded mild steel case). Similar to the previous case, this is caused by the simplifying assumption, in derivation of closed-form expressions, that the unconfined concrete is nonlinear at this limit state. A study of the results obtained from analytical models shows that, in all the parametric walls, the farthest unconfined concrete entered nonlinear segment of the stress-strain relationship and hence is not in the linear elastic range of the stress-strain relationship anymore.
6. Debonding the longitudinal mild steel reinforcement over a predetermined height at the base of the wall significantly increases the lateral drift value with small reduction in the base moment value for the limit states of: (a) yielding of longitudinal mild steel reinforcement (ELL-3 for bonded mild steel and YMS for debonded mild steel), (b) fracture of longitudinal mild steel reinforcement (FMS), (c) linear limit of post-tensioning steel (LLP) and (d) crushing of confined concrete (CCC).
7. At the limit state of crushing of confined concrete, difference in base moment values estimated from closed-form expressions and analytical models were high for the walls with debonded longitudinal mild steel reinforcement compared to their bonded longitudinal mild steel reinforcement cases. This effect was caused by the use of truss bar element in the analytical model for the debonded longitudinal mild steel reinforcement which could not be designed to have zero or constant stress after the ultimate strain was achieved. Therefore, stresses (and hence forces) in the reinforcement bar(s) continued to increase after the limit state of FMS was achieved, leading to large difference between the results.
8. At the limit state of crushing of confined concrete the analytical model result for drift is larger than the closed-form expression result for PW3.0.0. However, it is smaller than the closed-form expression result for PW4.0.0. This difference may be caused by a combination of factors including total area of PT steel, total initial PT force, area of the longitudinal mild steel reinforcement, and difference in material properties (concrete and longitudinal mild steel reinforcement) considered for the two cases.
9. In general, the limit state of LLP occurred before FMS for the parametric walls studied. Similarly, FMS occurred before CCC except for the cases with heavily reinforced parametric walls.

Parametric study on the effects of design parameters in the lateral load response of cast-in-place walls with longitudinal mild steel reinforcement:

10. The base moment response of the walls increases for all the limit states with increase in the total area of PT steel with constant initial prestress force, and increase in the initial prestress in PT steel with constant total PT area (except LLP).

11. The lateral drift response of the walls decreases for all the limit states with increase in the total area of PT steel with constant initial prestress force, and increase in the initial prestress in PT steel with constant total PT area.
12. The base moment response of the wall for LLP decreases when the initial prestress in PT steel (with constant PT steel area) is increased because when initial prestress increases, difference between the initial stress and yielding stress reduces and yielding of PT steel occur at a smaller drift with smaller forces in longitudinal mild steel reinforcement bar(s).
13. In case of constant initial prestress force, the lateral load responses of the parameter walls increases for the limit state of LLP, FMS and CCC for the walls with smaller initial prestress. This occurs because in order to achieve constant initial prestress force with smaller initial prestress a larger PT steel area is required and effects of this larger prestress area are more pronounced when stress in PT steel starts increasing at larger drift for the limit states of LLP, FMS and CCC.
14. Increasing the area of longitudinal mild steel reinforcement in the boundary region or in the web of the walls have same effect on the lateral load responses, the base moment value increases with nominal increase in the drift value for an increase in the longitudinal mild steel reinforcement area.
15. Spacing of web longitudinal mild steel reinforcement with constant total web reinforcement area did not produce any significant changes in either of the response quantities studied. Therefore, it can be concluded that this parameter does not affect the lateral load responses of the parametric walls.

7.3 FUTURE WORK

The following areas of analytical and experimental research are suggested:

1. This research analytically investigates the lateral load response of unbonded post-tensioned cast-in-place concrete walls with bonded or debonded longitudinal mild steel reinforcement under monotonic lateral load. Additional research is needed to analytically and experimentally investigate the wall response due to static cyclic and nonlinear dynamic lateral loads. An experimental program is in progress at Lehigh University to experimentally investigate the cyclic lateral load response of these walls. This experimental program will provide valuable information on static cyclic and hysteretic responses of the walls which can be used to verify the accuracy of closed-form expressions and improve the analytical models. This may also help in improving the closed-form expression for the limit state of yielding of mild steel reinforcement.
2. It was observed in this study that the base moment at the limit state of crushing of confined concrete was over predicted by the analytical model for the walls with debonded mild steel reinforcement. This is attributed to the use of truss bar elements for modeling debonded longitudinal reinforcement which uses strain hardening rate for modeling strain hardening without any limit on ultimate strength. Therefore, the analytical models require modification to eliminate this and incorporate fracture of mild steel at ultimate strain. This will give a realistic approximation of the lateral load responses of an unbonded post-tensioned cast-in-place concrete wall with bonded or debonded longitudinal mild steel reinforcement.

3. Research is also needed to investigate effects of other design parameters such as length of the wall, height of the wall, thickness of the wall, and eccentricity in the location of application of gravity load, on the lateral load responses of the walls.
4. This research studies isolated walls only. Research is needed to study the interaction of such walls with gravity load carrying members, floor and roof slabs, frames, and other walls.

REFERENCES

ACI Committee 318, "Building Code Requirements for Structural Concrete", American Concrete Institute, Farmington Hills, MI, August 2011.

Building Seismic Safety Council, "NEHRP Recommended Provisions for the Development of Seismic Regulations for New Buildings and Other Structures", BSSC, Washington, D.C. 2004.

El-Sheikh, M., Sause, R., Pessiki, S., Lu, L. –W., and Kurama, Y. C., "Seismic Analysis, Behavior, and Design of Unbonded Post-Tensioned Precast Concrete Frames", Earthquake Engineering Research Report, No. EQ-97-02, Department of Civil and Environmental Engineering, Lehigh University, Bethlehem, PA, November 1997.

Fintel, M., 'Performance of Buildings with Shear Walls in Earthquakes of the Last Thirty Years", PCI Journal, Precast/Prestressed Concrete Institute, Vol. 40, No. 3, May-June 1995, pp. 62-80.

Holden, T., Restrepo, J. and Mander, J. B., "Seismic Performance of Precast Reinforced and Prestressed Concrete Walls", Journal of Structural Engineering, American Society of Civil Engineers, Vol. 129, No. 3 , March 2003, pp. 286-296.

Kurama, Y. C., "Seismic Analysis, Behavior, and Design of Unbonded Post-Tensioned Precast Concrete Walls", Ph.D Dissertation, Department of Civil and Environmental Engineering, Lehigh University, Bethlehem, PA, May 1997.

Kurama, Y. C., Pessiki, S., Sause, R., Lu, L. W., El-Sheikh, M., "Analytical Modeling and Lateral Load Behavior of Unbonded Post-Tensioned Precast Concrete Walls", Research Report, No. EQ-96-02, Department of Civil and Environmental Engineering, Lehigh University, Bethlehem, PA, November 1996.

Mander, J., Priestley, M., and Park, R., "Theoretical Stress-Strain Model for Confined Concrete", Journal of Structural Engineering, American Society of Civil Engineers, Vol. 114, No. 8, August 1988a, pp. 1804-1826.

Mander, J., Priestley, M., and Park, R., "Observed Stress-Strain Behavior of Confined Concrete", Journal of Structural Engineering, American Society of Civil Engineers, Vol. 114, No. 8, August 1988b, pp. 1827-1849.

Perez, F. J., "Experimental and Analytical Lateral Load Response of Unbonded Post-Tensioned Precast Concrete Walls", Ph.D. Dissertation, Department of Civil and Environmental Engineering, Lehigh University, Bethlehem, PA, 2004.

Perez, F. J., Sause, R., and Pessiki, S., "Analytical and Experimental Lateral Load Behavior of Unbonded Post-Tensioned Precast Concrete Walls", Journal of Structural Engineering, American Society of Civil Engineers, Vol. 133, No. 11, November 2007, pp. 1531-1540.

Prakash, V. and Powell, G., "DRAIN-2DX Base Program Description and User Guide; Report No. UCB/SEMM-93/17, Structural Engineering Mechanics and Materials, Department of Civil Engineering, University of California, Berkeley, CA, November 1993.

Restrepo, J. and Rahman, A., "Seismic Performance of Self-Centering Structural Walls Incorporating Energy Dissipators", Journal of Structural Engineering, American Society of Civil Engineers, Vol. 133, No. 11, November 2007, pp. 1560-1570

Schultz, A. E. and Magana, R. A., "Seismic Behavior of Connections in Precast Concrete Walls", American Concrete Journal, SP162-12, August 1996, pp. 273-312.

Smith, B. J., and Kurama, Y. C., "Design of Hybrid Precast Concrete Walls for Seismic Regions", Proceedings of 2009 Structures Congress, American Society of Civil Engineers, 2009, pp. 1-10.

Smith, B. J., Kurama, Y. C. and McGinnis, M. J., "Design and Measured Behavior of a Hybrid Precast Concrete Wall Specimen for Seismic Regions", Journal of Structural Engineering, American Society of Civil Engineers, Vol. 137, No. 10, October 2011, pp. 1052-1062.

Wood, S. L., "Performance of Reinforced Concrete Buildings During the 1985 Chile Earthquake: Implications for the design of Structural Walls", Earthquake Spectra, Vol. 7, No. 4, November 1991, pp. 607-638.